THÈSE

En vue de l'obtention du

DOCTORAT DE L'UNIVERSITÉ DE TOULOUSE

Délivré par *l'Université Toulouse III - Paul Sabatier*
Discipline ou spécialité : *Chimie moléculaire*

Présentée et soutenue par *Olivier Back*
Le *29 Avril 2011*

Titre : *Stabilisation par les carbènes de fragments phosphorés paramagnétiques ou électro-déficients*

JURY

Jean-Marc Sotiropoulos (chargé de recherche C.N.R.S. à l'université de Pau)
Nicolas Mézailles (directeur de recherche C.N.R.S. à l'école polytechnique)
Marc Taillefer (directeur de recherche C.N.R.S. à l'E.N.S.C.M., Montpellier)
Guy Bertrand (professeur à l'université de Californie, Riverside)
Antoine Baceiredo (directeur de recherche C.N.R.S. à l'université Paul Sabatier, Toulouse)
Gérard Mignani (directeur-scientist fellow du groupe Rhodia)
Rémi Chauvin (professeur à l'université Paul Sabatier, Toulouse)

Ecole doctorale : *Ecole doctorale sciences de la matière*
Unité de recherche : *UCR-CNRS joint research chemistry laboratory (UMI 2957)*
Directeur(s) de Thèse : *Guy Bertrand , Antoine Baceiredo*
Rapporteurs : *Jean-Marc Sotiropoulos (chargé de recherche C.N.R.S. à l'université de Pau)*
Nicolas Mézailles (directeur de recherche C.N.R.S. à l'école polytechnique)

THESE

En vue de l'obtention du

DOCTORAT DE L'UNIVERSITE DE TOULOUSE

Délivrée par l'Université Toulouse III - Paul Sabatier
Spécialité: CHIMIE MOLECULAIRE

Présentée et soutenue par: Olivier Back
Le 29 Avril 2011

Titre: **Stabilisation par les carbènes de fragments phosphorés paramagnétiques ou électro-déficients**

Jury:

MM Jean-Marc Sotiropoulos (chargé de recherche C.N.R.S. à l'université de Pau) Rapporteur

Nicolas Mézailles (directeur de recherche C.N.R.S. à l'école polytechnique) Rapporteur

Marc Taillefer (directeur de recherche C.N.R.S. à l'E.N.S.C.M., Montpellier)

Guy Bertrand (professeur à l'université de Californie, Riverside)

Antoine Baceiredo (directeur de recherche C.N.R.S. à l'université Paul Sabatier, Toulouse)

Gérard Mignani (directeur-scientist fellow du groupe Rhodia)

Rémi Chauvin (professeur à l'université Paul Sabatier, Toulouse)

Remerciements

Je tiens dans un premier temps à exprimer ma plus profonde reconnaissance aux docteurs Jean-Marc Sotiropoulos et Nicolas Mézailles pour avoir accepté de juger ce travail en tant que rapporteurs, ainsi qu'aux docteurs Marc Taillefer, Gérard Mignani et Rémi Chauvin qui ont bien voulu participer à ce jury.

J'ai eu la chance et le bonheur d'effectuer ce travail au « CNRS-UCR joint laboratory » de l'université de Californie à Riverside dirigé par le professeur Guy Bertrand. Je le remercie d'avoir accepté de diriger ma thèse et de m'avoir fait bénéficier de ses compétences, de sa passion, de sa créativité et de ses qualités humaines. Je tiens également à remercier Antoine Baceiredo pour avoir accepté d'être co-directeur de ma thèse.

Je remercie aussi le groupe Rhodia pour avoir accepté de financer ma thèse, et particulièrement Gérard Mignani pour m'avoir fait confiance.

Bien qu'ayant effectué tous mes travaux outre-Atlantique, j'étais officiellement un étudiant de l'Université Paul Sabatier. C'est pourquoi je tiens à remercier particulièrement Maryse Béziat à Toulouse qui a su avec une grande efficacité gérer toutes les formalités administratives à distance.

L'analyse cristallographique par diffraction des rayons X est la méthode d'analyse indispensable et de loin la plus importante pour les composés discutés dans ce manuscrit. Je remercie donc Bruno Donnadieu (M^r Donnadieu) qui a réalisé toutes les études cristallographiques présentes dans ce rapport. Je tiens à remercier également Dan Borchardt du service ACIF à UCR pour son aide précieuse concernant les études RPE réalisées sur l'ensemble des composés paramagnétiques impliqués dans ces travaux.

Je tiens à remercier spécialement Mohand Melaïmi, Michèle Soleilhavoup, Grégorio Guisado Barrios, Martin Henry-Ellinger et Daniel Mendoza-Espinosa pour leur aide sans laquelle ce manuscrit n'aurait jamais pu voir le jour dans les délais prévus.

Je remercie tous les collègues de labo avec qui j'ai eu la chance de travailler et qui ont toujours été disponibles pour moi. Ainsi dans l'ordre chronologique je remercie :

Armelle Ouali pour m'avoir passé le projet sur P_4, Guido Frey (The Guido !!) pour toutes les soirées passées à San Diego ou Los Angeles à écumer les clubs de la ville. A ce sujet je remercie aussi Matt Assay (aka Giorgio Luiggi) pour les soirées passées à un certain institut, pour la croisière mémorable en basse Californie ou pour toutes les soirées passées au Getaway devant une (ou souvent plusieurs) bières....Glenn Kuchenbeiser pour avoir partagé avec moi la galère de la chimie du phosphore blanc et dans le même bureau Adam Dyker pour son aide et sa gentillesse.

Vince Lavallo chimiste hors-paire, Xiaoming Zeng et son vélo lévitant, David Weinberger pour les soirées pocker ainsi que les parties de squash, Rei Kinjo (Aka The Kinjo !!), Amos Rosenthal (Fabian !!) pour sa ponctualité tous les samedis et dimanches matins (t'inquiète pas on retournera à Végas très bientôt), Eugenia Aldeco-Perez (aka Clayton) pour m'avoir supporté pendant pratiquement deux longues années et Emrah Giziroglu pour sa sympathie et sa disponibilité. Un remerciement spécial à Alan Dehope

pour tous les bons moments passés à 777 chez les Schleiches ainsi que toutes les soirées passées à déguster du whisky ou de la bonne bière fait maison.

Un merci aussi aux « nouveaux » arrivés en fin 2009 : Grégorio Guisado Barrios (Tétas !) mon compagnon du café du matin, Gael Ung ainsi que Jean Bouffard pour s'être chargé de fermer le labo tous les soirs. Un grand merci à Daniel Mendoza mon très cher colloc à Spruce Village avec qui j'ai passé deux très bonnes années que je n'oublierai jamais. Merci également à Martin Ellinger mon compagnon de voyages et sans qui la découverte des parcs natinaux de Californie n'aurait pas été aussi fun. Merci également à Maria Lopez que j'ai connue seulement à la fin de mon séjour aux US pour sa gentillesse, sa disponiblité et pour tous les moments passés autours d'un expresso à la casa de puta ! Je tiens également à remercier David Ruiz qui j'en suis sur sera un très bon successeur pour le maintien et la diffusion des délires du " Bertrand's lab", merci également à Aholibama Escobar pour tous les délicieux gâteaux apportés au labo. Un grand merci à tous les permanents du CNRS : Mohand Melaimi, Michelle Soleilhavoup, David Martin et Hoa Tran Hui pour leur aide, leur disponibilité ansi que leurs talents de managers dont ils ont su faire appel pour la gestion du labo. Merci special à Bruno Donnadieu pour toutes les sorties dans les clubs à Los Angeles ainsi que les visites de San Francisco. Merci à toutes les personnes que j'ai pu rencontrer au cours de mon aventure à Riverside aussi bien aux Etats Unis qu'en France, croyez en ma sympathie...

Enfin, un grand merci également à tous mes amis en France aussi bien de Paris que de Lorraine qui m'ont supporté de loin durant cette thèse et que je retrouvais avec grand plaisir lors de mes retours en France. Je tiens enfin à remercier ma famille qui m'ont énormément supporté et sans qui le bon déroulement de cette thèse n'aurait pas été possible.

Stabilisation par les carbènes de fragments phosphorés paramagnétiques ou électro-déficients

Alors qu'à la fin du XX^{ème} siècle, les carbènes singulets stables étaient considérés comme une curiosité de laboratoire, de nombreuses applications leurs ont été découvertes. Parmis les plus importantes, on peut mentionner leur utilité en tant que ligands pour les métaux de transition. En effet les complexes qui en découlent s'avèrent être pour la plupart de très bons catalyseurs. L'exemple le plus frappant est le catalyseur de Grubbs 2nd génération comportant un ligand NHC qui possède une plus grande stabilité et de meilleures propriétés catalytiques que le catalyseur de 1ère génération (incluant un ligand tricyclohexylphosphine à la place du NHC). Il a été montré également que les carbènes stables étaient capables d'activer des petites molécules (CO, H_2, P_4). De plus ils s'avèrent être parfois plus efficaces dans ce domaine que les complexes de métaux de transition. En effet alors que ces derniers sont incapables d'activer l'ammoniaque formant après réaction avec NH_3 les fameux complexes de Werner, certains carbènes clivent l'ammoniaque à température ambiante. Très récemment une nouvelle application des carbènes stables a été découverte: la stabilisation de fragments homoatomiques constitués d'éléments du groupe principal dans leur état d'oxidation zéro. Ce concept a ete appliqué dans le cas du carbon, du silicium et du phosphore. En effet bien que Si_2 et P_2 soient des molécules fortement réactives qui ne peuvent être générées que dans des conditions extrêmes, une fois coordinées par des carbènes, les adduits qui en résultent sont parfaitement stables a température ambiante à la fois en solution et à l'état solide.

Ce manuscrit traite principalement de la stabilisation d'entités phosphorées electro-déficientes ou paramagnétiques.
Dans un premier chapitre, la réactivité des carbènes avec le phosphore blanc (P_4) sera étudiée. Nous allons voir qu'en choisissant les paramètres électroniques et stériques adéquats pour le carbène, la fragmentation de P_4 en entités P_1 et P_2 est possible. Bien que ces processus soient courants pour les métaux de transtion, aucun exemple n'a été rapporté concernant des fragments organiques.

Dans le second chapitre, nous nous concentrerons plus sur les adduits P_2-carbènes. Nous allons montrer qu'en réalisant l'oxydation à un électron de ces molécules, les adduits des fragments $P_2^{+\cdot}$ radical cation et P_2^{2+} dication avec les carbènes seront préparés. De plus cette étude va permettre de comparer l'influence des paramètres électroniques de différents carbènes sur les propriétés des adduits étudiés.

Enfin dans le dernier chapitre, la stabilisation d'entités paramagnétiques par les carbènes sera appliquée à la préparation de radicaux phosphinyls. Plus exactement, nous montrerons que l'oxydation a un électron d'un adduit carbène-phosphinidène conduit a un phosphinyl radical cation. Finalement la synthèse d'un radical phosphinyl neutre sera accomplie et nous permettra de comparer directement la capacité d'un carbène avec celle d'un métal de transition pour stabiliser les radicaux phosphinyls.

Mots clés : carbène singulet, phosphore blanc, radical, RPE, phosphinyl, densité de spin.

Résumé

1) Activation du phosphore blanc par les carbènes

Le phosphore blanc (P_4) est le principal produit de départ pour la synthèse industrielle de la plupart des composés organophosphorés. Les processus indutriels mis en place actuellement reposent sur la synthèse préliminaire de PCl_3. Ce composé est préparé directement par réaction entre P_4 et le dichlore gazeux (Cl_2). Ensuite les atomes de chlore sont substitués par des groupements organiques aux cours de réactions produisant HCl ou des sels comme produits secondaires. Afin de se conformer aux lois environnementales qui sont de plus en plus sévères, il est nécessaire de mettre au point de nouveaux processus basés sur P_4 mais évitant l'utilisation de chlore. Pour ces raisons, durant les 20 dernières années les recherches concernant l'activation de P_4 se sont intensifiées. Ces recherches concernent aussi bien l'activation par les métaux de transition que par des composés organiques basés sur les éléments du groupe principal. C'est dans ce carde que s'inscrit notre étude de la réactivité de P_4 avec les carbènes.

1.1) Activation de P_4 par les composés isoélectroniques aux carbènes basés sur les éléments de la troisième période ($Al^{(I)}$, silylènes et phosphéniums)

De manière générale nous pouvons dire que les composés organiques isoélectroniques aux carbènes basés sur les éléments de la 3 ème période réagissent avec P_4 pour donner des produits d'insertion. Ainsi le composé **1** incorporant un centre $Al^{(I)}$ effectue une double insertion dans deux liaisons P-P opposées du tétrahèdre (Cf Schéma 1).

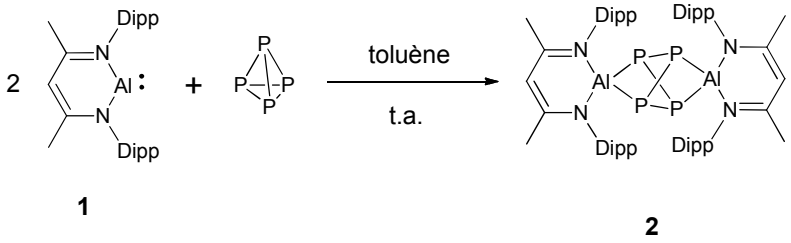

1 **2**

Schéma 1. Activation de P_4 par le composé **1**.

Lorsque le silylène **3** isoélectronique à **1** réagit avec P_4, une réaction similaire se produit. Cependant les insertions ne sont pas simultanées comme dans le cas de **1** et le produit **4** issu d'une mono-insertion de **3** dans une liaison P-P peut également être isolé (Cf Schéma 2).

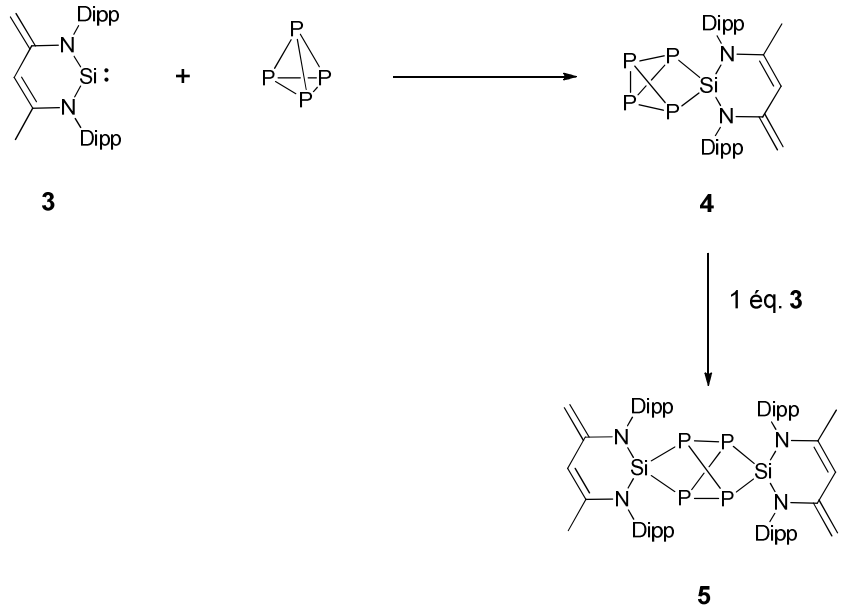

Schéma 2. Insertions successives du silylène **3** dans deux liaisons P-P de P_4.

Cette réactivité est également rencontrée dans les cas des cations phosphéniums électrophiles. L'exemple le plus marquant est la réaction du composé **6** avec P_4 en présence de $GaCl_3$. Au cours de cette réaction, le cation phosphénium **7**, qui est généré in situ par abstraction d'un chlorure, réalise également une insertion dans une liaison P-P du tétrahèdre conduisant à **8**.

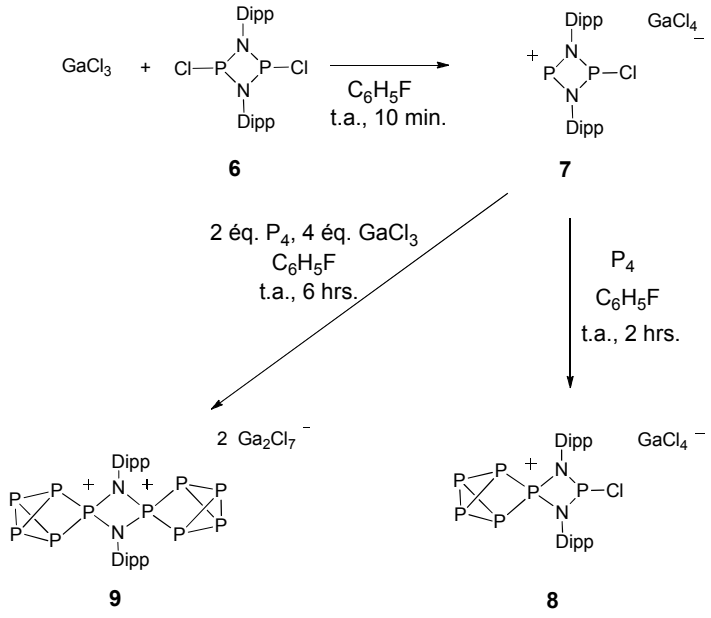

Schéma 3. Réactions d'insertion mises en jeu lors de la réaction de **6** avec P_4 en présence de $GaCl_3$.

Cependant lorsque la réaction est conduite dans des conditions plus acides en présence d'un excès de $GaCl_3$, une seconde insertion se produit après abstraction du deuxième atome de chlore restant. Cette seconde insertion implique une seconde molécule de P_4 pour conduire finallement au dication **9** (Cf Schéma 3).
Alors que ces composés isoélectroniques des carbènes réagissent avec P_4 en effectuant des insertions dans les liaisons P-P , les carbènes singulets stables plus nucléophiles régissent avec le phosphore blanc de manière différente.

1.2) Activation de P_4 par les carbènes singulets stables

1.2.1) Activation et aggrégation de P_4

Concernant l'activation du P_4 par les non-métaux, la réactivité offerte par les carbènes avec le phosphore blanc est probablement à ce jour la plus riche. En effet, en variant les paramètres électroniques et stériques du carbène l'activation, l'aggrégation ou la fragmentation de P_4 peuvent être observées.
Ainsi, lorsque le cyclic(alkyl)(amino)carbène CAAC **10** stériquement encombré de part la présence d'un groupement menthyle est mis en réaction avec P_4, le composé **11** est obtenu (Cf Schéma 4). Cet adduit comportant une fonction diphosphène est obtenu sous la forme d'un mélange de diastéréoisomères *E/Z*. Il est intéressant de noter par ailleurs que l'isomère *E* est largement majoritaire et peut être isolé par recristallisation dans l'hexane.

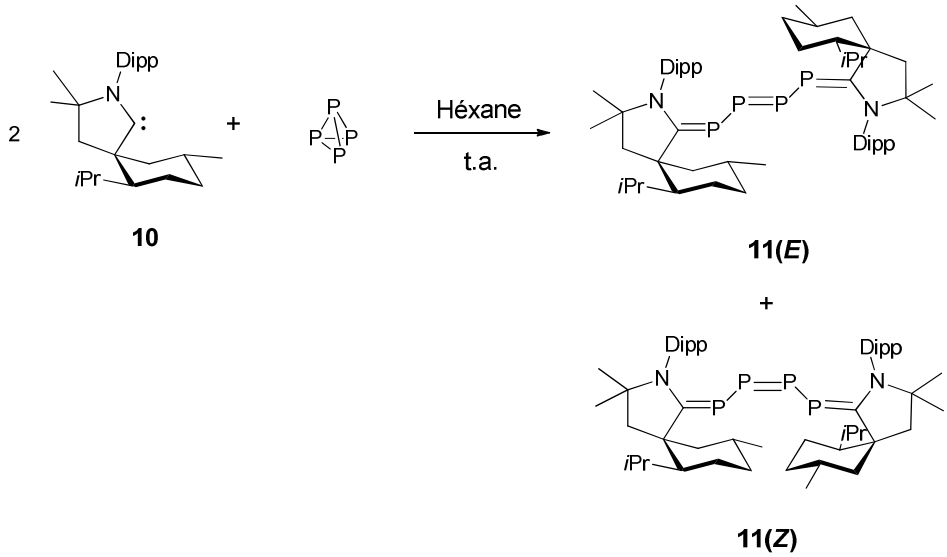

10

11(*E*)

11(*Z*)

Schéma 4. Activation de P_4 par le CAAC **10**.

De plus, quand **11(*E*)** est mis en présence d'un excès de 2,3-diméthylbutadiène dans l'hexane, le produit attendu **12** résultant de la cycloaddition [4+2] est obtenu avec une diastéréosélectivité supérieure à 95% (

Schéma 5). Cette réaction est conceptuellement importante puisque deux atomes de phosphore provenant directement de P_4 sont incorporés dans un substrat organique.

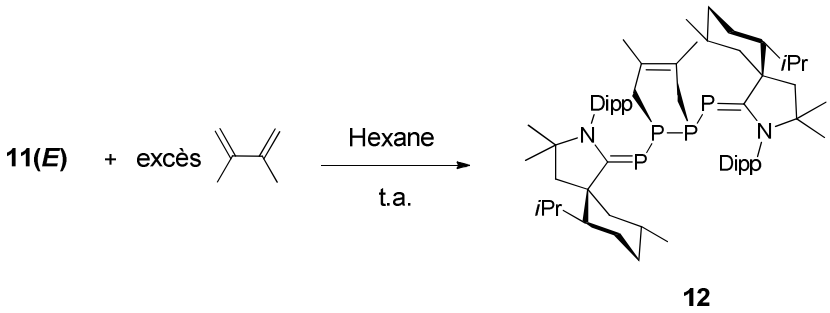

Schéma 5. Cycloaddition [4+2] mettant en jeu **11(*E*)** et le 2,3-diméthylbutadiène.

En changeant la nature du carbène et en effectuant la réaction de P_4 avec le carbène NHC **13**, un produit complétement différent est obtenu. En effet même si dans un premier temps les adduits similaires à **11(*E*)** et **11(*Z*)** sont formés, le NHC **13** induit au final l'aggrégation de P_4. En effet le cluster **14** composé d'un fragment central de 12 atomes de phosphore est isolé à la suite de cette réaction (Schéma 6).

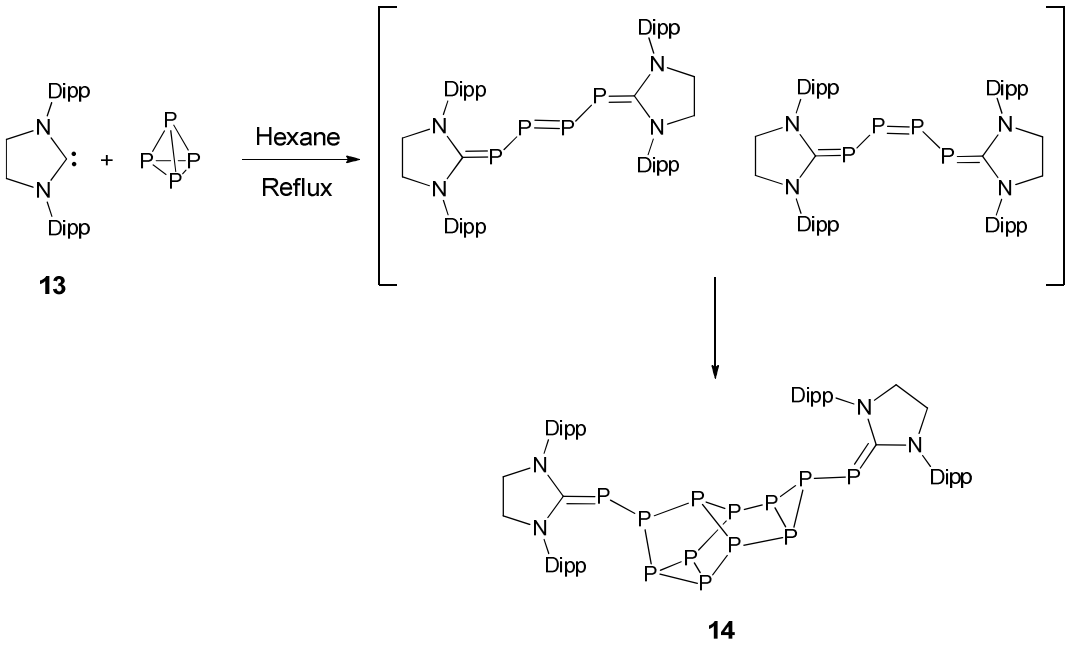

Schéma 6. Aggrégation du phosphore blanc obtenue par réaction de **13** avec P_4.

Le différence de réactivité observée avec les deux carbènes CAAC **10** et NHC **13** peut s'expliquer par les propriétés électroniques différentes de ces deux carbènes. Les CAACs qui sont π-accepteurs forment des adduits relativement forts avec les fragments phosphorés. Au contraire les NHCs sont de meilleurs groupes partant,

par conséquent au cours de la réaction, la dissociation des carbènes de l'adduit phosphoré conduit à l'aggrégation en un cluster de phosphore.
Cependant jusqu'à présent, l'influence des paramètres stériques des carbènes sur le devenir de la réaction avec P_4 n'a pas encore été étudiée. De plus il serait intéressant de voir si des carbènes seraient susceptibles d'effectuer la fragmentation de P_4 en fragments P_1 et P_3 ou en fragments P_2.

1.2.2) Fragmentation de P_4 par les carbènes

Comme les carbènes électrophiles semblent être plus aptes à réaliser la fragmentation du phosphore blanc, nous avons étudié dans un premier temps la réaction entre P_4 et le carbène acyclique **15** (Schéma 7). Cependant dans ce cas le carbène est tellement électrophile qu'il réagit avec le triphosphirène intermédiaire selon une réaction de cycloaddition [2+1] aboutissant au triphosphabicyclobutane **16**.

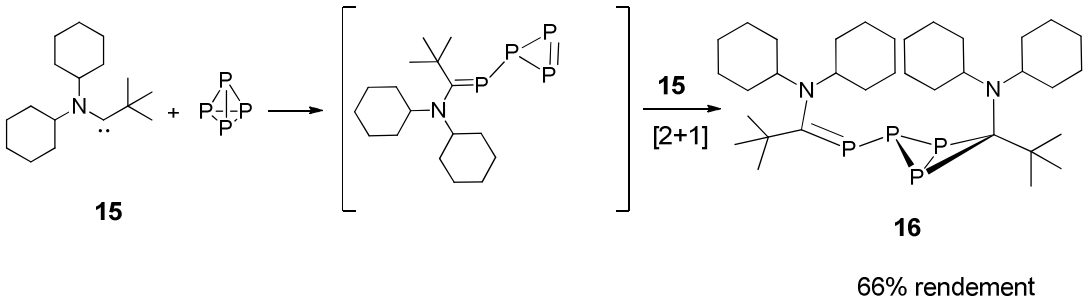

Schéma 7. Réaction de P_4 avec le carbène électrophile **15**.

Ces premiers résultats nous ont amenés à changer la nature du carbène et à étudier la réaction de P_4 avec le CAAC **17** moins électrophile que **15** mais aussi moins encombré que le CAAC **10** (Schéma 8). Dans ce cas, deux produits sont obtenus avec un rendement moyen: un adduit de P_4 avec trois carbènes **18** et le produit de fragmentation désiré **19** (Schéma 9).
L'obtention du produit **19** ne comportant que deux atomes de phosphore représente le premier exemple de fragmentation de P_4 par des molécules organiques neutres. Concernant le méchanisme de cette réaction , on peut imaginer que **19** résulte de la réaction de deux équivalents de carbène **17** avec un intermédiaire tétraphosphatriène du type **11** (*E*/*Z*). De la même manière, le composé **18** résulterait de la réaction entre deux équivalents de carbènes avec le triphosphirène initiallement formé après attaque nucléophile de **17** sur P_4.

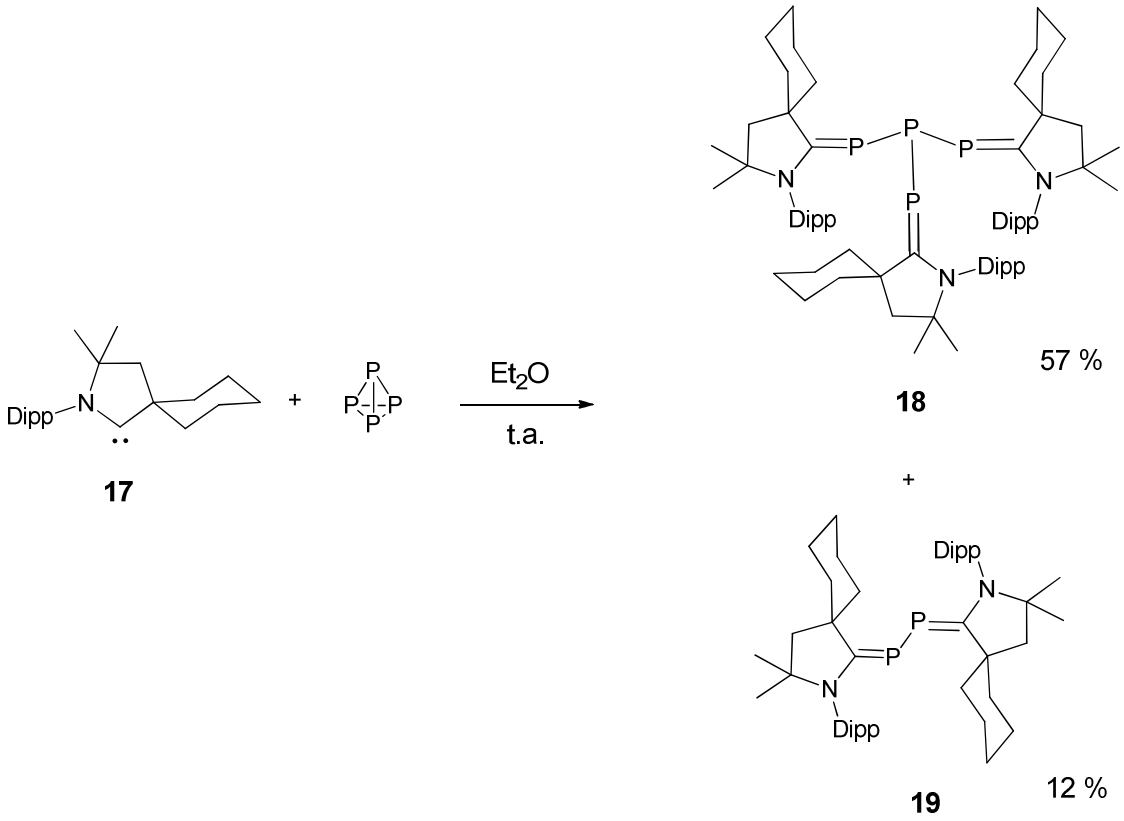

Schéma 9. Activation du phosphore blanc par le CAAC **17**.

Dans le but d'aboutir à la fragmentation de P_4 en unités P_1, la réaction de P_4 avec un carbène stable très peu encombré stériquement (le cyclopropénylidène **20**) a été étudiée (Schéma 10). Ainsi, selon une analyse RMN ^{31}P effectuée sur le brut réactionnel, la réaction de **20** avec P_4 résulte dans un premier temps en la formation d'un sel constitué du cation **21** et d'un fragment P_3^- jouant le rôle d'anion. Cependant il ne nous a pas été possible d'isoler ce sel. Nous observons dans tous les cas la disparition du fragment anionique P_3^-. Néanmoins, le composé **21**(Cl^-) a pu être obtenu par ajout de chloroforme au mélange réactionnel (Schéma 10).

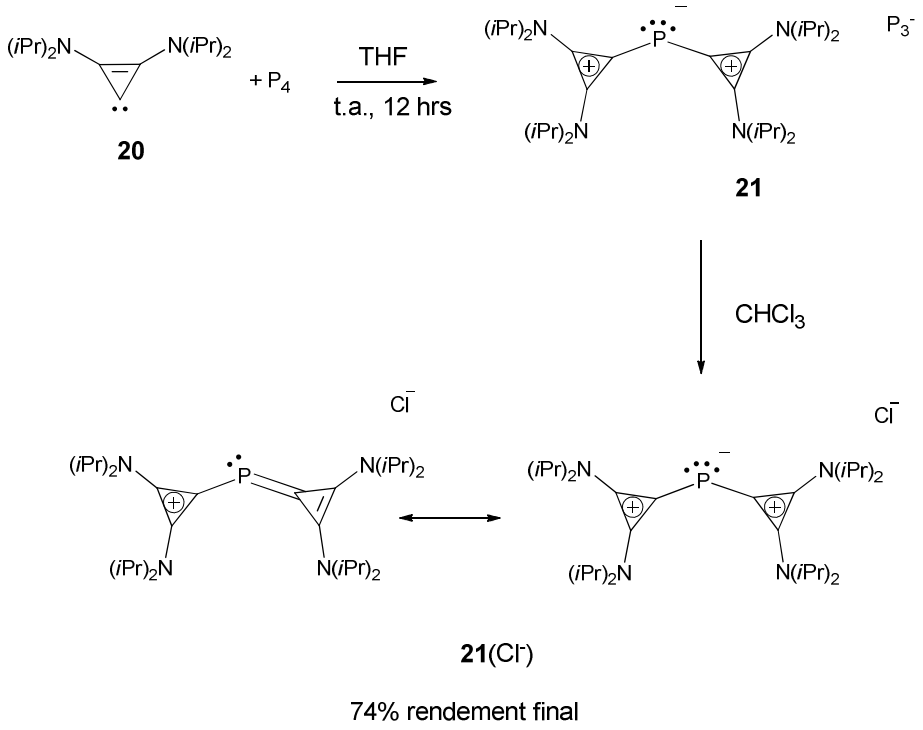

Schéma 10. Activation de P_4 par le cyclopropènylidène **20**.

Ces derniers résultats concernant la fragmentation de P_4 complètent donc l'étude de la réactivité du phosphore blanc avec les carbènes. Nous avons ainsi montré que les carbènes sont capables de réaliser l'activation, l'aggrégation ou la fragmentation de P_4 en jouant sur les paramètres électroniques et stériques des carbènes utilisés.

2) Stabilisation par les carbènes des fragments P_2, P_2-radical cation et P_2-dication

Récemment, une nouvelle application des carbènes stable est née : la stabilisation de fragments homoatomiques constitués d'éléments du groupe principal dans leur état d'oxydation zéro. Alors que sous leur forme libre ces fragments sont instables ou peuvent seulement être générés que dans des conditions particulières (par exemple vaporisation sous vide à haute température), une fois complexés par les carbènes, ils sont parfaitement stables en solution et à l'état solide. Par conséquent leur étude et leur complète caractérisation a été possible. Jusqu'à présent, les fragments concernés ont été : le carbone atomique, Si_2, P_2, P_4, P_{12} (voir premier paragraphe) et enfin As_2.

2.1) Synthèse et caractérisation d'un carbodicarbène : un carbone (0) complexé par deux carbènes

En 2008 notre groupe a rapporté la synthèse du carbodicarbène **22**, une molécule pouvant être décrite comme un complexe du carbone atomique à l'état d'oxydation zéro (Schéma 11).

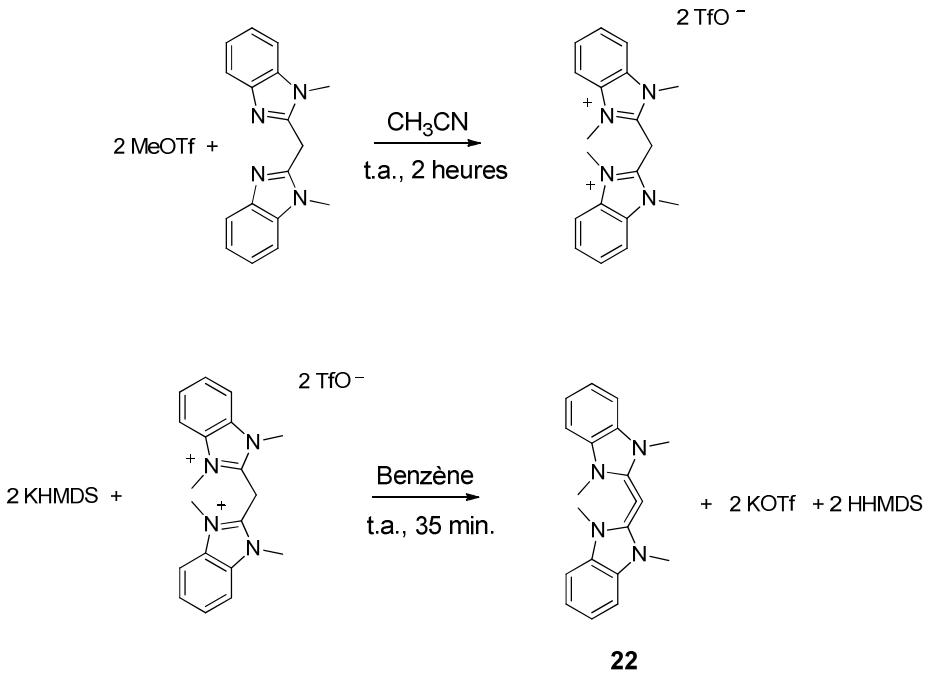

22

Schéma 11. Préparation du carbodicarbène **22**.

Des calculs théoriques réalisés par Frenking *et al.* un an avant la synthèse de **22** ont permis de mieux comprendre la structure électronique de cette molécule. En effet, selon ces calculs, les deux orbitales les plus hautes occupées (HOs) sont non liantes et sont principalement localisées sur l'atome de carbone central. La HO est principalement une orbitale de symétrie π et la HO-1 une orbitale de symétrie σ. Par conséquent ces orbitales correspondent à deux paires libres d'électrons. De plus ces calculs prédisent une structure coudée pour ce carbodicarbène ce qui a été confirmé par la structure à l'état solide de **22** déterminée par analyse de diffraction des rayons X. En conséquence, **22** peut être décrit en tant comme un atome de carbone (0) complexé par deux NHCs. Dans ce complexe les 4 électrons de valence du carbone sont répartis en deux doublets non liants (Schéma 12).

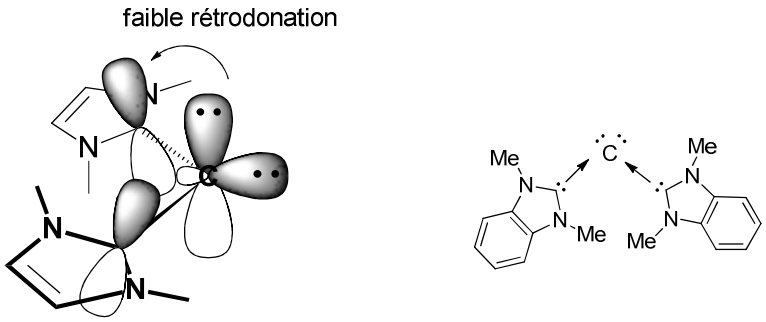

Schéma 12. Structure électronique du carbodicarbène **22**.

2.2) Synthèses et caractérisations des adduits Si_2-carbènes et P_2-carbènes

2.2.1) L'adduit Si_2-carbènes

Disilicium (Si_2) est une molécule qui a été caractérisée sous sa forme libre en matrice d'argon à 4 K. Cette molécule extrèmement instable peut être générée par vaporisation du silicium solide à très haute température suivie d'une condensation. A l'état fondamental Si_2 est dans un état triplet. Récemment Robinson *et al.* ont synthétisé l'adduit Si_2-carbènes **23** (Schéma 13) qui est stable aussi bien en solution qu'à l'état solide ce qui a permis sa caractérisation complète.

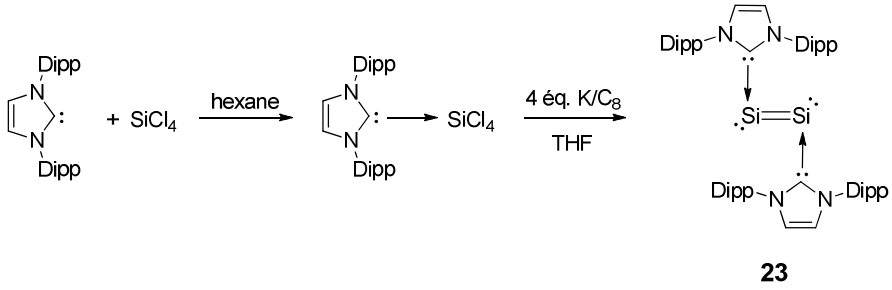

23

Schéma 13. Synthèse de l'adduit **23**.

A l'état solide, la molécule possède une géométrie « trans-bent » dans laquelle les carbènes sont liés presque orthogonalement au fragment central Si_2. La longueur de la liaison centrale Si=Si indique qu'il s'agit d'une liaison double et est également proche de la longueur de liaison Si-Si dans Si_2. Finallement des calculs DFT ont été réalisés sur le composé parent comportant des groupements phényles sur les fragments NHCs de **23**. Ces calculs montrent que les trois orbitales les plus hautes occupées sont centrées sur le fragment Si_2. L'orbitale HO correspond à l'orbitale moléculaire π de la liaison Si=Si et l'orbitale HO-1 correspond à l'orbitale moléculaire σ cette même liaison. L'orbitale HO-2 correspond à une des

orbitales non-liantes centrées sur les atomes de silicium. Cette analyse montre que **23** possède une double liaison Si=Si ainsi qu'une paire libre d'électrons sur chaque atome de silicium (Schéma 14). Aussi, cette molécule peut également être décrite comme un fragment Si_2 complexé par deux carbènes.

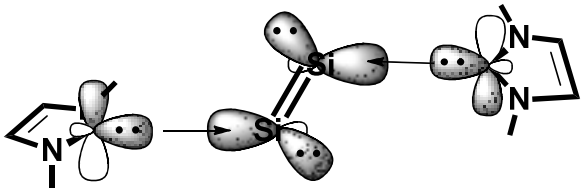

Schéma 14. Structure électronique pour le composé **23**.

2.2.2) L'adduit P_2-carbènes

Le diphosphore (P_2) est, à l'inverse du diazote, une molécule extrèmement réactive. Ce composé peut être formé en phase gazeuse par thermolyse du phosphore blanc dans des conditions extrèmes (chauffage au-delà de 1100 K). Cependant, de la même manière que Si_2, une fois la molécule de P_2 complexée par des carbènes, les adduits obtenus sont très stables à la fois à l'état solide et en solution.
Ainsi, Robinson *et al.* rapporta en 2008 la synthèse des adduits P_2-carbène **24a** et **24b**. Ces composés ont été préparés suivant une stratégie similaire à **23** (Schéma 15).

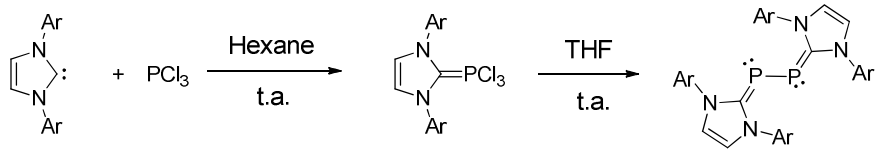

24a,b

24a: Ar = 2,6-*i*$Pr_2C_6H_3$
24b: Ar = 2,4,6-$Me_3C_6H_2$

Schéma 15. Préparation des adduits P_2-NHCs **24a** et **24b**.

Ces adduits sont analogues au composé **19** décrit dans le premier paragraphe et obtenu directement à partir de P_4. Du fait de la donation de la paire libre de chaque atome d'azote dans les orbitales $\pi^*_{C=P}$ des phosphaalcènes, les atomes de phosphore sont enrichis électroniquement. En conséquence, les atomes de phosphore de ces composés résonnent à un champ relativement fort en comparaison avec les phosphaalcènes classiques. Cependant, un déplacement chimique plus élevé est observé pour le composé **19** portant des ligands CAACs reflétant déjà le caractère plus électrophile de ces carbènes par rapport aux NHCs.

De manière générale, les composés **19**, **24a** et **24b** qui ont tous été caractérisés à l'état solide, possèdent une liaison P-P simple. L'adduit **24a** comportant des ligands NHCs stériquement encombrés (avec les groupements Dipp sur les atomes d'azote) possède une géométrie « trans bent » alors que les composés **19** et **24b** adoptent une conformation gauche à l'état solide. De plus, pour tous ces dérivés, les liaisons C=P sont relativement longues avec des longueurs de liaison similaires à celles habituellement rencontrées dans le cas des phosphaalcènes inversement polarisés. Les paramètres géométriques ainsi que les déplacements chimiques observés en RMN du phosphore sont résumés dans le tableau 1.

Composé:	**19**	**24a**	**24b**
Déplacement chimique $^{31}P\{^{1}H\}$:	+59.4 ppm	-52.4 ppm	-73.6 ppm
Longueur de liaison P-P:	2.18 Å	2.21 Å	2.19 Å
Angle de torsion C-P-P-C:	149.2°	180°	134.1°
Angle C-P-P (moyenne):	104.9°	103.2°	102.8°
Longueur de liaison P=C (moyenne):	1.73 Å	1.75 Å	1.75 Å

Table 1. Paramètres géométriques importants et déplacements chimiques observés en RMN du phosphore pour les adduits **19**, **24a** et **24b**.

La simulation des orbitales moléculaires localisées pour le composé parent analogue à **24a** (mais possédant des atomes d'hydrogène à la place des substituents Dipp) montre que dans cet adduit, chaque atome de phosphore possède deux paires libres d'électrons. Ces paires libres correspondent à deux orbitales moléculaires localisées esentiellement sur chaque atome de phosphore, une de symétrie σ et l'autre de symétrie π. Cette dernière subit également une rétro-donation dans les orbitales 2p vacantes des carbènes. Ainsi tous ces composés peuvent être également décrits par la forme de résonance B et même par la forme C consistant à un fragment bis-phosphinidène stabilisé par les ligands carbéniques (Schéma **16**).

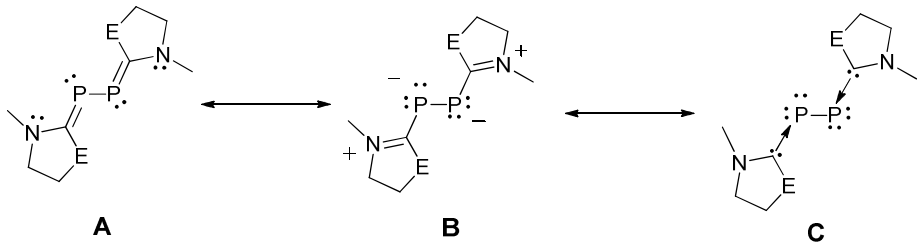

Schéma 16. Trois formes de résonnance extrèmes pour les aduits P_2-carbènes.

C'est pourquoi dans le cas du composé **19** comportant les carbènes CAACs plus électrophiles, cette rétro-donation est plus importante et résulte à une diminution de la densité électronique présente sur le fragment P_2. En conséquence, le déplacement chimique observé pour le composé **19** est nettement supérieur à ceux observés pour **24a** et **24b**. De même les liaisons C=P sont plus courtes dans le composé **19** que dans les adduits **24a** et **24b**.

2.2.3) Stabilisation par les carbènes des fragments $P_2^{+\cdot}$ et P_2^{2+}

La différence de propriétés électroniques entre les adduits **19** et **24a** a pu être mise en évidence par les voltamogrammes cycliques de ces composés (Figure 1).

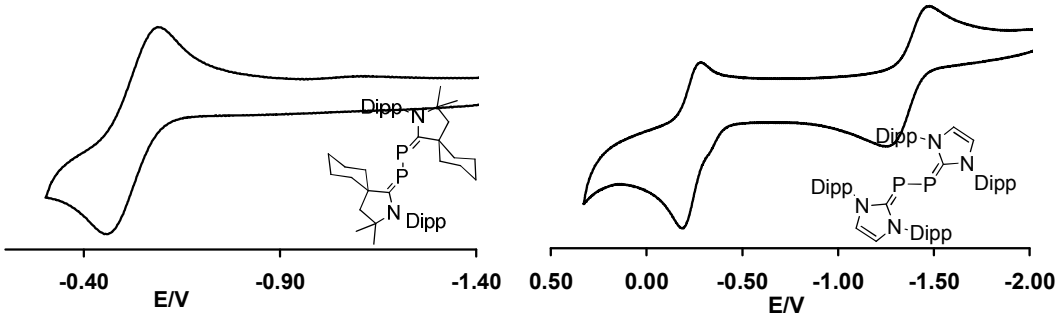

Figure 1. Voltamogrammes cycliques des composés **19** (gauche) et **24a** (droite) en solution dans le THF.

Alors que dans le cas de **19** seulement une oxydation réversible est observée, pour le composé **24a** deux oxydations réversibles sont possibles. De plus la première oxydation apparait à un potentiel bien plus bas que dans le cas de **19** (**24a** : $E_{1/2}$ = -1.408 V, **19** : $E_{1/2}$ = -0.536 V versus Fc^+/Fc). Ainsi ces résultats préliminaires nous ont conduits à réaliser la synthèse chimique des produits d'oxydation correspondant. Les radicaux cations $\mathbf{19}^{+\cdot}$ et $\mathbf{24a}^{+\cdot}$ issus respectivement de **19** et **24a** ont été préparés en utilisant $Ph_3C^+B(C_6F_5)_4^-$ en tant qu'agent oxydant. Ces composés paramagnétiques ont été caractérisés par R.P.E. (Figure 2).

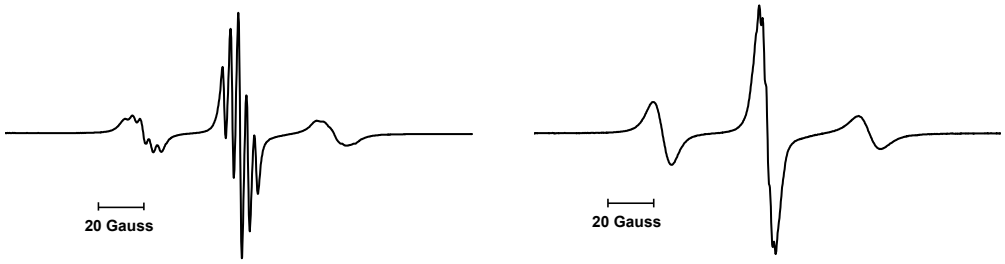

Figure 2. Spectres R.P.E. de $\mathbf{19}^{+\cdot}$ (gauche) et $\mathbf{24a}^{+\cdot}$ (droite) en solution dans le fluorobenzène enregistrés à température ambiante.

Dans les deux cas on peut observer un large couplage hyperfin avec les deux atomes de phosphore équivalents résultant en un triplet dans chaque spectre ($\mathbf{19}^{+\cdot}$: g = 2.009, a(^{31}P) = 42 G ; $\mathbf{24a}^{+\cdot}$: g = 2.008, a(^{31}P) = 44 G). De plus, dans le cas de $\mathbf{19}^{+\cdot}$, on peut également observer un couplage hyperfin supplémentaire avec deux atomes d'azote équivalents ($\mathbf{19}^{+\cdot}$: a(^{14}N) = 3 G). Afin de déterminer plus en détail la densité de spin présente dans chaque cas sur le fragment P_2 central, les spectres R.P.E. ont été enregistrés à 100 K pour les deux radicaux (figure 3).

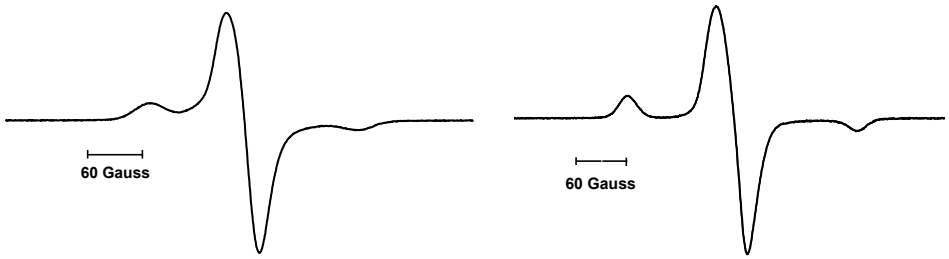

Figure 3. Spectres R.P.E. de $\mathbf{19}^{+\cdot}$ (gauche) et $\mathbf{24a}^{+\cdot}$ (droite) en solution congelée dans le fluorobenzène enregistrés à 100 K.

Après analyse de ces spectres, il a été conclu que pour $\mathbf{19}^{+\cdot}$ environ 58% de densité de spin est localisée sur le fragment central alors que dans le cas de $\mathbf{20a}^{+\cdot}$ la densité de spin sur les deux atomes de phosphore s'élève à 72%. Ces résultats reflètent encore une fois la différence de pouvoir π-accepteur entre les CAACs et les NHCs : en effet dans le cas de $\mathbf{19}^{+\cdot}$ l'électron célibataire est plus fortement délocalisé dans les orbitales 2p vacantes des carbènes que dans le cas de $\mathbf{24a}^{+\cdot}$. De plus, les radicaux ont également été caratérisés à l'état solide. Cette analyse montre que la liaison P-P des produits oxydés est plus courte que dans les composés neutres ($\mathbf{19}^{+\cdot}$: 2.094 Å, $\mathbf{24a}^{+\cdot}$: 2.091 Å). Au contraire, les liaisons P=C sont plus longues dans les radicaux que dans les produits de départ ($\mathbf{19}^{+\cdot}$: 1.777 Å pour chaque liaison P=C, $\mathbf{24a}^{+\cdot}$: 1.795 Å et 1.810 Å).

2.2.4) Synthèse et caractérisation de l'adduit P_2^{2+}-NHCs

Nous avons ensuite préparé le produit résultant de la double oxydation de **24a** en utilisant deux équivalents de triflate de ferrocénium ($[FeCp_2]^+TfO^-$). Le dication obtenu $\mathbf{24a}^{2+}$ est diamagnétique et par conséquent peut être caractérisé par RMN. Les atomes de phosphore de $\mathbf{24a}^{2+}$ résonnent à +452 ppm dans la région typique des diphosphènes. Par conséquent le composé $\mathbf{24a}^{2+}$ peut être décrit comme un diphosphène substitué par des groupements imidazoliums (Schéma 17).

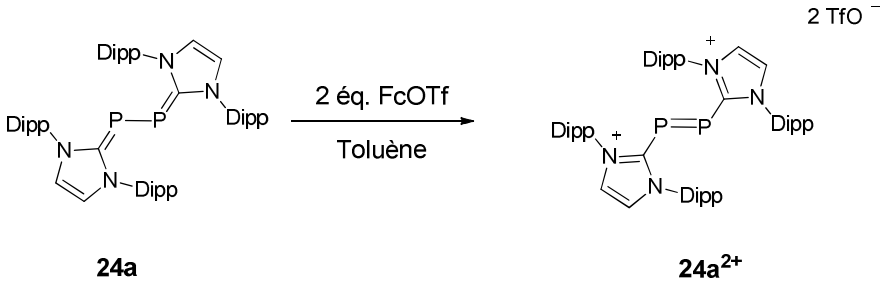

Schéma 17. Préparation du composé $\mathbf{24a}^{2+}$.

La structure du dication $\mathbf{24a}^{2+}$ a été également confirmée par analyse de diffraction des rayons. A l'état solide on observe un très léger raccourcissement de la liaison P-P par rapport à $\mathbf{24a}^{+\cdot}$ ($\mathbf{24}^{2+}$: 2.083 Å) et une légère élongation des liaisons P=C (1.840 Å pour chaque liaison P=C).
Tous ces résultats ont pu être interprétés grâce à des calculs DFT réalisés par le groupe de Frenking. Ces calculs révèlent que dans les composés **19** et **24a**, le fragment P_2 complexé est à l'état excité $^1\Gamma$ resultant de la promotion de deux électrons d'une orbitale π dans une orbitale antiliante π^*. Pour cette raison, dans les composés neutres, la longueur de la liaison P-P mesurée est en accord avec un indice de liaison de 1. De plus cette orbitale π^* doublement occupée qui est la HO des composés **19a** et **24a** subit une rétrodonation dans les orbitales 2p vacantes des carbènes (Figure 4)

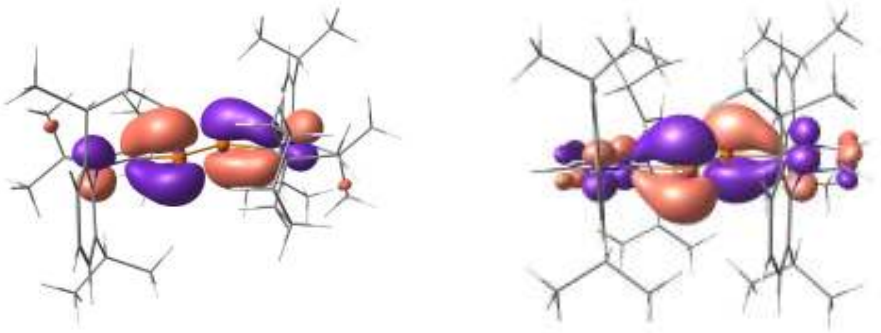

Figure 4. Orbitale moléculaire la plus haute occupée (HO) pour les composés **19** (gauche) et **24a** (droite).

Lorsqu'un électron est retiré par oxydation, ces orbitales HO dans **19** et **24a** deviennent les orbitales SO dans $\mathbf{19}^{+\cdot}$ et $\mathbf{24a}^{+\cdot}$. De plus, durant cette oxydation, le nombre d'électrons dans l'orbitale moléculaire antiliante est diminué. Par conséquent, l'indice de la liaison P=P augmente, ce qui se traduit expérimentallement par un raccourcissement de la liai
son P-P mais aussi par une élongation des liaisons P=C dans les radicaux (Figure 5).

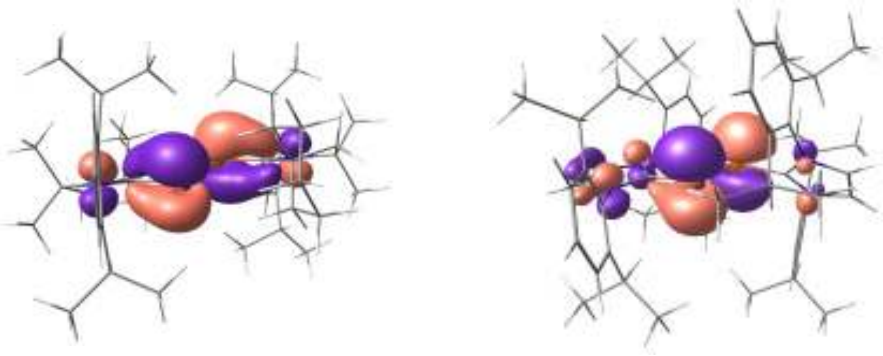

Figure 5. Orbitale moléculaire simplement occupée (SO) pour les composés $\mathbf{19}^{+\cdot}$ (gauche) et $\mathbf{24a}^{+\cdot}$ (droite).

Enfin lors de la seconde oxydation de **24a**, l'orbitale HO devient alors l'orbitale la plus basse vacante (BV) dans $\mathbf{24a}^{2+}$. En conséquence, l'absence d'électrons dans l'orbitale antiliante résulte en un indice de la liaison P=P de 2. Le produit de double oxydation peut donc être décrit comme un diphosphène substitué par des groupement imidazoliums liés au fragment central via des liaisons P-C simples (Figure 6).

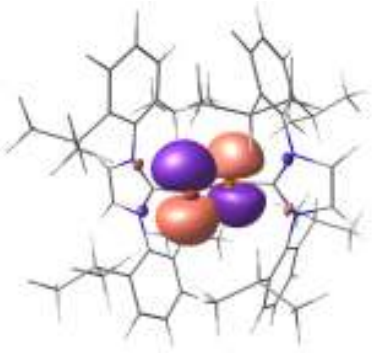

Figure 6. Orbitale moléculaire la plus basse vacante (BV) pour le dication $\mathbf{24a}^{2+}$.

En conclusion, nous avons montré dans ce paragraphe que les carbènes s'avéraient également efficaces pour la stabilisation d'entités paramagnétiques ou électrodéficientes. Nous allons dans un troisième paragraphe montrer que ce concept peut être également appliqué à la stabilisation de radicaux phosphinyles.

3) Stabilisation par les carbènes des radicaux phosphinyles

Les radicaux phosphinyles sont des composés paramagnétiques comportant un atome de phosphore divalent. Dans ces radicaux, l'électron célibataire réside principalement dans une orbitale 3p du phosphore (Schéma 18).

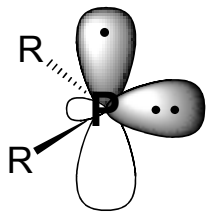

Schéma 18. Structure électronique des radicaux phosphinyles.

La première obervation spectroscopique d'un tel radical ($Ph_2P^{\bullet}$) date de 1966. Depuis, plusieurs exemples de radicaux phosphinyles persistents ou même stables à température ambiante ont été rapportés. De manière générale, deux stratégies ont été utilisées pour la stabilisation de ces espèces particulièrement réactives. La stabilisation cinétique qui consiste à protéger stériquement l'atome de phosphore à l'aide de substituants volumineux a permis la synthèse et la caractérisation de radicaux phosphinyles dont la durée de vie en solution excède 1 an. Enfin la stabilisation themodynamique consistant à utiliser des substituants capables de délocaliser la densité de spin de l'atome de phosphore a permis la préparation d'un radical phosphinyle stable, à la fois en solution et à l'état solide.

3.1) Utilisation de substituents flexibles et stériquement encombrés pour la stabilisation des radicaux phosphinyles

Les premiers travaux importants concernant la préparation de radicaux phosphinyles stables ont été effectués par le groupe de Power en 1976. Il a été montré que la réduction photochimique de la chlorophosphine **25** en présence d'un alcène électroniquement riche permettait de générer le radical **26** (Schéma 19).

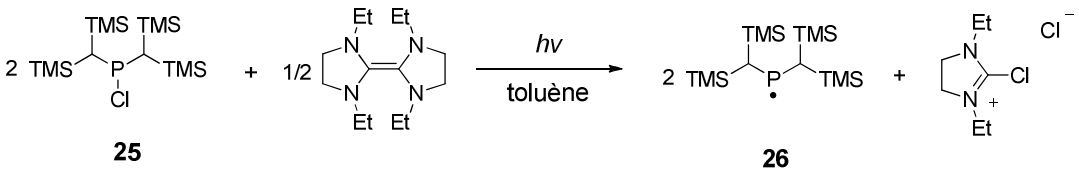

Schéma 19. Préparation du radical phosphinyle **26**.

En solution **26** possède une durée de demie-vie supérieure à une année. Le spectre RPE de **26** à température ambiante en solution consiste en un doublet de triplet (g = 2.009) dû au couplage hyperfin avec l'atome de phosphore (a(^{31}P) = 96.3 G) et aussi avec les deux protons équivalents appartenant au méthines des substituents du phosphore (a(^{1}H) = 6.4 G). Le spectre RPE à basse température en solution congelée a également été enregistré. Il en a été déduit que la densité de spin est principalement localisée dans une orbitale 3p de l'atome de phosphore confirmant le caractère phosphinyle du radical **26**. Cependant à l'état solide **26** dimérise pour donner la diphosphine correspondante **27** (Schéma 20).

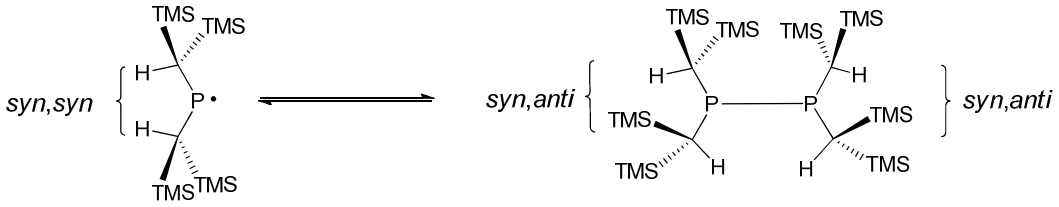

26 **27**

Schéma 20. Dimérisation réversible du radical **26**.

Cette dimérisation est néanmoins réversible et lorsque le composé **27** est redissout dans un solvant, sublimé ou fondu, le radical est regénéré.

Pour expliquer cette dimérisation réversible, il est nécessaire de regarder attentivement la conformation des groupements alkyles présent sur les atomes de phosphore dans le radical et dans le dimer. La structure de **26** a été déterminée en phase gazeuse par diffraction électronique. En phase gazeuse, le radical adopte une géométrie en V avec les substituants alkyles se trouvant dans une conformation *syn,syn* (Schéma 20). Dans cette conformation les atomes d'hydrogène des méthines de chaque substituent pointent vers le milieu de la structure en V. La géométrie de **26** optimisée par des calculs DFT est en accord avec la structure déterminée expérimentallement. La structure du dimer **27** a quant à elle été déterminée par diffraction des rayons X réalisée sur un monocristal. Danc ce cristal, la maille élémentaire ne contient qu'une seule molécule indépendante. Cependant dans le dimer, les substituents alkyles présents sur chaque atome de phosphore adoptent une conformation différente que dans le radical **26** (Schéma 20). En effet afin d'assurer un meilleur emboitement de chaque fragment lors de la dimérisation, les substituents sur chaque atome de phosphore adoptent une conformation *syn,anti*. Cette conformation en revanche entraine d'importantes tensions au sein de la molécule. Ces tensions sont dues principalement aux répulsions stériques entre chaque moitié du dimer (Schéma 21, intéractions **S1**) mais aussi à celles qui apparaissent entre les groupements TMS appartenant aux substituents d'un même atome de phosphore (Schéma 21, intéractions **S2** et **S3**).

En conséquence à l'état solide de nombreuses distortions géométriques sont apparentes dans la structure de **27**. En effet cette molécule possède des liaisons P-

C rallongées et met en jeu d'importantes variations pour les valeurs des angles autours des atomes de carbone des méthines au sein de la molécule.

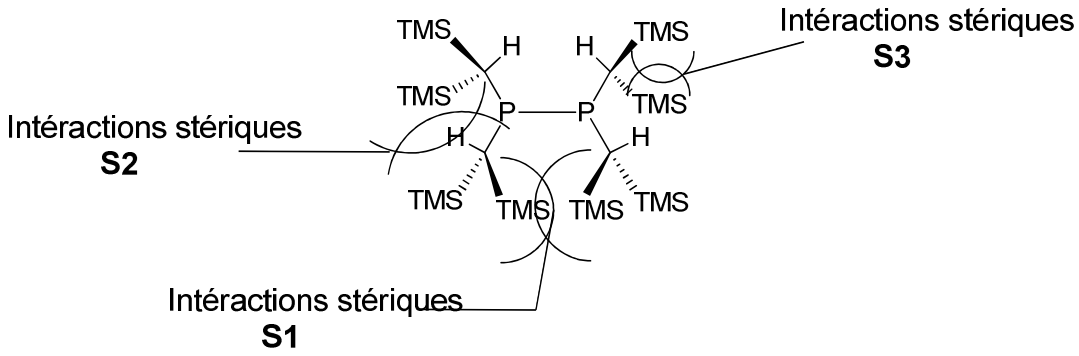

Schéma 21. Intéractions stériques apparaissant lors de la dimérisation du radical **26**.

Une étude théorique a permis alors de déterminer les énergies mises en jeu dans chaque étape de la dissociation du dimer conduisant aux radicaux **26** (Schéma 22).
Bien que la dissociation homolytique de la liaison P-P annule les répulsions stériques **S1** cette étape est endothermique de 96 kJ.mol^{-1}.

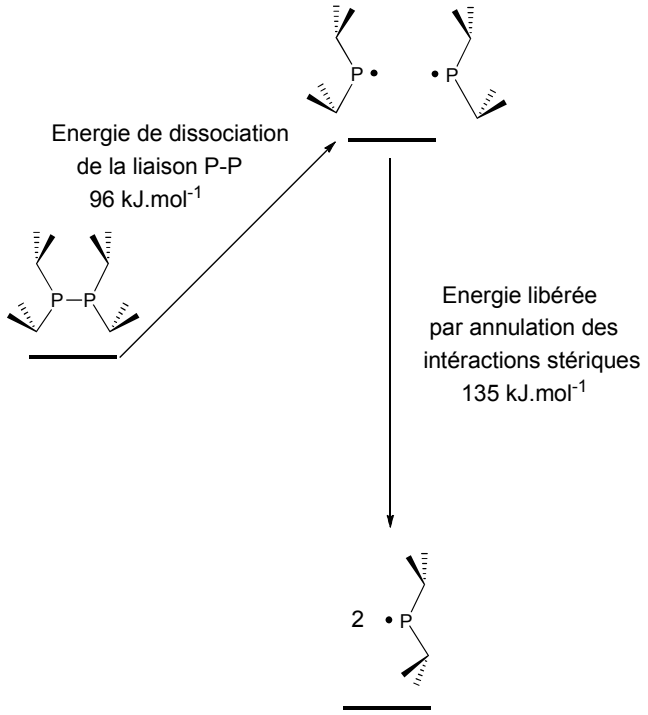

Schéma 22. Energies mises en jeu lors de la dissociation de la diphosphine **27** en radical **26**.

Cependant la relaxation des substituents alkyles au sein de chaque fragment obtenu et l'isomérisation permettant de passer de la conformtion *syn*,*anti* à la conformation *syn*,*syn* annulent les intéractions stériques **S2** et **S3**. Ce procédé est exothermique d'environ 135 kJ.mol^{-1} par dimer ce qui rend au final la dissociation thermodynamiquement favorable. Ainsi dans le radical **26**, du fait de leur flexibilité les substituents alkyles se comportent comme des ressorts. Durant la dimérisation ils accumulent suffisamment d'énergie potentielle permettant de compenser le cout énergétique nécessaire pour rompre la liaison P-P.
Cette analyse illustre clairement la tendance qu'ont ces espèces à dimériser à l'état solide. Cette tendance est si importante que l'énergie accumulée due aux intéractions stériques est supérieure à l'énergie de dissociation de la liaison P-P. Par consequent, la stabilisation cinétique n'apparait pas à première vue comme la stratégie idéale pour la préparation d'un radical phosphinyle monomérique à l'état solide. C'est pourquoi le premier exemple d'un tel radical a été possible grâce à la stabilisation thermodynamique apportée par la présence de métaux de transition dans la molécule.

3.2) Utilisation de métalloligands pour la stabilisation des radicaux phosphinyles

En 2007, le groupe de Cummins a rapporté la préparation et la caractérisation complète d'un radical phosphinyle neutre monomérique à l'état solide. Ce composé a pu être préparé par réduction de la chlorophosphine **28** en utilisant 1 équivalent de K/C_8 (Schéma 23).

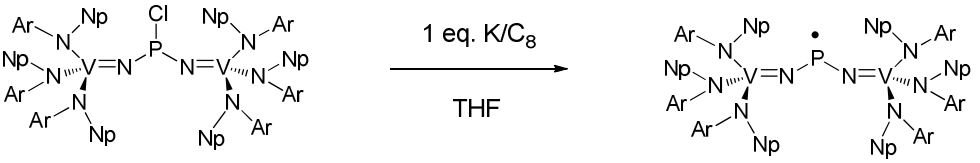

28 **29**

Schéma 23. Synthèse du radical **29**.

Le spectre RPE de **29** mesuré en solution à température ambiante consiste en un signal compliqué dû au couplage hyperfin avec l'atome de phosphore (a(^{31}P) = 42.5 G) et aussi avec les deux atomes de vanadium équivalents (a(^{51}V) = 23.8 G). La constante de couplage avec le phosphore observée pour **29** est relativement faible en comparaison avec les constantes habituellement mesurées pour les radicaux phosphinyles persistents décrits auparavant (63 G-100 G). Il en est de même pour la constante de couplage avec le vanadium qui est relativement faible par rapport aux valeurs mesurées pour $[V(NMe_2)_4]^{\cdot}$ (65 G) ou $[V(NEt_2)_4]^{\cdot}$ (66 G).

Ces valeurs signifient que la densité de spin est répartie sur ces trois atomes reflètant alors une importante délocalisation de l'électron célibataire (Schéma 24).

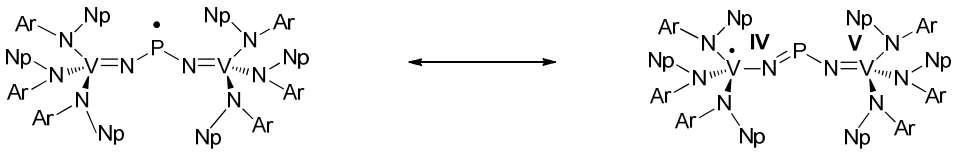

29

Ar = 3,5-$Me_2C_6H_3$
Np = Néopentyle

Schéma 24. Deux structures de résonance possibles pour le radical **29**.

Cette importante délocalisation a été également confirmée par la calcul de l'orbitale moléculaire simplement occupée de **29**. Selon ces calculs effectués pour le modèle simplifié (comportant les substituents phényles et méthyles sur les atomes d'azote) la densité de spin est localisée dans l'orbitale $3p_y$ du phosphore (31.30%) et aussi dans les orbitales $3d_{xy}$ et $3d_{x^2-y^2}$ de chaque vanadium (au total 39.49% et 8.33% respectivement sur les atomes de vanadium).
Du fait de cette délocalisation, le caractère phosphinyle pour le composé **29** est grandement diminué comme en témoigne l'étude de la réactivité de **29**. En effet, ce dernier ne réagit pas avec P_4, ou avec les donneurs d'atomes d'hydrogène $n$$Bu_3SnH$, $n$$Bu_2SnH_2$ et $[(\eta^5\text{-}C_5H_5)(CO)_3MoH]$.
En conlusion on peut dire que l'utilisation de métalloligands a permis d'isoler le premier exemple d'un radical phosphinyle stable même à l'état solide. Cependant la stabilisation apportée par les métaux est si importante que la nature du composé **29** peut être remise en question. En effet on peut également décrire **29** en tant qu'un complexe de valence mixte V^{IV}/V^{V} compprtant un pont NPN (Schéma 24).

3.3) Génération de radicaux phosphinyles hautement persistents par oxydation de phosphaalcènes inversement polarisés

Dans les exemples précédents, les radicaux phosphinyles ont été générés par la réduction à un électron des chlorophosphines correspondantes. Cependant certains phosphaalcènes s'avèrent être des precurseurs idéaux pour la préparation de radicaux ioniques.
En effet, le groupe de Geoffroy a montré que l'oxydation des phosphaalcènes neutres **31** et **32** comportant un atome de phosphore électroniquement riche permet de générer les radicaux cations correspondant (Schéma 25).
Ces radicaux générés ont une durée de vie très longue permettant alors leur caractérisation en solution par RPE.

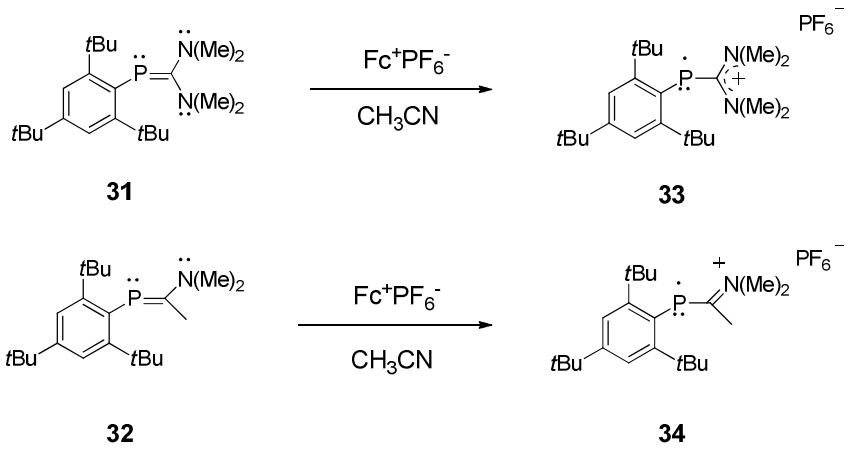

Schéma 25. Préparation des radicaux phosphinyles **33** et **34** par oxydation de phosphaalcènes neutres.

Les spectres RPE enregitrés en solution à tempérrture ambiante consistent pour chaque radical en un large doublet dû au couplage hyperfin avec le noyau de l'atome de phosphore (**33** : a(^{31}P) = 105 G, **34**: a(^{31}P) = 103 G). Ces valeurs de constante de couplage sont comparables aux valeurs habituellement observées pour des radicaux phosphinyles persistents. De plus les mesures RPE effectuées à basse température en solution congelée montrent clairement que dans les deux cas, la densité de spin est principalement localisée dans une orbitale 3p de l'atome de phosphore (75% dans les deux cas) confirmant ainsi la nature de ces radicaux.
Par conséquent ces derniers résultats nous ont inspirés par la suite pour la synthèse de radicaux cation qui seraient obtenus par oxydation d'adduits carbène-phosphinidène. En effet comme on l'a vu dans le paragraphe précédent, les carbènes singulets stables semblent être efficaces pour la stabilisation d'entités paramagnétiques.

3.4) Stabilisation par les carbènes d'un radical cation phosphinyle

3.4.1) Etude préliminaire

Afin de tester notre hypothèse, l'oxydation de l'adduit carbène-phosphinidène **35** qui est également un phosphaalcène inversement polarisé a été conduite afin d'identifier le produit d'oxydation. Le composé **35** est préparé en une seule étape à partir du carbène libre selon une procédure déjà décrite dans la littérature (Schéma 26).

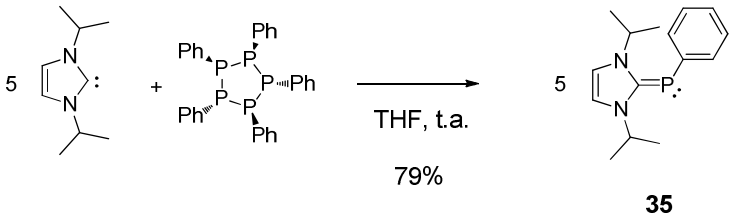

Schéma 26. Préparation de l'adduit carbène-phosphinidène **35**.

L'oxydation a été réalisée en utilisant le triflate de ferrocénium ($[FeCp_2]^+TfO^-$) en tant qu'agent oxydant. Après réaction le dimer **36** est obtenu sous la forme d'une poudre blanche avec un rendement moyen (30 %) et consiste en une mixture de diastéréoisomères *méso*/*rac* (Schéma 27).

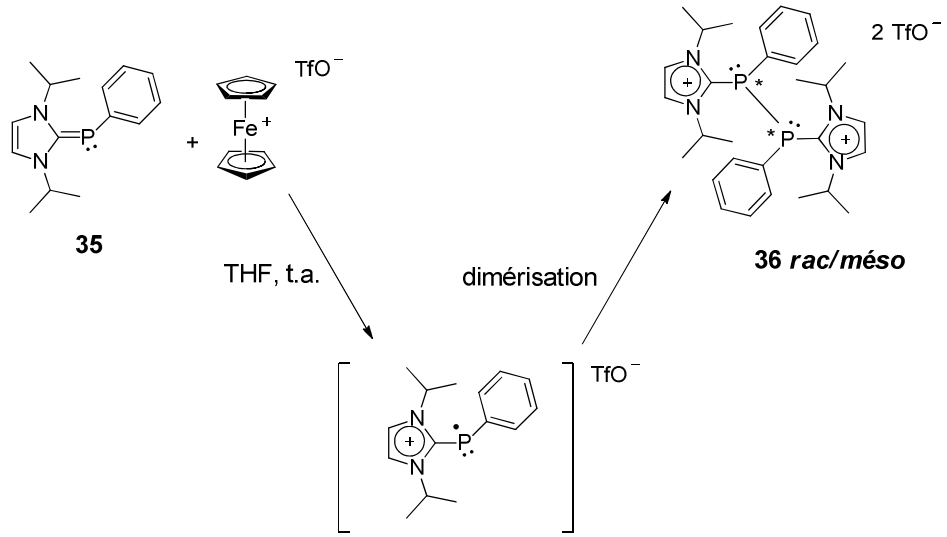

Schéma 27. Oxydation à un électron du phosphaalcène **35**.

La formation de **36** résulte probablement de la dimérisation du radical cation intermédiaire formé par l'oxydation à un électron de **35**. Ce résultat suggère que le radical peut effectivement être généré à partir de l'adduit carbène-phosphinidène **35**. De plus, nous avons vu dans le second paragraphe que les CAACs semblent être plus efficaces que les NHCs pour délocaliser la densité de spin de l'atome de phosphore résultant alors à une meilleure stabilisation du radical cation. Pour cette raison on a décidé dans un premier temps de préparer l'adduit **37** comportant le substituent menthyle sur le carbène offrant également une protection stérique importante (Schéma 28).

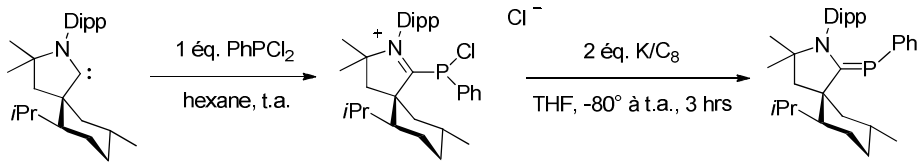

37

42 % rendement
sur les deux étapes

Schéma 28. Préparation de l'adduit carbène-phosphinidène **37**.

La voltampérométrie cyclique de **37** montre que ce composé subit une oxydation quasi réversible à un potentiel relativement élevé ($E_{1/2}$ = + 0.094 V vs Fc^+/Fc). Du fait de la valeur élevée de ce potentiel, les tentatives de générer le radical cation correspondant se sont soldées par un échec. En effet, les agents oxidant suffisamment puissants capables d'oxyder **37** sont souvent présents sous la forme de sels comportant des anions non anodins (PF_6^-, $SbCl_6^-$) qui réagissent avec le radical cation généré. Par exemple, lorsque l'oxydation de **37** est réalisée en utilisant $[N(C_6H_4Br\text{-}4)_3]^+SbCl_6^-$ commercialement disponible, la RMN du phosphore du brut réactionnel montre que la chlorophosphine précurseur de **37** est formée (Schéma 28). Cette chlorophosphine résulte probablement de l'abstraction d'un atome de chlore du contre anion $SbCl_6^-$ appartenant au radical intermédiaire. A la lueure de ces résultats nous avons décidé de préparer des adduits carbène-phosphinidènes analogues à **37** comportant toujours un carbène CAAC mais un fragment phosphinidène légèrement modifié afin de diminuer le potentiel d'oxydation de l'adduit.

3.4.2) Préparation d'adduits carbène-phosphinidènes possèdant des potentiels d'oxydation réduits

Dans ce but nous avons incorporé un groupement amino judicieusement placé dans l'adduit CAAC-phosphinidène capable de stabiliser l'atome de phosphore électro-déficient dans le radical cation généré. Dans un premier temps l'adduit **38** comportant un groupement 8-diméthylaminonaphtalène a été préparé (Schéma 29). En raison de la proximité du groupement diméthylamino par rapport à l'atome de phosphore, la stabilisation s'effectuerait dans ce cas directement par σ-donation de la paire d'électrons de l'atome d'azote à l'atome de phosphore. En effet, la voltampérométrie cyclique révèle que **38** subit une oxidation à un potentiel bien plus bas que **37** (**38** : E_o = - 300 mV vs Fc^+/Fc) en accord avec l'effet du substituant diméthylamino souhaité. Malheureusement cette oxydation est irréversible indiquant probablement que le radical cation correspondant n'est pas stable. Cependant nous avons tout de même décidé d'entreprendre l'oxydation chimique de **38**.

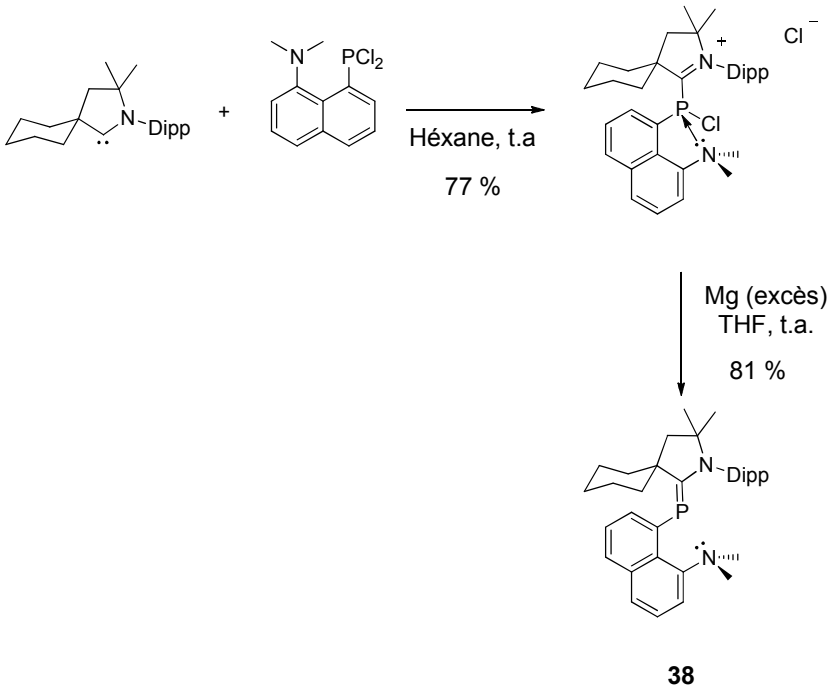

Schéma 29. Préparation du composé **38**

L'oxydation a été conduite en utilisant $Ph_3C^+B(C_6F_5)_4^-$ en tant qu'agent oxydant. Après réaction, l'analyse RMN du produit obtenu indique que l'oxydation résulte en une mixture équimolaire des produits **39** et **40** (Schéma 30). La structure du composé **39** a été également confirmée par analyse de diffraction des rayons X effectuée sur un monocristal de **39**.

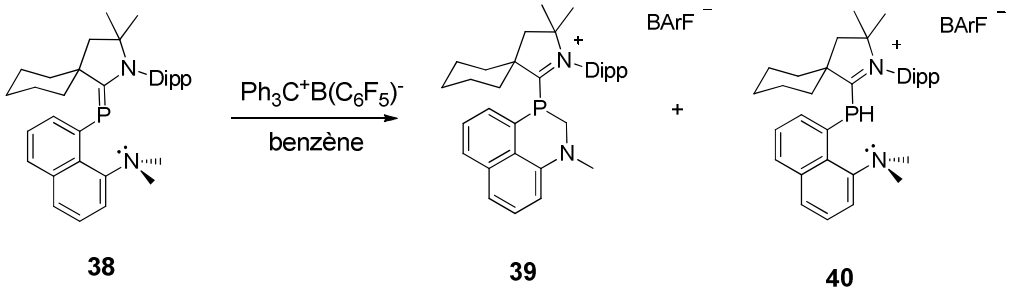

Schéma 30. Oxydation du phosphaalcène **38**

Les produits de cette réaction résultent probablement d'un transfert de H· provenant d'un substituent méthyle du groupement diméthylamino dans le radical cation formé suivi d'un réarrangement intermoléculaire donnant au final un mélange 1 :1 des composés **39** et **40**. Afin d'éviter ce réarrangement nous avons alors préparé le composé **41** comportant le groupement diméthylamino en *para* de l'atome de phosphore (Schéma 31). La stabilisation du radical cation se ferait dans ce cas par π-donation de la paire libre de l'azote à travers le cycle aromatique.

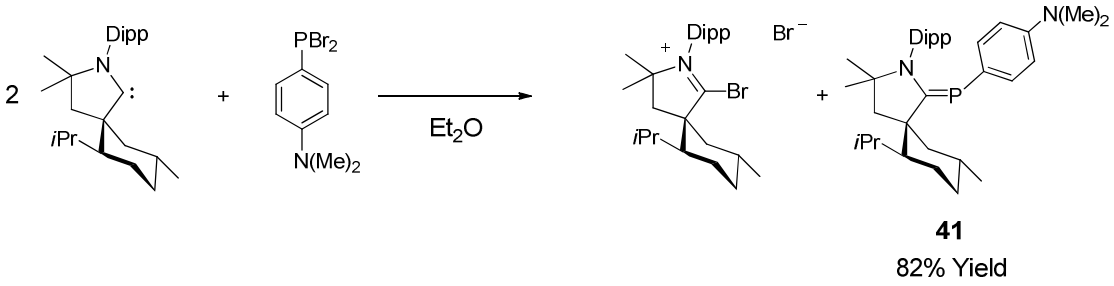

Schéma 31. Préparation du composé 41.

Encore une fois, la voltampérométrie cyclique de **41** réalisée dans le THF indique que ce dernier subit une oxydation irréversible à un potentiel $E_{ox} \approx$ -0.150 V plus bas que l'adduit **37**.
Cependant lorsque la réaction de **41** avec $Ph_3C^+B(C_6F_5)_4^-$ est conduite à -80 °C dans le dichlorométhane, le radical cation correspondant a pu être observé par RPE à basse température. Le spectre de ce radical consiste en un large doublet dû au couplage hyperfin avec l'atome de phosphore (g = 2.005, $a_{iso}(^{31}P)$ = 89 G). La valeur de cette constante de couplage est comparable à celles observées pour les radicaux phosphinyles confirmant la nature de ce dernier. Cependant à température ambiante ce radical est seulement persistent avec une demi-vie de l'ordre de quelques minutes.
Nous avons alors finalement préparé l'adduit **42** comportant un groupement tétraméthylpipéridine directement lié à l'atome de phosphore (Schéma 32). En effet grace à la π-donation de la paire libre de l'azote, le radical cation serait alors stabilisé. De plus l'absence d'hydrogène sur les méthylènes liés directement à l'atome d'azote du cycle pipéridine permettrait d'éviter une réaction secondaire similaire lors de l'oxydation de **38**.

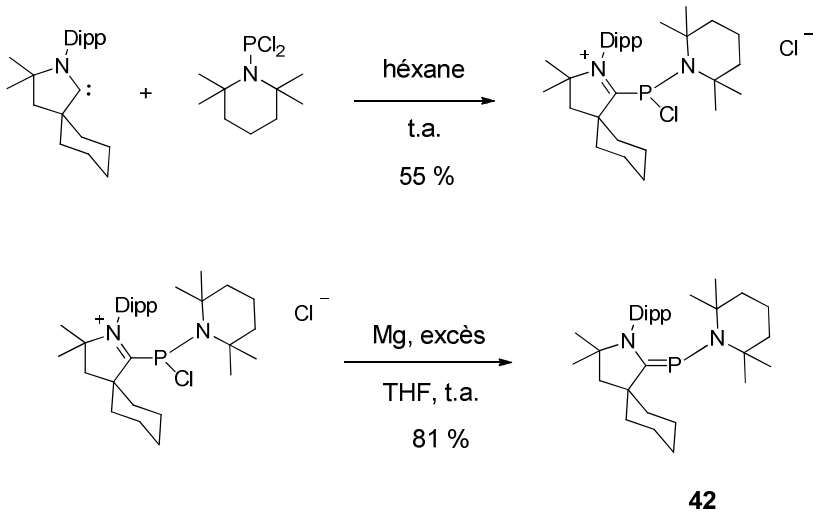

Schéma 32. Préparation de l'adduit **42**.

Finalement la voltampérométrie cyclique de **42** réalisée dans le fluorobenzène avec $K^+B(C_6F_5)^-_4$ en tant qu électrolyte montre que ce dernier subit une oxydation réversible à $E_{1/2}$ = -0.412 V vs. Fc^+/Fc. Ce résultat encourageant nous a alors amenés à réaliser l'oxydation chimique de l'adduit **42** en utilisant $Ph_3C^+B(C_6F_5)_4^-$ en tant qu'agent oxydant (Schéma 33).

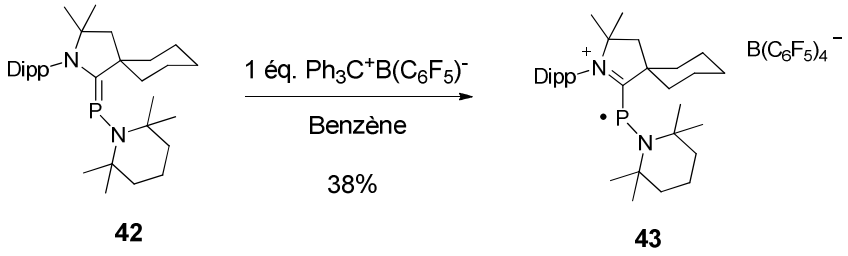

42 **43**

Schéma 33 Préparation du radical cation **42**.

Le radical **43** a été isolé sous la forme d'une poudre marron. Le spectre RPE de ce composé enregistré à température ambiante dans une solution de fluorobenzène consiste en un large doublet dû au couplage hyperfin avec le noyau de l'atome de phosphore (g = 2.007, a(^{31}P) = 99 G) (Figure 7).

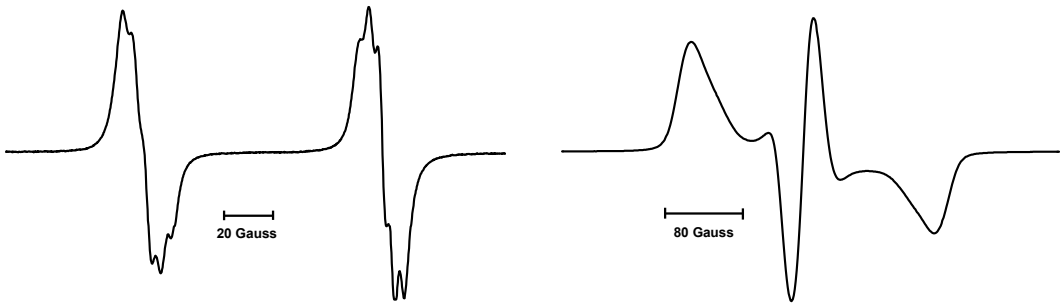

Figure 7. Spcetres RPE du radical cation **43** en solution dans le fluorobenzène, enregistré à température ambiante (gauche) et en solution congelée à 100 K (droite).

Un couplage additionel est également apparent et correspond probablement au couplage hyperfin avec un ou deux atomes d'azote (a(^{14}N) ≈ 4 G).
Afin de déterminer la densité de spin présente sur l'atome de phosphore le spectre RPE en solution congelée dans le fluorobenzène a également été enregistré à 100 K (Figure 7). Selon les valeurs principales du tenseur de couplage hyperfin avec l'atome de phosphore déterminées par cette analyse, nous pouvons conclure que 57% de densité de spin est localisé dans une des orbitales 3p du phosphore. L'orbitale 3s en revannche ne contient qu'environ 2% de densité de spin. Ces valeurs montrent bien qu'il s'agit d'un radical phosphinyle. La structure de **43** a également été confirmée par analyse de diffraction des rayons X effectuée sur un

monocristal. A l'état solide **43** possède une géométrie en V avec un angle C-P-N de 107.26°. De plus la longeur de la liaison P-N (1.68 Å) est relativement courte reflétant ainsi la π-donation de la paire libre d'électrons de l'atome d'azote. La liaison P-C est quant à elle relativement longue (1.81 Å) en accord avec une diminution de l'indice de la liaison P=C lors de l'oxydation. Selon des calculs théoriques utilisant la méthode NBO, la densité de spin présente sur l'atome de phosphore atteint 67%. De plus, l'atome d'azote du cycle pipéridine possède environ 16% de densité de spin. (Figure 8).

Figure 8. Densité de spin dans le radical **43** déterminée à l'aide de calculs théoriques.

Cette analyse confirme donc la nature de ce radical cation qui peut être décrit comme un radical phoshinyle. De plus contrairement au composé **29**, ce dernier réagit avec *n*-Bu_3SnH pour donner la phosphine **44** résultant du transfert de H· (Schéma 34).

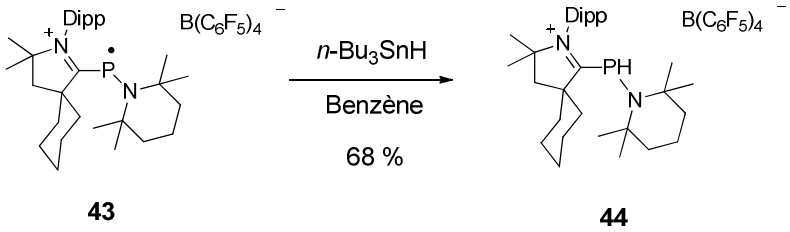

43 **44**

Schéma 44. Abstraction de H· intermoléculaire mise en jeu lors de la réaction entre le radical **43** et *n*-Bu_3SnH.

En conclusion, la synthèse du radical phosphinyle **43** stable aussi bien en solution qu'à l'état solide confirme l'aptitude des carbènes stables à stabiliser des espèces paramagnétiques. La stabilité de **43** est également attribuée à l'encombrement stérique autours de l'atome de phosphore ainsi qu'à la présence de la charge

positive qui empêche l'eventuelle dimérisation de **43** grâce aux réplusions électrostatiques.

3.5) Comparaison des NHCs et des métaux de transition pour la stabilisation de radicaux phosphinyles

3.5.1) Préparation et caractérisation d'un radical phosphinyle neutre

Dans le but de réaliser la synthèse d'un radical phosphinyle neutre, nous nous sommes inspirés des travaux de Cummins décrits auparavant. En effet le remplacement des centres organométalliques $V(NNpAr)_3$ dans le composé **29** par des carbènes pourrait éventuellement conduire au premier exemple d'un radical phosphinyle neutre purement organique. Cette hypothèse est basée sur le fait que les carbènes singulets stables sont capables d'imiter la réactivité des complexes de métaux de transition. En effet comme ces derniers, les carbènes sont capables d'activer CO, H_2 et P_4. Ainsi, dans un premier temps le composé **44** a été préparé selon la méthode décrite au schéma 35.

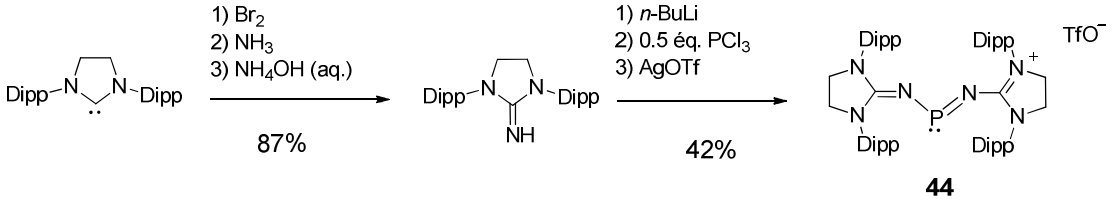

Schéma 35 Préparation du sel **44**.

La voltampérométrie cyclique de **44** montre que ce dernier subit une réduction réversible à $E_{1/2}$ = -1.84 V vs Fc^+/Fc. Ainsi la réduction chimique de **44** a été effectuée en utilisant K/C_8 en tant que réducteur ce qui a permis d'obtenir le radical **45** avec un rendement de 85 % sous la forme d'une poudre rouge (Schéma 36).

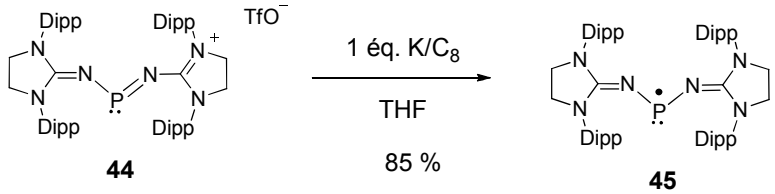

Schéma 36 Préparation du radical **45**

Le radical **45** a été caractérisé par RPE en solution dans le THF (Figure 9). Le spectre enregistré à température ambiante consiste simplement en un large doublet dû au couplage hyperfin avec l'atome de phosphore (g = 2.005, $a(^{31}P)$ = 78 G). Le spectre mesuré en solution congelée à 100K indique que 62 % de densité de spin sont localisés dans une orbitale 3p de l'atome de phosphore et seulement 2% dans

l'orbitale 3s confirmant ainsi la nature de **45**. De plus, pour ce radical, la densité de spin localisée à l'atome de phosphore est largement supérieure à celle déterminée dans la cas de **29 (**31.3 %).

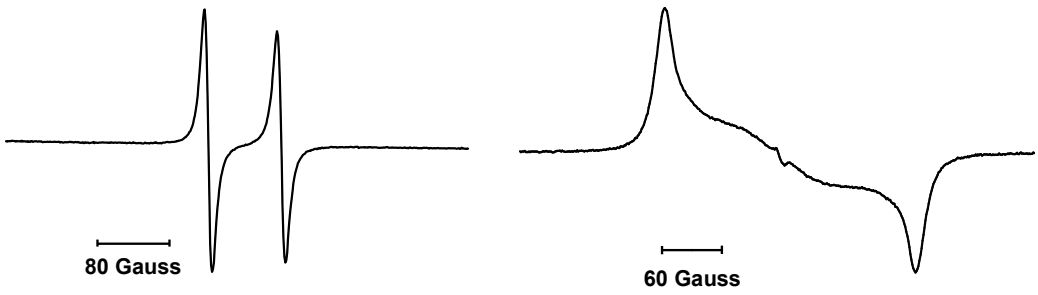

Figure 9. Spectres RPE du radical **45** en solution dans le THF, enregistré à température ambiante (gauche) et en solution congelée à 100K (droite).

La structure de **45** a été également confirmée à l'aide d'une analyse de diffraction des rayons X. A l'état solide la molécule adopte une géométrie en V avec un angle NPN de 97.8°. Les liaisons N-P (1.658 Å et 1.657 Å) sont relativement courtes et reflètent la délocalisation de l'électron célibataire dans les orbitales 2p vacantes des carbènes (Schéma 37).

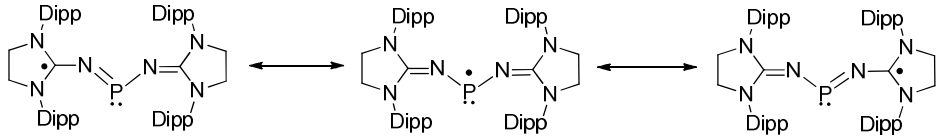

45

Schéma 37. Délocalisation de l'électron célibataire dans le composé **45**.

Afin de comparer expérimentalement l'aptitude du centre organométallique $V(NNpAr)_3$ à délocaliser la densité de spin de l'atome de phosphore avec celle du NHC, nous avons réalisé la synthèse du composé mixte **46** (Schéma 38).
Ce composé paramagnétique a été caractérisé par RPE (Figure 10). Le spectre enregistré à température ambiante dans le THF consiste en un octuplet dû au couplage hyperfin avec l'atome de vanadium (g = 1.981, a(^{51}V) = 58 G). Le couplage avec le phosphore est par contre relativement faible résultant seulement à un léger épaulement des lignes et ne peut être résolu. Le spectre RPE enregistré en solution congelée indique que la densité de spin est majoritairement localisée sur le vanadium (67 %) et très faiblement sur le phosphore (environ 1 %).

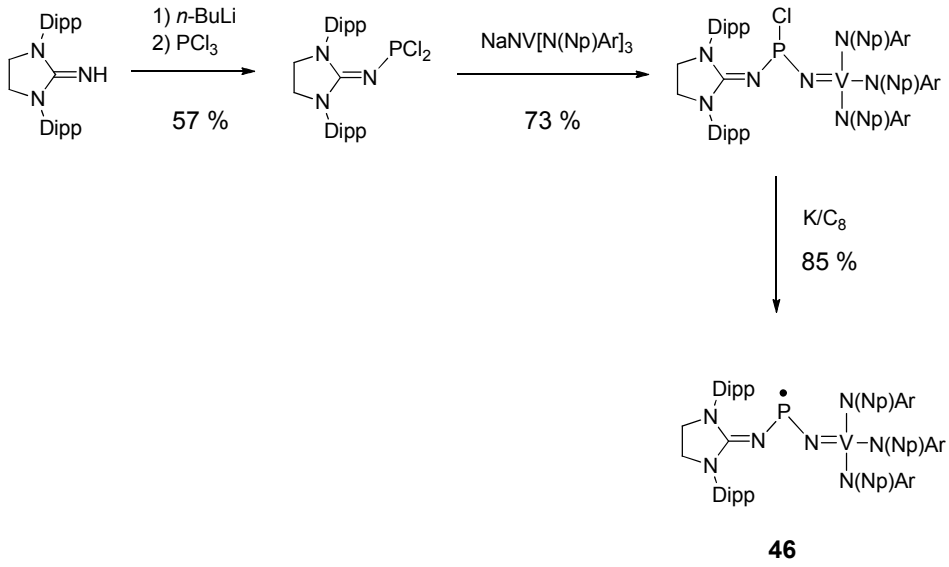

Schéma 38. Préparation du composé mixte **46** (Np = neopentyl, Ar = 3,5-$Me_2C_6H_3$).

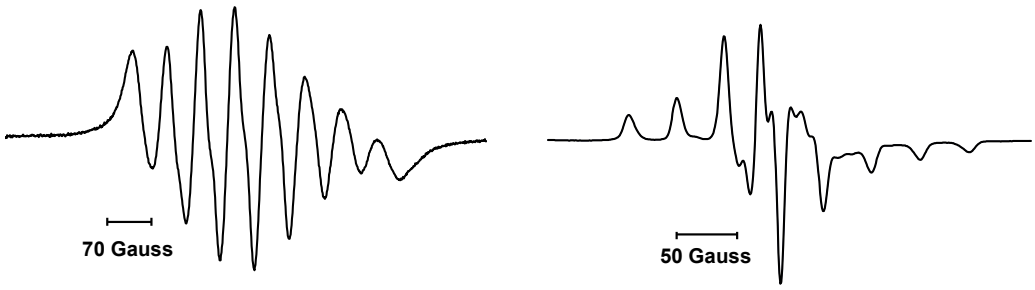

Figure 10. Spectres RPE du radical **46** en solution dans le THF, enregistré à température ambiante (gauche) et en solution congelée à 100K (droite).

Ces résultats suggestent clairement que l'électron célibataire est principalement localisé sur l'atome de vanadium, par conséquent le radical **46** peut être décrit comme un complexe de vanadium (IV) comportant un ligand imidazolidin-2-iminato (Schéma 39).

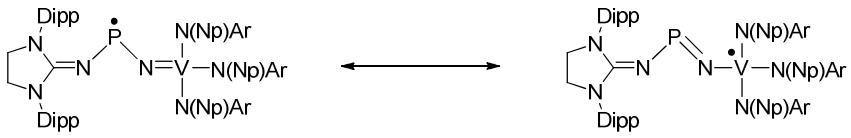

Schéma 39. Structures de resonance possibles pour le compose **46** (Np = neopentyl, Ar = 3,5-$Me_2C_6H_3$).

Cette description est également supportée par la structure à l'état solide. En effet, la longueur de la liaison N-P (impliquant l'atome d'azote directement lié au vanadium) est de 1.572 Å indiquant un caractère de double liaison. De plus, la liaison V-N (1.806 Å) est plus longue que les liaisons correspondantes dans le radical **29** et est proche de la longueur d'une liaison simple. Les calculs théoriques de densité de spin réalisés sur les composés expérimentaux **29**, **45** et **46** sont également en accord avec les résultats experimentaux. Ces analyses montrent bien au final que le metalloligand $NV(NNpAr)_3$ est plus efficace que le fragment organique NNHC pour délocaliser la densité de spin de l'atome de phosphore. Cependant, les substituents imidazolidine-2-iminato ont tout de même permis l'isolation du radical **45** stable à l'état solide. La stabilité de ce dernier est probablement attribuée en grande partie à la protection stérique offerte par les groupements Dipp des NHCs. Par conséquent la densité de spin pour le composé **45** est plus fortement localisée sur l'atome de phosphore que dans le radical **29** et par conséquent **45** possède un caractère phosphinyle plus marqué.

Carbene-stabilization of paramagnetic or electron deficient phosphorus based fragments.

Considered as a laboratory curiosity at the end of the twentieth century, stable singlet carbenes have quickly found numerous applications. For example, they can serve as ligands for transition metals resulting in more active and more robust catalysts. Interestingly, they can also mimic the reactivity of transition metal complexes, for example they can activate small molecules (CO, H_2, P_4) and for this last purpose they sometimes even surpass transition metals as shown by the carbene mediated activation of NH_3. Recently a new application of singlet carbenes has emerged, namely the stabilization of main group elements in their zero oxidation state. This has been applied in the preparation of the so-called carbodicarbenes (featuring a carbon (0) center) and more strikingly in the preparation of disilicon and diphosphorus carbene adducts. Although Si_2 and P_2 are extremely reactive molecules, which usually can only be generated under harsh conditions and cannot be observed in solution, the carbene adducts are perfectly stable at room temperature and in the solid state.

This manuscript is devoted to the stabilization by stable carbenes of even more reactive electron-deficient or paramagnetic species based on phosphorus.
In the first chapter, the activation of white phosphorus by carbenes is discussed. It is shown that, by choosing the right steric and electronic parameters for the carbenes, fragmentation of P_4 can be performed, a well-known task for transition metal complexes but unprecedented for organic molecules. This fragmentation pathway led to the preparation of compounds which can be described as P_2 and P^+ carbenes adducts.

The second chapter focuses on one-electron oxidations of diphosphorus-carbene adducts. The synthesis and characterizations of the new $P_2^{+\cdot}$-radical cation and P_2^{2+}-dication bis-carbenes adducts are achieved. This study has allowed for the direct comparison of the stabilization effects on the adducts by two different types of carbenes, NHCs and CAACs. These last results reveal a new application for stable singlet carbenes: the stabilization of paramagnetic and electron-deficient species.

This concept will then be extended in the third chapter to the preparation of new phosphinyl radical cations by taking advantage of the stabilization induced by carbenes. These $P^{+\cdot}$ carbene adducts are perfectly stable at room temperature in solution and in the solid state allowing for their complete characterization. Finally, the stabilizing effects of the carbene on the phosphinyl radical will be directly compared with a vanadium metalloligand which had been previously used for the successful isolation of a neutral phosphinyl radical.

Key words: Singlet carbene, white phosphorus, diphosphorus, radical, EPR, phosphinyl, spin density.

Preface

It was in 1669, while looking for the philosopher's stone that the alchemist Hennig Brandt accidentally discovered the elemental phosphorus from the distillation of urine. Nowadays, it is known that phosphorus plays an important role in our life. It is largely found as phosphate in the human body where it is a constituent of the DNA (deoxyribonucleic acid) and the ATP (adenosine-5'-triphosphate). Moreover, since 1831 when the first matches based on white phosphorus were invented, the number of industrial applications involving phosphorus has been growing. These applications range from new materials to pharmaceutical drugs.

On the other hand, this element displays strikingly different fundamental properties when compared to its lighter congener, the element nitrogen. For example, contrary to nitrogen, phosphorus can be present in different allotropic forms (red, white and black forms). Furthermore, it does not readily hybridize and does not form strong π bonds. These last intrinsic characteristics result in interesting properties for the organic species where it is incorporated.

This manuscript is devoted to the stabilization of highly reactive phosphorus-based fragments by the use of stable carbenes. Stable carbenes are neutral dicoordinate carbon compounds which have only six valence electrons. While the use of carbenes as ligands for transition metals is well recognized, it is only recently that these species have been used for the coordination of main group elements.

In the first chapter we will discuss about the activation of white phosphorus (P_4) mediated by carbenes. We will show that, by changing the electronic and steric parameters of the carbenes, the aggregation or the fragmentation of P_4 can be performed. These reactions lead to products which can be described as P_n-carbene adducts.

In the second chapter, we will focus exclusively on the P_2-carbene adducts and we will study the influence of the carbenes parameters to the properties of these adducts. By performing one-electron oxidations on these species, the synthesis and characterizations of the new $P_2^{+\cdot}$-radical cation and P_2^{2+}-dication bis-carbenes adducts are achieved. This reveals a new application of stable carbenes: the stabilization of paramagnetic and electron-deficient species.

This new concept will then be extended in the third chapter to the stabilization of paramagnetic fragments containing only one phosphorus center. The resulting phosphinyl radicals are stable in solution and in the solid state allowing their complete characterization. In addition, the abilities of a carbene and a transition metal to stabilize a phosphinyl radical will be compared.

The work presented in this manuscript has been carried out in the CNRS-UCR joint laboratory at the University of California at Riverside (USA).

General Considerations:

All manipulations were performed under an atmosphere of dry argon using standard Schlenk techniques. Solvents were dried by standard methods and distilled under argon. ^{1}H, ^{31}P, ^{19}F and ^{13}C NMR spectra were recorded on Varian Inova 400, 500 and Bruker 300 spectrometers at 25 °C.
NMR multiplicities are abbreviated as follows: *s* = singlet, *d* = doublet, *t* = triplet, *sept* = septet, *oct* = octuplet, *m* = multiplet, *br* = broad signal.
EPR spectra were recorded on a Bruker EMX spectrometer.
X-ray diffraction studies were performed by Bruno Donnadieu on a Bruker X8-APEX instrument using Mo-radiation for data collection.
Cyclic voltammetries were performed in a glove box at room temperature. Unless mentioned otherwise, the experiments were carried out in THF solutions containing 0.1M of *n*-Bu_4NPF_6 as electrolyte with a scan rate of 100 $mV.s^{-1}$.
Masse spectrometry experiments were performed at the UC Riverside Mass Spectrometry Laboratory.
Melting points were measured with a Büchi melting point apparatus system.

Abbreviations:

DFT: Density Functional Theory
EPR: Electron Paramagnetic Resonance
NMR: Nuclear Magnetic Resonance
MO: Molecular Orbital
HOMO: Highest Occupied Molecular Orbital
LUMO: Lowest Unoccupied Molecular Orbital
SOMO: Singly Occupied Molecular Orbital
SCE: Saturated Calomel Electrode
BArF: tertrakis(pentafluorophenyl)borate
CAAC: Cyclic (Alkyl)(Amino)Carbene
Cp^*: pentamethylcyclopentadienyl
Dipp: 2,6-diisopropylphenyl
DME: dimethoxyethane
dppm: bis(diphenylphosphino)methane
Fc: ferrocene
Fc^+: ferrocenium
Hex: cyclohexyl
*i*Pr: isopropyl
KHMDS: Potassium Bis(trimethylsilyl)amide
Me: methyl
MeOTf: Methyl Trifluoromethanesulfonate
Mes: 2,4,6-trimethylphenyl (Mesityl)
Mes^*: 2,4,6-tri-*tert*-butylphenyl
NHC: N-heterocyclic carbene
Np: Neopentyl
Ph: Phenyl
Pftb: perfluoro-*tert*-butoxyaluminate
*t*Bu: *tert*-butyl
TBME: *tert*-butyl methyl ether
THF: tetrahydrofuran
TfO: trifluoromethanesulfonate
TMS: trimenthylsilyl

Table of contents

Chapter I

Carbene mediated activation of white phosphorus: preparation of P_1, P_2 and P_4 carbenes adducts

1.1) Industrial importance of white phosphorous

P_4, also known as white phosphorous is the most reactive allotropes of the phosphorus element. This waxy white solid is extremely pyrophoric and burns instantaneously in the air giving phosphorus pentoxide (P_2O_5) by the very exothermic reaction with dioxygen. Nevertheless, despite its high reactivity, P_4 is widely produced nowadays from phosphate minerals and it is the starting material for the industrial preparation of various organophosphorus compounds.[1] These industrial processes lay on the transformation of P_4 to PCl_3 or PCl_5 using Cl_2 gas and then on the substitution of the chlorines by organic fragments through HCl or salts elimination reactions. However to meet the increasingly stringent environmental regulations, new catalytic processes starting from white phosphorus and avoiding the use of chlorine are highly desirable.

Despite many efforts, no catalytic process combining directly P_4 and organic molecules has been described and so far only one catalytic cycle based on a Niobium complex has been reported.[2] Whereas transition metal mediated activation of white phosphorus is a well established field,[3] research concerning activation by main group fragments has been less developed.[4] One of the reasons may be the fact that the reactions are often not predictable and there is no general trend for the reactivity of P_4 with main group compounds. Therefore this domain suffers from a considerable lack of mechanistic knowledge.

1.2) Structure, electronical properties and general behavior of P_4

Solid white phosphorus occurs in three modifications: the α form which is the common form observed at room temperature, the β form which was discovered in 1914[5] and is obtained below -77 °C by a reversible phase transformation from α-P_4 and finally the γ form discovered in 1974[6] obtained when α-P_4 is quenched and kept at -165 °C during several hours. Although no single crystal X-ray structure of α-P_4 and γ-P_4 has been obtained so far, a X-ray structure diffraction study has been performed for β-P_4[7]. The asymmetric unit contains three independent molecules which exhibit slight deviation from T_d symmetry. In the β form, the measured P-P distances lie between 2.199 Å and 2.212 Å after applying a rigid body correction. However, in the gas phase at 197°C, P_4 has a regular tetrahedron structure with a P-P distance of 2.21 Å measured using electrons diffraction technique.[8] Finally, according to quantum chemical calculations, a value of 2.194 Å has been computed [9]. Moreover, according to an other computational study in the singlet state (predicted to be 24.44 kcal/mol lower in energy than the triplet state) the molecule adopts a regular tetrahedron structure.[10]

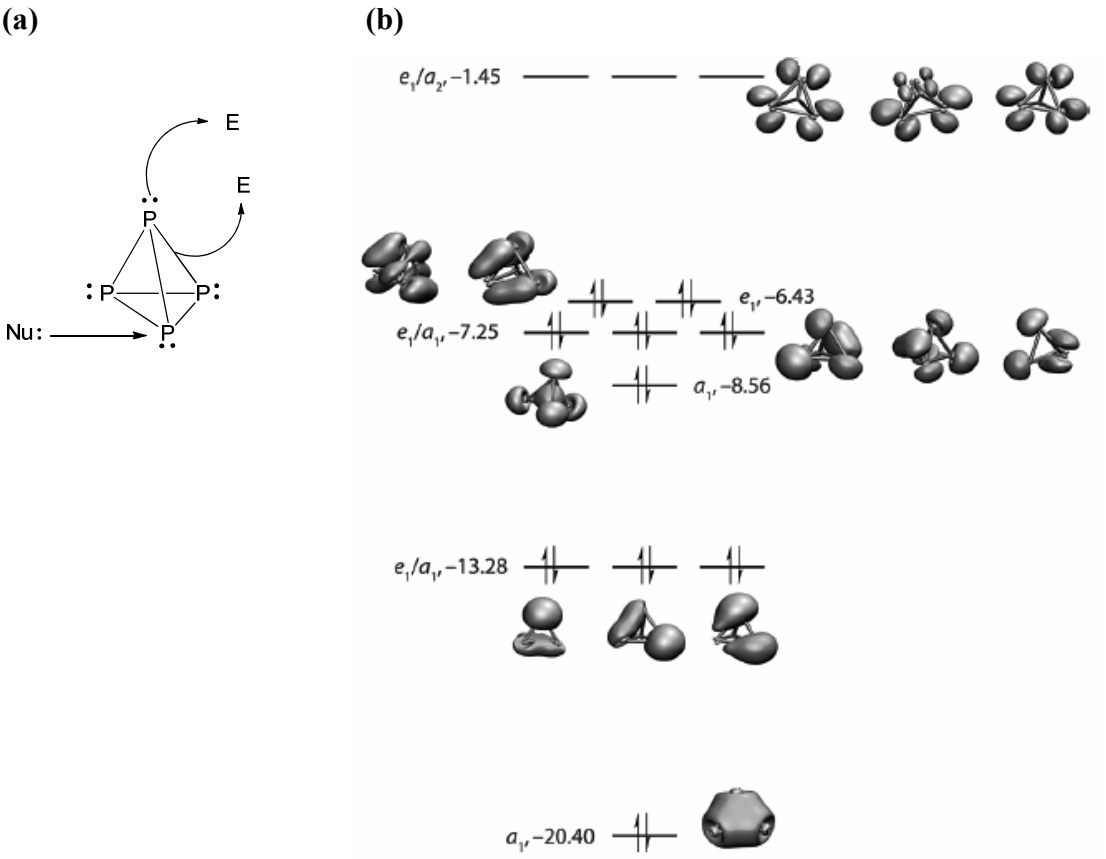

Figure 1. (a) Reactivity pattern of P_4 showing the nucleophilic and electrophilic sites of the molecule (E = Electrophile or Nu = Nucleophile refers to the attacking reactant). **(b)** Molecular orbitals diagram of P_4 (adapted from ref. 11).

To understand better the complex reactivity of white phosphorus we have to look closely to the molecule in order to localize the reactive sites. According to the computed molecular orbitals diagram (figure 1(b)), the HOMO in P_4 is mainly localized at the edges of the tetrahedron.[11] Moreover each phosphorus atom of P_4 possesses a non-bonding electron lone-pair which contribute to the HOMO-1, HOMO-2 and HOMO-3 molecular orbitals (figure 1(b)). Therefore the nucleophilic sites of the molecule are localized at the edges and also to a less extend at the apexes of the tetrahedron (figure 1(a)).

This is well exemplified by the synthesis of the organometallic complexes **A**-**E** (Scheme 1).[12] In the complexes **A**-**C**, the P_4 entity is coordinated to the metal in a mono-*hapto* fashion (η^1) through one of the phosphorus atom. This was assigned in the case of **A** by the $^{31}P\{^1H\}$ NMR spectrum which consists of a temperature-invariant AB_2MX_3 spin system. The coordinated phosphorus atom displays a complex signal at δ = -390.5 ppm and the three remaining basal P atoms display a doublet at δ = - 488.9 ppm suggesting free rotation around the Re-P bond. Interestingly the chemical shifts of these phosphorus atoms are slightly

shifted downfield in comparison of the free P_4 molecule (δ = -526.9 ppm) suggesting a minor perturbation of the P_4 tetrahedron upon coordination.

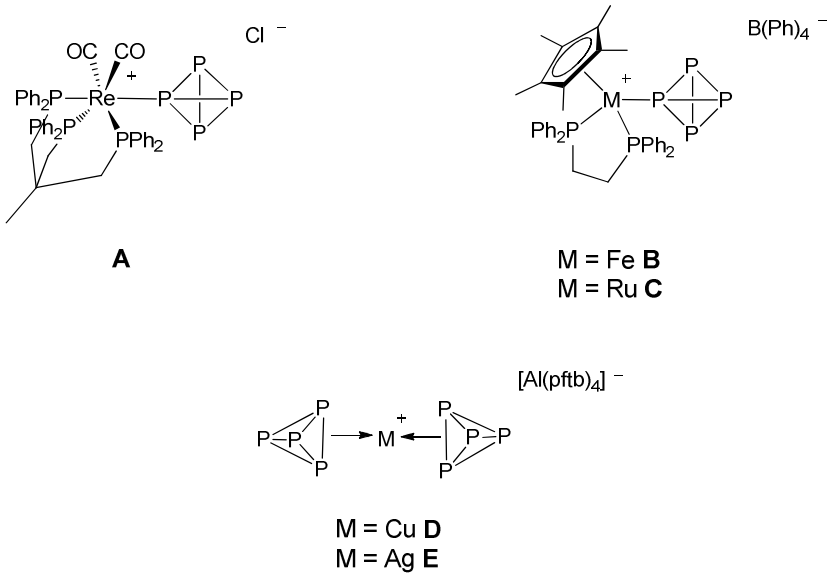

A

M = Fe **B**
M = Ru **C**

M = Cu **D**
M = Ag **E**

Scheme 1. Previously reported organometallic complexes containing an intact *tetrahedro*-tetraphosphorus ligand (pftb = perfluoro-*tert*-butoxyaluminate).

The complexes **B** and **C** display a A_2MX_3 spin system in the $^{31}P\{^1H\}$-NMR spectrum. However upon coordination more important variations of the chemical shifts of the tetrahedron's phosphorus atoms are observed (**B**: δ_M = -299.54 ppm, δ_X = -482. 12 ppm; **C**: δ_M = -308.46 ppm, δ_X = -490.29 ppm) suggesting a more pronounced perturbation of the electronic density in the P_4 fragment. The η^1 coordination mode of P_4 was unambiguously confirmed by X-ray diffraction analysis performed on a single crystal of **B**. Finally, the complexes **D** and **E** have been isolated using the weakly coordinating anion $Al(OC(CF_3)_3)_4^-$ and have been characterized using X-ray diffraction studies. For each complex, the $^{31}P\{^1H\}$ NMR spectrum displays only a sharp singlet even at low temperature (**D**: δ = -460 ppm in CD_2Cl_2 at -90 °C; **E**: δ = -486 ppm in CD_2Cl_2 at -100 °C) suggesting dynamic behavior making all the phosphorus equivalent. In the solid state in both cases, the local coordination sphere at the metal center is nearly planar and the P_4 fragment is bonded to the metal center via a η^2 mode. The coordinated edge of the tetrahedron is elongated in average by 0.13 Å for **D** and 0.12 Å for **E** while the other P-P bonds shrunk by 0.01 to 0.06 Å due to a weak perturbation of the P_4 molecule upon coordination. The bonding situation in **E** was also investigated by calculations [13] and it was concluded that the complex results mainly from electrostatic interactions between the Ag^+ ion and the two electron pairs of the two coordinated P-P bonds. The energetically preferred planar arrangement of the ion was explained by $d_{x^2-y^2}(Ag) \rightarrow \sigma^*(P\text{-}P)$ back bonding reducing also the positive charge on the coordinated phosphorus atom. This type of side-on attack has also been evocated to explain the reactivity of

more electrophilic carbene-like fragments with P_4 (silylene and phosphenium cations) which will be developed in the next paragraphs.

Not only white phosphorus reacts with electrophiles, but it has been known for a long time that P_4 is also able to react with nucleophiles such as sodium hydroxide or sodium ethoxide,[14] cyanides[15], diphenylphosphinite[16] or with bulky organic nucleophiles such as the supersilyl anion tBu$_3$Si$^-$Na$^+$[17] or tBu$_3$C$_6$H$_2^-$Li$^+$.[18] This observation suggests a pronounced electrophilic character in P_4 which is clearly apparent on the molecular orbitals diagram (see figure 1(b)). The LUMO of P_4, mainly constituted by the phosphorus 3p orbitals is localized at the apexes of the tetrahedron. This suggests that the attack of a nucleophile on P_4 will proceed according to the pathway represented in figure 1(a). This is well illustrated experimentally by the reaction with tBu$_3$C$_6$H$_2^-$Li$^+$ (**1**). The reaction was conducted in the presence of the electrophilic and trapping agent 1-bromo-2,4,6-tri-*tert*-butylbenzene (Scheme 2). After the reaction bis(2,4,6,- *tert*-butylphenyl)bicyclotetraphosphane (**2**) was isolated. Its formation was rationalized by the first nucleophilic attack of tBu$_3$C$_6$H$_2^-$Li$^+$ to one of the phosphorus center at the apex of the tetrahedron which consequently undergoes a P-P bond cleavage and opens to an anionic butterfly intermediate. This intermediate reacts then with 1-bromo-2,4,6-tri-*tert*-butylbenzene providing the bicyclotetraphosphane as ivory-colored crystals.

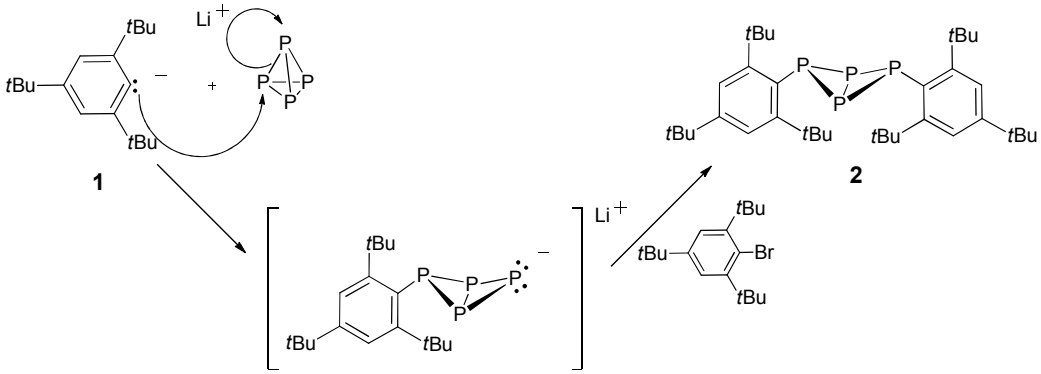

Scheme 2. Nucleophilic activation of P_4 and subsequent trapping of the butterfly intermediate.

Similar nucleophilic cage opening of P_4 can be triggered by the reaction with the highly nuclophilic supersilyl anion tBu$_3$Si$^-$ (**3**). However in this case the outcome of the reaction is dependent on the conditions and various products can be obtained. Thus, when 2 equivalents of **3**(Na$^+$) is reacted with white phosphorus in THF or DME, the tetraphosphabutadienediide (**6**(Na$^+$)$_2$) is obtained (Scheme 3).
It is proposed that **6**(Na$^+$)$_2$ is formed by the addition of a second molecule of **3**(Na$^+$) to the butterfly intermediate **4** or to the transient triphosphirene **5** resulting from a first nucleophilic attack of **3**(Na$^+$) to P_4 (scheme 3).[17, 19]

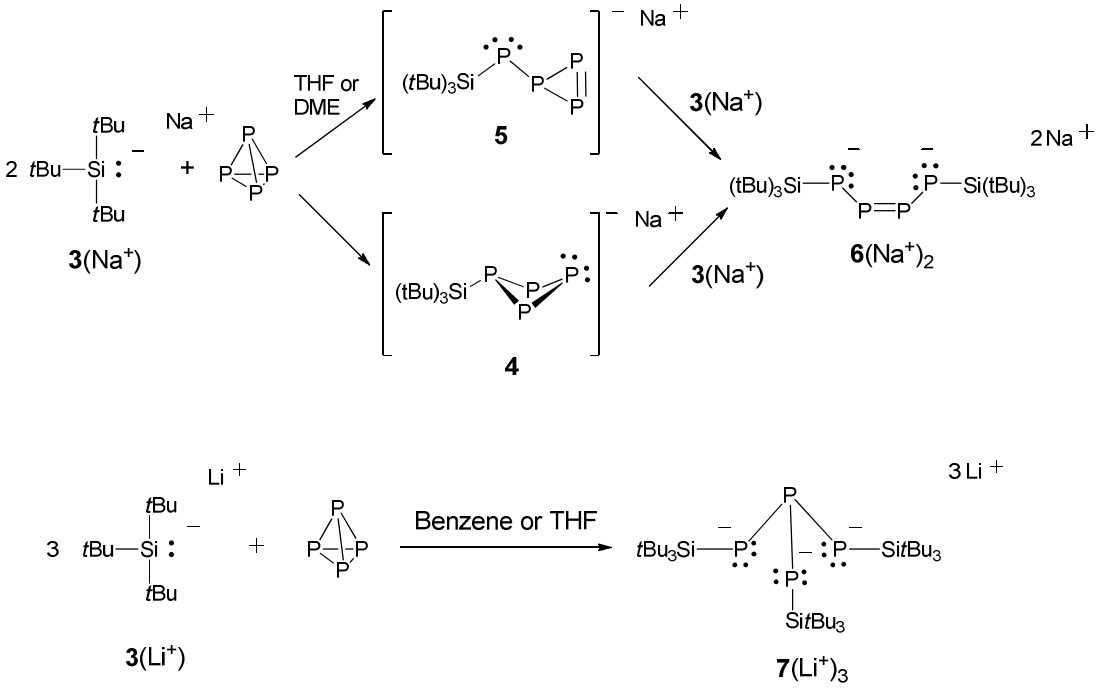

Scheme 3. Nucleophilic activation of P_4 mediated by the supersilyl anion tBu$_3$Si$^-$ **3**. On top, it is shown that when using 2 equivalents of **3**(Na$^+$) the tetraphosphabudienediide **6**(Na$^+$)$_2$ is obtained. However when 3 equivalents of **3**(Li$^+$ or Na$^+$) are used, the tetraphosphide **7**(Li$^+$ or Na$^+$)$_3$ is obtained (bottom).

Interestingly when the reaction is performed with 3 equivalents of **3**(Li$^+$ or Na$^+$) in benzene or in THF, the tetraphosphide **7**(Li$^+$ or Na$^+$)$_3$ is obtained. The lithium salt was characterized in the solid state (scheme 3).[20]
However the latter is not stable in THF and it undergoes a slow cleavage to give after one week at room temperature the allylic anion **8**(Li$^+$) along with tBu$_3$SiPLi$_2$ (scheme 4).[20] The sodium salt of the allylic anion (**8**(Na$^+$)) prepared by an other way was characterized in the solid state by X-ray diffraction analysis and displays an AX_2 spin system in the $^{31}P\{^1H\}$ NMR spectrum. The central P_A phosphorus nucleus gives rise to an extremely low field chemical shift (δ_A = 732.5 ppm).[21]

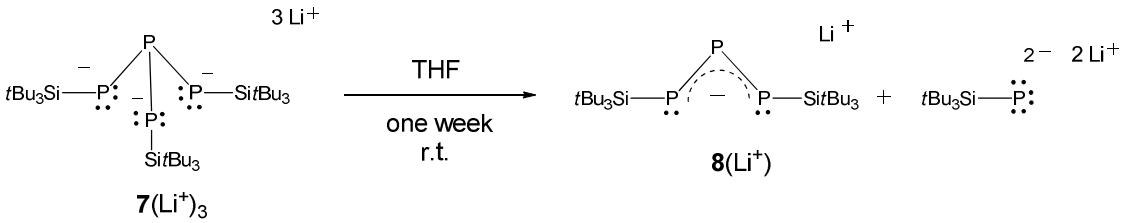

Scheme 4. Degradation of P_4 induced by the supersilyl anion tBu$_3$Si$^-$Li$^+$ **3**(Li$^+$).

The outcome of the reaction depends also on the steric hindrance around the silicon center. For example, the reaction between P_4 and 1 equivalent of the bulky potassium hypersilyl complex $[(Me_3Si)_3Si^-K^+([18]crown-6)]$ **9** in toluene proceeds differently and gives the P_8 aggregate **10** (scheme 5).[22] The aggregation of P_4 to **10** is explained by the dimerization of the initially formed butterfly anion analogous to **4**. Then subsequent rearrangements lead to the P_8 cluster.

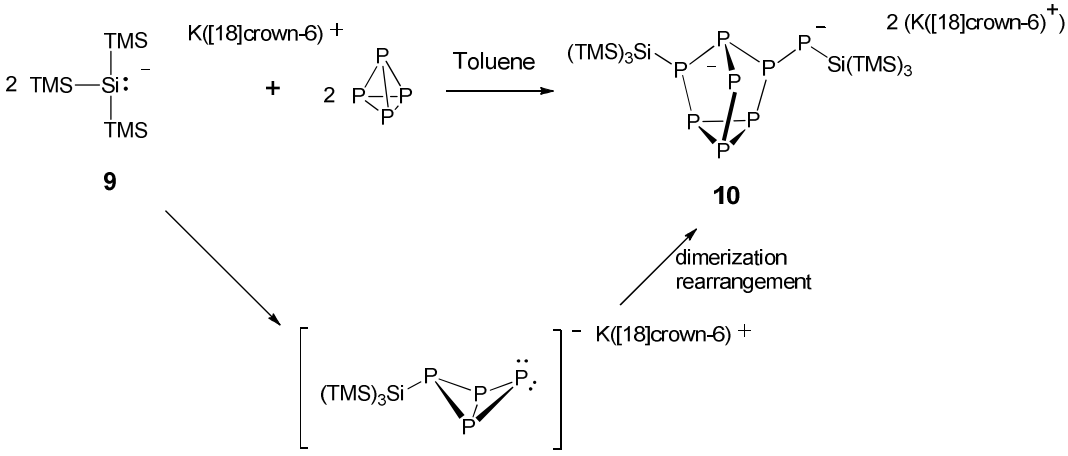

Scheme 5. Aggregation of P_4 mediated by the hypersilyl complex **9**.

After this general description of the reactivity of white phosphorus, we will focus now on the reactions of the latter with main group compounds. We will show that the electrophilic carbenoid species such as Ga^I or Al^I compounds, silylene and phospheniums cations will lead to P-P bond insertions according to a side-on attack pathway mentioned earlier. On the contrary, the reactions with strong nucleophiles and most importantly carbenes proceed in a first step by nucleophilic cage opening of P_4. However, as we will discuss later, after the first step different reaction pathways can be followed depending on the nucleophile, the conditions of the reaction or the stoichiometry.
Transition metal mediated P_4 activation has been extensively studied in the past, therefore we won't provide a complete overview of this field but when possible, we will mention the analogy between the reactions performed with main group compounds and the ones performed with relevant transition metals.

1.3) Activation of P_4 by the electrophilic and electrodeficient group 13 elements compounds, silylene and phosphenium cations

1.3.1) Group 13 element compounds

The first reaction between white phosphorus and a group 13 element based fragment was reported in 1991.[23] After reaction between P_4 and two equivalents of the electrophilic Ga*t*Bu_3, product **11** was isolated in 84% yield (Scheme 6). X-

ray diffraction analysis showed that the product contains two tetracoordinated gallium centers: one results formally from the addition of a Ga-C bond across one P-P bond of the P_4 molecule while the other one is coordinated to one phosphorus atom via a dative bond. Because the Ga^{III} center is electrophilic and features a vacant p orbital, this addition can occur via a side-on electrophilic attack of the Ga center to a P-P bond of the initial P_4 tetrahedron (cf figure 1(a), page 43). Frameworks similar to the GaP_4 core of **11** are more commonly found in transition metal complexes. For example some group 9 metal complexes undergo oxidative addition upon reaction with white phosphorus. We can mention the Co complex **F** and the Rh complex **G**: the former is formed by the cothermolysis of $[Cp^*Co(\mu\text{-}CO)]_2$ in the presence of three equivalents of P_4 and the latter is prepared by reaction at -78 °C between P_4 and the Wilkinson complex $[RhCl(PPh_3)_3]$ (Scheme 6).[24] In addition, a similar reaction has been reported when the Ir^I cationic complex $[Ir(dppm)_2]^+OTf^-$ is reacted with white phosphorus in CH_2Cl_2 at -40°C giving the $Ir^{III}P_4$ complex **H**.[25]

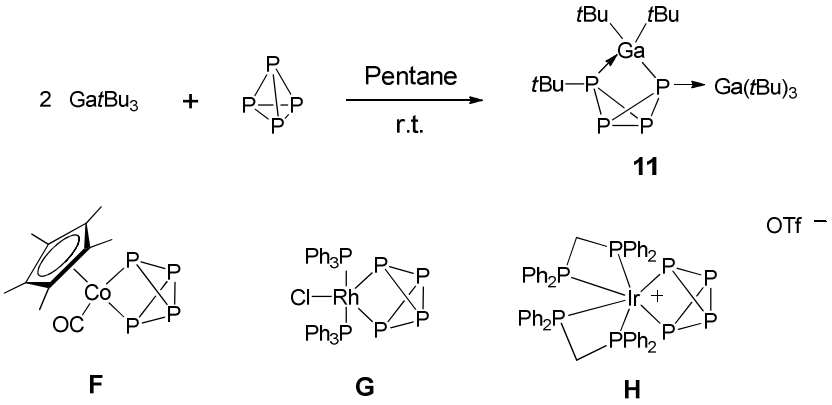

Scheme 6. Preparation of the tetrahedrane type compound **11** from Ga*t*Bu$_3$ and structurally related transition metal complexes **F**, **G** and **H**.

The reaction between white phosphorus and the Ga(I) compound $((TMS)_3CGa)_4$ (**12)** proceeds differently and gives the threefold insertion product **13** (Scheme 7).[26] This compound was characterized by X-ray diffraction study and its nortricyclane skeleton Ga_3P_4 is structurally similar to P_4S_3 or the Zintl-type anion $[P_7]^{3-}$.

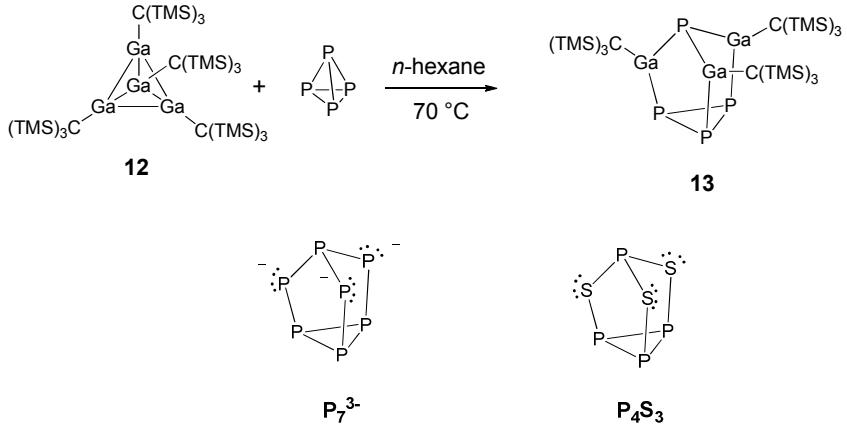

Scheme 7. Activation of P_4 by the tetrameric Ga(I) compound **12** and structure of the related compounds P_7^{3-} and P_4S_3.

Interestingly the apical phosphorus atom attached to the three gallium atoms displays a very upfield chemical shift (-521.9 ppm). Besides it has been shown that in solution the tetrameric compound **12** is in equilibrium with the monomeric Ga(I) species $GaC(TMS)_3$[27] (Scheme 8). Therefore the product **13** probably arises from the reaction between P_4 and the latter which inserts into the P-P bonds of P_4.

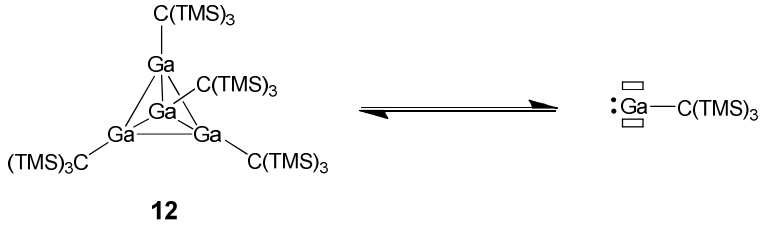

Scheme 8. Dissociation of the tetrameric Ga(I) compound **12** to the corresponding monomer in solution.

Moreover, the reaction of P_4 with the Al(I) compound $(Cp^*Al)_4$ (**14**) has been investigated by the group of Schnöckel in 1994.[28] When P_4 was reacted with 1.5 equivalents of **14** the insoluble compound **15** was isolated as bright yellow crystals (Scheme 9).

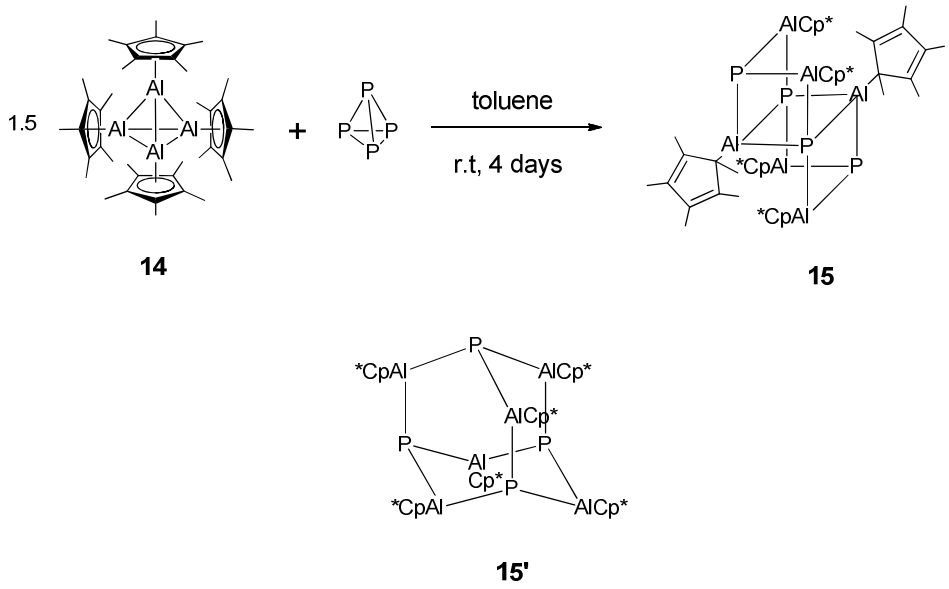

Scheme 9. Preparation of the polyheterocyclic compound **15** from P_4 and $(Cp^*Al)_4$. Calculated isomer **15'** which is predicted to be higher in energy than **15**.

Whereas no NMR spectroscopy analysis of a solution of **15** could be done, a single crystal X-ray diffraction study was performed. In the solid state, **15** is a centrosymmetric polycyclic molecule consisting of two distorted face-sharing Al_4P_4 heterocubanes with two phosphorus atoms missing at the opposite corners. In **15** two of the phosphorus atoms are tricoordinated whereas the two others are tetracoordinated. Also interestingly, four Cp* rings are η^5 bonded to the external aluminum centers and the two other are η^1 bonded to the inner aluminum atoms.
It has been shown on the basis of a ^{27}Al NMR study that like compound **12**, in solution the tetrameric form **14** is in equilibrium with the monomeric species Cp^*Al[29] , therefore **15** is probably formed by reaction between P_4 and the monovalent species. However the expected product directly derived from the insertion of a Cp*Al fragment in each of the six P-P bonds of the P_4 tetrahedron would be the isomer **15'** possessing an adamantane-like structure. According to calculation **15** is more stable than **15'** by 30 to 80 $kJ.mol^{-1}$ depending on the method of calculation explaining why only **15** is observed.

Another example of insertion reaction has been reported by Roesky using the LAl^I compound **16** featuring the bulky ligand nacnac (L = $HC(CMeNDipp)_2$, Dipp = 2,6-*i*$Pr_2C_6H_3$).[30] After the reaction of two equivalents of **16** with P_4 in toluene at room temperature during one week, compound **17** was isolated as red crystals (Scheme 10).

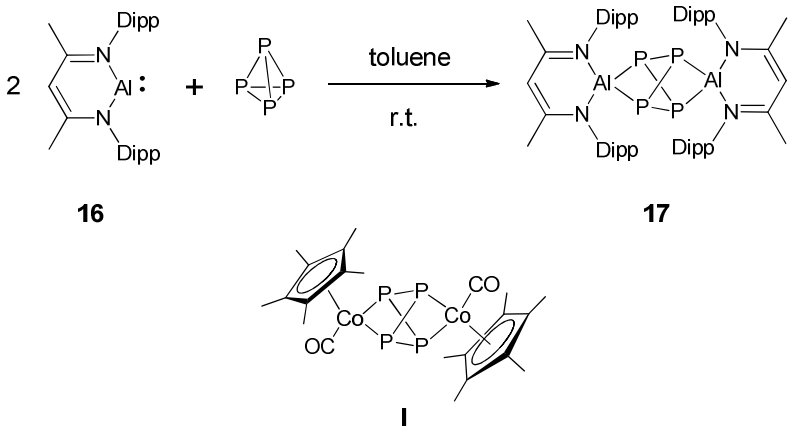

Scheme 10. Preparation of compound **17** by reaction between white phosphorus and the carbene-like fragment **16** (Dipp = 2,6-*i*$Pr_2C_6H_3$). Structurally analog transition metal complex **I.**

Due to the presence of an electron lone pair and a vacant orbital at the aluminum center, **16** features a singlet carbene-like character. The structure of **17** was unambiguously confirmed by the use of X-ray diffraction analysis. In the solid state **17** contains a P_4Al_2 core structure which arises formally from the insertion of two Al(I) fragments into two opposite P-P bonds of the P_4 tetrahedron. Importantly in comparison to **13** and **15**, because of the steric hindrance of the ligand L, only two insertions were observed. The distances between the aluminum bridged phosphorus atoms (3.049(2) and 3.063(2) Å) confirm the full cleavage of the corresponding P-P bonds in the P_4 tetrahedron.
It was concluded that the latter reaction proceeds through oxidative addition at the aluminum centers of **16** resulting to the derivative **17** containing two Al(III) centers linked by a P_4^{4-} moiety. Noteworthy, a structure similar to the P_4Al_2 core is found in the complex **I** (Scheme 10).[24a]

A different reactivity has been observed by the group of Power with the reaction of white phosphorus and the weakly dimerized dithallene $(TlAr^{Dipp})_2$ **18** (Scheme 11).[31]

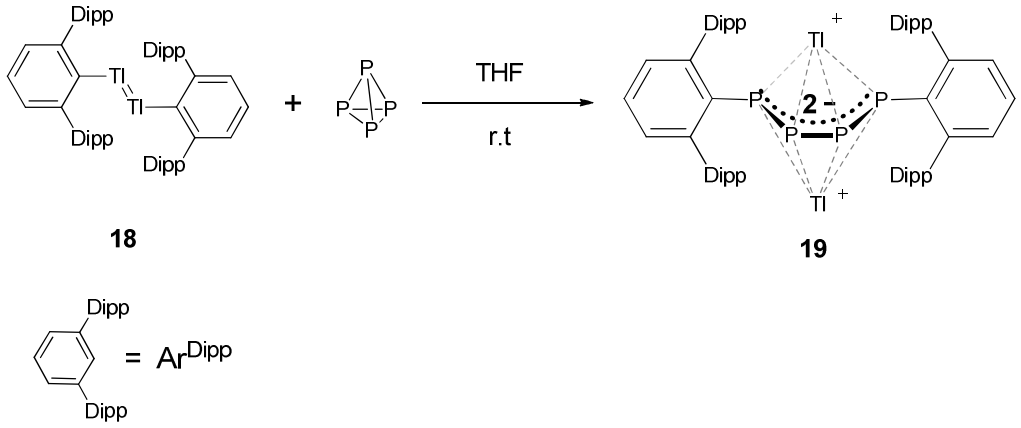

Scheme 11. Synthesis of the tetraphosphabutadienediide **19** from P_4 and the dithallene **18**.

The resulting compound **19** was obtained as burgundy crystals in moderate yield (40%) and was characterized by X-ray diffraction study. In the solid state, the molecule adopts a planar *cis* conformation with the four central phosphorus atoms and the two ipso carbon atoms from the phenyl rings lying in the same plane. This geometry suggests a complete delocalization of the two negative charges in the central tetraphosphabutadienediide core. This is also confirmed by the three P-P bond distances which are almost identical. Due to the symmetry in **19**, the two external P-P bonds in the central P_4 fragment are identical (2.136(4) Å) and the central P-P bond length is 2.143(6). These bond lengths lie between those observed for P=P double bonds (1.98-2.05 Å) and P-P single bonds (2.21 Å). The two positively charged thallium atoms are coordinated to the four phosphorus atoms and are equidistant above and below the P_4 array. According to ^{203}Tl and ^{205}Tl NMR, this coordination is also maintained in solution. This structure is reminiscent of the already mentioned tetraphosphabutadienediide **6** (see scheme 3, page 46) prepared by the nucleophilic addition of 2 equivalents of the supersilyl anion tBu$_3$Si$^-$ (**3**) to P_4. Therefore by analogy and considering the fact that in the dithallene **18** the Ar^{Dipp} groups display a strong anionic character we can imagine that the observed product **19** arises actually by the nucleophilic additions of two equivalents of the TlAr^{Dipp} fragments on P_4.

1.3.2) Activation of P_4 mediated by silylenes

Prior to the investigation of the reactivity of stable carbenes toward white phosphorus, the group of Driess reported in 2007 the reaction between P_4 and the electrophilic silylene **20a** (Scheme 12).[32] The silylene **20a** reacts differently with P_4 in comparison with the silicon analog of the nucleophilic Arduengo-type carbenes **20b**. Whereas the latter apparently catalyzes the polymerization of white phosphorus to red phosphorus,[33] **20a** (which is isoelectronic to the Al(I) fragment **16**) undergoes stepwise insertions into the P-P bonds of the P_4 tetrahedron. Thus when 1 equivalent of **20a** is reacted with P_4, the 1:1 adduct **21** is isolated in 60 % yield.

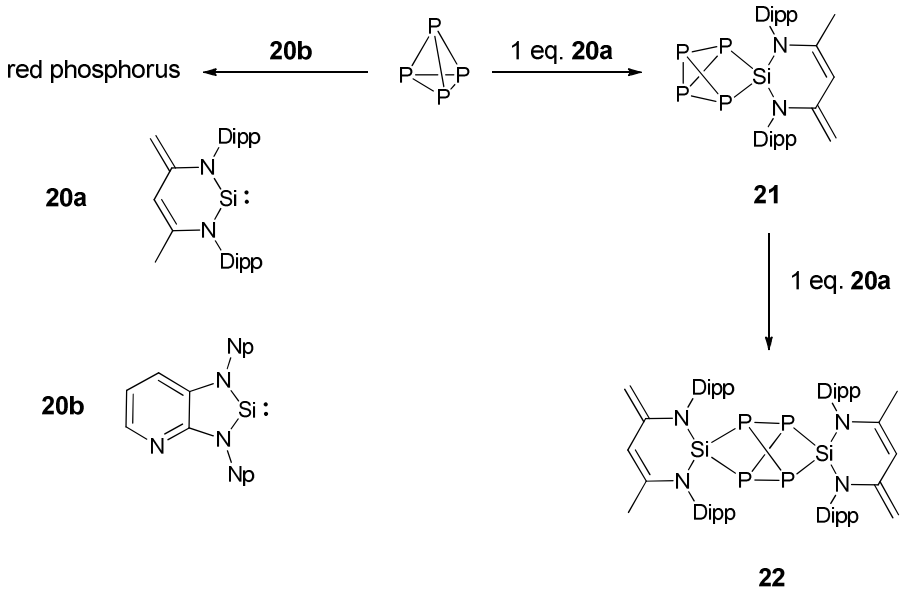

Scheme 12. Reactivity of P_4 with stable silylenes **20a** and **20b**.

In the solid state, compound **21** displays a SiP_4 core with similar structural features than the transition metal complexes **F**, **G** and **H** (Scheme 6, page 48). The bridgehead P-P bond length is slightly shorter than typical P-P single bonds (**21**: 2.159 Å, **F**: 2.158 Å, **G**: 2.188 Å, **H**: 2.162 Å, $\mathbf{P_4}$: 2.21 Å) whereas the average value of the remaining P-P bonds lengths is closer to the single P-P bond length (**21**: 2.228 Å, **F**: 2.210 Å, **G**: 2.212 Å, **H**: 2.228 Å). Interestingly, when **21** is treated with another equivalent of **20a**, a second insertion occurs affording the bis-adduct **22**. The Si_2P_4 core in **22** is structurally similar to the Al_2P_4 or Co_2P_4 cores in **17** and **I** respectively (Scheme 10, page 51) where the two metal centers are formally linked by a P_4^{4-} fragment. Ab initio calculations were performed in order to better understand the reactivity of this electrophilic silylene. It was concluded that in the case of the parent singlet SiH_2, the insertion product was the most stable adduct among other possible products located in the potential energy surface which is consistent with the experiment.[34] Importantly, a recent computational study shows that because of the inertness of the σ orbital at the silicon center, **20a** reacts according to an electrophilic side-on approach (see Figure 1(a), page 43). However this electrophilic attack involves high energy barrier which could be lowered by coordination of a second P_4 molecule to the Si center in the transition state. Therefore in the first step of the mechanism, a P_4 molecule coordinates reversibly via its lone-pair the silylene (Scheme 13). Then, the obtained complex reacts with a second molecule of P_4. The relatively high energy barrier of the insertion step is then lowered by coordination of a second P_4 molecule to the Si in the transition state resulting in a trigonal bipyramidal geometry at the silicon center.[35] The evolution of the transition state leads then to the insertion product along with the release of one molecule of P_4

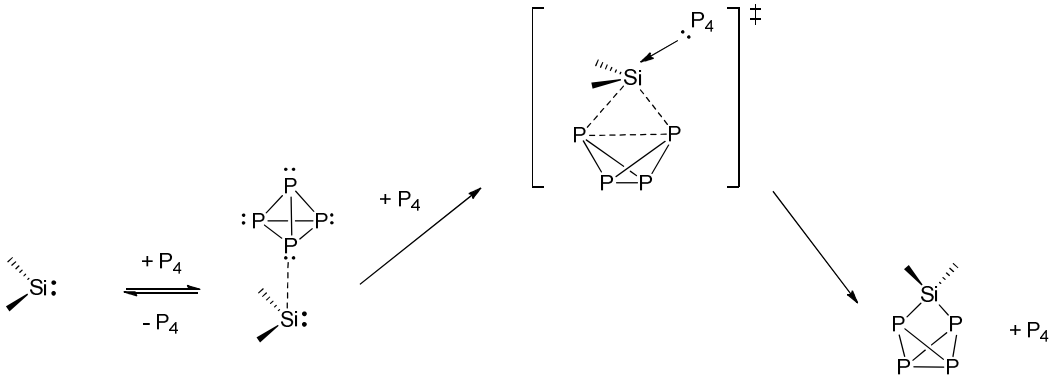

Scheme 13. Proposed mechanism for the activation of P_4 by the electrophilic silylene **20a**.

Silylenes are not the only silicon based fragments able to activate P_4. It is worth to mention that the disilene Mes_4Si_2 (**23a**), the phosphasilenes $Tipp_2SiPSiMe_2tBu$ (**23b**) and $Tipp_2SiPSi(iPr)_3$ (**23c**) are able to react with white phosphorus providing the heterobicyclo[1.1.0]butane derivatives **24a-c** respectively (Scheme 14) (Tipp = 2,4,6-$iPr_3C_6H_2$).

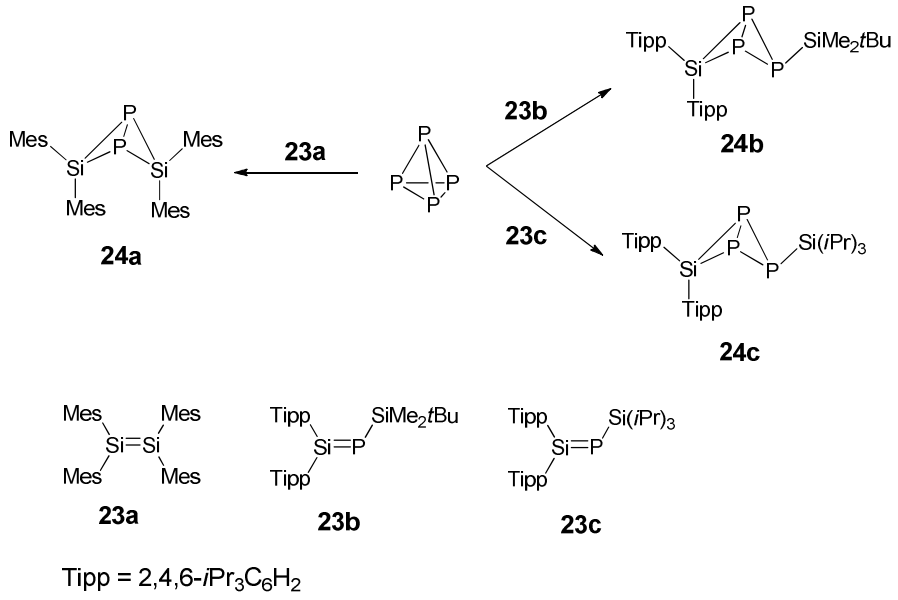

Scheme 14. White phosphorus activation by stable disilene and phosphasilenes.

1.3.3) Activation of P_4 mediated by phosphenium cations

The electrophilic reactivity toward P_4 described above is not only encountered with the silylenes, but also with the isoelectronic phosphenium

cations. The first example was reported in 2001 by the group of Krossing when it was observed that the addition of 3.5 equivalents of iodine to a solution of $[Ag(P_4)_2]^+[Al(pftb)_4]^-$ **E** (Scheme 1, page 44) in CD_2Cl_2 at -78°C resulted in the formation of the salt $[P_5I_2]^+[Al(pftb)_4]^-$ **25a** along with the generation of P_4 and PI_3. This reaction was interpreted by the initial reaction of I_2 and P_4 which gives PI_3, the latter reacts with the silver cation of **E** and gives the transient phosphenium PI_2^+ following a halide abstraction reaction. Finally, this species then inserts into one of the P-P bonds of P_4 providing the cation $P_5I_2^+$ (Scheme 15).

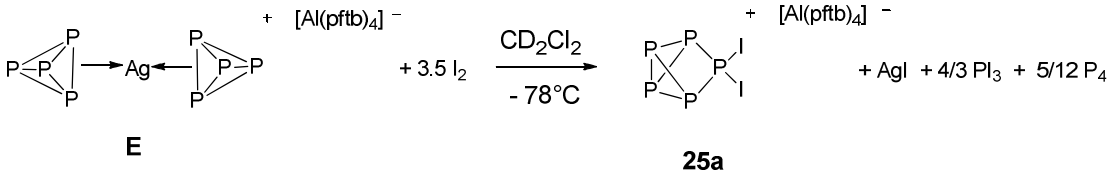

Scheme 15. In situ generation of the salt **25a** from the silver complex **E**.

In order to confirm this mechanistic hypothesis, the reaction between P_4, PBr_3 and the silver complex $Ag^+[Al(pftb)_4]^-$ was conducted at -78°C in CH_2Cl_2. The in-situ ^{31}P NMR spectroscopy showed that in solution only $[P_5Br_2]^+[Al(pftb)_4]^-$ **25b** was present after a reaction of ten days at -78°C (Scheme 16). Finally, **25b** was isolated quantitatively as a crystalline material stable below -30°C.
In the solid state the cation adopts a pseudo C_{2v} symmetry. The two P-P bond lengths involving the tetracoordinated phosphonium center (2.156 Å) are shorter than a typical single bond whereas the other bond lengths are in the range expected for single bonds (2.211 Å and 2.239 Å).

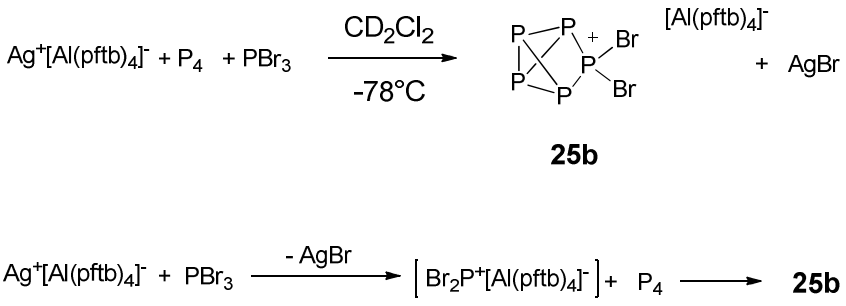

Scheme 16. Reaction pathway for the formation of **25b** involving the transient PBr_2^+ cation.

In the latter reaction, only one insertion of the dihalophosphenium fragment to the P_4 tetrahedron was observed.

However, by employing more drastic conditions, two insertions and even three insertions of the more reactive phosphenium cation Ph_2P^+ could be obtained. Thus, when one equivalent of P_4 was allowed to react at 70°C during 7 hours

without any solvent with a mixture of 8 equivalents of Ph_2PCl and 5 equivalents of $GaCl_3$, the formation of the dication **27** was observed along with the monocation **26** (Scheme 17; Eq. 1).[36] Interestingly the insertions didn't take place in two opposite P-P bonds of the tetrahedron, a situation encountered for **17** and **22** (Scheme 10 (page 51) and scheme 12 (page 53), respectively). On the contrary, the insertions involved two adjacent edges of the tetrahedron. Whereas any attempts to isolate the dication **27** failed, the monocation was formed quantitatively by changing the ratio of the reactants $P_4/Ph_2PCl/GaCl_3$ to1:1:1 (Scheme 17; Eq. 2). However, **26** is stable at room temperature in the solid state and in solution which is not the case for **25b**.

In the solid state the nearly C_{2v}-symmetric cation **26** adopts a similar structure to **25b** featuring two short bonds between the tri- and tetracoordinated phosphorus atoms (2.182 Å and 2.186 Å) and a short bond between the bridgehead phosphorus centers (2.179 Å).

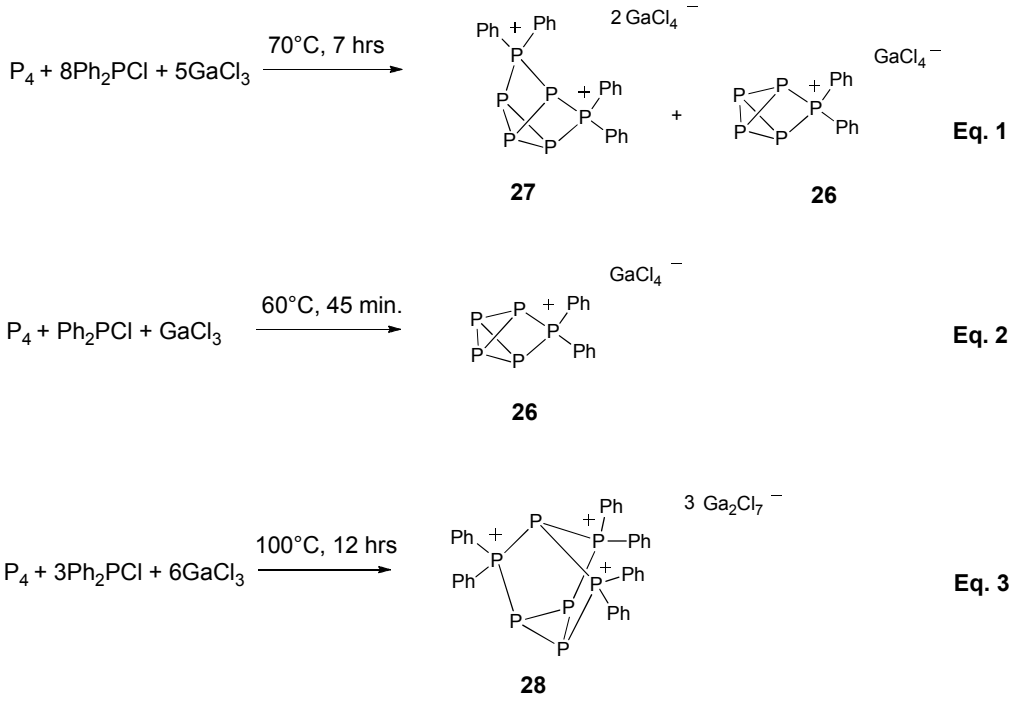

Scheme 17. Solvent free synthesis of the mono- (**26**), di- (**27**) and trication (**28**).

Increasing the ratio of the Lewis acid $GaCl_3$ by performing a 1:3:6 reaction of P_4, Ph_2PCl and $GaCl_3$ at 100°C during 12 hours gave the $(Ga_2Cl_7^-)_3$ salt **28** (Scheme 17; Eq. 3). In the solid state **28** displays a nortricyclane skeleton similar to the Ga_3P_4 core found in **13** or to the Zintl anion $[P_7]^{3-}$ (Scheme 7, page 49) but incorporating three bridging phosphonium centers and therefore being a trication.

Another interesting example of multiple insertions involving formally the diphosphenium dication $[DippNP]_2^{2+}$ and two molecules of P_4 has been reported (Scheme 18).[37] The insertion reactions proceed stepwise and each one involves a different molecule of P_4. Then, when P_4 is reacted with the in-situ generated

phosphenium cation **29**, the monocation **30** is first formed as a $[GaCl_4]^-$ salt (Scheme 18). In the solid state **30** contains a P_5 core comparable to the ones in **25a**, **25b** and **26** with the P-P bonds connecting the bridgehead phosphorus atoms and the ones involving the tetracoordinated phosphorus center being shorter (2.146-2.164 Å) than typical single bonds.
When the phosphenium cation **29** was reacted with two equivalents of P_4 in the presence of an excess of $GaCl_3$ (4 eq.), the dication **31** crystallizes as a conglomerate with **30** and contains the $[Ga_2Cl_7]^-$ counteranions. In the solid state, **31** is centrosymmetric and each P_5 core is similar to the one in the monocation **30**. However, the dication is not very stable and it undergoes decomposition in solution.

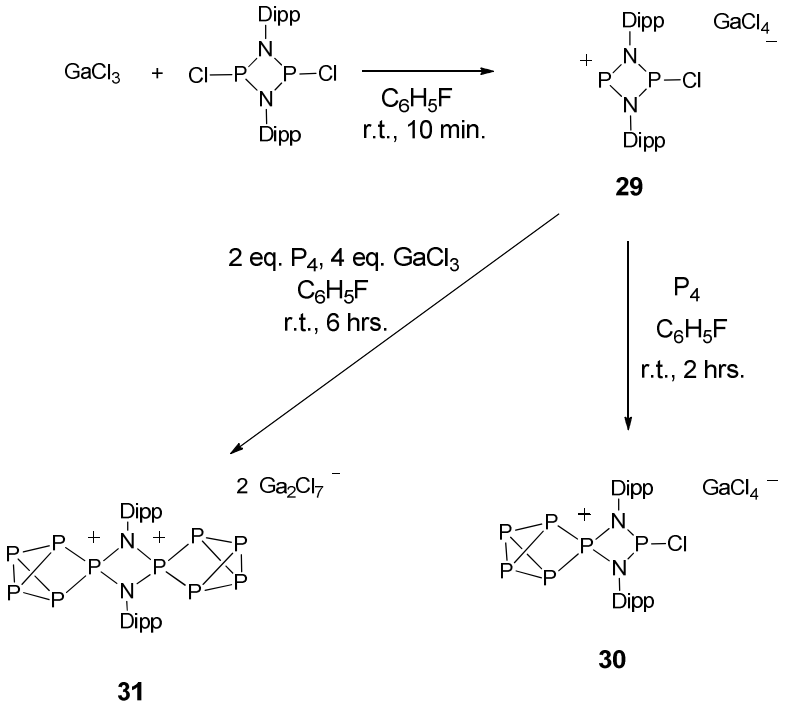

Scheme 18. Synthesis of the monocation **30** and the dication **31**.

It is also worth mentioning the unique activation of white phosphorus by the sterically hindered diphosphine **32a**. Indeed when the latter is heated in the presence of P_4 at the reflux of toluene during 2 hours, the tetraphosphabicyclobutane **33** is obtained (Scheme 19). It is proposed that the reaction proceeds through the dissociation of the diphosphine into the phosphinyl radicals **32b** which react then with P_4.[38]

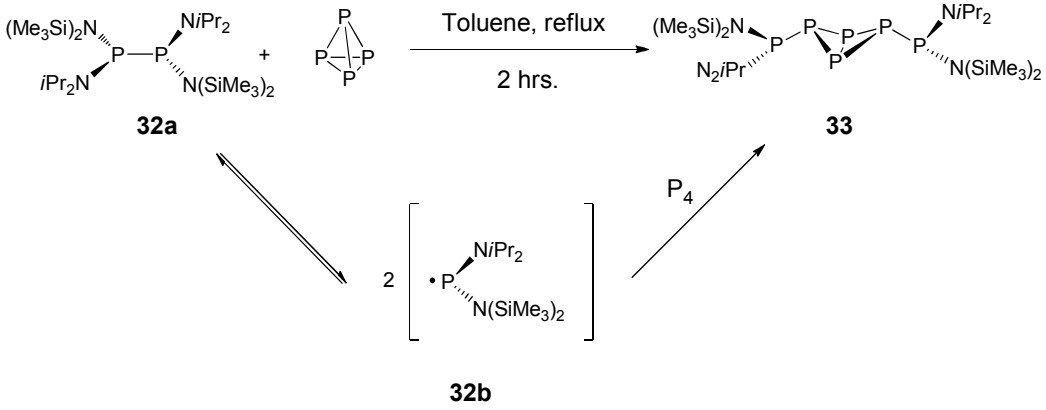

Scheme 19. Activation of P_4 mediated by the sterically hindered phosphinyl radical **32b** generated upon dissociation of the diphosphine **32a**.

To conclude, the majority of the examples of main group fragments mediated activations of P_4 mentioned above are likely to proceed through side-on electrophilic attack on the P_4 tetrahedron (Figure 1(a), page 43). However as we will see in the next chapter, the activation mediated by stable carbenes proceeds differently through nuclophilic attack by the carbene center on P_4.

1.4) P_4 activation by stable carbenes

1.4.1) Activation of P_4 by Cyclic(Alkyl)(Amino)Carbenes (CAAC)

In 2007, our group reported the first activation of P_4 by a stable carbene using the optically active, bulky, strongly electron releasing cyclic (alkyl)(amino)carbene CAAC **34** (Scheme 20).[39] When the free carbene CAAC **34** was added at room temperature to a stirred suspension of P_4 in hexane, the solution turned immediately dark blue. The ^{31}P NMR spectrum of the solution consists of two sets of AA'XX' spin systems in a 9:1 ratio (major: δ = 566 ppm and 121 ppm; minor: δ = 451 ppm and 115 ppm) revealing that the adducts contain a diphosphene moiety (δ = 566 and 451 ppm)[40] bearing phosphaalkene substituents (δ = 121 and 115 ppm)[41]. The solution contains actually a mixture of two diastereoisomers **35**(*E*) (major) and **35**(*Z*) (minor). After work-up, the product **35** was obtained as a mixture of diastereoisomers *E*/*Z* as a dark blue microcrystalline powder in 65 % yield.

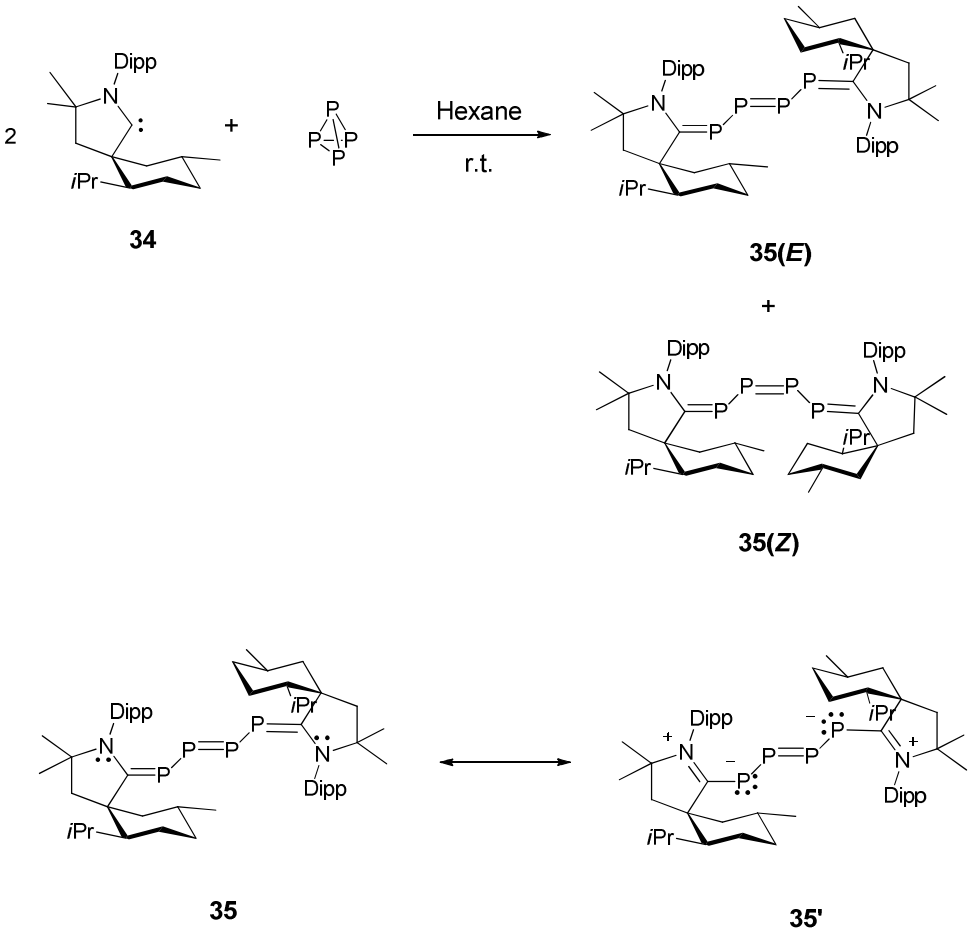

Scheme 20. Activation of P_4 by the bulky stable carbene CAAC **34** and the two resonance structures for the adduct **35**.

An X-ray diffraction study performed on a single crystal of the major diastereoisomer **35**(*E*) confirmed the structure of the latter. Compound **35**(*E*) consists of a planar P_4 fragment capped by two carbenes which displays one central P=P double bond (2.083 Å) and two external P-P single bonds (2.19 and 2.20 Å) (Figure 2). The two carbenes are connected to the central P_4 fragment through phosphaalkenes functions which contain elongated P=C bonds (1.75-1.76 Å) due to the donations of the lone pairs of the nitrogen atoms into the $\pi^*_{P=C}$ double bonds (regular non-conjugated phosphaalkenes usually display P=C double bond lengths from 1.65 to 1.67 Å).[42]

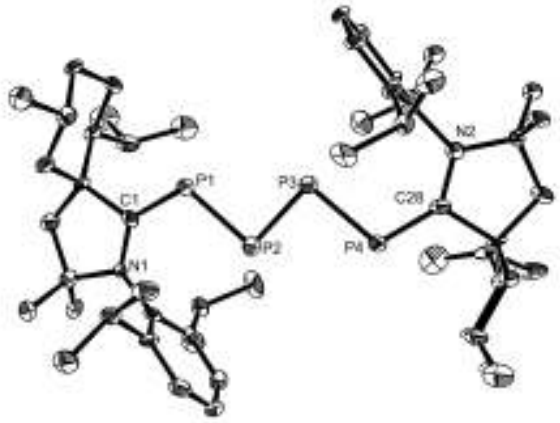

Figure 2. Solid state structure of **35(*E*)**, 50% thermal ellipsoids are shown. Hydrogen atoms are omitted for clarity.

We can also write the resonance form **35'** featuring a negative charge at each terminal phosphorus atom of the P_4 chain which becomes consequently a tetraphosphabutadienediide fragment (Scheme 20).
This tetraphosphabutadienediide core was already found in the previously mentioned adducts **6** (see Scheme 3, page 46) and **19** (see Scheme 11, page 52) obtained by nucleophilic activation of P_4 by the supersilyl anion tBu$_3$Si$^-$Na$^+$ (**3**(Na$^+$)) and the weakly dimerized dithallene (TlAr^{Dipp})$_2$ **18**, respectively. Calculations performed on the parent model CAAC **36** showed that the formation of **35** could be rationalized by a nucleophilic activation of P_4. The computed mechanism is provided in details in Scheme 21.

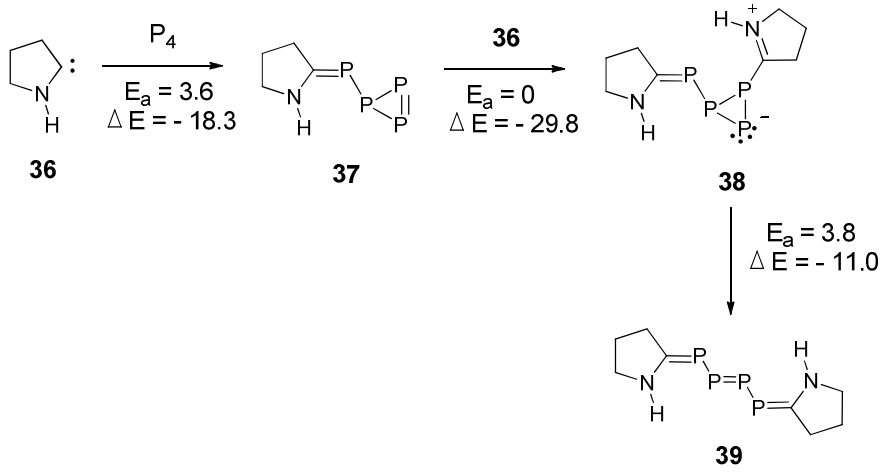

Scheme 21. Calculated pathway for the nucleophilic activation of P_4 mediated by the parent CAAC **36** (Energy values are given in kcal.mol^{-1}).

In the first step the triphosphirene **37** is formed after nucleophilic attack by the carbene on P_4. This process is exothermic by 18.3 kcal.mol^{-1} and involves a very small energy barrier of 3.6 kcal.mol^{-1}. Then in a second step, the attack by a

second carbene on **37** takes place without activation barrier giving the zwitterionic adduct **38**. The latter undergoes a ring opening with an energy barrier of 3.8 kcal.mol^{-1} affording finally the P_4 adduct **39** being 11 kcal.mol^{-1} lower in energy than **38**. This pathway is in agreement with the postulated mechanism for the nucleophilic activation of white phosphorus by tBu$_3$Si$^-$ (**3**) which was supposed to take place through the formation of the transient triphosphirene **5** (Scheme 3, page 46).[17, 19] The existence of a triphosphirene intermediate analogous to **37** was also confirmed experimentally by performing the reaction in the presence of a large excess of 2,3-dimethylbutadiene (45 eq.). In this case, the transient triphosphirene **40** was trapped by the diene giving the corresponding [4+2] cycloadduct **41** in 52 % yield as a single diastereoisomer (Scheme 22). The structure of the latter was proved by X-ray diffraction analysis (Figure 3).

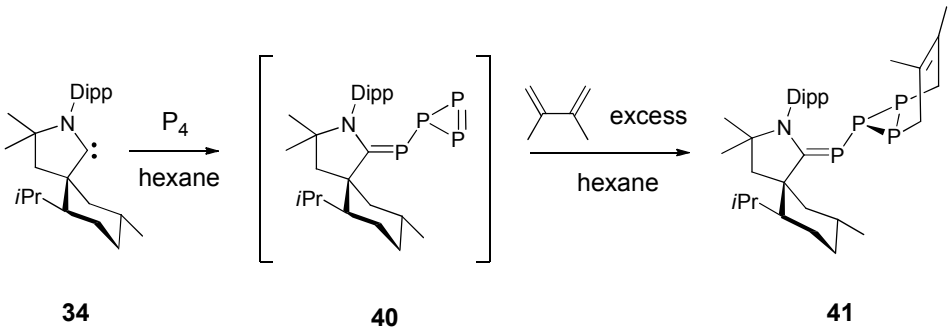

Scheme 22. Trapping of the transitient triphosphirene by 2,3-dimethylbutadiene.

Figure 3. Solid state structure of **41**, 50% thermal ellipsoids are shown. Hydrogen atoms are omitted for clarity.

To probe the reactivity of the diphosphene fragment, the adduct **35**(*E*) was reacted with 2,3-dimethylbutadiene. The Diels-Alder reaction proceeded cleanly at room temperature affording the [4+2] cycloadduct **42** in good yield (Figure 4). Interestingly due to the chirality brought by the CAAC fragments, according to the ^{31}P NMR spectroscopy, the reaction proceeded with more than 95% of diastereoselectively (Scheme 23).

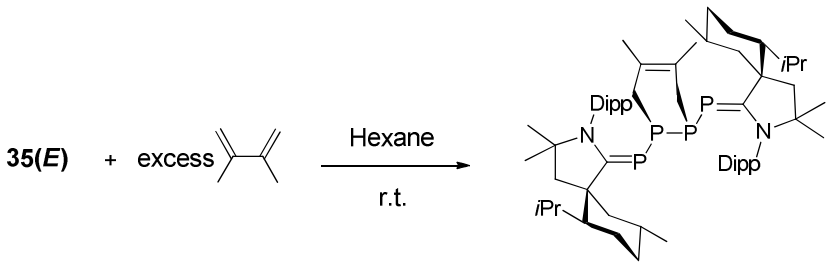

42

Scheme 23. Diastereoselective [4+2] cycloaddition of 2,3-dimethylbutadiene and P_4 adduct **35(*E*)**.

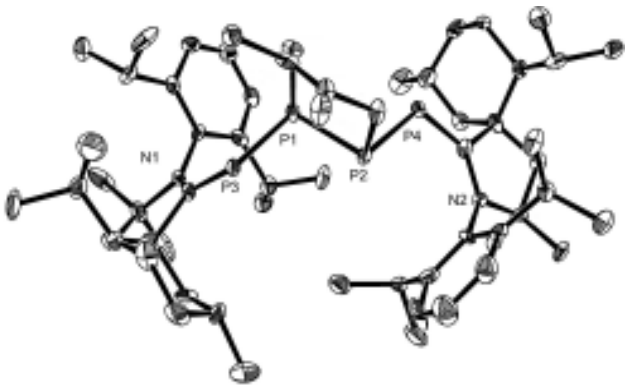

Figure 4. Solid state structure of **42**, 50% thermal ellipsoids are shown. Hydrogen atoms are omitted for clarity.

It is worth mentioning that, in this reaction two phosphorus atoms directly provided from white phosphorus are linked to an external organic substrate (2,3-dimethylbutadiene). Therefore, it paves the way for the elaboration of a catalytic cycle combining directly white phosphorus and organic molecules.
Interestingly, similar P_4 activation pathways giving linear P_4 chains but taking places in the coordination sphere of transition metals have been reported. The most relevant examples concern the group 9 transition metals. However, here the role of the nucleophile which was in the previous case the carbene is now played by the metal ligand and can be a phosphine, an alkyl, an aryl or a hydride. When white phosphorus was reacted with $Co^{+}(BF_4^{-})_2.6H_2O$ in the presence of dppm, the complex cation **J** containing the zigzag ligand $Ph_2PCH_2PPh_2(PPPP)PPh_2CH_2PPh_2^{2+}$ **43b** was obtained and was characterized by X-ray diffraction (Scheme 24).[43] It was concluded that the Co metal is in a (-I) oxidation state and is coordinated to the dicationic η^6 ligand **43b** in a pseudotetrahedral geometry. During this reaction, the P_4 fragment is *formally*

oxidized into the tetraphosphabutadiene dication **43a** which is then nucleophilically attacked twice by the dppm at the external positively charged phosphorus atoms giving finally the zigzag ligand **43b** (Scheme 24).

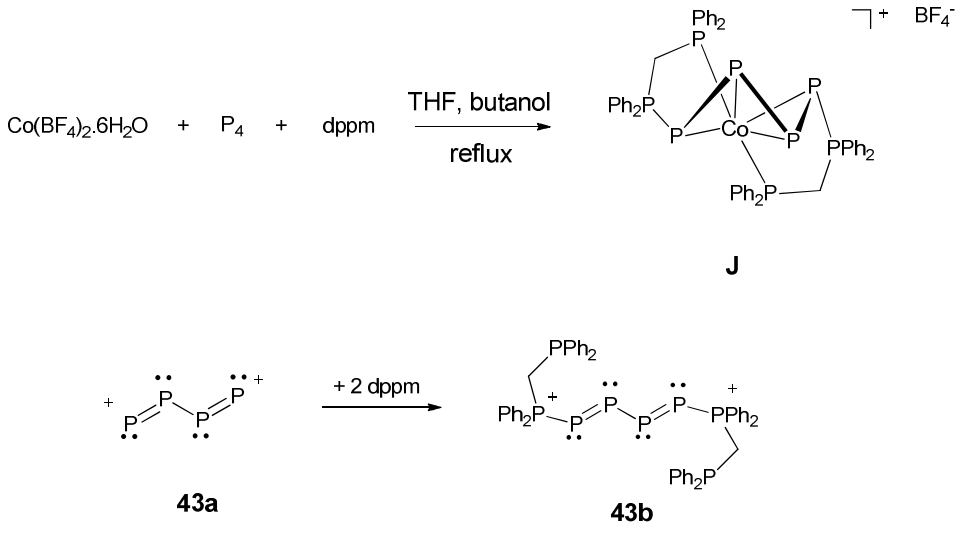

Scheme 24. Formation of the cationic cobalt complex **J** carrying the η^6 ligand **43b** obtained formally by nucleophilic attack of the dppm on **43a**.

Similar frameworks to the intermediate triphosphirene **40** (Scheme 22) stabilized in the coordination sphere of a metal could also be obtained. Thus, when the complexes $[Rh(dppm)_2]^+OTf^-$ or $[Ir(dppm)_2]^+OTf^-$ are reacted with P_4 in CH_2Cl_2 at room temperature, the complexes **K** and **L** containing the triphosphirene $Ph_2PCH_2PPh_2(PPPP)^+$ ligand **44** are obtained (Scheme 25). Again, like **43b** this ligand probably arises from the nucleophilic attack of one of the dppm ligand initially present in the complexes on P_4. Consequently, the triphosphirene **44** can be seen as an intermediate along the reaction pathway leading to **43b** in the same way that the triphosphirene **40** was an intermediate in the formation of **35**(*E*/*Z*) (see scheme 21, page 60).[25]

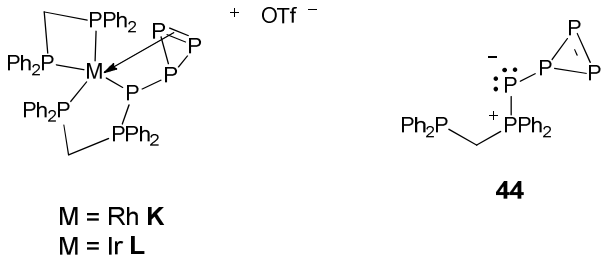

Scheme 25. Previously reported complexes **K** and **L** carrying the triphosphirene ligand **44** formed by a nuclophilic attack of a dppm ligand from the starting Rh(I) or Ir(I) complexes on P_4.

Similar reactions leading to the neutral Rh(I) complexes **M-Q** have been reported (scheme 26). However in this case the hydride or alkyl ligands initially present on the metal play the role of the nucleophiles. For the formation of complex **Q**, it is supposed that first ethene inserts into the Rh-H bond and secondly the resulting ethyl migrates from Rh to the phosphorus atom of P_4. The structures of the complexes **M-Q** were assigned on the basis of multinuclear and multidimensional NMR studies.[44]

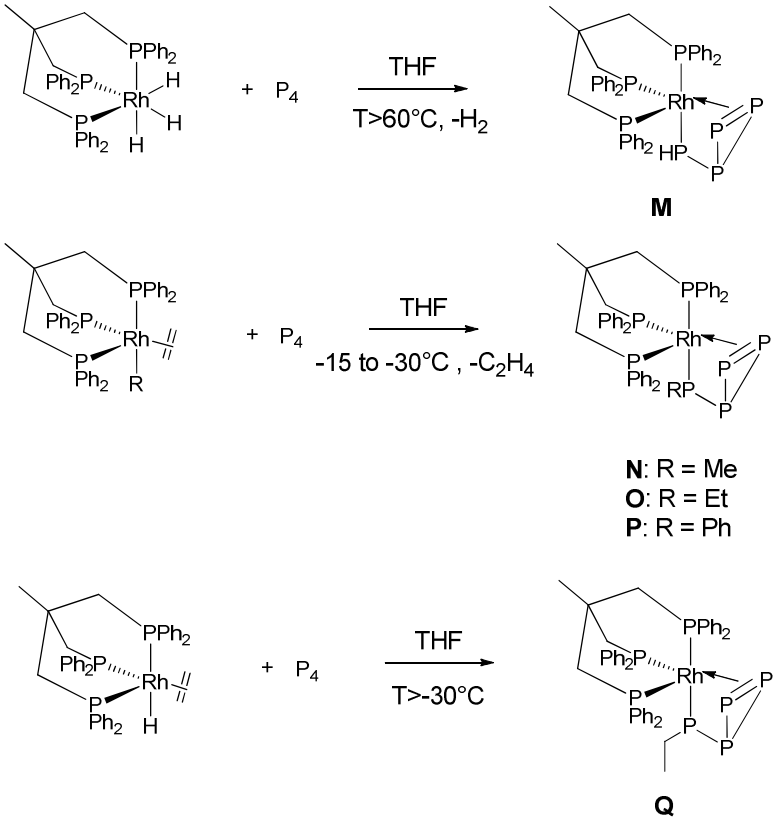

Scheme 26. Formation of the η^3-triphosphirene rhodium complexes **M-Q**.

1.4.2) Aggregation of P_4 mediated by N-Heterocyclic carbenes (NHCs)

When the less basic but also less electrophilic NHC **45** is used in the reaction with white phosphorus a very different product is obtained (Scheme 27).[45] Indeed, when the free carbene was added at room temperature to a suspension of P_4 in hexane, the ^{31}P NMR spectrum of the crude revealed the formation of the P_4 adducts **46**(*E*/*Z*) similar to the 2,3,4,5-tetraphosphatriene adducts **35**(*E*/*Z*) (Two sets of signals are observed: major, δ = 396.7 ppm and 69.4 ppm; minor, δ = 506.5 ppm and 63.0 ppm). However, on the contrary of the latter, the adducts **46**(*E*/*Z*) could not be isolated and appeared to be transient. On the other hand, when the mixture was stirred at 70 °C overnight, a yellow precipitate

appeared. The ^{31}P NMR spectrum of a THF solution of the obtained compound displayed a scarry set of 10 broad peaks from +120 ppm to -160 ppm in a 1:1:1:1:1:1:1:3:1:1 ratio suggesting the presence of a species containing twelve phosphorus atoms. Thanks to X-ray diffraction analysis, the structure was unambiguously assigned revealing that the compound **47** consists of a P_{12} cluster capped by two NHC fragments (Scheme 27 and figure 5).

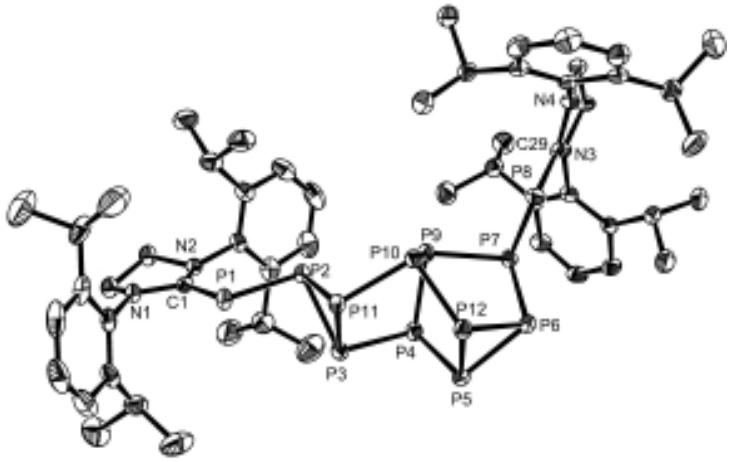

Figure 5. Solid state structure of **47**, 50% thermal ellipsoids are shown. Hydrogen atoms are omitted for clarity.

In the solid state, the P-P bond lengths within the P_{12} core lay between 2.176 and 2.233 Å which are close to the typical value for a P-P single bond. Also interestingly the P_{12} cluster includes the nortricyclane P_7 framework (P_4-P_5-P_6-P_7-P_9-P_{10}-P_{12} in figure 5) which is often encountered in the polyphosphides obtained by reduction of white phosphorus with alkali metals and subsequent agglomeration.[46]

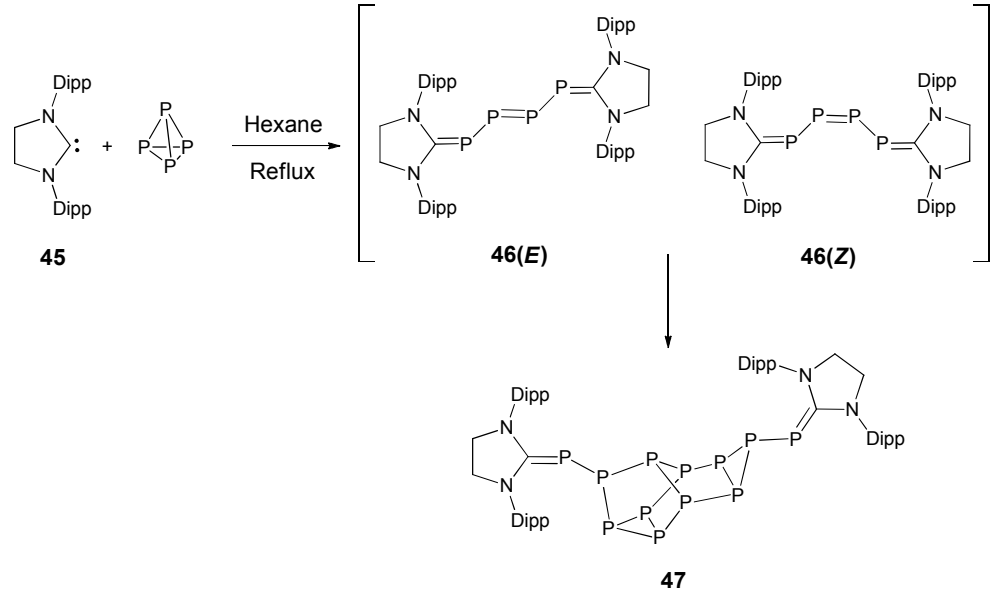

Scheme 27. NHC mediated aggregation of P_4 leading to the P_{12} cluster **47**.

Aggregation of P_4 is commonly observed for transition metal complexes. For example, we can mention the P_8Fe_4 complex **R** prepared by cophotolysis of $[Cp'Fe(CO)_2]_2$ (Cp' = C_5H_4Me) in the presence of P_4 at room temperature,[47] the $P_{10}Rh_4$ complex **S** prepared by the reaction at 190°C between $[Cp''Rh(CO)_2]$ (Cp'' = 1,3-tBu$_2$C$_5$H$_3$) and P_4,[48] and the $P_{12}Co_3$ complex **T** prepared by cophotolysis of $[Cp''Co(CO)_2]$ and P_4 at room temperature[49] (Scheme 28). However, aggregation mediated by main group fragments has been elusive and so far the two largest P_n aggregates obtained prior to **47** contain only eight phosphorus atoms (Scheme 28).

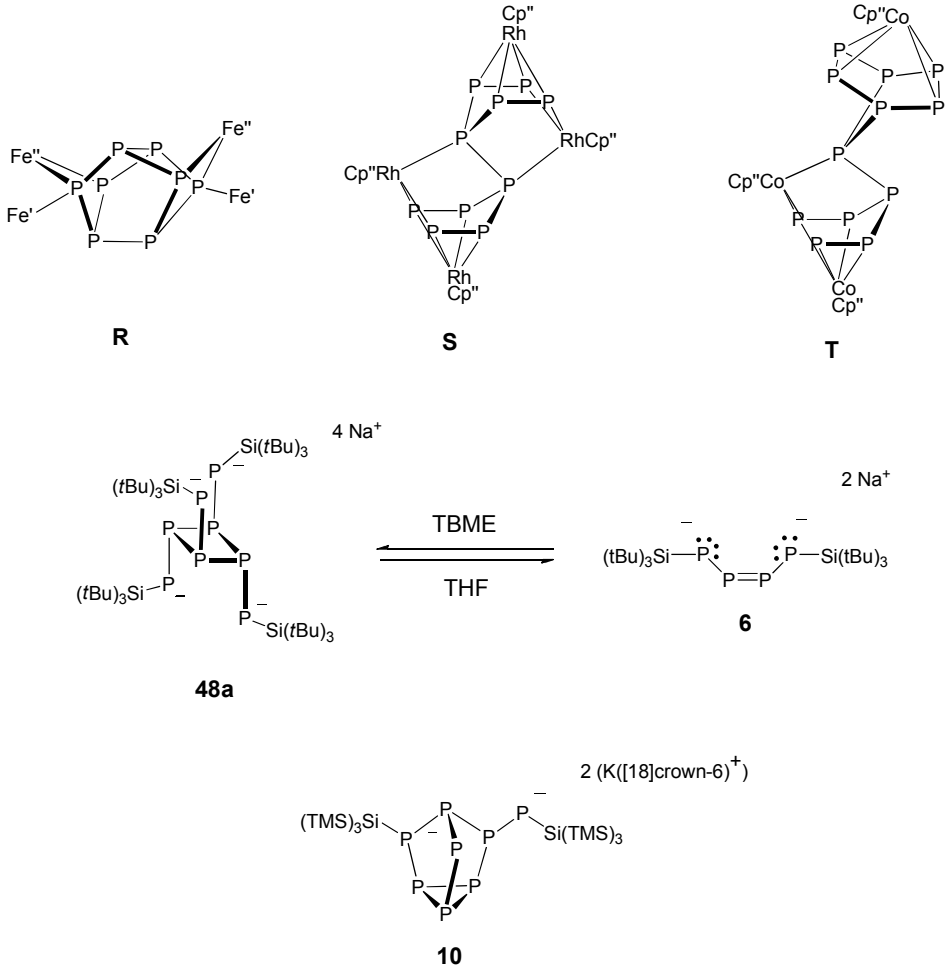

Scheme 28. Previously reported P_n aggregates coordinated by transition metal fragments (**R**, **S** and **T**) or obtained from the highly nucleophilic silyl anions tBu$_3$Si$^-$Na$^+$ or [(Me$_3$Si)$_3$Si$^-$K$^+$([18]crown-6)] (**10** and **48a**). (Fe' = [Fe(CO)$_2$Cp']; Fe" = [Fe(CO)Cp']; Cp' = C_6H_5Me and Cp" = 1,3-tBu$_2$C$_5$H$_3$).

Indeed we have already mentioned the aggregate **10** (see scheme 5, page 47) formed by reaction between P_4 and the hypersilyl complex $[(Me_3Si)_3Si^-K^+([18]crown-6)]$ **9**.[22] The other adduct **48a** is obtained by reaction between two equivalents of the super silyl anion tBu$_3$Si$^-$Na$^+$ **3**(Na$^+$) and white phosphorus in the non polar solvent TBME (*tert*-butyl methyl ether)[17]. Interestingly, **48a** results from the solvent dependant dimerization of the already discussed tetraphosphabutadienediide **6** (see Scheme 3, page 46) which takes place in TBME. The dimerisation is reversible and when **48a** is resolved in THF, compound **6** is reformed via a [2+2] cycloreversion (Scheme 28).

The very different products obtained upon reaction with white phosphorus when moving from the CAAC to the NHC outlines the importance of the electronic parameters of the carbenes on the outcome of the reaction. In order to better understand the difference of reactivity between **34** and **45**, calculations concerning the aggregation mechanism were performed starting from the parent model **49** (Scheme 29). Like for the CAAC **34**, the first step of the aggregation consists on the nucleophilic attack of the NHC on P_4 affording the usual triphosphirene **50**. Then, a second NHC adds to the latter to give the diphosphene **51**. Compound **51** undergoes a [3+2] cycloaddition with **50**, which is exothermic by 13.3 kcal.mol^{-1} and proceeds without energy barrier. Then the cycloadduct **52** rearranges with the loss of two NHCs into the heptaphosphanorbornadiene **53** undergoing (without energy barrier) a $[\pi^2 + \pi^2 + \pi^2]$ reaction with an other triphosphirene **50** to give the final P_{12} cluster similar to **47**. The last step is exothermic by 54.9 kcal.mol^{-1}.

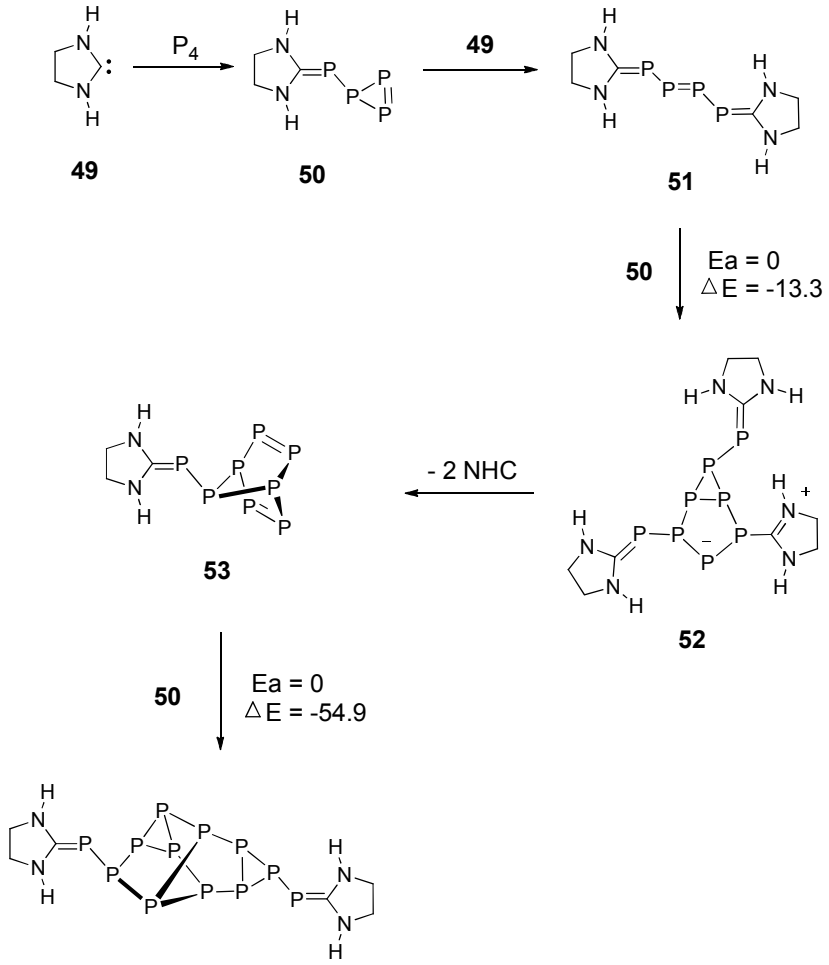

Scheme 29. Calculated mechanism for the aggregation of P_4 into the P_{12} cluster mediated by NHC (Energy values are given in kcal.mol^{-1}).

Again, performing the reaction of **45** and P_4 in the presence of 2,3-dimethylbutadiene confirmed the mechanism proposed above. The two products **54** and **55** resulting respectively from the trapping of the intermediate triphosphirene analogous to **50** and the intermediate diphosphene **46**(*E*) were isolated (Scheme 30) and structurally confirmed by X-ray diffraction studies (figure 6).

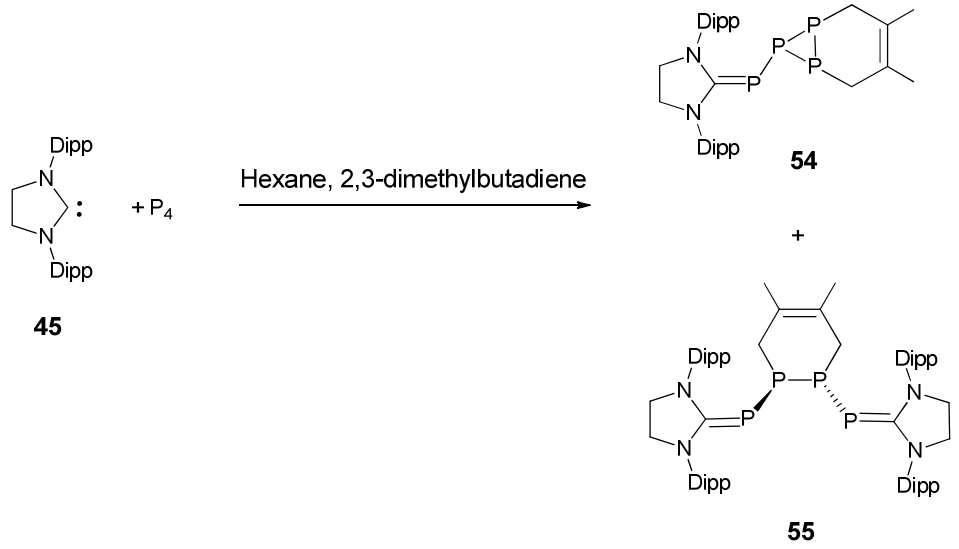

Scheme 30. Products **54** and **55** resulting from the trapping with 2,3-dimethylbutadiene.

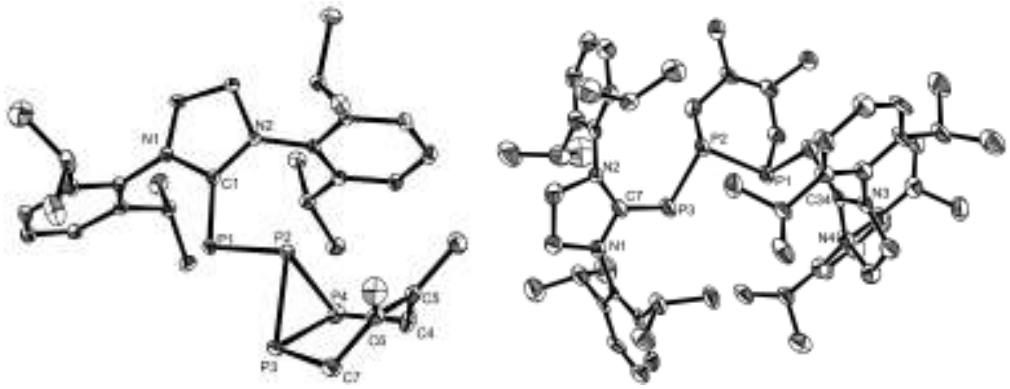

Figure 6. Solid state structure of **54** (left) and **55** (right), 50% thermal ellipsoids are shown. Hydrogen atoms are omitted for clarity.

1.5) Summary and objectives

To summerize, the important influence of the electronic parameters of the carbenes on the final result of the reaction with P_4 is obvious. Indeed CAACs are more electrophilic (more π accepting) than NHCs (see Scheme 31), therefore the P=C bonds in the P_4 adducts **35**(*E*/*Z*) (Scheme 20, page 59) are less polarized than the corresponding bonds in the transient adducts **46**(*E*/*Z)* (Scheme 27, page 65). Moreover, NHCs are less basic than CAACs and therefore they are better leaving groups. In consequence CAACs make stronger P=C bonds than the NHCs and are harder to dissociate from the phosphorus fragment. For this reason, the reaction involving the NHC results in the formation of the cluster **47** through the dissociation of the free carbene during the aggregation process (see

transformation of **52** to **53** in scheme 29, page 68). No cluster formation mediated by the CAACs has been observed. However, the steric parameters of the carbenes should also play an important role in the outcome of these reactions. It would be then interesting to study their influence and particularly to perform the reaction with smaller carbenes.

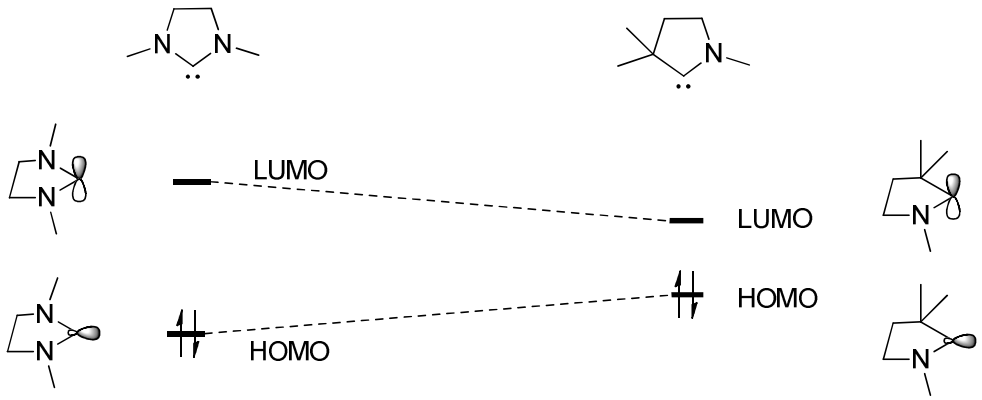

Scheme 31. Comparison of the electronic properties of NHCs versus CAACs.

Although the preparation and characterization of large phosphorus clusters is fundamentally interesting due to the possibility of discovering new phosphorus allotropes with the aim of making phosphorus-based nanoparticules, the most synthetic useful organophosphorus compounds contain only one or two phosphorus atoms. Therefore it is of particular interest of developing new tools which are able to perform the fragmentation of white phosphorus into P_1 or P_2 fragments. In a first project we tried to see if some carbenes were able to accomplish this task.

1.6) Results and discussion

1.6.1) Reaction between P_4 and an electrophilic acyclic(alkyl)(amino)carbene: formation of a triphosphabicyclo[1.1.0]butane

As we pointed out before, the ideal carbene for the fragmentation of P_4 must be quite electrophilic in order to make strong bonds with the phosphorus fragment but also must be basic enough in order to be a "bad" leaving group. In 2004 our group reported the synthesis of the acyclic(alkyl)(amino)carbene **I**.[50] The reactivity of this species showed that **I** is more electrophilic and also more nucleophilic than diamino-carbenes. This was well illustrated by the cyclopropanation reaction between **I** and methyl acrylate.
Consequently, the acyclic(alkyl)(amino)carbene **I** appears to be the best candidate for the fragmentation of P_4. Thus, when an excess of **I** (3.5 eq.) was reacted with white phosphorus in diethyl ether at room temperature for two hours, a clean reaction occurred (Scheme 32).[51]

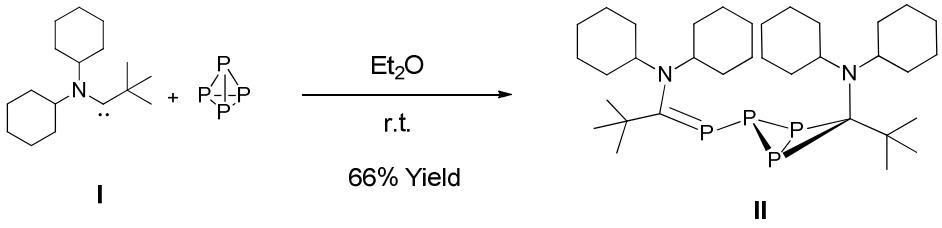

Scheme 32. Reaction of white phosphorus with acyclic (alkyl)(amino)carbene **I**

The $^{31}P\{^{1}H\}$ NMR spectrum of the solution showed that the reaction was complete and displayed one set of three signals consistent with an AMX_2 spin system (Figure 7). One phosphorus center (P_A) displays a relatively low field chemical shift (δ_A = 238.8 ppm, dt) and exhibits a strong ^{1}J coupling ($^{1}J_{AM}$ = 220 Hz) with one phosphorus center (P_M) and a ^{2}J coupling with two equivalent phosphorus nuclei (P_X) ($^{2}J_{AX}$ = 87 Hz).

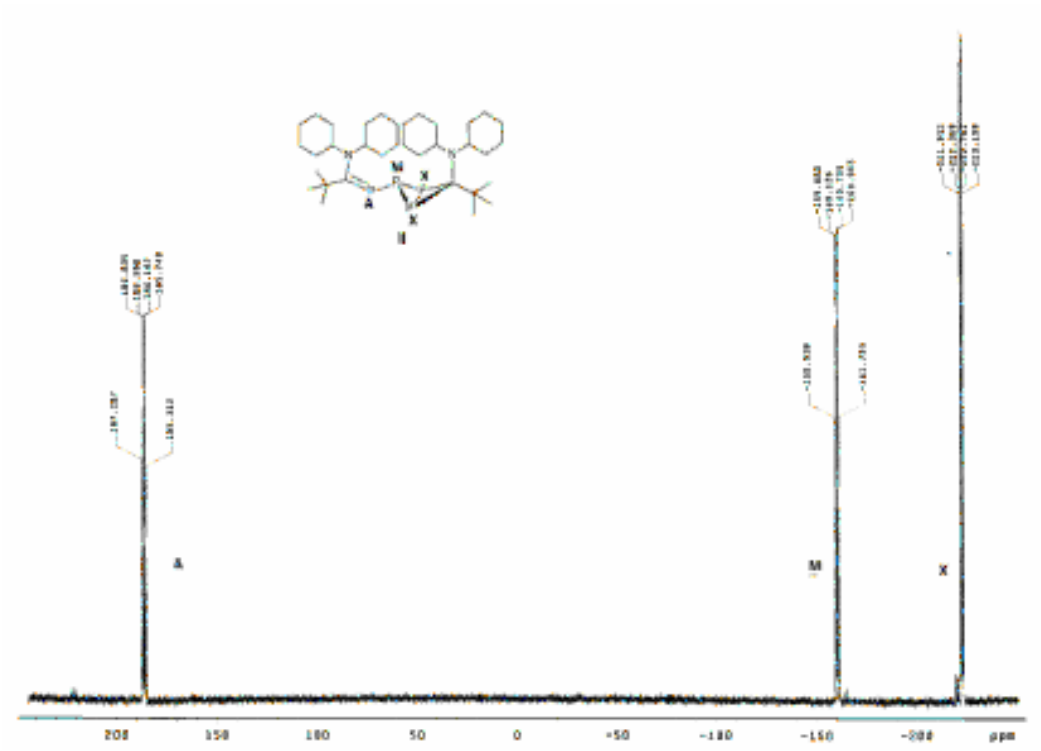

Figure 7. $^{31}P\{^{1}H\}$ spectrum of compound **II** displaying an AMX_2 spin system.

Also the two other phosphorus signals are shifted high field: one phosphorus nucleus (P_M) displays a signal at δ_M = -105.8 ppm (dt) and exhibits two strong ^{1}J coupling, one with the already mentioned P_A center ($^{1}J_{MA}$ = 220 Hz), and the other one with two equivalent phosphorus nuclei (P_X) ($^{1}J_{MX}$ = 167 Hz)). The other signal corresponds to the two remaining equivalent phosphorus nuclei, δ_X = -168.2 ppm (dd). It exhibits a strong ^{1}J coupling with the P_M center and a ^{2}J

coupling with the P_A center ($^1J_{XM}$ = 167 Hz and $^2J_{XA}$ = 87 Hz). The chemical shift of the P_A nucleus (δ_A = 238.8 ppm) is in the range of the observed values for inversed polarized phosphaalkene moiety[41] but is quite higher than the corresponding chemical shift values in the P_4 adducts **35**(*E*) (δ = 121ppm) and **35**(*Z*) (115 ppm) obtained with the cyclic version (Scheme 20, page 59). The high field chemical shifts displayed by the three other phosphorus centers are usually observed for phosphorus atoms involved in three members rings suggesting that the phosphorus centers P_M and P_X are linked together in a triphosphirane ring.[52] After work-up the product **II** was obtained as a yellow powder in 66 % yield based on P_4. The $^{13}C\{^1H\}$ NMR spectrum of **II** in THF-d_8 displays one doublet at 227.6 ppm ($^1J_{PC}$ = 89 Hz) confirming the presence of the phosphaalkene moiety. However the ^1H NMR spectrum indicates two different sets of protons in a 1:1 ratio corresponding each to the organic fragment [cHex$_2$NC*t*Bu] derived from the starting carbene **I** (for example one singlet for each *tert*-butyl fragment at δ = 1.33 ppm and at δ = 1.16 ppm). This suggests that the adduct **II** contains two non equivalent carbene fragments. All together these results are consistent with the triphosphabicyclo[1.1.0]butane structure assigned for **II** (Scheme 32).
The structure of the latter was unambiguously confirmed by X-ray diffraction study performed on a single crystal of **II** grown by layering acetonitrile on top of a THF solution (Figure 7).

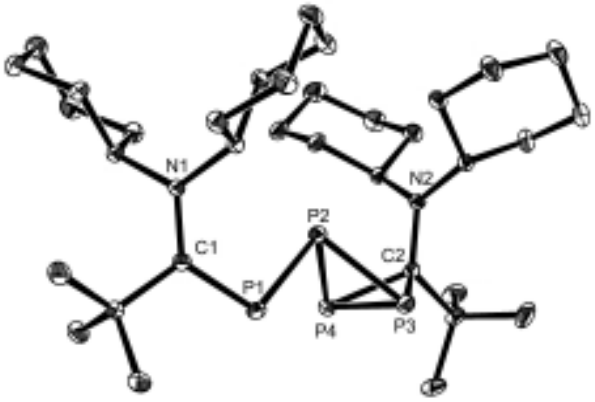

Figure 7. Solid state structure of **II**, 50% thermal ellipsoids are shown. Hydrogen atoms are omitted for clarity. Selected bond distances [Å] and angles[°]:P(1)–P(2) 2.2320(19), P(2)–P(3) 2.220(2), P(2)–P(4) 2.2342(17), P(3)–P(4) 2.1700(19), C(1)–P(1) 1.747(2), C(2)–P(3) 1.912(2), C(2)–P(4) 1.925(2), N(1)–C(1) 1.3893(19), N(2)–C(2) 1.4472(18); P(1)-P(2)-P(3) 93.29(3), P(1)-P(2)-P(4) 91.99(6), P(3)-P(2)-P(4) 58.31(7), P(2)-P(4)-P(3) 60.51(5), P(3)-P(4)-P(2) 60.51(5).

In the solid state, the dihedral angle in the bicycle between the two three-members rings is 107.7°. The P-P bond lengths [2.17-2.23 Å] are in the range expected for single P-P bonds with the distance between the bridgehead phosphorus atoms being slightly shorter. The P-C bonds within the bicycle (1.912 and 1.925 Å) are

longer than typical acyclic P-C single bonds (1.85 Å). The triphosphabicyclo[1.1.0]butane core in **II** is structurally similar to the ones in the previously known triphosphabicyclobutanes reported by Appel and Niecke in 1988.[53] The P=C double bond length (1.75 Å) compares well with the corresponding bond in **35**(*E*) (1.75-1.76) (Figure 2, page 60) and is consistent with an inversed polarized phosphaalkene.[41] Moreover, like in **35**(*E*), the phosphaalkene has a *Z* configuration due to the steric hindrance provided by the *tert*-butyl fragment.
Interestingly, the C(1)-P(1)-P(2)-P(3)-P(4)-C(2) core in **II** (see figure 7) and the 2,3,4,5-tetraphosphatriene core in **35**(*E*) are valence isomers of one another. The formation of **II** can be readily rationalized if one recalls the first step of the P_4 nucleophilic activation's mechanism. As in the former cases, first a triphosphirene is formed but here the carbene **I** is so electrophilic that instead of inducing the ring opening it undergoes a cyclopropanation-like reaction (Scheme 33).

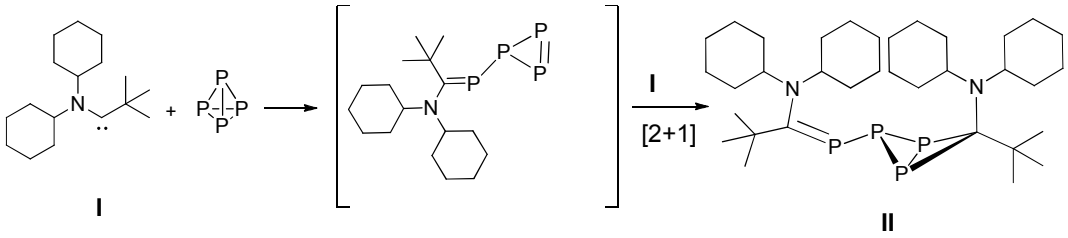

Scheme 33. Postulated mechanism for the reaction between **I** and P_4.

1.6.2) Reaction between P_4 and the small cyclohexyl cyclic(alkyl)(amino)carbene: isolation of P_4 and P_2 adducts

Considering the results obtained above, we then decided to move to the less electrophilic cyclohexyl CAAC **III** (scheme 35). We were hoping that such a cyclic CAAC would be able to induce the formation of the 2,3,4,5-tetraphosphatriene adduct analogous to **35**(*E*/*Z*) (see scheme 20, page 59) or **46**(*E*/*Z*) (see scheme 27, page 65), but then would react again (Scheme 34). The second attack of another carbene to the central P_4 chain would then lead to the unprecedented fragmentation of P_4 into P_2 or P_1 and P_3 units.

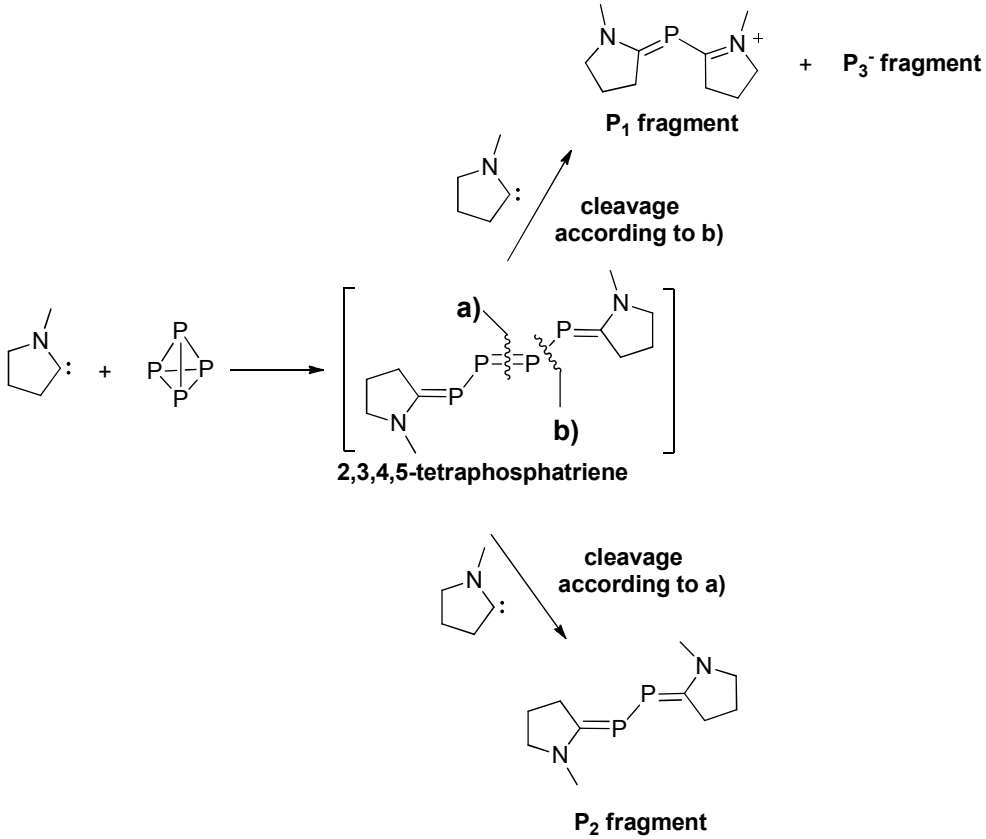

Scheme 34. Targeted fragmentation of P_4 mediated by carbenes.

Thus, addition of three equivalents of **III** to a suspension of P_4 in ether resulted immediately in a color change from light yellow to dark red. After two hours of stirring at room temperature, the ^{31}P $\{^1H\}$ NMR spectrum of the solution indicated the total consumption of P_4. Instead, two new products were present, one displaying an AX_3 spin system with a strong ^1J coupling (**IV**: δ_A = -66.2 ppm (q) and δ_X = 68.1 ppm (d), $^1J_{AX}$ = 227 Hz) and the other one displaying a singlet at δ = 59.38 ppm (**V**). After work-up, the two products were isolated in moderate yields (**IV**: 57% and **V**: 12% based on P_4).

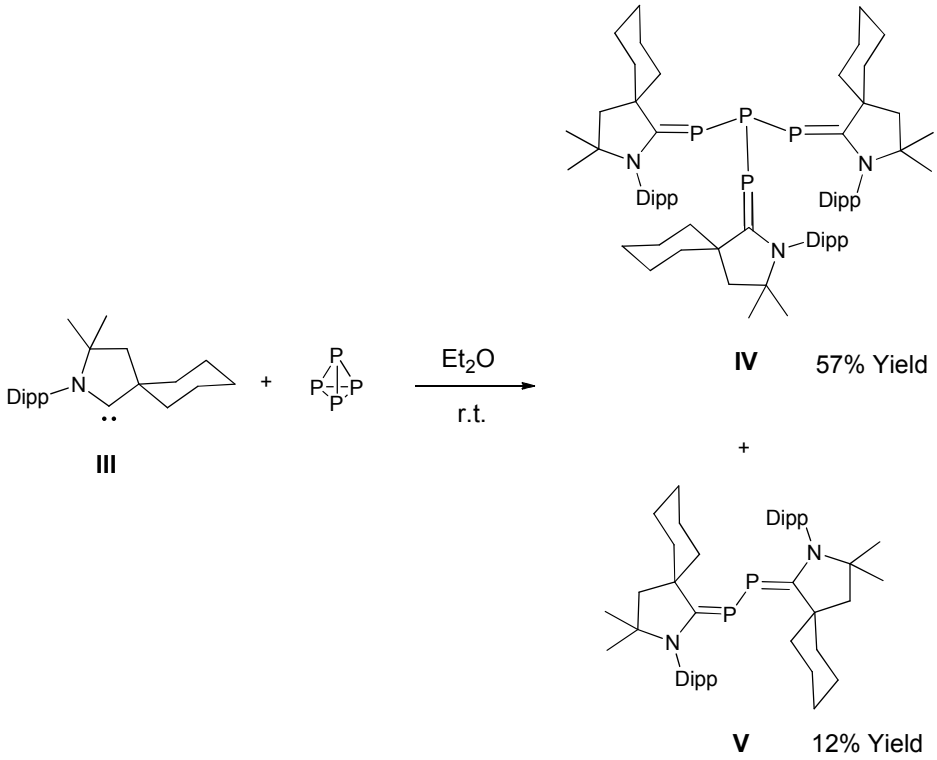

Scheme 35. Reaction of white phosphorus with the non-hindered cyclohexyl CAAC **III**.

For the major product (**IV**), the $^{31}P\{^{1}H\}$ NMR data indicates the presence of three magnetically equivalent phosphorus nuclei which are directly connected to a central one. Moreover, the chemical shift of theses three equivalent phosphorus atoms (δ_A = 68.1 ppm) is indicative of an inversed polarized phosphaalkene. However, this chemical shift is relatively high field in comparison with the ones in **35**(*E*) (+115 ppm) and **35**(*Z*) (+121 ppm).[41] This is also confirmed by the $^{13}C\{^{1}H\}$ NMR spectrum in C_6D_6 which displays a low field signal at δ = 207.4 ppm. The ^{1}H NMR spectrum shows only one set of signals for the carbene fragment, consequently all together, these data are consistent with a tripodal molecule incorporating three carbene fragments. This product (**IV**) results formally from the breaking of three P-P bonds of the same face of the P_4 tetrahedron (Scheme 35). This structure was confirmed by X-ray diffraction analysis performed on a single crystal of **IV** grown by slow evaporation of a hexane solution at room temperature (Figure 8). In the solid state, compound **IV** displays P-P bond lengths consistent with P-P single bonds (average 2.22 Å) and the P=C bond lengths (average 1.73 Å) are comparable to the ones in the adduct **35**(*E*) (figure 2, page 60) (1.75 Å and 1.76 Å).

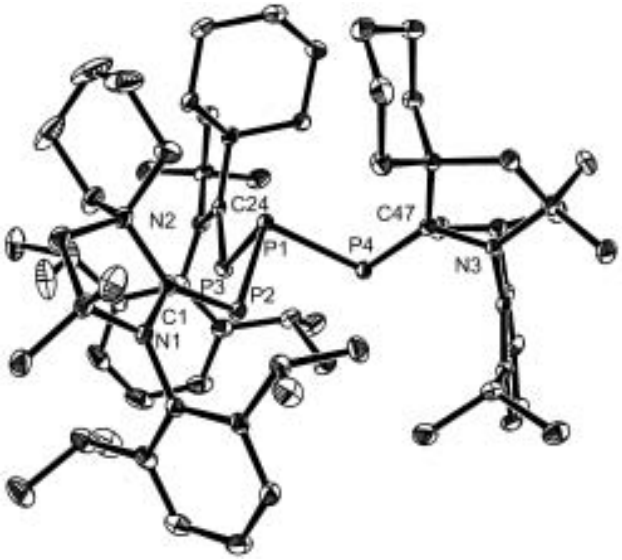

Figure 8. Solid state structure of **IV**, 50% thermal ellipsoids are shown. Hydrogen atoms are omitted for clarity. Selected bond distances [Å] and angles [°]: P(1)–P(2) 2.2168(6), P(1)–P(3) 2.2270(6), P(1)–P(4) 2.2192(7), C(1)–P(2) 1.7328(19), C(24)–P(3) 1.7343(18), C(47)–P(4) 1.7324(18), N(1)–C(1) 1.374(2), N(2)–C(24) 1.370(2), N(3)–C(47) 1.368(2); P(2)-P(1)-P(4) 90.15(2), P(3)-P(1)-P(4) 90.15(2), P(2)-P(1)-P(4) 90.15(2), C(1)-P(2)-P(a) 108.22(6), C-(24)-P(3)-P(1) 106.62(6), C(47)-P(4)-P(1) 108.45(7).

Concerning now the minor product (**V**) obtained along with **IV**, the $^{31}P\{^{1}H\}$ NMR spectrum displays a unique singlet at δ = 59.38 ppm. In addition, the $^{13}C\{^{1}H\}$ NMR spectrum in C_6D_6 displays also a low field signal at δ = 202.2 ppm consisting of a doublet of doublet due to coupling with two phosphorus centers ($^{1}J_{PC}$ = 32 Hz and $^{2}J_{PC}$ = 26 Hz). These two features suggest the presence of a phosphaalkene function in the molecule. As for **IV**, the ^{1}H NMR spectrum contains only one set of signals for the organic fragment derived from the starting carbene. The solid state structure of **V** depicted in figure 9 reveals that, differently than all the previously described P_4-carbene adducts, **V** contains only two phosphorus atoms. The central P-P bond length in **V** (2.184 Å) is slightly shorter than a typical single bond and the P=C bonds lengths (average 1.73 Å) remain comparable to the corresponding ones in **II** and **IV**, characteristic of inversed polarized phosphaalkenes. The molecule adopts a gauche conformation with a torsion angle C(24)-P(2)-P(1)-C(1) of 149.22°.

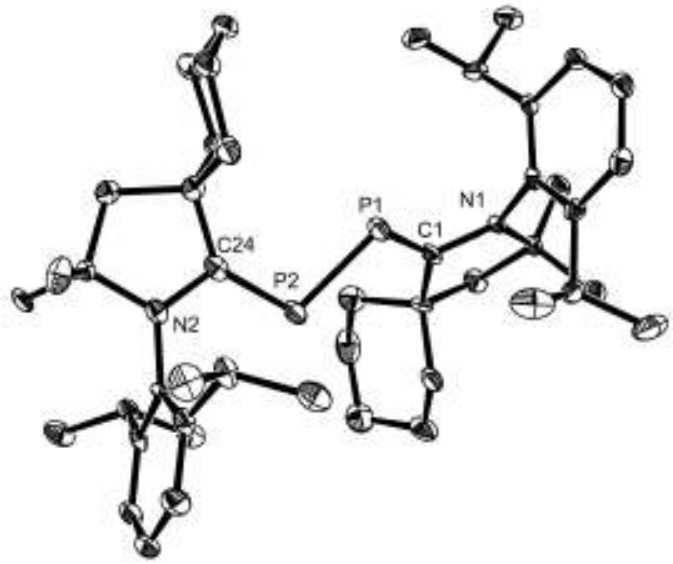

Figure 9. Solid state structure of **V**, 50% thermal ellipsoids are shown. Hydrogen atoms are omitted for clarity. Selected bond distances [Å] and angles [°]: P(1)–P(2) 2.184(3), C(1)–P(1) 1.719(7), C(24)–P(1) 1.737(8), N(1)–C(1) 1.387(9); C(1)-P(1)-P(2) 105.1(2); C(1)-P(1)-P(2)-C(24) 149.22.

Also due to the donation of the lone-pairs of the nitrogen atoms into the $\pi^*_{P=C}$ double bonds, **V** can also be represented by the resonance form **Vb** where each phosphorus center carries two electron lone-pairs and even by the resonance form **Vc** where a bisphosphinidene fragment is stabilized by two carbenes (Scheme 36).

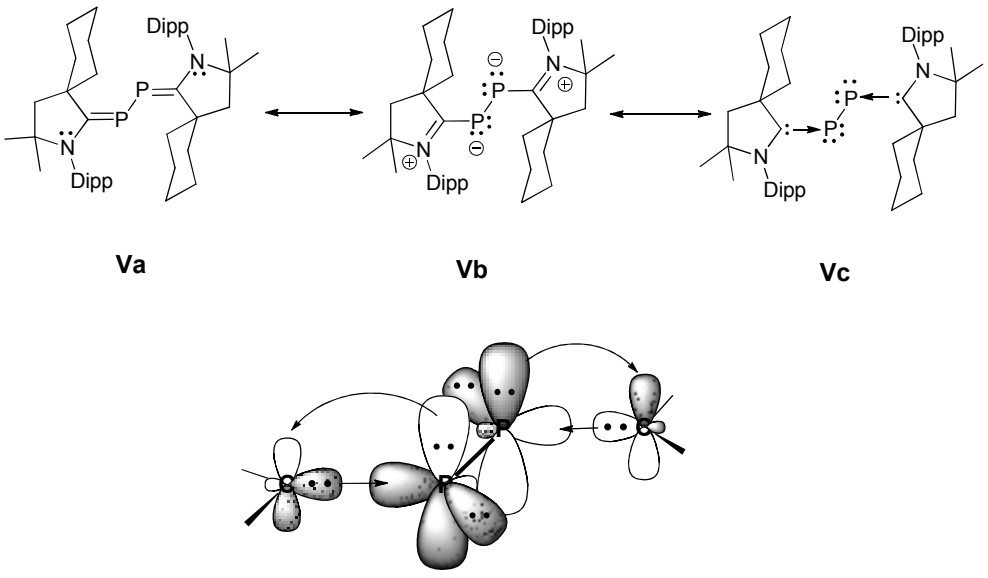

Scheme 36. Resonnance structures of the P_2-bis(carbene) adduct **V** and bonding situation showing the σ donation from the carbenes to P_2 and the π back bonding from the lone-pairs of the phosphorus atoms to the vacant p orbital of the carbene.

In **Vc**, the carbene units donate their electron lone-pair into the vacant orbital of each phosphorus center (σ donation). Simultaneously there is also some significant π back bonding from one lone pair of each phosphorus atom into the vacant p orbital of each carbene. This aspect will be discussed in detail in the next chapter.

Regarding the mechanism of formation of compound **V** (see Scheme 37), we can imagine that this adduct most probably results from the attack of a carbene to the β-phosphorus centers of the initially formed P_4-Bis(carbene) adduct structurally similar to **35**(*E*/*Z*). However, very surprisingly the formation of the tris(carbene)-P_4 adduct **IV** would imply that two CAACs **III** react on the transient triphosphirene analogous to **40** (see scheme 22, page 61) initially formed by the first nucleophilic attack of **III** on P_4.

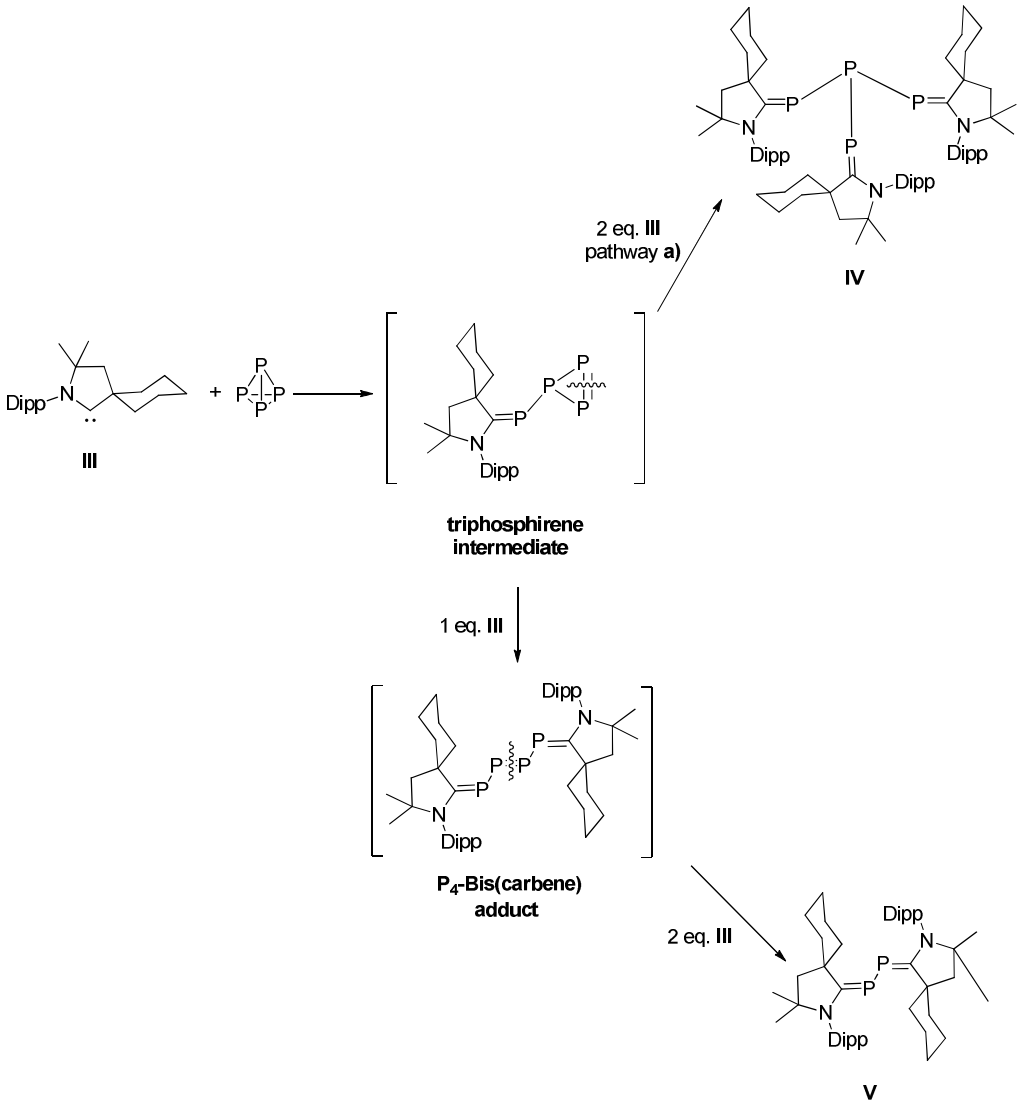

Scheme 37. Proposed mechanism for the reaction between **III** and P_4.

The general reactivity of carbenes toward white phosphorus is schematized in scheme 43 (page 86).
The formation of the major product **IV** in this reaction outlines again the analogy between the reactivity of highly nucleophilic CAACs toward P_4 and the reactivity of the supersilyl anion **3**(Li^+ or Na^+) (see schemes 3 and 4, page 46). Indeed we already mentioned that the reaction of three equivalents of **3**(Li^+ or Na^+) and white phosphorus in benzene afforded the tetraphosphide **7**(Li^+ or Na^+)$_3$ which was characterized in the solid state as the lithium salt.[20] In the solid state, the latter displays slightly longer P-P bond lengths than **IV** (average 2.28 Å) which is probably due to the presence of negative charges at the three phosphorus centers.
Whereas the fragmentation of P_4 leading to P_2 adducts mediated by neutral organic molecules is unprecedented, this process is well known for transition metals. The first reported P_2 complexes featured a tetrahedral M_2P_2 core. We can mention for example the molybdenum complex **U** prepared from the dimer $[MoCp(CO)_2]_2$ and white phosphorus[54] or the related chromium complex ***V*** prepared in the same way from $[CrCp(CO)_3]_2$ (Scheme 38).[55]

U ***V***

Scheme 38. Some examples of previously reported P_2 transition metal complexes featuring a M_2P_2 tetrahedral core.

Structurally different is the dinuclear Re butterfly complex **W** formed by reaction between $[Cp^*(CO)_2Re]_2$ and white phosphorus in the temperature range -18°C to 23°C. The complex **W** contains a bridging μ-$\eta^{2:2}$ P_2 fragment and can be described as the side-on coordination of P≡P (acting as a 4 electrons donor) by the two metal fragments as suggested by the relatively short P-P bond (2.032(8) Å) (Scheme 39).[56] Interestingly, when the same reaction is performed at room temperature, complex **W** was formed as a by-product along with the tetranuclear complex **X** containing the bridging diphosphinidene ligand.[57] On going from **W** to **X** the P-P bond length increases from 2.032 Å to 2.226 Å which is consistent with a P-P single bond in the last case reinforcing the diphosphinidene ligand description. Interestingly, this disphosphinidene ligand acts as an 8 electrons donor and is coordinated to the Re fragments via the four electron lone-pairs at the phosphorus centers (Scheme 39). This bonding situation is opposite to the one encountered in **V** where the carbenes are coordinated to the diphosphinidene fragment via donation from the lone pairs at the carbenes centers to the vacant orbitals at the phosphorus centers (Scheme 36). However, an analogous structure to **V** is found in the dinuclear Ta complex **Y** as well as in the related Nb complex **Z** (Scheme 39) where each metal center is linked to a phosphorus atom through a

double bond as suggested by the P=M bond lengths (M = Ta (**Y**): 2.3158 Å; M = Nb (**Z**): 2.3249 Å). Also, in both cases the P-P bond lengths (**Y**: 2.1709 Å, **Z**: 2.1430 Å) are slightly shorter than typical single bonds and are comparable to the ones in **V**.[58]

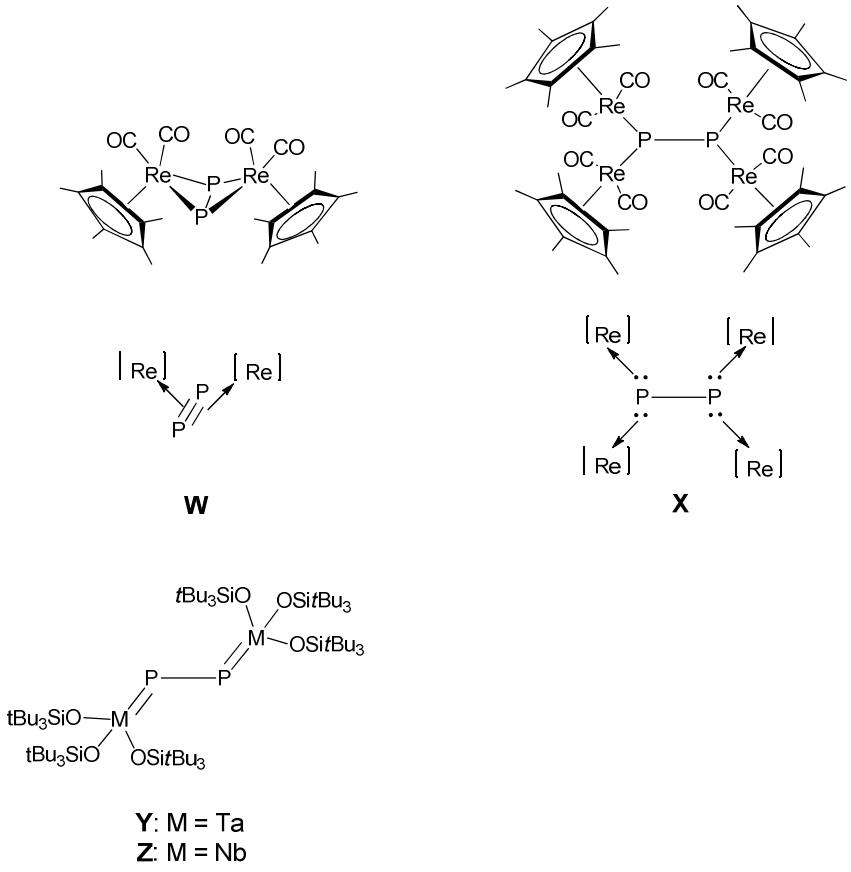

Scheme 39. Some examples of previously reported P_2- transition metal complexes ([Re] = $Re(CO)_2Cp^*$).

Concerning non-metal fragments, a similar fragmentation of P_4 mediated by nucleophilic phosphinite anions was already reported in 1984 by the group of Schmidpeter. They showed that sodium diphenylphosphinite $Na^+OPPh_2^-$ is able to cleave P_4 in a similar way to give the corresponding P_2 adduct **56a** when the reaction was carried out using a 1:4 molar ratio of P_4 to $Na^+OPPh_2^-$. However, when the amount of phosphinite was reduced to a 1:2.4 ratio, disproportionation occurred leading to a P^+–Bis(phosphinite) adduct **56b** along with Na_3P_7 (Scheme 40).[16]

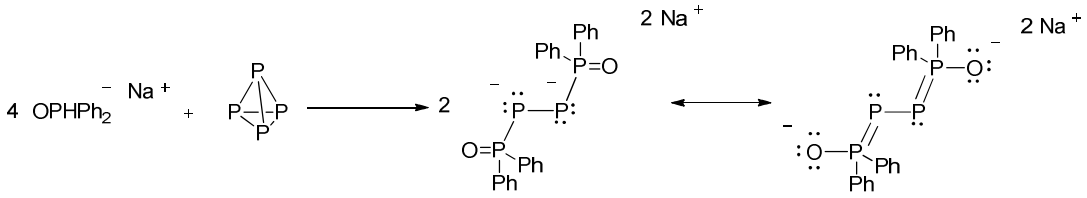

56a

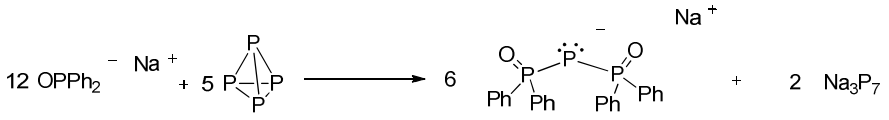

56b

Scheme 40. Degradation of white phosphorus mediated by the diphenylphosphinite anion.

To summarize, the formation of **V** confirmed our starting hypothesis. Indeed, by the careful choice of the carbene, we were able to perform the fragmentation of white phosphorus to a P_2 unit. Moreover, we have also shown that the steric parameters of the carbene have an important influence on the outcome of the reaction.

1.6.3) Reaction between P_4 and the very small bis(diisopropylamino)cyclopropenylidene: non symmetrical fragmentation of P_4

Our next target for white phosphorus degradation was the cleavage leading to a P_1 fragment. Such fragmentation would result from the carbene attack at a phosphorus center in the α position of the carbene fragments in the triphosphirene or tetraphosphatriene intermediates (Scheme 41). For this purpose we moved on the least sterically demanding stable carbene known to date, namely bis(diisopropylamino)cyclopropenylidene **VI**.

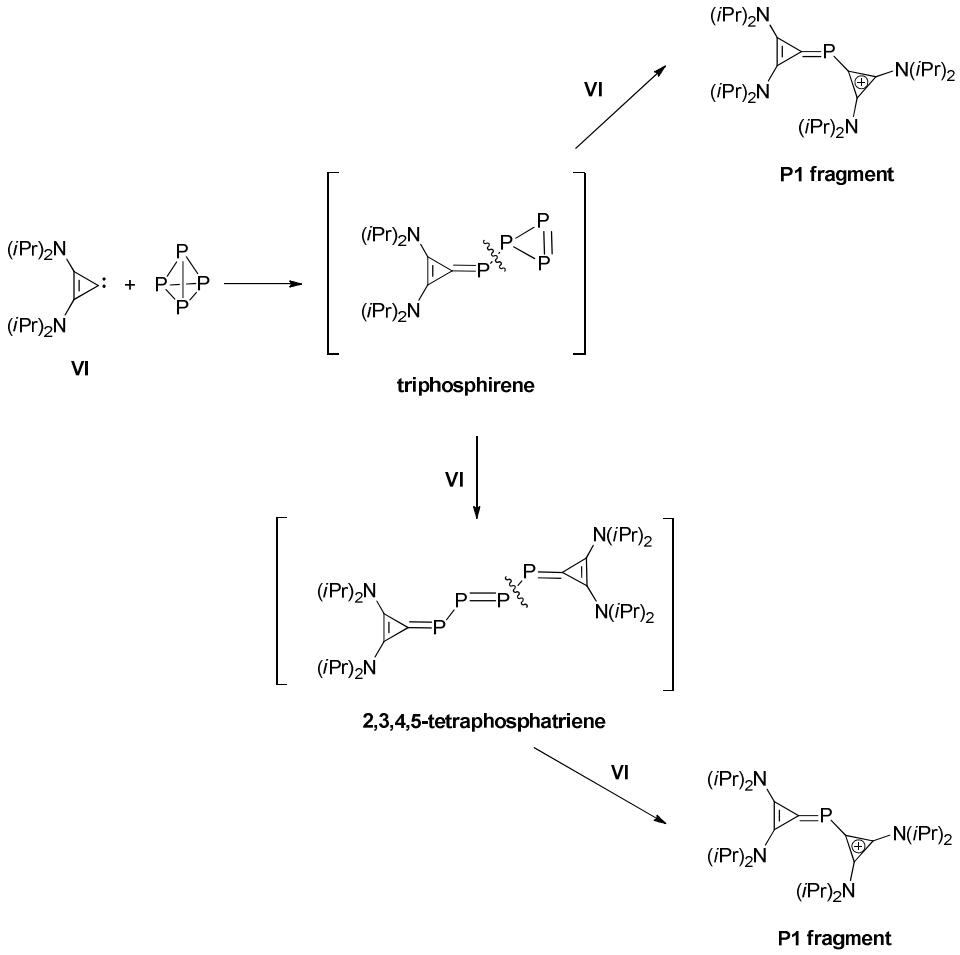

Scheme 41. Possible fragmentation of P_4 to a P_1 adduct mediated by the cyclopropenylidene **VI.**

When three equivalents of **VI** were reacted with white phosphorus in THF at room temperature, the color of the solution turned deep red. After 12 hours of stirring, the $^{31}P\{^1H\}$ NMR spectrum of the solution indicated total consumption of white phosphorus giving instead two sets of signals: an ABX spin system (δ_A = 242.8, δ_B = 237.0, δ_X = 157.0, J_{AX} = -484.7 Hz, J_{AB} = 38.8 Hz and J_{BX} = -481.1 Hz) and a singlet at -93.2 ppm. This ABX system may be the fingerprint for the P_3^- anion of the product (see Scheme 42). All attempts to purify this compound led to the disappearance of the second order spin system reflecting the high sensitivity of the product. However when chloroform was added to the crude solution and after work-up, compound **VII**(Cl^-) was obtained in 74% yield based on P_4 (Scheme 42). In the $^{31}P\{^1H\}$ NMR spectrum, only the high-filed singlet is displayed. The $^{13}C\{^1H\}$ as well as the ^1H NMR spectra of **VII**(Cl^-) reveal only one set of signals for the carbene fragment. The structure of the product was assigned on the basis of X-ray diffraction analysis and consists of the P_1-Bis(carbene) cation **VII** with Cl^- as counteranion (Scheme 42 and figure 9).

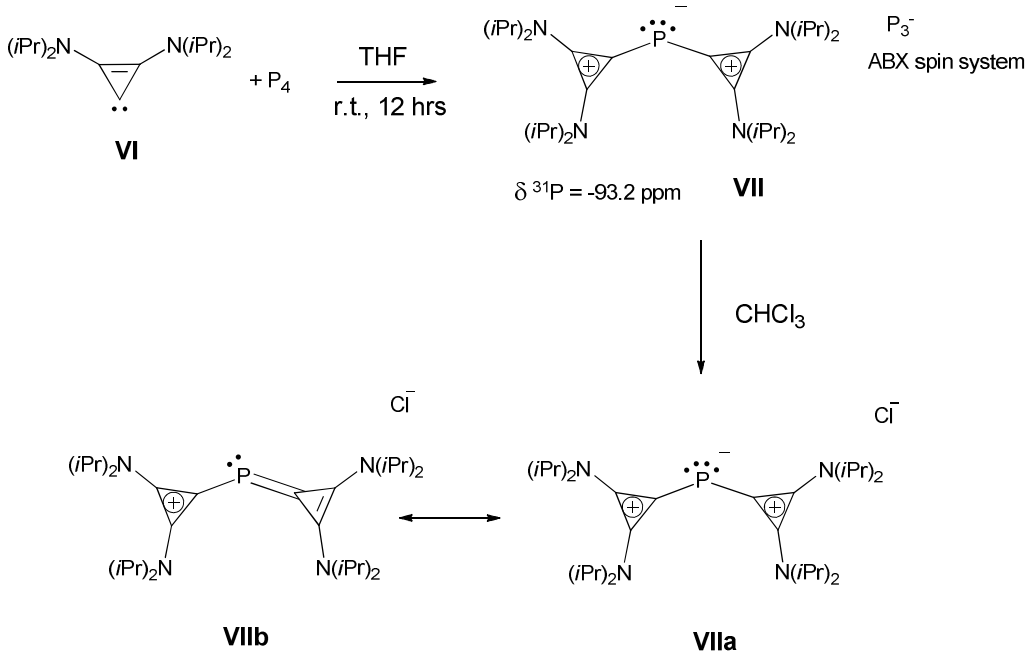

Scheme 42. Reaction of P_4 with cyclopropenylidene **VI**.

In the solid state, the two P-C bonds lengths in **VII**(Cl^-) are almost identical (1.787 Å and 1.788 Å) and are slightly longer than the corresponding P=C double bonds in the previous adducts suggesting a more important polarization. The bond angle value at the central phosphorus center is 104.68(9)° and interestingly the two cyclopropenyl rings are twisted from the C-P-C plane (36.74° and 45.76°) suggesting weak interaction between the π systems of the rings and the filled 3p orbitals at the phosphorus atom. Consequently **VII** is best described as a singlet P^+ cation complexed by two carbene ligands as outlined by the resonance structure **VIIa** in scheme 42. It is important to mention that similar cations were previously reported by Schmidpeter and MacDonald et al. where $(R_3P)_2P^+$, $(RNPCl)_2$, or PCl_3 were used as a source of P^+.[59] The characterized $P(NHC)_2^+$ adduct displayed similar geometrical parameters than **VII** and gave also a high field singlet (-126.2 ppm) in the $^{31}P\ \{^1H\}$ NMR spectrum.

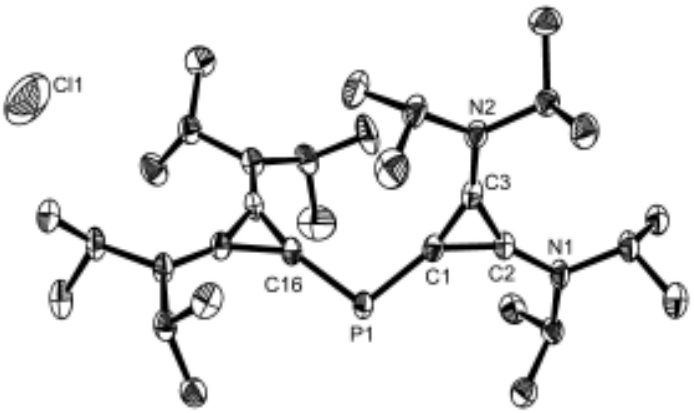

Figure 9. Solid state structure of **VII**(Cl^-), 50% thermal ellipsoids are shown. Hydrogen atoms are omitted for clarity. Selected bond distances [Å] and angles [°]:P(1)–C(1) 1.787(2), P(1)–C(16) 1.788(2), N(1)–C(2) 1.323(3), N(2)–C(3) 1.328(3), C(1)–C(3) 1.397(3), C(1)–C(2) 1.404(3), C(2)–C(3) 1.388(3); C(1)-P(1)-C(16) 104.68(9).

This last example represents a unique example of degradation of white phosphorus to P_1 and P_3 fragments induced by a neutral organic molecule. However, a long time ago, Schmidpeter showed that the cyanide anion is able to induce the disproportionation of white phosphorus into $P(CN)_2^-$ which was characterized in the solid state.[15] The same kind of reactions was also performed using sodium diphenylphosphinite as already mentioned (see scheme 40).

A similar degradation leading to P_1 and P_3 fragments triggered by a strongly nucleophilic anion has been reported before. Indeed we have already seen in the first paragraph of this chapter that the reaction between the supersilyl anion tBu$_3$Si$^-$Li$^+$ **3**(Li^+) and P_4 in a 3:1 ratio in THF leads first to the triphosphide **7**(Li^+)$_3$ (see Scheme 3, page 46). However, after one week at room temperature in THF the latter undergoes a fragmentation and the allylic anion **8**(Li^+) is formed along with the tBu$_3$SiPLi$_2$ (see Scheme 4, page 46).[20] The sodium salt **8**(Na^+) prepared by an other way was characterized in the solid state by X-rays diffraction analysis and displays an AX_2 spin system in the $^{31}P\{^1H\}$ NMR spectrum with a relatively low field chemical shift signal for the central phosphorus nuclei (δ_A = 732.5 ppm and δ_X = 212.5 ppm).[21] Therefore by analogy, although in our case the nature of the P_3 fragment is still unclear, we can imagine that it consists also of an allylic triphosphorus anion substituted by cyclopropenylidenes. However the chemical shift displayed by the P_3 fragment is very different from the ones reported for **8**(Na^+).

The formation of **VII** along with the P_3 anion is still not understood. It probably results from the attack of a second equivalent of the carbene to the substituted phosphorus center in the usual triphosphirene intermediate or in the P_4-bis(carbene) adduct with the simultaneous elimination of the P_3^- fragment (see scheme 41).

1.7) Conclusion

The reactivity pattern of carbenes toward white phosphorus is depicted in scheme 43. It shows clearly that the chemistry displayed by stable carbenes toward P_4 is very rich due to the fact that the electronic and steric parameters of the carbenes are easily tunable. Like transition metals, carbenes are able to activate P_4, inducing its agglomeration to large clusters and more importantly inducing its fragmentation. Therefore, regarding the activation of white phosphorus by main group compounds the reactivity of carbenes toward white phosphorus is so far the most promising and also the best understood. We can imagine that, because of the on going discovery of new types of carbenes (we can mention for example the very recently reported mesoionic carbenes),[60] some other interesting reactions with P_4 will be found. The next step in this field is to use the previously described adducts (especially the P_1 and P_2 adducts) to transfer the phosphorus fragment into organic substrates. The ultimate goal would be to make this reaction catalytic by regenerating the free carbene.

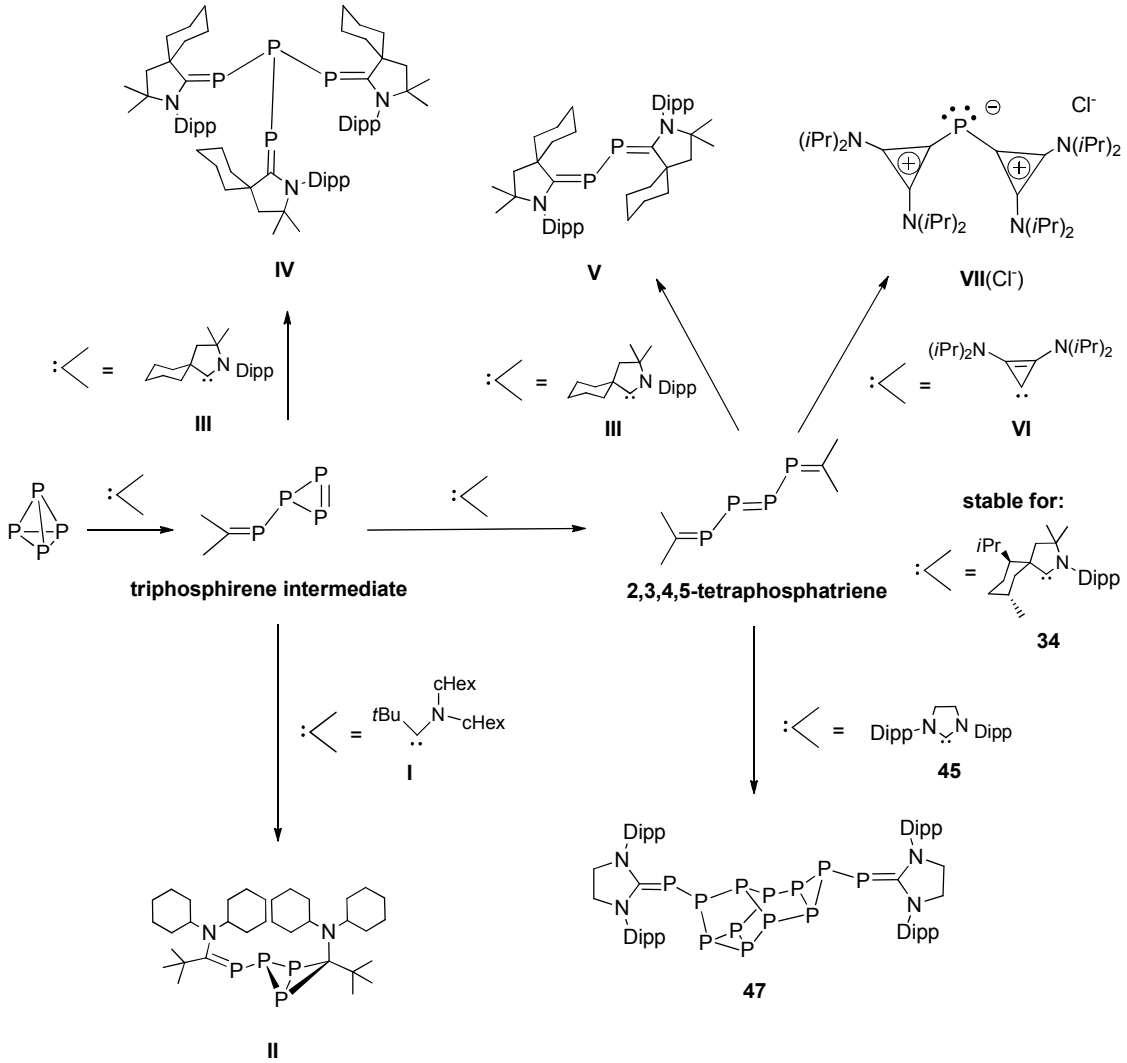

Scheme 43. Summary for the reactivity of stable carbenes toward P_4.

References

[1] D. E. C. Corbridge, *Phosphorus 2000: Chemistry, Biochemistry & Technology*, **2000**, p. 1267 pp.
[2] B. M. Cossairt and C. C. Cummins, *Angew. Chem., Int. Ed.* **2008**, *47*, 8863-8866.
[3] a) B. M. Cossairt, N. A. Piro and C. C. Cummins, *Chem. Rev. (Washington, DC, U. S.)* **2010**, *110*, 4164-4177; b) M. Caporali, L. Gonsalvi, A. Rossin and M. Peruzzini, *Chem Rev* **2010**, *110*, 4178-4235.
[4] M. Scheer, G. Balazs and A. Seitz, *Chem. Rev. (Washington, DC, U. S.)* **2010**, *110*, 4236-4256.
[5] P. W. Bridgman, *J. Am. Chem. Soc.* **1914**, *36*, 1344-1363.
[6] H. W. Spiess, R. Grosescu and U. Haeberlen, *Chem. Phys.* **1974**, *6*, 226-234.
[7] A. Simon, H. Borrmann and J. Horakh, *Chem. Ber./Recl.* **1997**, *130*, 1235-1240.
[8] L. R. Maxwell, S. B. Hendricks and V. M. Mosley, *J. Chem. Phys.* **1935**, *3*, 699-709.
[9] M. Haser and O. Treutler, *J. Chem. Phys.* **1995**, *102*, 3703-3711.
[10] V. G. Tsirelson, N. P. Tarasova, M. F. Bobrov and Y. V. Smetannikov, *Heteroat. Chem.* **2006**, *17*, 572-578.
[11] B. M. Cossairt and C. C. Cummins, *J. Am. Chem. Soc.* **2009**, *131*, 15501-15511.
[12] a) M. Peruzzini, L. Marvelli, A. Romerosa, R. Rossi, F. Vizza and F. Zanobini, *Eur. J. Inorg. Chem.* **1999**, 931-933; b) I. De los Rios, J.-R. Hamon, P. Hamon, C. Lapinte, L. Toupel, A. Romerosa and M. Peruzzini, *Angew. Chem., Int. Ed.* **2001**, *40*, 3910-3912; c) I. Krossing, *J. Am. Chem. Soc.* **2001**, *123*, 4603-4604; d) G. Santiso-Quinones, A. Reisinger, J. Slattery and I. Krossing, *Chem. Commun. (Cambridge, U. K.)* **2007**, 5046-5048.
[13] I. Krossing and L. Van Wullen, *Chem.--Eur. J.* **2002**, *8*, 700-711.
[14] a) A. Michaelis and M. Pitsch, *Ber. Dtsch. chem. Ges.* **1899**, *32*, 337-339; b) C. H. Burgess and D. L. Chapman, *J. Chem. Soc., Trans.* **1901**, *79*, 1235.
[15] A. Schmidpeter, G. Burget, F. Zwaschka and W. S. Sheldrick, *Z. Anorg. Allg. Chem.* **1985**, *527*, 17-32.
[16] A. Schmidpeter, G. Burget, H. G. Von Schnering and D. Weber, *Angew. Chem.* **1984**, *96*, 795-796.
[17] N. Wiberg, A. Woerner, K. Karaghiosoff and D. Fenske, *Chem. Ber./Recl.* **1997**, *130*, 135-140.
[18] R. Riedel, H. D. Hausen and E. Fluck, *Angew. Chem.* **1985**, *97*, 1050.
[19] A. Lorbach, A. Nadj, S. Tuellmann, F. Dornhaus, F. Schoedel, I. Saenger, G. Margraf, J. W. Bats, M. Bolte, M. C. Holthausen, M. Wagner and H.-W. Lerner, *Inorg. Chem. (Washington, DC, U. S.)* **2009**, *48*, 1005-1017.
[20] H.-W. Lerner, M. Wagner and M. Bolte, *Chem. Commun. (Cambridge, U. K.)* **2003**, 990-991.
[21] N. Wiberg, A. Woerner, H.-W. Lerner, K. Karaghiosoff, D. Fenske, G. Baum, A. Dransfeld and P. v. R. Schleyer, *Eur. J. Inorg. Chem.* **1998**, 833-841.
[22] W. T. K. Chan, F. Garcia, A. D. Hopkins, L. C. Martin, M. McPartlin and D. S. Wright, *Angew. Chem., Int. Ed.* **2007**, *46*, 3084-3086.
[23] M. B. Power and A. R. Barron, *Angew. Chem.* **1991**, *103*, 1403-1404 (See also Angew Chem , Int Ed Engl , 1991, (1430)1410, 1353-1404).

[24] a) O. J. Scherer, M. Swarowsky and G. Wolmershaeuser, *Organometallics* **1989**, *8*, 841-842; b) A. P. Ginsberg and W. E. Lindsell, *J. Amer. Chem. Soc.* **1971**, *93*, 2082-2084.
[25] D. Yakhvarov, P. Barbaro, L. Gonsalvi, S. M. Carpio, S. Midollini, A. Orlandini, M. Peruzzini, O. Sinyashin and F. Zanobini, *Angew. Chem., Int. Ed.* **2006**, *45*, 4182-4185.
[26] W. Uhl and M. Benter, *Chem. Commun. (Cambridge)* **1999**, 771-772.
[27] W. Uhl, W. Hiller, M. Layh and W. Schwarz, *Angew. Chem.* **1992**, *104*, 1378-1380 (See also Angew Chem , Int Ed Engl , 1992, 1331(1310), 1364-1376).
[28] C. Dohmeier, H. Krautscheid and H. Schnockel, *Angew. Chem.* **1994**, *106*, 2570-2571 (See also Angew Chem , Int Ed Engl , 1994, 2533(2523/2524), 2482-2573).
[29] J. Gauss, U. Schneider, R. Ahlrichs, C. Dohmeier and H. Schnoeckel, *J. Am. Chem. Soc.* **1993**, *115*, 2402-2408.
[30] Y. Peng, H. Fan, H. Zhu, H. W. Roesky, J. Magull and C. E. Hughes, *Angew. Chem., Int. Ed.* **2004**, *43*, 3443-3445.
[31] A. R. Fox, R. J. Wright, E. Rivard and P. P. Power, *Angew. Chem., Int. Ed.* **2005**, *44*, 7729-7733.
[32] Y. Xiong, S. Yao, M. Brym and M. Driess, *Angew. Chem., Int. Ed.* **2007**, *46*, 4511-4513.
[33] M. Haaf, A. Schmiedl, T. A. Schmedake, D. R. Powell, A. J. Millevolte, M. Denk and R. West, *J. Am. Chem. Soc.* **1998**, *120*, 12714-12719.
[34] R. Damrauer and S. E. Pusede, *Organometallics* **2009**, *28*, 1289-1294.
[35] W. W. Schoeller, *Phys. Chem. Chem. Phys.* **2009**, *11*, 5273-5280.
[36] J. J. Weigand, M. Holthausen and R. Frohlich, *Angew. Chem., Int. Ed.* **2009**, *48*, 295-298.
[37] M. H. Holthausen and J. J. Weigand, *J. Am. Chem. Soc.* **2009**, *131*, 14210-14211.
[38] J.-P. Bezombes, P. B. Hitchcock, M. F. Lappert and J. E. Nycz, *Dalton Trans.* **2004**, 499-501.
[39] a) J. D. Masuda, W. W. Schoeller, B. Donnadieu and G. Bertrand, *Angew. Chem., Int. Ed.* **2007**, *46*, 7052-7055; b) V. Lavallo, Y. Canac, C. Prasang, B. Donnadieu and G. Bertrand, *Angew. Chem., Int. Ed.* **2005**, *44*, 5705-5709.
[40] a) M. Yoshifuji, I. Shima, N. Inamoto, K. Hirotsu and T. Higuchi, *J. Am. Chem. Soc.* **1981**, *103*, 4587-4589; b) M. Yoshifuji, T. Sato and N. Inamoto, *Chem. Lett.* **1988**, 1735-1738; c) A. M. Caminade, M. Verrier, C. Ades, N. Paillous and M. Koenig, *J. Chem. Soc., Chem. Commun.* **1984**, 875-877.
[41] L. Weber, *Eur. J. Inorg. Chem.* **2000**, 2425-2441.
[42] a) M. Regitz, O. J. Scherer and Editors, *Multiple Bonds and Low Coordination in Phosphorus Chemistry*, **1990**, p. 478 pp; b) R. Appel and F. Knoll, *Adv. Inorg. Chem.* **1989**, *33*, 259-361.
[43] F. Cecconi, C. A. Ghilardi, S. Midollini and A. Orlandini, *J. Am. Chem. Soc.* **1984**, *106*, 3667-3668.
[44] P. Barbaro, A. Ienco, C. Mealli, M. Peruzzini, O. J. Scherer, G. Schmitt, F. Vizza and G. Wolmershaeuser, *Chem.--Eur. J.* **2003**, *9*, 5195-5210.
[45] J. D. Masuda, W. W. Schoeller, B. Donnadieu and G. Bertrand, *J. Am. Chem. Soc.* **2007**, *129*, 14180-14181.
[46] a) M. Baudler and W. Faber, *Chem. Ber.* **1980**, *113*, 3394-3395; b) H. G. Von Schnering, V. Manriquez and W. Hoenle, *Angew. Chem.* **1981**, *93*, 606-607; c) F. Kraus

and N. Korber, *Chem.--Eur. J.* **2005**, *11*, 5945-5959; d) T. Hanauer, J. C. Aschenbrenner and N. Korber, *Inorg. Chem.* **2006**, *45*, 6723-6727.
[47] M. E. Barr, B. R. Adams, R. R. Weller and L. F. Dahl, *J. Am. Chem. Soc.* **1991**, *113*, 3052-3060.
[48] O. J. Scherer, B. Hoebel and G. Wolmershaeuser, *Angew. Chem.* **1992**, *104*, 1042-1043 (See also Angew Chem , Int Ed Engl , 1992, 1031(1048), 1027-1048).
[49] O. J. Scherer, G. Berg and G. Wolmershaeuser, *Chem. Ber.* **1996**, *129*, 53-58.
[50] V. Lavallo, J. Mafhouz, Y. Canac, B. Donnadieu, W. W. Schoeller and G. Bertrand, *J. Am. Chem. Soc.* **2004**, *126*, 8670-8671.
[51] O. Back, G. Kuchenbeiser, B. Donnadieu and G. Bertrand, *Angew. Chem., Int. Ed.* **2009**, *48*, 5530-5533, S5530/5531-S5530/5539.
[52] F. Mathey and Editor, *Phosphorus-Carbon Heterocyclic Chemistry: The Rise of a New Domain*, **2001**, p. 846 pp.
[53] a) R. Appel, B. Niemann and M. Nieger, *Angew. Chem.* **1988**, *100*, 957-958; b) E. Niecke, O. Altmeyer and M. Nieger, *J. Chem. Soc., Chem. Commun.* **1988**, 945-946; c) W. W. Schoeller, V. Staemmler, P. Rademacher and E. Niecke, *Inorg. Chem.* **1986**, *25*, 4382-4385.
[54] O. J. Scherer, H. Sitzmann and G. Wolmershaeuser, *J. Organomet. Chem.* **1984**, *268*, C9-C12.
[55] L. Y. Goh, C. K. Chu, R. C. S. Wong and T. W. Hambley, *J. Chem. Soc., Dalton Trans.* **1989**, 1951-1956.
[56] O. J. Scherer, M. Ehses and G. Wolmershaeuser, *J. Organomet. Chem.* **1997**, *531*, 217-221.
[57] O. J. Scherer, M. Ehses and G. Wolmershauser, *Angew. Chem., Int. Ed.* **1998**, *37*, 507-510.
[58] E. B. Hulley, P. T. Wolczanski and E. B. Lobkovsky, *Chem. Commun. (Cambridge, U. K.)* **2009**, 6412-6414.
[59] a) A. Schmidpeter, S. Lochschmidt and A. Willhalm, *Angew. Chem.* **1983**, *95*, 561-562; b) B. D. Ellis, C. A. Dyker, A. Decken and C. L. B. Macdonald, *Chem. Commun. (Cambridge, U. K.)* **2005**, 1965-1967.
[60] a) E. Aldeco-Perez, A. J. Rosenthal, B. Donnadieu, P. Parameswaran, G. Frenking and G. Bertrand, *Science (Washington, DC, U. S.)* **2009**, *326*, 556-559; b) G. Guisado-Barrios, J. Bouffard, B. Donnadieu and G. Bertrand, *Angew Chem Int Ed Engl* **2010**, *49*, 4759-4762.

Experimental part

Synthesis of II:

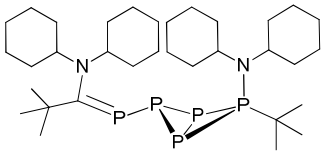

40 mL of ether was added at room temperature to a mixture of acyclic (alkyl)(amino)carbene **I** (1.014 g, 4.07 mmol) and P_4 (0.143 g, 1.16 mmol). The suspension was then stirred at room temperature during 2 hours. The solvent was removed under vacuum, and the yellow residue was washed with 6 ml of hexane at -35°C. The resulting solid was dried under vacuum to afford **II** as a yellow powder. Single crystals of **II** were grown by layering acetonitrile on top of a THF solution. Yield: 66.4 % in respect to P_4 (0.480 g, 0.77 mmol).

Mp: 150°C.

$^{31}P\{^1H\}$ NMR (THF-d_8, 202.5 MHz): δ -168.2 (dd, J_{PP} = 167 Hz, J_{PP} = 87 Hz), -105.8 (dt, J_{PP} = 220 Hz, J_{PP} = 167 Hz), 238.8 (dt, J_{PP} = 220 Hz, J_{PP} = 87 Hz).

^1H NMR (THF-d_8, 500 MHz): δ 1.06-1.36 (m, 12 H), 1.16 (s, 9 H), 1.33 (s, 9 H), 1.48-1.66 (m, 10 H), 1.70-1.82 (m, 10 H), 2.12 (d, J =12.0 Hz, 2 H), 2.23 (d, J =12.0 Hz, 4 H), 2.46 (d, J = 12.0 Hz, 2 H), 2.70 (t, J =12.0 Hz, 2 H), 3.64 (t, J = 12.0 Hz, 2 H).

$^{13}C\{^1H\}$ NMR (THF-d_8, 125.75 MHz): δ 27.1, 27.5, 28.5, 28.7, 28.9, 29.3, 32.4, 34.3 (d, J_{PC} = 17 Hz), 35.7, 36.8 (d, J_{PC} = 10 Hz), 37.2, 37.5, 38.9 (d, J_{PC} = 6 Hz), 39.7, 45.3 (t, J_{PC} = 15 Hz), 46.3 (d, J_{PC} = 29 Hz), 54.9, 62.7, 67.0 (d, J_{PC} = 5 Hz), 69.8, 101.5 (br s, $C_{carbene}$), 227.6 (d, J_{PC} =89 Hz, $C_{carbene}$).

Synthesis of IV and V:

A solution of cyclohexyl CAAC **III** (3.250 g, 10.01 mmol) in 20 ml of ether was added at room temperature to a suspension of P_4 (0.412 g, 3.34 mmol) in 20 ml of ether while stirring. Immediately upon addition the color of the solution turned dark red. The mixture was stirred at room temperature during 2 hours and then half of the solvent was removed under vacuum. A precipitate was formed when the remaining solution was cooled down to -30°C. Filtration via cannula gave **V** as a bright yellow powder (0.580 g, 0.81 mmol). Yield: 67 % in respect to P_4 (2.5 g, 2.27 mmol). Single crystals of **V** were grown from a saturated diethyl ether solution at room temperature. Evaporation of the filtrate gave a dark red powder which was washed 3 times with 30 mL of acetonitrile and then dried under vacuum to give **IV** (2.5 g, 2.27 mmol) as a

yellow powder. Yield: 12 % in respect to P_4 (0.580 g, 0.81 mmol). Single crystals of **IV** where obtained by slow evaporation of a hexane solution at room temperature.

Compound IV:

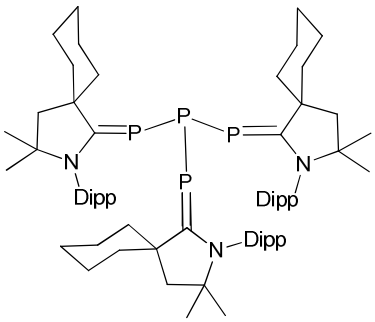

Mp: 142°C.

$^{31}P\{^1H\}$ NMR (C_6D_6, 162 MHz): δ -66.2 (q, J_{PP} = 228 Hz), 68.13 (d, J_{PP} = 228 Hz).

^1H NMR (C_6D_6, 500 MHz): δ 1.0-1.9 (m, 24 H), 1.08 (s, 18 H), 1.24 (d, J = 6.0 Hz, 18 H), 1.34 (d, J = 6.0 Hz, 18 H), 1.97 (s, 6 H), 2.92 (sept, J = 6.0 Hz, 6 H), 3.39 (m, 6 H), 7.07 (d, J = 8.0 Hz, 6 H), 7.19 (t, J = 8.0 Hz, 3 H).

$^{13}C\{^1H\}$ NMR (C_6D_6, 125.75 MHz): δ 24.3, 25.1, 25.7, 28.2, 29.4, 30.2, 38.1 (d, J_{PC} = 13 Hz), 50.9, 55.4, 68.1, 125.5, 128.9, 134.8, 149.1, 207.4 (m, $C_{carbene}$).

Compound V:

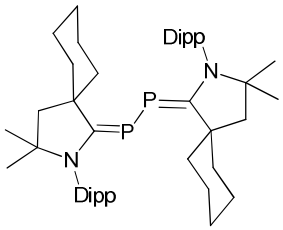

Mp: 216°C.

$^{31}P\{^1H\}$ NMR (C_6D_6, 162 MHz): δ 59.38.

^{1}H NMR (C_6D_6, 500 MHz): δ 1.0-1.6 (m, 16 H), 1.04 (s, 12 H), 1.27 (d, J = 7.0 Hz, 12 H), 1.59 (d, J = 7.0 Hz, 12 H), 1.92 (s, 4 H), 3.11 (sept, J = 7.0 Hz, 4 H), 3.36 (m, 4 H), 7.17 (d, J = 6.0 Hz, 4 H), 7.20 (t, J = 6.0 Hz, 2 H)**.**

^{13}C{^{1}H} NMR (C_6D_6, 125.75 MHz): δ 24.2, 24.8, 25.4, 27.4, 29.5, 30.2, 36.9 (t, J_{PC} = 12 Hz), 51.3, 55.4, 67.8, 125.4, 128.9, 136.1, 149.3, 202.2 (dd, J_{PC} = 32 Hz, J_{PC} = 26 Hz, $C_{carbene}$).

Synthesis of VII(Cl^-)**:**

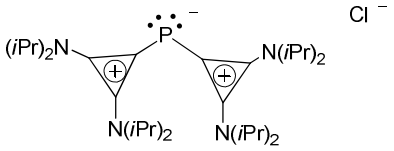

P_4 (0.170 g, 1.40 mmol) was added at room temperature to a solution of bis(diisopropylamino)cyclopropenylidene **VI** (1.000 g, 4.24 mmol) in 5 mL of THF. Immediately upon addition the solution turned deep red. The mixture was then stirred at room temperature overnight and 5 mL of chloroform was added. The mixture was then stirred for an additional 30 min and all the volatiles were removed under vacuum. The resulting solid was washed twice with 20 mL of ether and then dried under vacuum to afford **VII**(Cl^-) as a dark orange powder. Yield: 74 % in respect to P_4 (0.564 g, 1.05 mmol).

Mp: 174 °C (dec.).

^{31}P{^{1}H} NMR ($CDCl_3$, 121 MHz): δ -93.2.

^{1}H NMR ($CDCl_3$, 300 MHz): δ 1.25 (d, J = 6.5 Hz, 48 H), 3.79 (sept, J = 6.5 Hz, 8 H)**.**

^{13}C{^{1}H} NMR ($CDCl_3$, 75 MHz): δ 21.5, 51.3, 123.7 (d, J_{PC} = 105 Hz, $C_{carbene}$), 136.5.

Chapter II

Stable carbenes for the stabilization of diphosphorus (P_2), P_2-radical cation and P_2-dication

2.1) Introduction

Although at the end of the twentieth century stable carbenes were considered as laboratory curiosities, they quickly found numerous applications. The most important of them is their use as transition metal ligands. Due to their unique properties such as strong σ-donation and weak π-accepting, the resulting complexes display excellent catalytic activities and robustness.[1] This is well exemplified by the superior catalytic activity of the Grubbs second generation olefin metathesis catalyst bearing a NHC ligand in comparison with the first generation catalyst containing tricyclohexylphosphine.[2] Also importantly, carbenes are catalysts in their own right[3] and in addition they are able to activate small molecules (H_2, NH_3,[4] P_4 (First chapter), CO[5]) paving therefore the way for metal free catalytic process. Very recently, a new application of carbenes has emerged: the coordination of main group elements in their zero oxidation state leading to stable species.[6] In this regard, the concerned coordinated fragments have been: carbon[7], disilicon (Si_2)[8], diphosphorus (P_2)[9] and diarsenic (As_2).[10] We will show that although diphosphorus is an extremely reactive molecule that can be generated only under harsh conditions, once coordinated by carbenes, it exhibits totally different electronic properties and is stable under standard conditions. In consequence it was possible to study its reactivity in solution which revealed interesting electrochemical properties leading to the synthesis of carbene adducts of the even more reactive P_2-radical cation and P_2-dication. These last results unveiled a new application of stable carbenes, namely the stabilization of paramagnetic and electrodeficient species.[11]

2.1.1) Carbodiphosphorane and carbodicarbene: two stable carbon (0) complexes

The carbodiphosphorane **2** (Scheme 1) was the first reported compound stable in solution at room temperature that can be described as a carbon (0) complex. The first synthesis of this species was reported as early as 1961.[12] However it was only in 2006 thanks to experimental and theoretical studies that the bonding situation in **2** was fully understood.[13] Compound **2** can be made conveniently in two steps starting from readily available CCl_4 and triphenylphosphine. In a first step, the salt **1** is formed in quantitative yield along with dichlorotriphenylphosphorane.[14] Then, in a second step **2** is formed by dechlorination of **1** using tris(dimethylamino)phosphane (Scheme 1).[15]

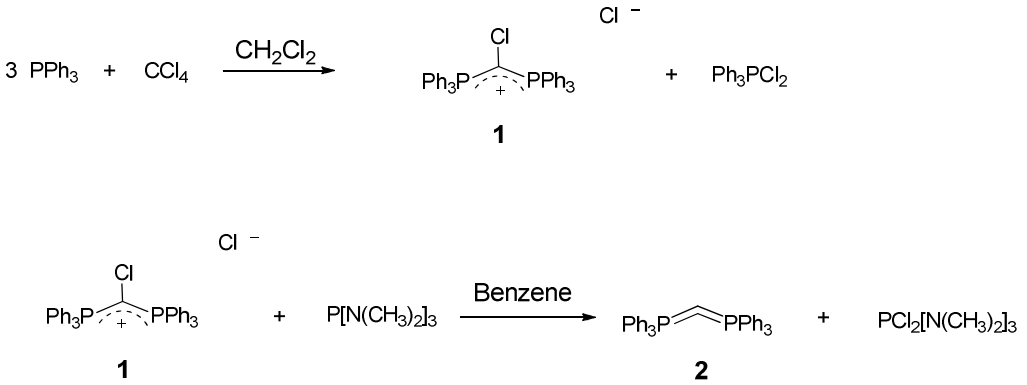

Scheme 1. Synthesis of the carbodiphosphorane **2.**

In the solid state, the molecule is bent with an P-C-P angle around the central carbon atom of 131.7° and the corresponding P=C bond lengths being 1.635 Å.[16] Importantly, the calculations performed by Frenking in 2006 indicate that the two highest-lying MOs of **2** are almost exclusively centered on the central carbon atom and correspond to two lone-pairs MOs of π and σ symmetry (Figure 1) consistent with the bent geometry of the molecule.[13]

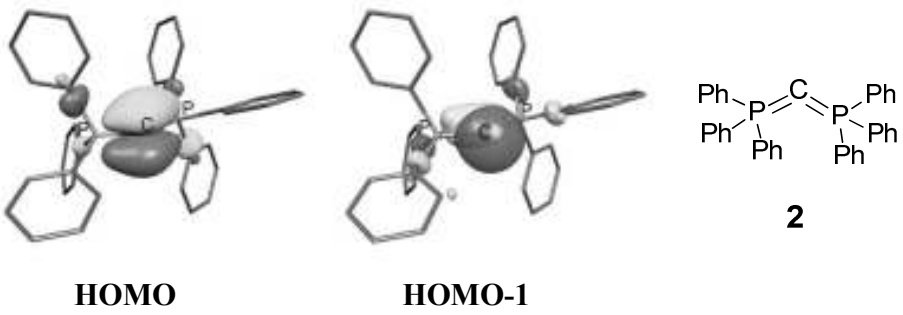

HOMO **HOMO-1**

Figure 1. Calculated molecular orbitals HOMO (left) and HOMO-1 (right) of carbodiphosphorane **2** (adapted from ref. 13).

Therefore, the four valence electrons of the carbon atom are non bonding and make up two lone-pairs orbitals. This suggests weak back-donation of the lone-pairs into the antibonding P-C^{Ph} orbitals. In conclusion, **2** is better described as a carbon (0) center complexed by triphenylphosphine ligands (resonance form **2b**, Scheme 2) than as a regular bisylide (resonance form **2a**, Scheme 2). In **2b**, the triphenylphosphine ligands are linked to the carbon center through dative bonds.

2a **2b**

Scheme 2. The two extreme resonance forms of **2**: on the left a regular bisylide (**2a**) and on the right a carbon (0) center complexed by two triphenylphosphine ligands (**2b**).

The carbon(0) concept was then extended in our group by the synthesis of a carbodicarbene featuring the better donor NHC ligands instead of triphenylphosphines.[7] The desired compound **5** was made in two steps from the readily prepared bis(*N*-methylbenzimidazol-2-yl)methane **3** (Scheme 3).[17]

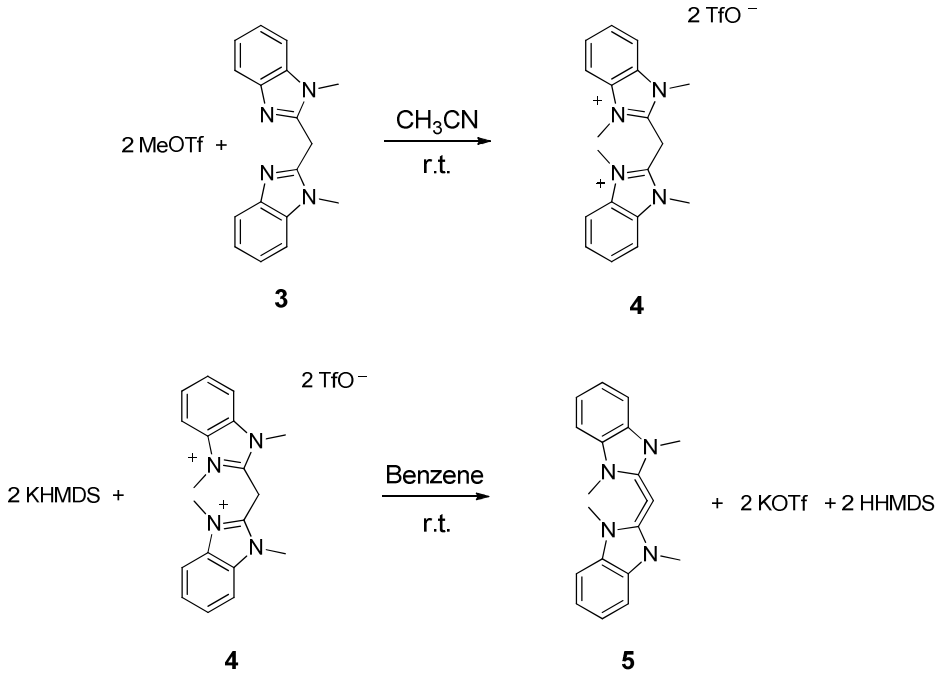

Scheme 3. Synthesis of the carbodicarbene **5**.

In the first step, the dication **4** is prepared by bismethylation of **3** using methyl triflate (MeOTf). Then, the former is deprotonated twice in one step by KHMDS affording the desired product **5** as a crystalline yellow material. Interestingly, the $^{13}C\{^{1}H\}$ NMR of **5** in C_6D_6 displays unusual chemical shifts for the three carbon nuclei involved in the allene framework (δ = 110.2 ppm for the central atom and δ = 144.8 ppm for the two terminal carbon centers). Indeed the inverse situation is usually encountered for regular allenes where the central nucleus displays lower field chemical shift than the terminal ones (δ = 185-215 ppm and δ = 60-130 ppm respectively).[18] This observation indicates already the peculiar electronic properties of **5**.

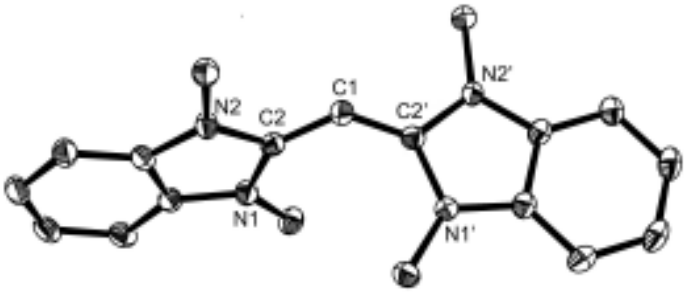

Figure 3. Solid state structure of **5**, 50% thermal ellipsoids are shown. Hydrogen atoms are omitted for clarity.

In the solid state, the main feature of the allene **5** is the bent geometry around the central carbon atom with a C-C-C angle of 134.8° (see figure 3). This special feature, already encountered in the case of **2**, was also predicted one year prior its discovery by Toner and Frenking in a theoretical study.[19] The calculations indicated that the two highest-lying molecular orbitals in the parent compound **5'** (containing the imidazol-2-ylidene fragments) were located on the central carbon atom and corresponded to two non bonding lone-pairs orbitals of π and σ symmetry in agreement with the bent geometry (Figure 4).

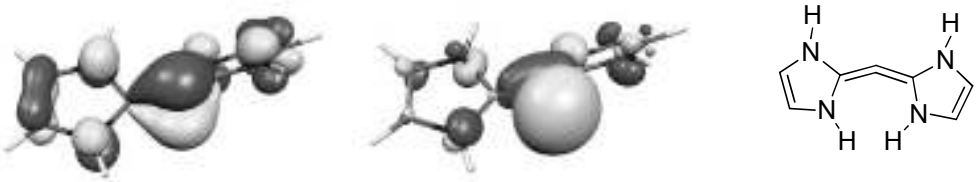

5'

HOMO **HOMO-1**

Figure 4. Calculated molecular orbitals HOMO (left) and HOMO-1 (right) of carbodicarbene **5'** (adapted from ref. 19).

In conclusion, we can say that like for **2**, the allene **5** is best described as a carbon (0) center complexed by two NHC ligands through donation of the carbenes lone-pairs into the two vacant orbitals of the carbon. The four valence electrons of the carbon atom remain then localized at the carbon center due to weak π back-bonding into the NHC 2p vacant orbitals. This weak π back-bonding is apparent by the twisting of the NHC rings by 35.8° from the plane defined by the three central carbon atoms. The bonding situation for the carbodicarbene is represented in figure 5.

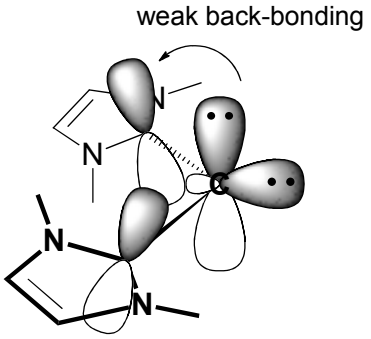

Figure 5. Bonding situation in carbodicarbene **5** showing the weak π back-bonding from the carbon lone-pairs to the p vacant orbitals of the NHC.

2.1.2) Disilicon Si_2 fragment stabilized by NHCs

Disilicon (Si_2) is an extremely reactive molecule which has been only characterized in the gas phase or in an argon matrix at 4K after vaporization of silicon powder at very high temperature followed by condensation.[20] At the same time, there has been some interest in the Si_2 study because it may also be formed during chemical vapor deposition processes which are involved in the manufacture of integrated circuits.[21]

In the ground state, according to theoretical studies[22] Si_2 is a triplet molecule with the electronic configuration: $(\sigma_g)^2(\sigma_u)^2(\sigma_g)^2(\pi_u)^2$ which has been confirmed experimentally[20a].

Interestingly in 2008, the group of Robinson succeeded in the isolation of a stable Si_2-bis(NHC) adduct **8** which is perfectly stable in solution and in the solid state at room temperature (Scheme 4).[8] Compound **8** was made readily in two steps starting from the free bulky NHC **6a** and $SiCl_4$. First, the adduct **7** was prepared in a quantitative yield. Then reduction of the latter using 4 equivalents of potassium graphite (KC_8) in THF at room temperature afforded **8** as dark red crystals in low yield (23.2 %).

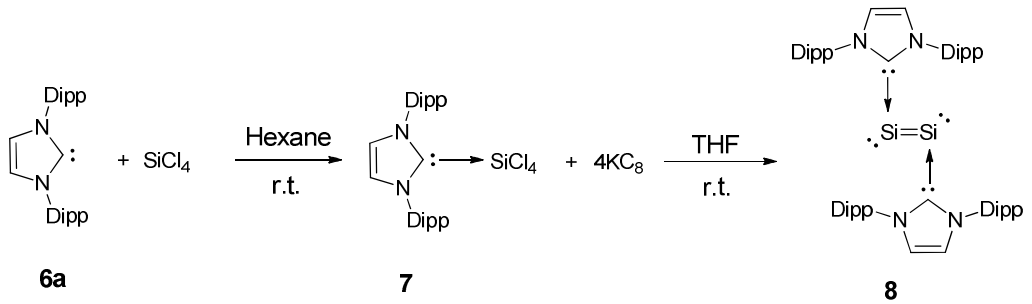

Scheme 4. Synthesis of the Si_2-bis(NHC) adduct **8**.

Very importantly, **8** displays in the solid state a trans-bent geometry where the NHC ligands are attached almost orthogonally to the central Si_2 fragment (The C-Si-Si angles being 93.37°). The Si-C bond lengths are rather long (1.927 Å), while

the Si=Si bond length (2.229 Å) is in the range expected for disilenes (2.14 to 2.29 Å) and is comparable with the experimental bond length of Si_2 (2.246 Å).[20b, 23] DFT calcultions were performed in order to gain insight into the electronic structure of this interesting molecule. It was shown that the three highest lying MOs are centered on the Si_2 fragment. The HOMO corresponds to the Si=Si π bond, the HOMO-1 is attributed to the Si=Si σ bond and finally the HOMO-2 is one of the two non-bonding lone-pair molecular orbitals centered on the central silicon atoms (Figure 6). This analysis suggests that compound **8** features a central Si=Si double bond where each Si center has a non bonding electron lone-pair, two attributes which are usually associated with extreme unstability.

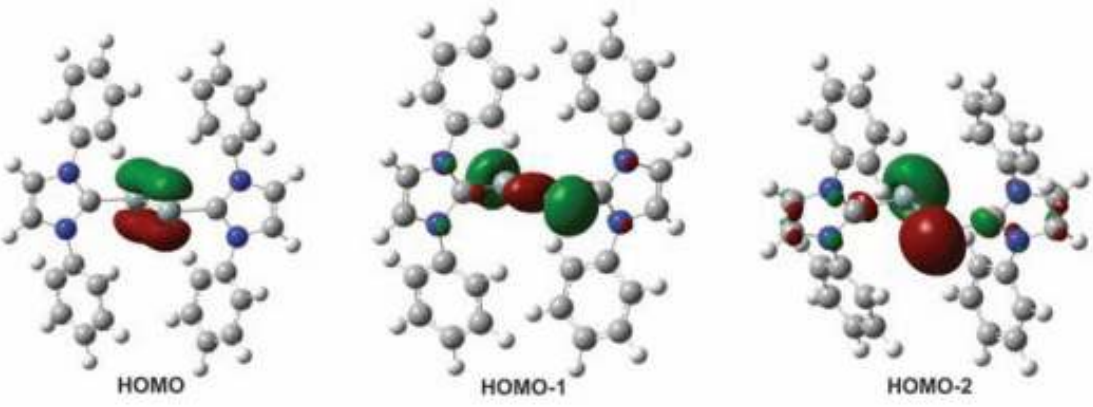

Figure 6. The three highest-lying MOs of compound **8** (Adapted from ref. 8).

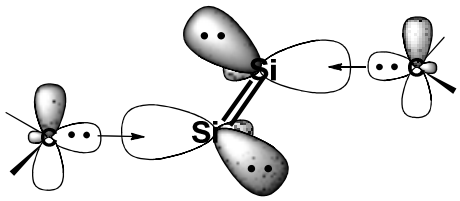

Figure 7. Bonding situation in compound **8** showing the σ donation from the electron lone-pairs at the carbene centers to the vacant orbitals at the silicon centers (The π orbital is omitted for clarity).

This analysis shows also clearly that compound **8** can be formally described as a Si_2 fragment coordinated by two NHC (Figure 7). However, once coordinated, the disilicon fragment displays a completely different electronic structure than the free Si_2 molecule. Indeed in the singlet molecule **8**, all valence orbitals of the Si centers are occupied whereas disilicon is an electro-deficient triplet molecule.

The binding energy of the parent NHCs (L:) (Featuring methyl groups on the nitrogen atoms instead of Dipp) to the Si_2 moiety has been calculated to be: -80.9 kcal.mol^{-1}. This confirms the large stabilization brought by the NHCs ligands.

$$Si_2(X^3\Sigma_g) + 2\ L: \longrightarrow L: Si{=}Si :L \quad (-80.9\ kcal.mol^{-1})$$
$$L: = :C(NMeCH)_2$$

2.1.3) Diphosphorus (P_2) fragment stabilized by carbenes

Whereas N_2 is a very stable and inert molecule, the heavier analog P_2 is on the contrary extremely reactive. This is due to the fact that elements from the 3rd period and beyond are unlikely to hybridize.[24] This is well illustrated when the bond dissociation energy for dinitrogen (236.08 kcal.mol^{-1}) is compared with the one for diphosphorus (117.18 kcal.mol^{-1}).[22] However, P_2 can still be generated in the gas phase from white phosphorus at temperatures above 1100 K. Interestingly, in 2006, the group of Cummins reported that P_2 could be generated under mild conditions from a niobium complex containing a P_2 substituted organic azide ligand.[25] The same group showed in 2010 that diphosphorus can also be generated by photolysis of white phosphorus in solution at room temperature. However, in all the cases, P_2 is only a transient species which cannot be observed in solution.

In the gas phase the P-P bond length of diphosphorus (1.89 Å) is quite short in comparison with the P-P bond length in P_4 (2.21 Å) or with the P=P double bond lengths in organic disphosphenes (2.00 Å to 2.05 Å)[26], suggesting a triple bond character.[27] However, despite its high reactivity, the P_2 fragment can still be stabilized in the coordination sphere of transition metals where it acts as four, six or eight-electrons donor ligands. In 2008, Robinson et al. reported the first P_2-bis(NHC) adducts **11a** and **11b** which were prepared from the corresponding free NHCs **6a** and **6b** and PCl_3 following a similar methodology than the one employed for the preparation of **8** (Scheme 5).[28] These adducts are closely related to the already mentioned P_2-bis(CAAC) adduct **10** which was made directly from P_4 (see 1st chapter).[29]

In the first step the hypervalent phosphorus compound **9a,b** was made by addition of the free NHC **6a,b** to PCl_3. Then reduction of the adduct **9a,b** using 3.1 equivalents of KC_8 in THF at room temperature afforded the desired product **11a,b** as red crystals in moderate yields (**11a**: 57 % and **11b**: 21 %).

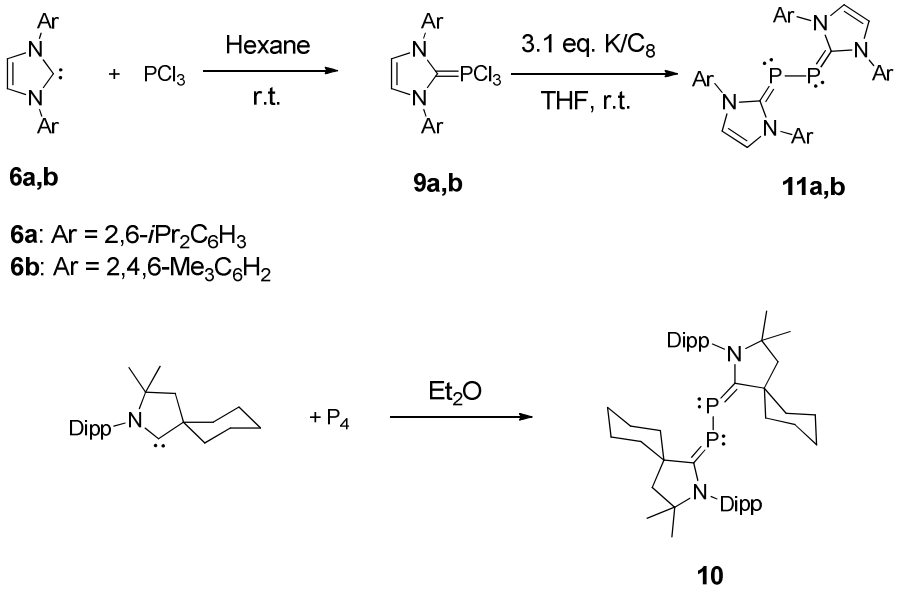

Scheme 5. Synthesis of the P_2-bis(NHC) adducts **11a** and **11b** and the already mentioned P_2-bis(CAAC) **10**.

Interestingly, the phosphorus centers of the adducts **11a,b** display high field chemical shifts in the $^{31}P\{^1H\}$ NMR spectra (**11a**: -52.4 ppm and **11b**: -73.6 ppm). These chemical shifts are quite different from the one displayed by the related P_2-bis(CAAC) **10** (+59.4 ppm) outlining already the different electronic properties of CAACs in comparison with NHCs. In the solid state, because of the difference of steric environment of the NHCs, the conformations of **11a** and **11b** are slightly different. Compound **11a**, featuring the bulky NHC (with Dipp on the nitrogen atoms), has C_i symmetry and adopts a perfect trans-bent geometry with a C-P-P-C torsion angle of 180°. However, the gauche conformation is preferred for the less sterically hindered adduct **11b** (with Mes on the nitrogen atoms) where the C-P-P-C angle is 134.1°. We have already mentioned that the gauche conformation is also preferred for the P_2-bis(CAAC) adduct **10** (torsion angle: 149.2°). Importantly, in all of these compounds the central P-P bond lengths lay within the range of single P-P bond lengths (**10**: 2.18 Å, **11a**: 2.21 Å, **11b**: 2.19 Å). Also, the C-P-P angles are comparable in all cases (**10**: 104.9° (average), **11a**: 103.2°, **11b**: 102.8° (average)) and each adduct display relatively long P=C double bonds lengths consistent with inversely polarized phosphaalkenes (**10**: 1.73 Å (average), **11a**: 1.75 Å, **11b**: 1.75 Å (average)).[30]
Table 1 summarizes NMR and geometrical features for the three adducts.

Compound:	10	11a	11b
$^{31}P\{^{1}H\}$ NMR chemical shift:	+59.4 ppm	-52.4 ppm	-73.6 ppm
P-P bond length:	2.18 Å	2.21 Å	2.19 Å
C-P-P-C torsion angle:	149.2°	180°	134.1°
C-P-P angle (average):	104.9°	103.2°	102.8°
P=C double bond length (average):	1.73 Å	1.75 Å	1.75 Å

Table 1. ^{31}P NMR and geometrical parameters for the P_2-bis(carbene) adducts **10**, **11a** and **11b**.

Three resonance forms for these species are shown in scheme 6. The first resonance structure (**A**) features two regular phosphoalkene functions, whereas in the second resonance form (**B**) because of the donation of the nitrogen atoms lone pairs into the $\pi^*_{P=C}$ orbitals, each P centers are formally negatively charged and have two electrons lone pairs. We can also write the extreme resonance form **C** where the compounds are formally described as bis-phosphinidene fragments coordinated by two carbenes.

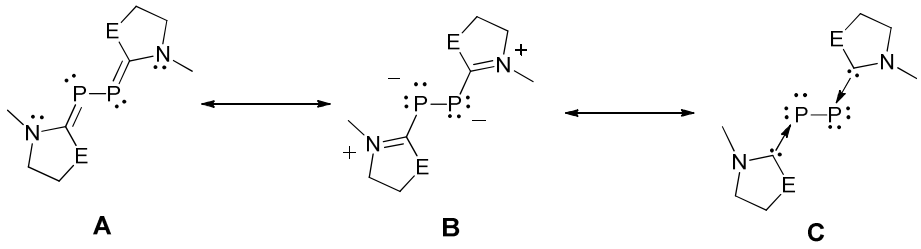

Scheme 6. Three possible resonance structures for the P_2-bis(carbene) adducts.

The localized molecular orbitals for the parent compounds containing the simplified carbene (L: = :C(NHCH)$_2$) have been calculated (Figure 8). They reveal that in the parent model the phosphorus centers are linked through a P-P σ-bond (**a**) and they are bonded to the carbene centers via P-C σ-bonds (**b**). In addition, two lone-pair orbitals are localized on each phosphorus centers: one of σ symmetry (**d**) and one of π symmetry (**c**). However, because of the π back donation, the latter is also slightly delocalized on the carbene center.

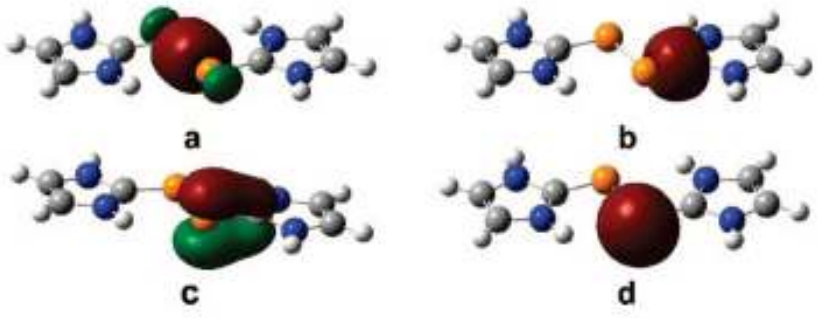

Figure 8. Localized molecular orbitals of the parent P_2-bis(NHC) adduct (L:P-P:L) showing: **a**) P-P σ bond, **b**) P-C σ bond, **c**) Phosphorus center's lone pair orbital of π symmetry and **d**) Phosphorus center's lone pair orbital of σ symmetry (Adapted from ref. 9).

Overall, compounds **10**, **11a** and **11b** can be described by the formalism according to the resonance form **C** (Scheme 6)**.** This description allows us to explain the difference of properties of the resulting P_2-bis(carbene) adducts by considering the difference of steric and electronic properties of the carbenes.

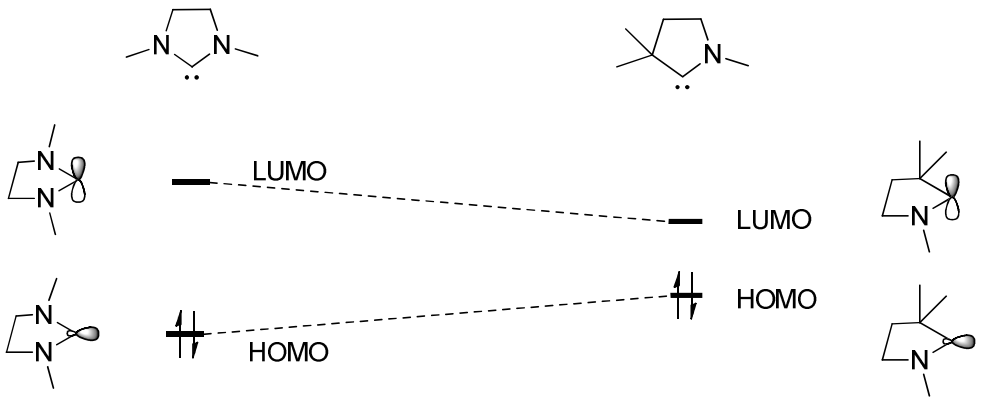

Scheme 7. Comparison of the electronic properties of NHCs versus CAACs.

For example, due to the more electrophilic character of the CAAC in comparison with the NHC (see Scheme 7), the π back bonding from the lone pair at the phosphorus center into the vacant p orbital of the carbene is more pronounced in **10** than in **11a,b**. Consequently in **10**, the electronic density at the central P_2 fragment is decreased, resulting in the lower field chemical shift displayed by the phosphorus nuclei and the shorter P=C bond length in **10**. The bonding situation is depicted in figure 9.

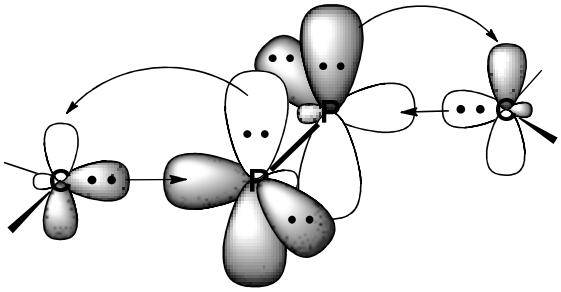

Figure 9. Bonding situation in the P_2-bis(carbene) adducts showing the σ donation from the carbenes to P_2 and the π back bonding from the lone pairs of the phosphorus atoms to the vacant p orbital of the carbene.

2.2) Conclusion

In summary, it has been shown very recently that carbenes are able to stabilize highly reactive fragments which are otherwise transient or inexistent. Once coordinated by carbenes, the resulting adducts are stable both in solution and in the solid state at room temperature allowing for their characterization. However, we have also to keep in mind that the stabilized adducts display different electronic properties than the parent fragments. This is well exemplified by the P_2-bis(carbene) compounds. Indeed the free P_2 molecule displays a P≡P triple bond but once complexed by the carbenes, the resulting central fragment features a single bond. Also, the latter is electron rich due to the presence of two lone pairs at each phoshorus atom. It would be thus interesting to study the electronic properties of those adducts and to analyze what is the influence of the electronic properties of the carbenes (CAAC vs NHC). In addition, through modification of the central fragment, the stabilization of other highly reactive fragments will be achieved. Our findings will be developed in the following section.

2.3) Results and discussion

2.3.1) Electrochemical study of the adducts 10 and 11a

In order to evaluate the electrochemical properties of compounds **10** and **11a**, a cyclic voltammetry for each species in a THF solution containing 0.1 M of n-Bu_4NPF_6 as electrolyte was performed. The obtained voltammograms are shown in figure 10.

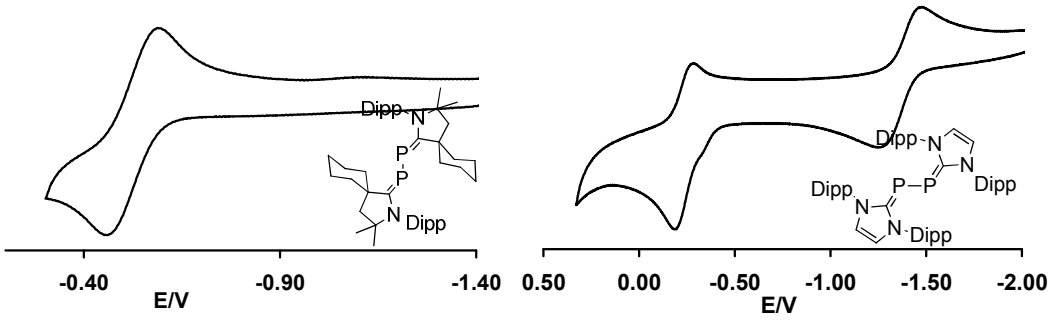

Figure 10. Cyclic voltammograms of the THF solutions of **10** (Left) and **11a** (Right) containing 0.1 M n-Bu_4PF_6 as electrolyte (potential versus Fc^+/Fc, scan rate 100 $mV.s^{-1}$).

The voltammogram of **10** shows a reversible one-electron oxidation at $E_{1/2}$ = -0.536 V versus Fc^+/Fc). Interestingly the voltammogram of **11a** displays two reversible one-electron oxidations with the first one occurring at a much lower potential than **10** ($E_{1/2}$ = -1.408 V versus Fc^+/Fc) and the second one being 1.230 V higher than the first one ($E_{1/2}$ = -0.178 V versus Fc^+/Fc). It is worth to mention that the cyclic voltammogram of **10** shows also a second oxidation around +0.02 V but irreversible which is not shown here. This analysis suggests that the radical cation $\mathbf{10}^{+\cdot}$ obtained by one-electron oxidation of the corresponding neutral compound **10** should be accessible whereas, starting from **11a** not only the radical cation $\mathbf{11a}^{+\cdot}$ but also the dication $\mathbf{11a}^{++}$ could be prepared. These striking differences in the electrochemical properties of **10** and **11a** indicate that the P_2 fragment in the latter is more electron-rich than the one in the former consistent with the phosphorus higher-field chemical shift displayed by **11a** in comparison with **10** (**10**: +59.4 ppm and **11a**: -52.4 ppm). Therefore, these encouraging results prompted us to carry out the synthesis of the corresponding radical cations $\mathbf{10}^{+\cdot}$ and $\mathbf{11a}^{+\cdot}$.

2.3.2) Synthesis and characterization of the radical cations $\mathbf{10}^{+\cdot}$ and $\mathbf{11a}^{+\cdot}$

Considering the relatively low oxidation potentials displayed by both adducts (**10**: -0.536 V versus Fc^+/Fc and **11a**: -1.408 V versus Fc^+/Fc) we reasoned that the mild organic oxidative agent $Ph_3C^+B(C_6F_5)_4^-$ should be suitable for the corresponding chemical one-electron oxidations of **10** and **11a** (the reported potential for $Ph_3C^+BF_4^-$ is -0.11 V versus Fc^+/Fc)[31] (scheme 8).
When toluene was added at room temperature to an equimolar mixture of **10** and $Ph_3C^+B(C_6F_5)_4^-$ under an argon atmosphere, the resulting solution turned immediately purple. After two hours of stirring, the $^{31}P\{^1H\}$ NMR spectrum was silent indicating the paramagnetic nature of the resulting products.

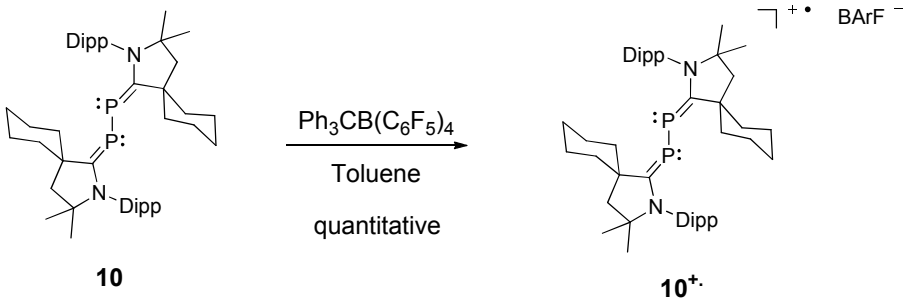

Scheme 8. Preparation of the radical cation $\mathbf{10}^{+\cdot}$.

After work-up the radical cation $\mathbf{10}^{+\cdot}$ was obtained in quantitative yield as an air-sensitive microcrystalline purple powder. The room temperature EPR spectrum (Figure 11, left) of a fluorobenzene solution of $\mathbf{10}^{+\cdot}$ displays a triplet of quintets (g = 2.009) due to a large coupling with two equivalent phosphorus nuclei (a(^{31}P) = 42 G) and a small coupling with two equivalent nitrogen nuclei (a(^{14}N) = 3 G) (^{31}P: I = ½, 100% and ^{14}N: I = 1, 99.63%).

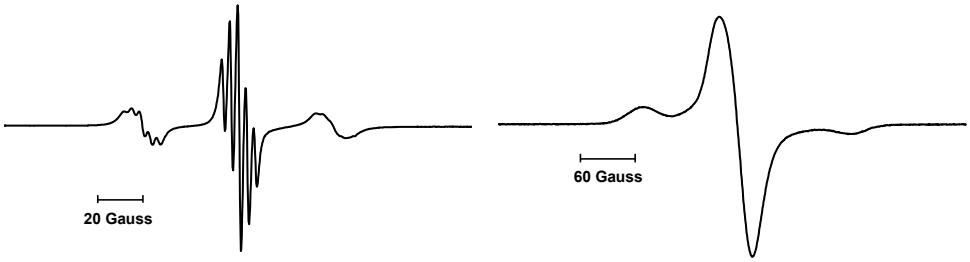

Figure 11. EPR spectra of $\mathbf{10}^{+\cdot}$ in fluorobenzene recorded at room temperature (left) and in a frozene solution at -173°C (right).

To gain more insight into the electronic structure of $\mathbf{10}^{+\cdot}$, the frozen fluorobenzene solution EPR spectrum was recorded at -173°C and is shown in figure 11 (right). Simulation of the spectrum shows that the g and ^{31}P hyperfine tensors are aligned and display axial symmetry. The following principal values for the ^{31}P and g hyperfine coupling tensors are obtained: $A_{xx}(^{31}P) = A_{yy}(^{31}P) = 0$ and $A_{zz}(^{31}P) =$ 117 G; $g_{xx} = 2.011$, $g_{yy} = 2.009$ and $g_{zz} = 2.004$. These values indicate that 28% of spin density is localized in the 3p orbital of each phosphorus atom and less than 1% is localized in the 3s orbital, consistent with the π^* geometry of the SOMO. Moreover these EPR features are comparable to the ones observed for the radical anions obtained by reduction of diphosphenes where the single electron resides in the π^* orbital of the P=P double bond, suggesting a similar electronic situation for $\mathbf{10}^{+\cdot}$.[32]

X-rays diffraction study was performed on a single crystal of $\mathbf{10}^{+\cdot}$ (Figure 12, left). In the solid state $\mathbf{10}^{+\cdot}$ has C_i symmetry and displays a planar trans-bent geometry (C-P-P-C torsion angle: 180°). The P-C bond lengths in $\mathbf{10}^{+\cdot}$ (1.777(3) Å) are slightly longer than in **10** (1.719(7) Å), moreover the P-P bond distance

become shorter upon oxidation and is in the mid-way between a P=P double bond (2.00 Å to 2.05 Å) and a P-P single bond (2.094(2) Å in $\mathbf{10}^{+\cdot}$ and 2.184(3) Å in **10**).

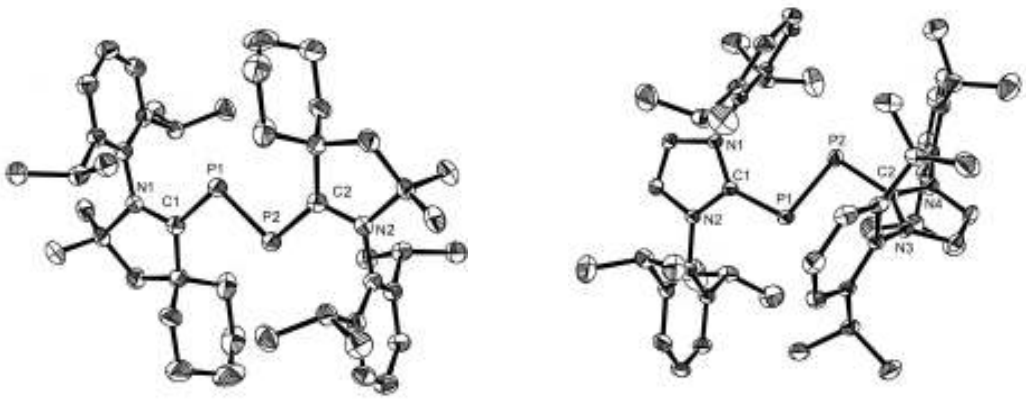

Figure 12. Solid-state structure of $\mathbf{10}^{+\cdot}$ (left) and $\mathbf{11a}^{+\cdot}$ (right). 50% thermal ellipsoids are shown. Hydrogen atoms and the counter anions ($B(C_6F_5)_4^-$)are omitted for clarity in both cases. Selected bond distances [Å] and angles [°]: $\mathbf{10}^{+\cdot}$: P(1)–P(2) 2.094(2), C(1)–P(1) 1.777(3), N(1)–C(1) 1.326(4); C(1)–P(1)–P(2) 102.24(13). $\mathbf{11a}^{+\cdot}$: P(1)–C(1) 1.795(2), P(2)–C(2) 1.810(2), P(1)–P(2) 2.0907(10); C(1)–P(1)–P(2) 102.70(8), C(2)–P(2)–P(1) 96.73(8).

The radical cation $\mathbf{11a}^{+\cdot}$ prepared using the same method than $\mathbf{11}^{+\cdot}$, was isolated quantitatively as a dark red microcrystalline powder (Scheme 9).

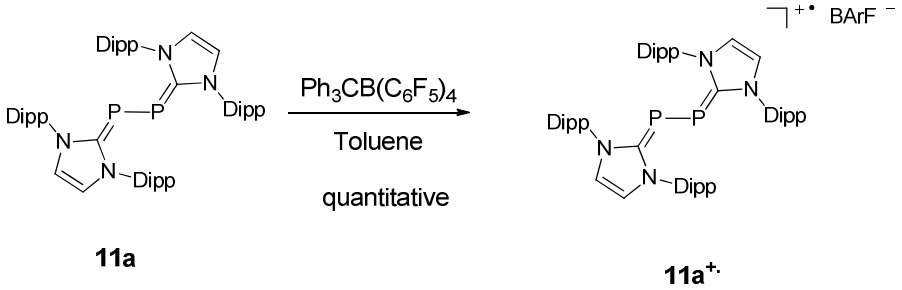

11a **$\mathbf{11a}^{+\cdot}$**

Scheme 9. Preparation of the radical cation $\mathbf{11a}^{+\cdot}$.

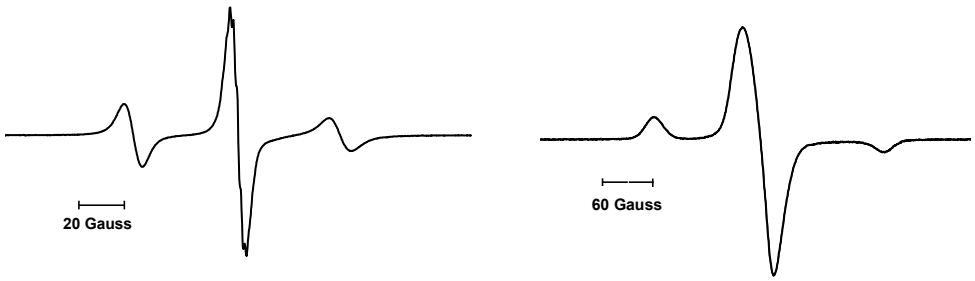

Figure 13. EPR spectra of $\mathbf{11a}^{+\cdot}$ in fluorobenzene recorded at room temperature (left) and in a frozen solution at -173°C (right).

The room temperature EPR spectrum of $\mathbf{11a}^{+\cdot}$ in a fluorobenzene solution (Figure 13, left) appears as a broad triplet (g = 2.008) due to coupling with two equivalent phosphorus centers ($a(^{31}P)$ = 44 G) similar to the one observed for $\mathbf{10}^{+\cdot}$ ($a(^{31}P)$ = 42 G). However the hyperfine coupling with the nitrogen nuclei is too small and could not be resolved. The frozen fluorobenzene solution EPR spectrum recorded at -173°C (Figure 13, right) is also very similar to that of $\mathbf{10}^{+\cdot}$ indicating that the g and the axially symmetric ^{31}P hyperfine tensors are aligned. After simulation, the following principal values were obtained: $A_{xx}(^{31}P) = A_{yy}(^{31}P) = 0$ and $A_{zz}(^{31}P)$ = 136 G and g_{xx} = 2.015, g_{yy} = 2.007 and g_{zz} = 2.004. These values indicate that 35% of spin density is localized in the 3p orbital of each phosphorus atom and less than 1% is localized in the 3s orbital. Therefore, in $\mathbf{11a}^{+\cdot}$ the spin density is more localized on the P_2 fragment than in $\mathbf{10}^{+\cdot}$ (spin density on each P center in $\mathbf{10}^{+\cdot}$: 29%) which is readily explained by the weaker π-accepting properties of the NHCs in comparison with the CAACs.
In the solid state, $\mathbf{11a}^{+\cdot}$ adopts almost a trans-bent geometry (C-P-P-C torsion angle: 172.4°) with similar trends than $\mathbf{10}^{+\cdot}$ (Figure 12, right). As already observed for **10**, upon oxidation the central P-P bond length becomes shorter (in $\mathbf{11a}^{+\cdot}$ 2.09 Å and in **11a**: 2.21 Å) and lay in the mid-way between a P=P double bond and a P-P single bond. Also the P-C bond lengths (average 1.80 Å) in the radical cation are slightly longer than in the neutral molecule (1.75 Å).

2.3.3) Synthesis and characterisation of the dication $\mathbf{11a}^{++}$

As indicated by the voltammogram (Figure 10, right), **11a** undergoes a second reversible one-electron oxidation at $E_{1/2}$ = -0.178 V versus Fc^+/Fc suggesting that the dication may be accessible. Therefore, we performed the reaction between **11a** and two equivalents of $[FeCp_2]^+TfO^-$ (Fc^+TfO^-) in THF at room temperature (scheme 10).
After stirring for two hours and subsequent work-up, the dication $\mathbf{11a}^{++}$ was obtained as a pale yellow powder in a moderate yield (42%).

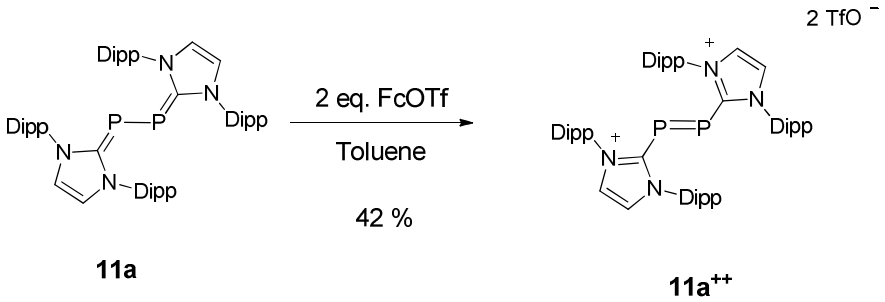

Scheme 10. Preparation of the dication **11a**$^{++}$.

The $^{31}P\{^{1}H\}$ NMR spectrum shows a broad singlet at +452 ppm, in the range expected for diphosphene.[33] In addition the ^{1}H NMR spectrum of **11a**$^{++}$ in CD_3CN displays only one set of signals for the carbene fragments. Noteworthy, the imidazole protons give rise to a broad signal between 8.1 and 8.5 ppm considerably down field in comparison to the corresponding signal in the free NHC (6.73 ppm in C_6D_6) consistent with the presence of two imidazolium rings. In consequence, compound **11a**$^{++}$ probably consists of a diphosphene in which the substituents at the phosphorus centers are the imidazolium groups.
The structure of **11a**$^{++}$ was unambiguously confirmed by X-ray diffraction analysis which shows that the dication has C_i symmetry and adopts a perfect trans-bent geometry (C-P-P-C torsion angle: 180 °) (Figure 14). Interestingly, the imidazol rings are almost orthogonal to the plane defined by the four central atoms C(1)–P(1)–P(2)–C(2) (86.82°), a geometry which was already encountered in the isoelectronic silicon adduct **8** (see paragraph 2.1.2)**.** Also in **11a**$^{++}$, the P–C (1.840 Å) and the P=P (2.083 Å) bond lengths are respectively longer and shorter than in the corresponding radical cation **11a**$^{+\cdot}$ (**11a**$^{+\cdot}$: P–C: 1.80 Å (average) and P=P: 2.09 Å).

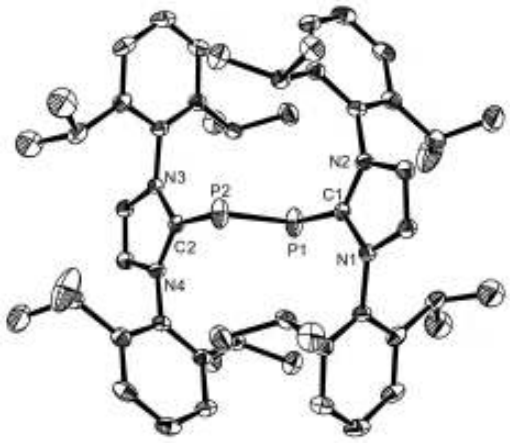

Figure 14. Solid-state structure of **11a**$^{++}$. 50% thermal ellipsoids are shown. Hydrogen atoms and the counter anions (TfO^-) are omitted for clarity.
Selected bond distances [Å] and angles [°]: P(1)–P(2) 2.0826(12), C(1)–P(1) 1.840(2); C(1)–P(1)–P(2) 97.23(7).

2.3.4) Interpretation of the results

To explain the geometry change upon oxidation of the P_2-bis(carbene) adducts (**10** and **11a**), and the spectroscopic differences between the adducts containing the CAAC ligands and the corresponding ones containing the NHC ligands, calculations were performed in collaboration with the group of Frenking at the MO5-2X/def-SVP level of theory.

As previously mentioned, the neutral P_2 adducts are better described as P_2 fragments stabilized by two carbenes. This description allows us to interpret the results discussed above by considering the difference in electronic properties between CAACs and NHCs. Indeed, some relevant molecular orbitals have been calculated for the experimentally observed molecules **10**, **11a**, $\mathbf{10}^{+\cdot}$, $\mathbf{11a}^{+\cdot}$, $\mathbf{11a}^{++}$ as well as for the elusive dication $\mathbf{10}^{++}$ and are shown in figure 15. As we see for the neutral complexes **10** and **11a**, the HOMO is mainly centered on the central P_2 moiety and corresponds to the doubly occupied π^* molecular orbital of P_2 which mixes in a bonding fashion with the 2p vacant orbitals at the carbene centers. Therefore, upon coordination, the electronic reference state of P_2 in **10** or **11a** is the doubly excited $^1\Gamma$ state due to the promotion of two electrons from one π molecular orbital to an antibonding π^* molecular orbital in the free P_2 molecule. The resulting in plane vacant $\pi(P_2)_{\|}$ molecular orbital is then involved in the bonding with the carbene ligands which occurs by donation from the σ lone pairs at the carbene centers giving rise to two low-lying molecular orbitals which are not shown here.

Therefore the more electrophilic character of the CAACs results in a more pronounced π back donation from the $\pi^*(P_2)$ MO to the carbene centers in **10** than in **11a**. Consequently the dissociation energy of the P_2-carbene bonds of **10** is higher than in **11a** (94.9 kcal.mol^{-1} versus 62.3 kcal.mol^{-1}) and in addition, the P-C bond lengths are slightly shorter in **10** than in **11a** (**10**: 1.73 Å and **11a**: 1.75 Å).This difference of π back donation results also in a lowering of the energy of the HOMO in **10** (**10**: -0.19 u.a. and **11a**: -0.15 u.a.) as observed in the voltammograms by the higher oxidation potential of **10** in comparison with **11a** (**10**: -0.536V, **11a**: -1.408 V).

When removing one electron, the HOMO in **10** or in **11a** becomes the SOMO in the radical cations $\mathbf{10}^{+\cdot}$ or $\mathbf{11a}^{+\cdot}$ and by removing a second electron it becomes the LUMO of $\mathbf{10}^{++}$ or $\mathbf{11a}^{++}$ (see figure 15). Consequently as observed experimentally in the EPR spectrums of the radical cations, because of the difference of the back donation strengths, the spin density is more localized on the P_2 fragment in $\mathbf{11a}^{+\cdot}$ than in $\mathbf{10}^{+\cdot}$ (this is also confirmed by the computed spin density in the radicals: $\mathbf{11a}^{+\cdot}$: 0.33e and 0.44e at each P center and $\mathbf{10}^{+\cdot}$**:** 0.27e at each P center).

Furthermore, when going from the neutral adducts to the radical cations and to the dications, because of the decrease of the number of electrons in the antibonding $\pi^*(P_2)$ orbital, the length of the P-P bond becomes shorter and the length of the P-C bonds become longer as observed experimentally.

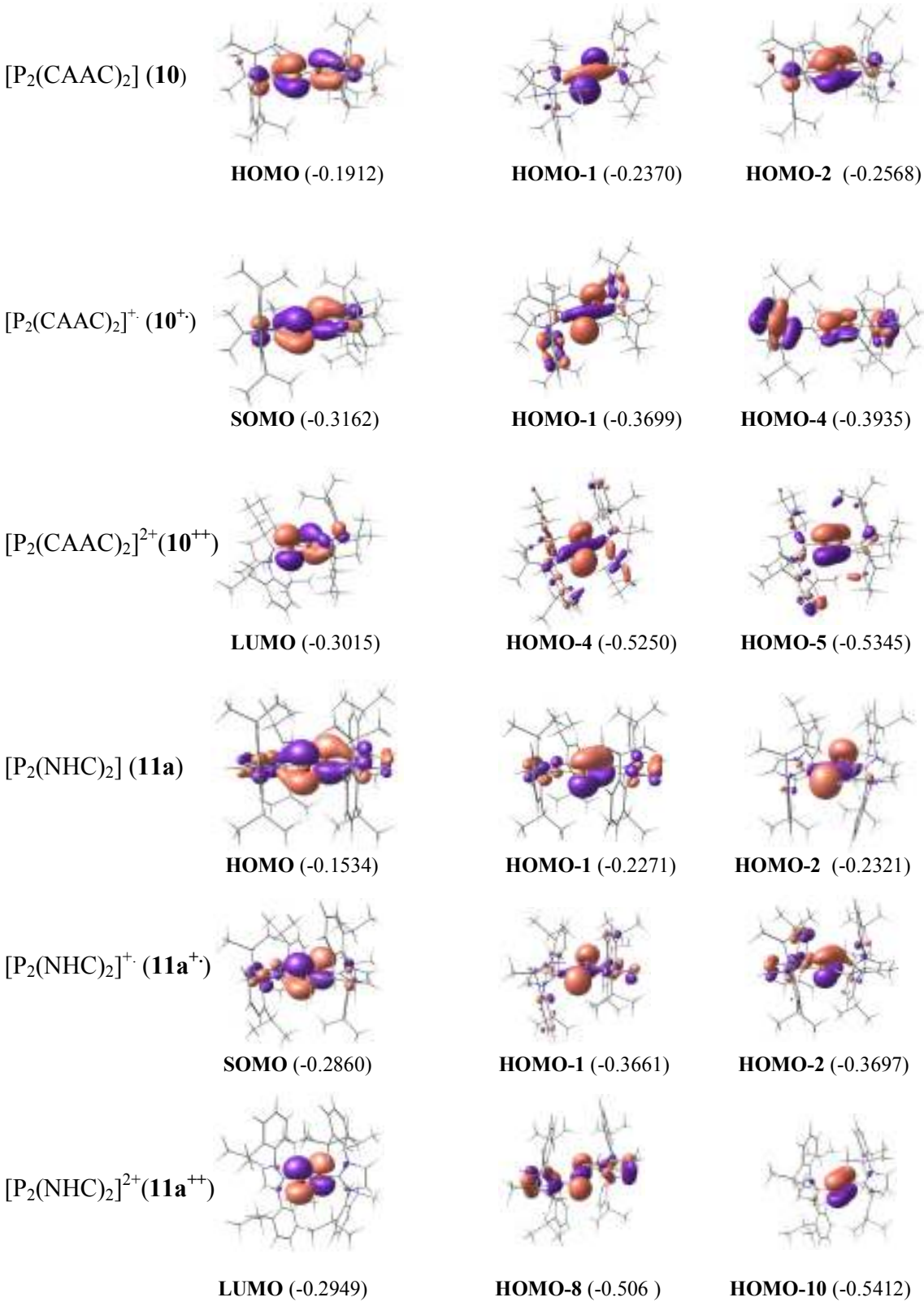

Figure 15. Selected molecular orbitals for the experimental molecules **10**, **10**$^{+\cdot}$, **11a**, **11a**$^{+\cdot}$, **11a**$^{++}$ and for the elusive dication **11**$^{++}$.

The calculated difference of dissociation energy between the CAACs adducts and the NHC adducts goes from $\Delta De = 32.6$ kcal.mol^{-1} in the neutral species to $\Delta De = 8.8$ kcal.mol^{-1} in the radical cations and reach finally $\Delta De = 0.2$ kcal.mol^{-1} in the dications. This is due to the fact that NHCs and CAACs have barely the same σ donor strength but the CAACs are more electrophilic.

2.4) Conclusion

In conclusion, a new and interesting application of stable carbenes has emerged: the stabilization of main group fragments in their zero oxidation state. Throughout this chapter, the resulting adducts were often described as carbene complexes in analogy with transition metals. We have shown, by observing the consequences of the successive one-electron oxidations of two P_2-adducts bearing different carbenes, that this description is actually correct. Moreover, these oxidations resulted in the synthesis and characterization of two kinds of new compounds that can be described as the carbene complexes of the extremely reactive $P_2^{+\cdot}$ radical cation and P_2^{2+} dication. Therefore, the stabilisation of paramagnetic and electron deficient fragments was achieved with the use of carbenes. As we will see in the last chapter, this concept will be applied with success to the isolation of other paramagnetic species.

References

[1] a) S. Diez-Gonzalez, N. Marion and S. P. Nolan, *Chem. Rev. (Washington, DC, U. S.)* **2009**, *109*, 3612-3676; b) J. C. Y. Lin, R. T. W. Huang, C. S. Lee, A. Bhattacharyya, W. S. Hwang and I. J. B. Lin, *Chem. Rev. (Washington, DC, U. S.)* **2009**, *109*, 3561-3598.
[2] G. C. Vougioukalakis and R. H. Grubbs, *Chem. Rev. (Washington, DC, U. S.)* **2010**, *110*, 1746-1787.
[3] a) D. Enders, O. Niemeier and A. Henseler, *Chem. Rev. (Washington, DC, U. S.)* **2007**, *107*, 5606-5655; b) N. Marion, S. Diez-Gonzalez and S. P. Nolan, *Angew. Chem., Int. Ed.* **2007**, *46*, 2988-3000; c) N. E. Kamber, W. Jeong, R. M. Waymouth, R. C. Pratt, B. G. G. Lohmeijer and J. L. Hedrick, *Chem. Rev. (Washington, DC, U. S.)* **2007**, *107*, 5813-5840.
[4] G. D. Frey, V. Lavallo, B. Donnadieu, W. W. Schoeller and G. Bertrand, *Science (Washington, DC, U. S.)* **2007**, *316*, 439-441.
[5] V. Lavallo, Y. Canac, B. Donnadieu, W. W. Schoeller and G. Bertrand, *Angew. Chem., Int. Ed.* **2006**, *45*, 3488-3491.
[6] C. A. Dyker and G. Bertrand, *Science (Washington, DC, U. S.)* **2008**, *321*, 1050-1051.
[7] C. A. Dyker, V. Lavallo, B. Donnadieu and G. Bertrand, *Angew. Chem., Int. Ed.* **2008**, *47*, 3206-3209.
[8] Y. Wang, Y. Xie, P. Wei, R. B. King, H. F. Schaefer, III, P. v. R. Schleyer and G. H. Robinson, *Science (Washington, DC, U. S.)* **2008**, *321*, 1069-1071.
[9] Y. Wang, Y. Xie, P. Wei, R. B. King, H. F. Schaefer, III, P. v. R. Schleyer and G. H. Robinson, *J. Am. Chem. Soc.* **2008**, *130*, 14970-14971.
[10] M. Y. Abraham, Y. Wang, Y. Xie, P. Wei, H. F. Schaefer, III, P. v. R. Schleyer and G. H. Robinson, *Chem.--Eur. J.* **2010**, *16*, 432-435, S432/431-S432/435.
[11] O. Back, B. Donnadieu, P. Parameswaran, G. Frenking and G. Bertrand, *Nat. Chem.* **2010**, *2*, 369-373.
[12] F. Ramirez, N. B. Desai, B. Hansen and N. McKelvie, *J. Am. Chem. Soc.* **1961**, *83*, 3539-3540.
[13] R. Tonner, F. Oexler, B. Neumueller, W. Petz and G. Frenking, *Angew. Chem., Int. Ed.* **2006**, *45*, 8038-8042.
[14] R. Appel, F. Knoll, W. Michel, W. Morbach, H. D. Wihler and H. Veltmann, *Chem. Ber.* **1976**, *109*, 58-70.
[15] R. Appel, F. Knoll, H. Schoeler and H. D. Wihler, *Angew. Chem.* **1976**, *88*, 769-770.
[16] G. E. Hardy, J. I. Zink, W. C. Kaska and J. C. Baldwin, *J. Am. Chem. Soc.* **1978**, *100*, 8001.
[17] S. Elgafi, L. D. Field, B. A. Messerle, P. Turner and T. W. Hambley, *J. Organomet. Chem.* **1999**, *588*, 69-77.
[18] R. W. Saalfrank, *Isr. J. Chem.* **1985**, *26*, 181-190.
[19] R. Tonner and G. Frenking, *Angew. Chem., Int. Ed.* **2007**, *46*, 8695-8698.
[20] a) R. J. Van Zee, R. F. Ferrante and W. Weltner, Jr., *J. Chem. Phys.* **1985**, *83*, 6181-6187; b) M. R. Nimlos, L. B. Harding and G. B. Ellison, *J. Chem. Phys.* **1987**, *87*, 5116-5124.
[21] J. Steinwandel and J. Hoeschele, *Chem. Phys. Lett.* **1985**, *116*, 25-29.
[22] A. Krapp, F. M. Bickelhaupt and G. Frenking, *Chem.--Eur. J.* **2006**, *12*, 9196-9216.
[23] M. Weidenbruch, *Chem. Org. Silicon Compd.* **2001**, *3*, 391-428.

[24] M. Regitz, O. J. Scherer and Editors, *Multiple Bonds and Low Coordination in Phosphorus Chemistry*, **1990**, p. 478 pp.
[25] N. A. Piro, J. S. Figueroa, J. T. McKellar and C. C. Cummins, *Science (Washington, DC, U. S.)* **2006**, *313*, 1276-1279.
[26] L. Weber, *Chem. Rev.* **1992**, *92*, 1839-1906.
[27] L. R. Maxwell, S. B. Hendricks and V. M. Mosley, *J. Chem. Phys.* **1935**, *3*, 699-709.
[28] Y. Wang, Y. Xie, P. Wei, R. B. King, F. Schaefer Henry, 3rd, R. Schleyer Paul v and H. Robinson Gregory, *J Am Chem Soc* **2008**, *130*, 14970-14971.
[29] O. Back, G. Kuchenbeiser, B. Donnadieu and G. Bertrand, *Angew. Chem., Int. Ed.* **2009**, *48*, 5530-5533.
[30] L. Weber, *Eur. J. Inorg. Chem.* **2000**, 2425-2441.
[31] N. G. Connelly and W. E. Geiger, *Chem. Rev. (Washington, D. C.)* **1996**, *96*, 877-910.
[32] a) M. Geoffroy, A. Jouaiti, G. Terron, M. Cattani-Lorente and Y. Ellinger, *J. Phys. Chem.* **1992**, *96*, 8241-8245; b) T. Sasamori, E. Mieda, N. Nagahora, K. Sato, D. Shiomi, T. Takui, Y. Hosoi, Y. Furukawa, N. Takagi, S. Nagase and N. Tokitoh, *J. Am. Chem. Soc.* **2006**, *128*, 12582-12588.
[33] a) P. P. Power, *Chem. Rev. (Washington, D. C.)* 1999, *99*, 3463-3503; b) T. Sasamori and N. Tokitoh, *Dalton Trans.* **2008**, 1395-1408.

Experimental part

Synthesis of 9a:

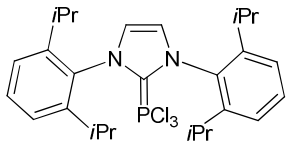

PCl_3 (1.840 g, 13.40 mmol) was added at room temperature to a slurry of the free NHC **6a** (5.200 g, 13.40 mmol) in 50 mL of hexane. The mixture is then stirred at room temperature during two days. The white precipitate is then filtered via cannula and is dried under vacuum to afford **9a** as a white powder. Yield: 97 % (6.840 g, 13.05 mmol).

$^{31}P\{^1H\}$ ($CDCl_3$, 162 MHz): δ 109.14.

^1H ($CDCl_3$, 400 MHz): δ 1.15 (d, J = 7.2 Hz, 12 H), 1.18 (d, J = 7.2 Hz, 12 H), 2.25 (sept, J = 7.2 Hz, 4 H), 7.26 (d, J = 7.6 Hz, 4 H), 7.52 (t, J = 7.6 Hz, 2 H), 8.82 (s, 2 H).

$^{13}C\{^1H\}$ ($CDCl_3$, 100 MHz): δ 22.6, 26.1, 29.7, 125.0, 129.3, 132.2, 133.1, 142.0 (d, J_{PC} = 120 Hz, $C_{carbene}$), 145.3.

Synthesis of 11a:

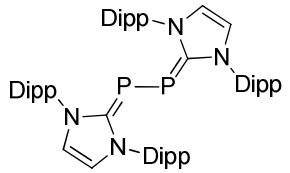

80 mL of THF is added at -80°C to a mixture of **9a** (5.620 g, 10.72 mmol) and potassium graphite (4.500 g, 33.29 mmol). The mixture is then stirred at room temperature overnight and the graphite is removed by filtration. The filtrate is then concentrated to 5 mL. After three days at -30°C, **11a** was obtained as dark red crystals extremely sensitive to air and moisture. Yield: 24 % (1.100 g, 1.31 mmol).

$^{31}P\{^1H\}$ (C_6D_6, 162 MHz): δ -51.8.

^1H (C_6D_6, 400 MHz): δ 1.06 (d, J = 7.2 Hz, 24 H), 1.28 (d, J = 7.2 Hz, 24 H), 2.97 (br s, 8 H), 5.7-6.2 (br s, 4 H), 6.94 (d, J = 6.8 Hz, 8 H), 7.10 (t, J = 6.8 Hz, 4 H).

$^{13}C\{^1H\}$ (THF, 125.75 MHz): δ 23.2, 24.4, 28.7 (d, J_{PC} = 6 Hz), 120 (br s), 123.4, 123.5, 128.8, 133.1, 148 (br s).

Synthesis of $10^{+\cdot}$:

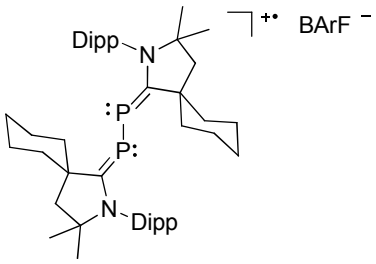

Toluene (5 mL) was added at room temperature to a mixture of **10** (0.385 g, 0.54 mmol) and $Ph_3CB(C_6F_5)_4$ (0.498 g, 0.54 mmol). Immediately upon addition the color of the solution turned dark purple. The mixture was then stirred at room temperature during 2 hours and the solvent was removed under vacuum. The purple residue was washed 5 times with 10 mL of hexane and was finally dried under vacuum to afford quantitatively compound $\mathbf{10}^{+\cdot}$ as a highly air sensitive fine purple powder. Single crystals of $\mathbf{10}^{+\cdot}$ were grown by layering hexane on top of a fluorobenzene solution at 0°C. Yield 100 % (0.750 g, 0.54 mmol).

Mp: 193 ^{o}C.

Synthesis of $\mathbf{11a}^{+\cdot}$:

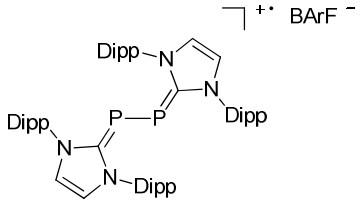

Toluene (10 mL) was added at room temperature to a mixture of **11a** (0.558 g, 0.67 mmol) and $C(Ph)_3B(C_6F_5)_4$ (0.613 g, 0.67 mmol). Immediately upon addition the color of the solution turned black. The mixture was then stirred at room temperature during 3 hours and the solvent was removed under vacuum. The black residue was washed 4 times with 20 mL of hexane and was finally dried under vacuum to afford quantitatively compound $\mathbf{11a}^{+\cdot}$ as a fine black powder. Single dark red crystals of $\mathbf{11a}^{+\cdot}$ were grown by layering hexane on top of a fluorobenzene solution at room temperature. Yield 100 % (1.020 g, 0.67 mmol).

Mp: 103 ^{o}C.

Synthesis of $11a^{++}$:

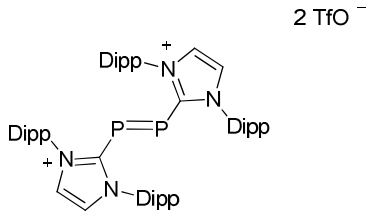

THF (8 mL) was added at room temperature to a mixture of **11a** (0.400 g, 0.48 mmol) and ferrocenium triflate (0.320 g, 0.96 mmol). The mixture was then stirred at room temperature in the dark. After 2 hours, the color of the solution turned brown and a precipitate appeared. After filtration, the residue was washed 3 times with 10 mL of ether and then dried under vacuum to afford compound $\mathbf{11a}^{++}$ as a fine pale yellow powder. Single crystals of $\mathbf{11a}^{++}$ were grown by slow evaporation of an acetonitrile solution at room temperature. Yield: 42 % (0.230 g, 0.20 mmol).

Mp: 262°C, dec.

$^{31}\mathbf{P}\{^{1}\mathbf{H}\}$ NMR (CD_3CN, 162 MHz): δ 451.8.

$^{1}\mathbf{H}$ NMR (CD_3CN, 400 MHz): δ 0.87 (d, J = 6 Hz, 24 H), 1.11 (d, J = 6 Hz, 24 H), 2.11 (sept, J = 6 Hz, 8 H), 7.35 (d, J = 8 Hz, 8 H), 7.61 (t, J = 8 Hz, 4 H), 8.1-8.5 (br s, 4 H).

Chapter III

Carbene stabilization of phosphinyl radicals

3.1) Stable phosphinyl radicals: a chemical challenge

The involvement of a variety of phosphorus radicals in chemical reactions has been recognized for many decades.[1] Since then, several persistent and even stable phosphorus based radicals have been reported. However, by examining the literature we can observe that overall, the rare phosphorus radicals that have been previously characterized in the solid state are resonance-stabilized. Therefore, the reduced spin density at the phosphorus center makes them less prone to dimerization. For instance, the oxidation of the allylic anion **1** using iodine affords the phosphaallyl radical **2**,[2] and the photolysis of the complex **3** in the presence of the diphosphene $Mes^*P{=}PMes^*$ leads to the triphosphaallyl radical **4** (Scheme 1).[3] In addition, Cummins *et al.* reported in 2007 the synthesis of a stable phosphorus radical **5** which is resonance stabilized by the vanadium (IV/V) redox couple. We will discuss later about this interesting compound which can also be viewed as a stable phosphinyl radical bearing the bulky metalloligands $NV[N(Np)Ar]_3$ (Np = neopentyl, Ar = 3,5-$Me_2C_6H_3$) (Scheme 1).[4]

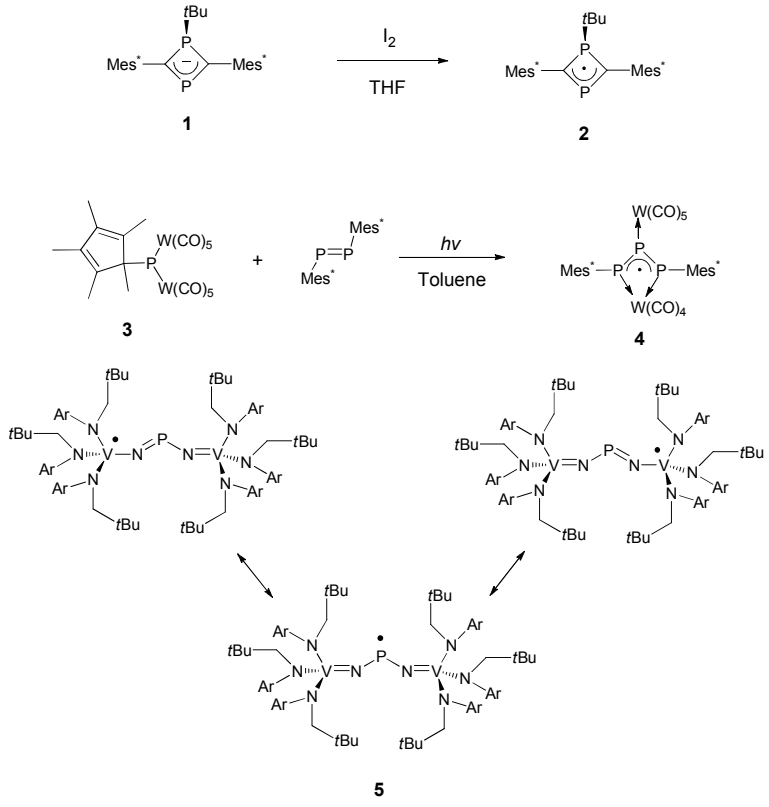

Scheme 1. Previously described resonance-stabilized phosphorus radicals **2**, **4** and **5** (Ar = 3,5-$Me_2C_6H_3$).

Phosphinyl radicals constitute a family of phosphorus centered radicals of the general formula: $R_2P^{\bullet}$. In this species, the single electron resides mainly in a

3p orbital of the divalent phosphorus atom. The electronic structure of a phosphinyl radical is depicted in Figure 1.

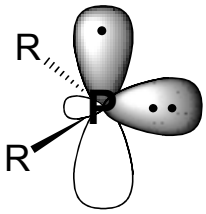

Figure 1. Electronic structure of a phosphinyl radical $R_2P^{\cdot}$

The first spectroscopic observation at low temperature of the diphenylphosphinyl radical $Ph_2P^{\cdot}$ was reported in 1966.[5] Since then, several persistent examples of such radicals[6] have been described. However, despite many efforts, no example of a neutral organic phosphinyl radical was found to be stable at room temperature in solution and in the solid state. Indeed, due to their high reactivity and their tendency to dimerize, the isolation of a stable phosphinyl radical represents a significant chemical challenge.

Phosphorus radicals are also interesting due to their characteristic signature in the EPR spectrum resulting from the hyperfine coupling with the ^{31}P nucleus. This feature allows for an easy experimental determination of their electronic structure which is interesting in a fundamental point of view. In addition, it opens the way for a potential application as spin labels.[7] Indeed, because of the large anisotropy of the hyperfine coupling tensor, phosphorus radicals would provide details about much faster molecular movements than the widely used nitroxide radicals. The latter advantage was indeed exploited by the groups of Grutzmacher and Geoffroy who studied the temperature dependence of the solution EPR spectrum of the diphosphanyl radical $[(Mes^{*})MePPMes^{*}]^{\cdot}$.[8]

In summary, due to the fundamental importance of phosphinyl radicals, their potential application as spin labels, and the challenge associated to the design and the synthesis of stable derivatives, different research groups have tried various strategies for their stabilization. We can also say that almost all the persistent phosphinyl radicals previously reported are prepared by a controlled one-electron oxidation or reduction of a suitable precursor. This precursor can be for example a simple chlorophosphine but it can also consist in a more complex phosphorus derivative like a phosphaalkene.

3.2) Previously reported persistent phosphinyl radicals: kinetic versus thermodynamic stabilization

3.2.1) Highly persistent sterically hindered phosphinyl radicals

In the field of persistent phosphinyl radicals, the pioneer work was done by Power *et al*. in 1976. They reported the synthesis and characterization in solution of the highly persistent phosphinyl radicals **9** ($t_{1/2}$ > 1 year) and **10a** ($t_{1/2} \approx$

5 days) which are kinetically stabilized by the presence of very bulky organic substituents (Scheme 2).[9] The radicals were generated by the photochemical reduction using the electron-rich alkene **6** of the corresponding chlorophosphines **7** and **8a**.

In solution, at room temperature both radicals exhibit in the EPR spectra a large doublet due to the hyperfine coupling with the ^{31}P nucleus (**9**: a(^{31}P) = 96.3 G and **10a**: a(^{31}P) = 91.8 G). The radical **9** displays an additional small splitting caused by the two equivalent methine protons of the alkyl substituents (**9**: a(^{1}H) = 6.4 G). The measured ^{31}P isotropic hyperfine coupling constants are comparable to the ones usually observed for other persistent phosphinyl radicals (a_{iso}(^{31}P) = 63-100 G).[6]

The frozen solution EPR spectra at -153°C of the two radicals are quite similar and display a relatively large parallel hyperfine splitting (**9**: $A_{\parallel}$(^{31}P) = 291 G and **10a**: $A_{\parallel}$(^{31}P) = 294 G) and a small perpendicular component (**9**: $A_{\perp}$(^{31}P) = -1.0 G and **10a**: $A_{\perp}$(^{31}P) = -9.3 G). These values suggest that that the SOMO is centered on the phosphorus atom and is mainly constituted of a 3p(P) orbital, in agreement with a phosphinyl radical.

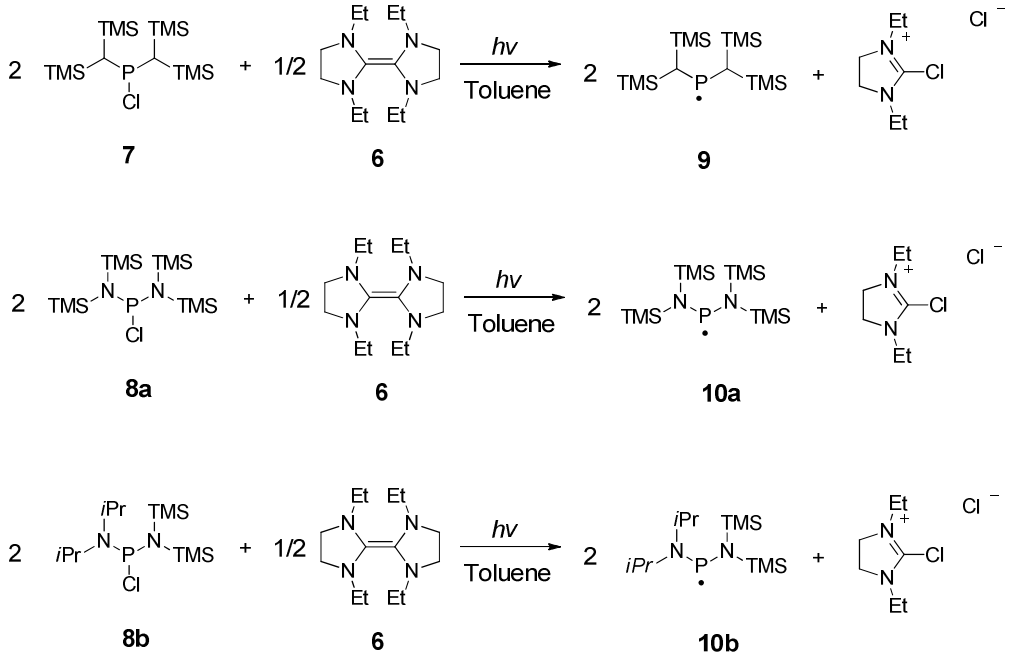

Scheme 2. Preparation of the highly persistent radicals **9**, **10a** and **10b**.

Four years later, the same group reported the generation and characterization of the phophinyl radical **10b** ($t_{1/2}$ ≈ 1 day) (see Scheme 2). This radical exhibits a slightly lower isotropic hyperfine coupling with the ^{31}P nucleus than **10a** (**10b**: a(^{31}P) = 77 G, *g* = 2.007). Also an additional splitting is observed in the EPR spectrum of **10b** attributed to the hyperfine coupling with a nitrogen nucleus (**10b**: a(^{14}N) = 5 G). This additional coupling, which is not apparent in the spectrum of **10a** and the lower ^{31}P hyperfine coupling constant suggest a slight delocalization

of the spin density from the phosphorus center to one nitrogen atom in **10b**. This delocalization occurs probably through a P-N p_π-p_π interaction.
Among those species, the most stable one (**9)** has a half-life longer than one year in solution. However, in the solid state the latter readily dimerizes to give the corresponding diphosphine **11a** despite the bulkiness of the phosphorus substituents (Scheme 3).[10] Moreover, **11a** can redissociate to the radical **9** through a homolytic P-P bond cleavage occurring by melting, sublimation or dissolution in a solvent. In order to explain this reversible dimerization of the radical, it is necessary to look closely to the conformations adopted by **9** and **11a**.
According to a gas-phase electron diffraction study, the radical **9** adopts a V-shaped geometry with a *syn*, *syn* conformation for the -C*H*(TMS)$_2$ substituents. In this conformation, the methine hydrogens of the -C*H*(TMS)$_2$ groups point toward the middle of the V-shaped structure reducing therefore the steric repulsions between these bulky groups (Scheme 3). This conformation is supposed to be maintained also in solution.

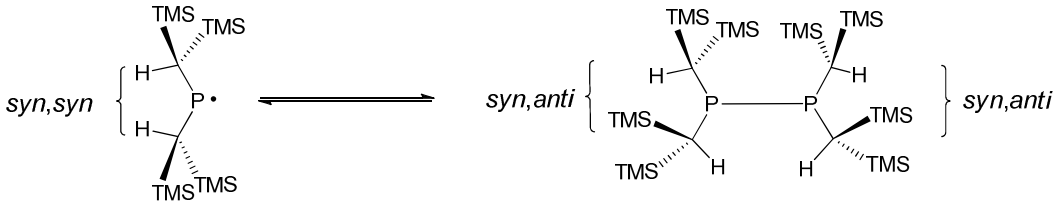

Scheme 3. Dimerization in the solid state of the radical **9** affording the diphosphine **11a**.

The solid-state structure of the dimer was determined thanks to an X-ray diffraction study performed on a single crystal of **11a**. The asymmetric unit contains one independent molecule. In the solid state, the molecule **11a** possesses approximately C_2 symmetry. Each phosphorus center is pyramidized (sum of the angles at the phosphorus centers: 315.3° and 316.3°) and the molecule adopts an overall *anti* configuration. In this conformation the phosphorus lone pairs are pointing toward opposite directions.
When looking at each phosphorus center, the pair of (-CH(TMS)$_2$) substituents display a *syn*, *anti* configuration (see Scheme 3). Due to this conformation, additional steric strains appear in the molecule.
These additional strains add to the repulsions already occurring between the two PR$_2$ fragments (interactions **S1** in Scheme 4) indicated by the elongated P-P single bond (0.1 Å longer than the average value for typical P-P single bonds).

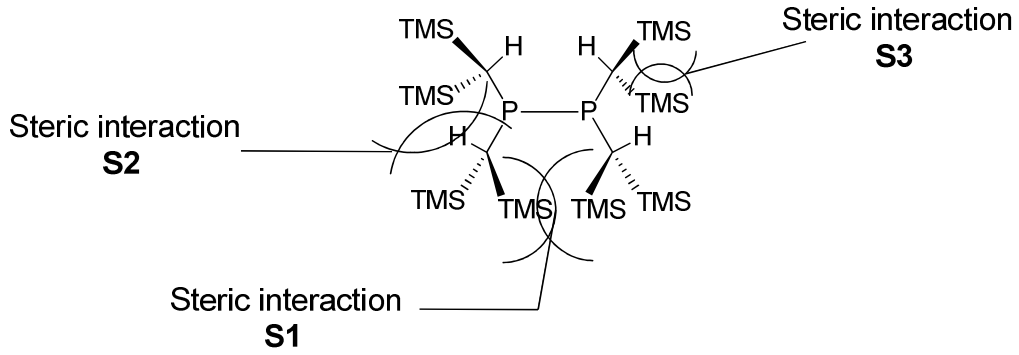

Scheme 4. Steric interactions occurring in the dimer **11a**.

Those additional strains are due to the repulsions taking place between the two (-$CH(TMS)_2$) ligands at each phosphorus center (steric interactions **S2** in Scheme 4) and also between the –TMS groups within each substituent (steric interactions **S3** in Scheme 4).

These strains result in important structural distortions in the molecule. This is well reflected on one hand by the important variation of the bond angles at the methine carbon and silicon atoms in the molecule. The root-mean-square variances are 17.96° for the angles at the methine carbon atom and 4.06° for the ones at the silicon atom. These values are significantly larger than the corresponding values in the gas-phase structure of radical **9** (3.88° and 2.55°) in agreement with more important distortions in **11a**. The deformation of the (-$CH(TMS)_2$) ligands is also apparent on the other hand by the elongation of the bonds: for example the average value for the P-C bond lengths in **11a** is: 1.89 Å (the average value for typical acyclic P-C single bonds is 1.85 Å).

Calculations were performed in order to gain insight into the dissociation process. In this computational study the calculated geometry of the radical **9** was in very good agreement with the experiment. Concerning the dimer **11a**, full optimization was not performed and the geometry was restricted to the crystallographically determined geometry.

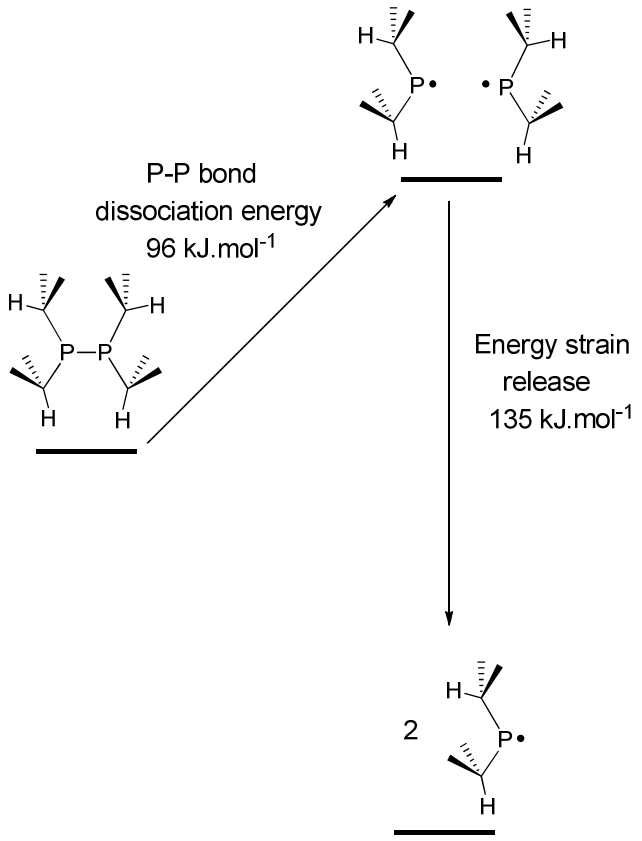

Scheme 5. DFT computed P-P bond cleavage energy of the diphosphine **11a** and subsequent energy strain released in each radical fragment.

These calculations indicate that the experimentally observed P-P bond elongation of 0.1 Å corresponds to a decrease of the P-P bond strenght of only 4 kJ.mol^{-1} and therefore cannot explain the easy dissociation. Although that during the P-P bond cleavage the **S1** steric repulsions are released (see Scheme 4), the splitting of **11a** remains still endothermic (96 kJ.mol^{-1} according to calculations). However, after dissociation the conformation change of the (-CH(TMS)$_2$) ligands from *syn*, *anti* to *syn*, *syn* in the resulting fragments cancel the important steric strains **S2** and **S3** (see scheme 4). According to calculations, the energy release during this process is 67 kJ.mol^{-1} per PR_2 fragment (135 kJ.mol^{-1} per dimer) compensating largely the energy cost for the P-P cleavage (see Scheme 5). In consequence, the bulky but flexible (-CH(TMS)$_2$) ligands in **11a** behave as energy reservoirs and can be compared to springs.
Whereas the radical **10a** has not been further studied, its derivative **10b** ·P[N(TMS)$_2$][N*i*Pr$_2$] displays a behavior similar to **9** (Scheme 6).[11] The corresponding dimers **11b** (*rac*- and *meso*- diastereoisomers) were directly made from the chlorophosphine **8b** by reduction with K/C_8. The latters undergoe reversible cleavage to the radical **10b** upon warming a hexane solution of **11b** (Scheme 6).

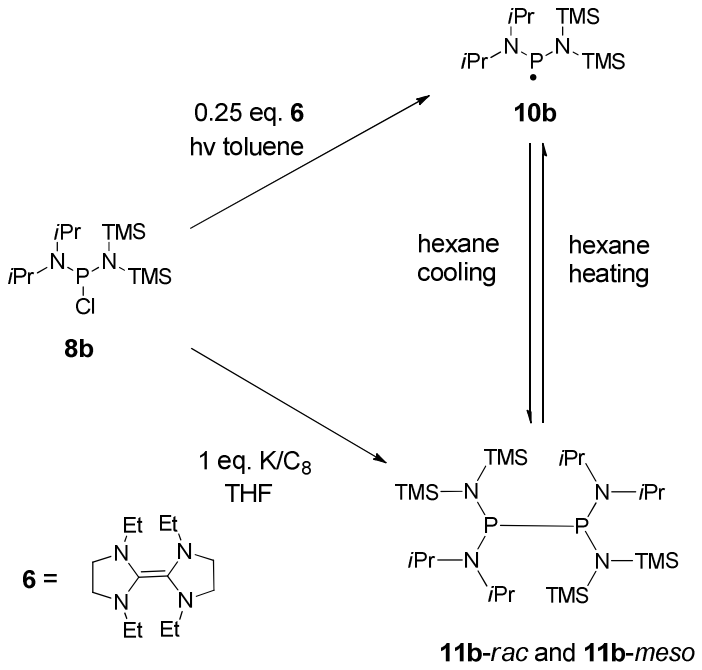

Scheme 6. Preparation of the radical **10b** and the diphosphines **11b**.

Interestingly, when the dimers **11b** are reacted with white phosphorus in toluene at reflux, the products **12**-*rac*/*meso* are formed together in 63% yield.[12] It was proposed that the radical **10b** is an intermediate generated during the reaction which consequently reacts with white phosphorus (Scheme 7)

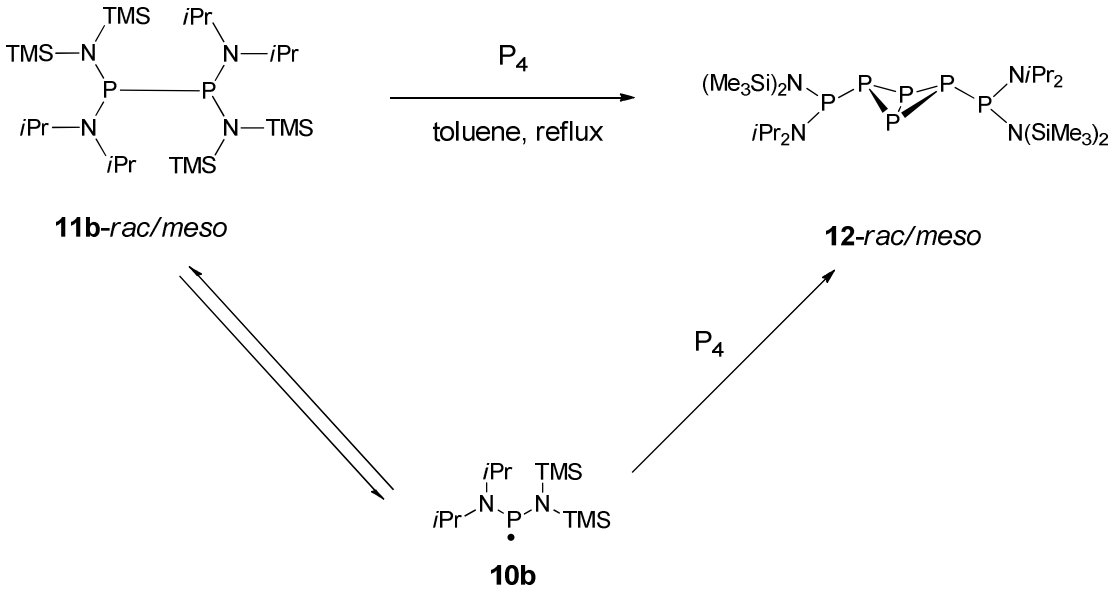

Scheme 7. Reaction between **11b**-*rac/meso* and P_4.

In conclusion, these results clearly outline the high propensity of phosphinyl radicals to dimerize in the solid state even in the presence of bulky substituents. This tendency is so strong that the strain energy accumulated in the molecule is even higher that the P-P bond dissociation energy. It appears therefore that kinetic protection strategy is not efficient enough for the stabilization of phosphinyl radicals. For this reason, the first synthesis of a stable phosphinyl radical avoiding the dimerization in the solid state was possible thanks mainly to thermodynamic stabilization.

3.2.2) Transition metal stabilization of phosphinyl radicals

It was only in 2007 that the first example of a phosphinyl radical stable in the solid state (the already mentioned compound **5**) was reported by Cummins *et al*.[4] In order to achieve this goal, the author took advantage of the electronic stabilization afforded by transition metals. Indeed, on the contrary to main group elements, transition metals are susceptible to undergo one-electron redox process. Thus, the radical **5** was prepared smoothly by one-electron reduction of the chlorophosphine precursor **13** bearing the metalloligand $NV[N(Np)Ar]_3$ using potassium graphite (K/C_8) (Np = neopentyl, Ar = 3,5-$Me_2C_6H_3$) (Scheme 8).

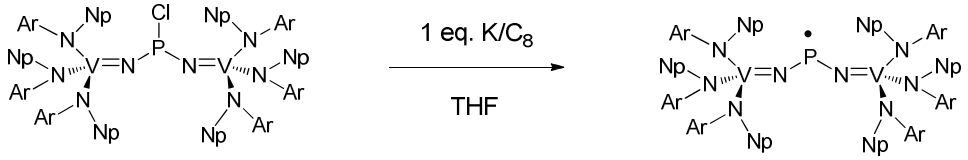

13 **5**

Scheme 8. Preparation of the stable radical **5** bearing the metalloligand $NV[N(Np)Ar]_3$ (Np = neopentyl, Ar = 3,5-$Me_2C_6H_3$).

Compound **5** is stable at room temperature both in solution and in the solid state allowing its complete characterization. The room temperature solution EPR spectrum of **5** displays a complex splitting pattern due to the hyperfine coupling with the ^{31}P nucleus (I =1/2, 100%, a(^{31}P) = 42.5 G) and the hyperfine coupling with the two equivalent ^{51}V nuclei (I = 7/2, 99.75%, a(^{51}V) = 23.8 G). The hyperfine coupling constant with the phosphorus nucleus is only half of the one observed for radicals **9** and **10a** suggesting a significantly reduced spin density at the phosphorus center. The observed hyperfine coupling constant with the vanadium nuclei is also small in comparison with the ones reported for $[V(NMe_2)_4]^{\cdot}$ (65 G) or for $[V(NEt_2)_4]^{\cdot}$ (66 G).[13] All together these results suggest clearly a significant delocalization of the spin density over the two vanadium and the phosphorus atoms. To gain more insight into the electronic situation in compound **5**, calculations were performed on the model system **5'** $[P\{NV(N(Me)Ph]_3\}_2]^{\cdot}$.

The calculations indicate that the SOMO in **5'** is mainly constituted of the phosphorus $3p_y$ orbital (31.30%) and the vanadium $3d_{xy}$ and $3d_{x^2-y^2}$ orbitals

(39.49% and 8.33% respectively over the two vanadium atoms) (See figure 2). Therefore, the calculations are in agreement with a significant delocalization of the single electron from the phosphorus center to the vanadium atoms as illustrated by the resonance structures depicted in Scheme 1.

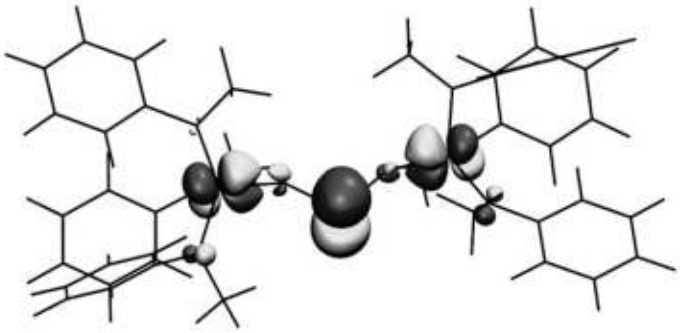

Figure 2. Calculated SOMO of the model radical **5'** showing the delocalization of the spin density over the vanadium and phosphorus centers (adapted from ref. 4).

In the solid state, the NPN bond angle of **5** is 110.9° and importantly the P-N bonds (average 1.62 Å) are shorter than a regular P-N single bond (1.77 Å).[14] This last geometrical parameter is in agreement with the delocalization of the radical over the vanadium centers increasing the P-N bond order (see resonance structures in Scheme 1). Importantly, reactivity studies showed that on the contrary to the bulky phosphinyl radical ·P[N(TMS)$_2$][N*i*Pr$_2$] **10b**,[11-12] compound **5** is not able to activate P_4. Also no reaction was observed with the common H-atom sources *n*Bu$_3$SnH, *n*Bu$_2$SnH$_2$ and [(η^5-C$_5$H$_5$)(CO)$_3$MoH]. This lack of reactivity is attributed to the reduced spin density at the phosphorus center in the radical **5**.

Therefore, the use of metalloligands to stabilize thermodynamically the phosphinyl radical proves to be efficient enough to prevent dimerization in the solid state. This is mainly due to a significantly reduced spin density at the phosphorus center. Also, the steric shielding provided by the bulky metalloligands around the phosphorus center may account as well for the stability of **5**. As a consequence of the important radical delocalization some concern may be raised about the phosphinyl nature of **5** which can alternatively be viewed as a mixed valence vanadium (IV/V) system bridged by a NPN ligand (Scheme 9).

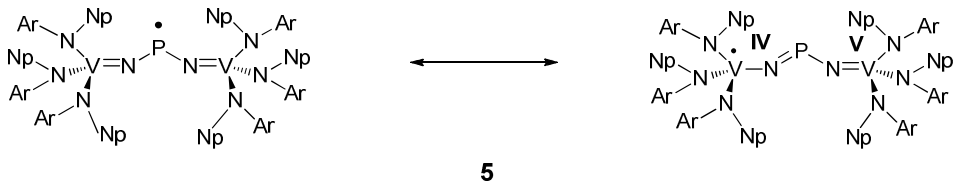

Scheme 9. Two possible descriptions of the compound **5**: on the left a phosphinyl radical, on the right a mixed valence complex vanadium (IV/V).

To summerize, two different ways have been used for the stabilization of phosphinyl radicals: kinetic protection and electronic stabilization. In the first case, the radicals display an important spin density at the phosphorus center and are highly persistent. However, despite steric hindrance around the phosphorus center, they readily dimerize in the solid state. In the second case, electronic stabilization along with steric protection offered by the vanadium metalloligands allowed the phosphorus radical to be stable even in the solid state. However, EPR as well as computational analysis revealed a significant decrease of the spin density at the phosphorus center. For the latter, one of the main consequence is its lack of reactivity.

3.3) Polarized phosphaalkenes as precursors for the synthesis of phosphinyl radicals

The previously discussed neutral radicals were prepared by the one-electron reduction of the corresponding chlorophosphines. It will be shown in this section that some neutral phosphaalkenes can also be suitable precursors of phosphorus radicals. In fact, by choosing carefully the substituents of the phosphaalkene, the polarity of the latter can be modified. In consequence, it is possible to generate the corresponding radical cation or radical anion respectively by one-electron oxidation or one-electron reduction of the phosphaalkene. In addition, the generated radicals are persistent in solution allowing their characterization. Moreover, EPR and computational analysis indicate that these phosphorus radicals feature an important phosphinyl character.

3.3.1) Reduction of phosphaalkenes containing an electron-deficient phosphorus center

In 1997, Geoffroy *et al*. generated and characterized the radical anions **15a** and **15b** obtained by the one-electron reduction of the respective phosphaalkenes **14a** and **14b**.[15] These phosphaalkenes can be prepared easily in two steps starting from cyclopentadienide or fluorenide lithium respectively (Scheme 10).[16]
Due to the incorporation of the phosphaalkenic carbon into the cyclopentadiene or the fluorene ring in **14a** or **14b**, respectively, the phosphorus center in each compound is electron-deficient as outlined by the resonance forms depicted in scheme 11.

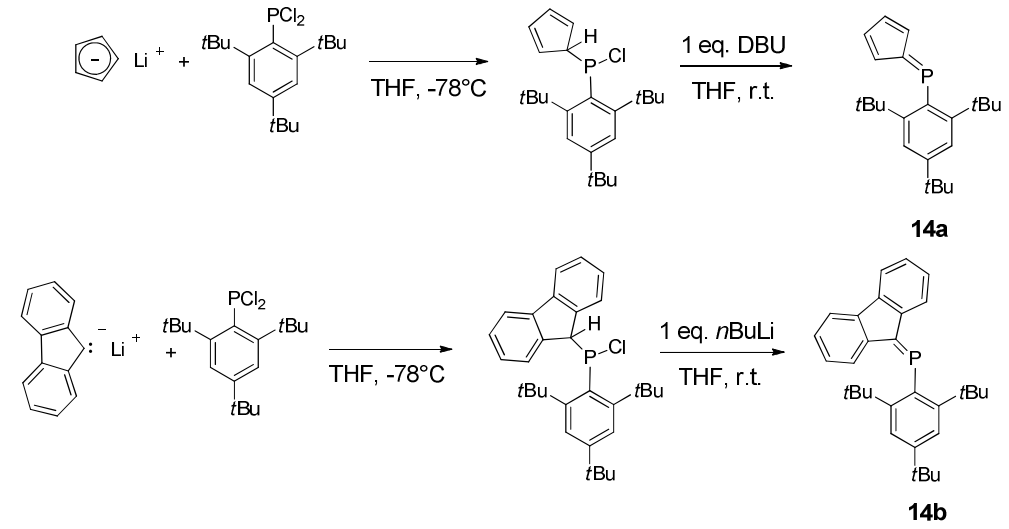

Scheme 10. Preparation of the phosphalkenes **14a** and **14b**.

This is also confirmed by the cyclic voltammetries carried out for both species in THF at room temperature. Indeed, **14a** and **14b** undergo a reversible one-electron reduction at $E_{1/2}$ = -1.339 V and $E_{1/2}$ = -1.494 V, respectively (vs saturated calomel electrode (SCE)). These potentials are significantly higher than the previously reported reduction potential for the "typical" phosphaalkene **14c** (see scheme 11) featuring a phenyl substituent at the phosphaalkenic carbon ($E_{1/2}$ = -1.980 V vs SCE).[17]

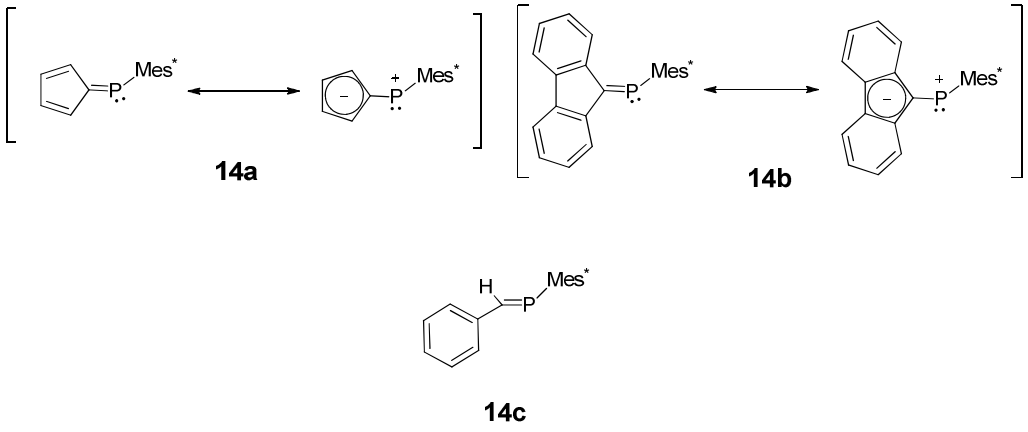

Mes* = 2,4,6-tri-*tert*-butylphenyl

Scheme 11. Resonance structures of the phosphaalkenes **14a** and **14b** (Mes* = 2,4,6-tri-*tert*-butylphenyl).

These results clearly indicate that it is easier to reduce **14a** or **14b** than **14c** in agreement with the more electrodeficient phosphorus center in the two phosphafulvenes. The radical anions **15a** and **15b** were then generated by electrochemical reduction of **14a** and **14b** in THF or by reduction with a

potassium mirror in THF (only for **14a**) (Scheme 12). The EPR spectra recorded in solution were similar in both cases. In the room temperature measurement, each spectrum displays a large splitting due to the isotropic hyperfine coupling with the ^{31}P nucleus. The measured hyperfine coupling constants (**15a**: a(^{31}P) = 90 G, g = 2.0039 and **15b**: a(^{31}P) = 79 G, g = 2.0059) are in the range of the corresponding values observed for other persistent neutral phosphinyl radicals (a(^{31}P) = 63-100 G).[6] Moreover, the frozen solution EPR spectra show that in each case the hyperfine coupling tensor displays axial symmetry with a large parallel hyperfine splitting and a small perpendicular component (**15a:** $A_{\parallel}$(^{31}P) = 250 G, $A_{\perp}$(^{31}P) = 10 G, $g_{\parallel}$ = 2.0018, $g_{\perp}$ = 2.005; **15b:** $A_{\parallel}$(^{31}P) = 218 G, $A_{\perp}$(^{31}P) = 8 G, $g_{\parallel}$ = 2.003, $g_{\perp}$ = 2.0104). According to these results, the SOMO is mainly composed of a phosphorus 3p orbital (**15a**: 61 % and **15b**: 53%) with a little contribution of the 3s orbital (**15a**: 2 % and **15b**: 2%). Also, according to calculations the remaining spin density is localized on the cyclopentadienyl substituent in **15a** and on the fluorenyl substituent in **15b**. Therefore, similar to the species **9** and **10a**, the spin density for **15a** and **15b** is mainly localized on the phosphorus center suggesting that these species can actually be described as phosphinyl radicals featuring a cyclopentadienide or a fluorenide substituent respectively (scheme 12).

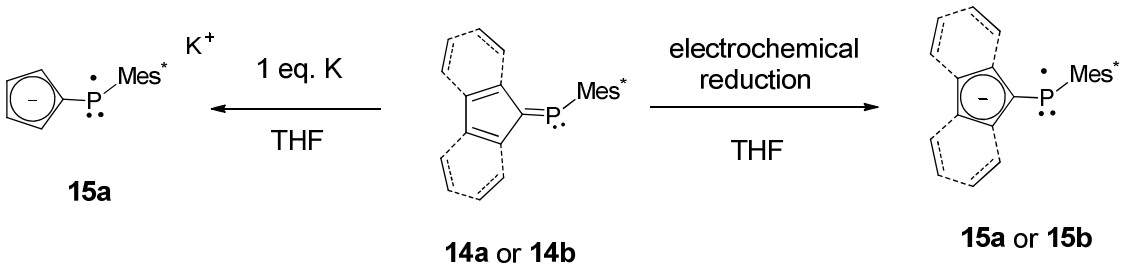

Scheme 12. Preparation of the phosphinyl radical anions **15a** and **15b**.

A similar strategy has been employed by Yoshifuji *et al*. two years later for the synthesis of the persistent radical **17** obtained by the reduction of the *para*-phosphaquinone **16**.[18]
The phosphaquinone was prepared readily from 2,6-di-*tert*-butyl-4-iodophenol and dichlorosupermesitylphosphine according to Scheme 13.

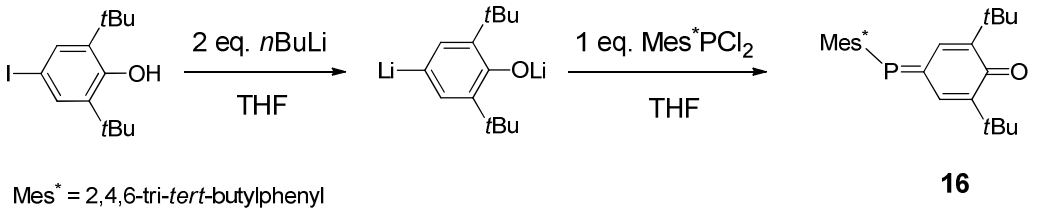

Scheme 13. Preparation of the *para*-phosphaquinone **16**.

The cyclic voltammetry measured for **16** in THF indicated that the latter undergoes a reversible one-electron reduction at $E_{1/2}$ = -1.43 V (vs Ag^{+}/Ag). The corresponding reduction of **16** was then carried out chemically using sodium as a reducing agent which afforded the persistent radical anion **17** (Scheme 14).

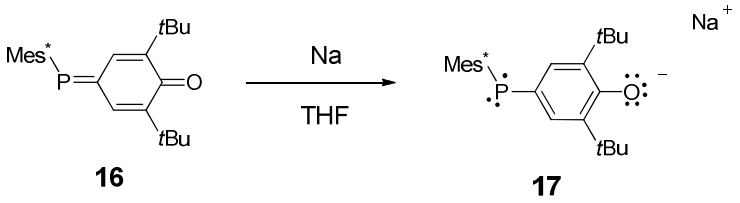

16 **17**

Scheme 14. One-electron reduction of the phosphaquinone **16** affording the phosphinyl radical anion **17**.

According to EPR analysis, the radical **17** displays a large hyperfine coupling with the ^{31}P nucleus ($a(^{31}P)$ = 93 G, g = 2.0069). Moreover, the frozen solution EPR spectrum shows that the ^{31}P hyperfine coupling tensor displays axial symmetry and also exhibits a large parallel hyperfine splitting and a small perpendicular component, indicative of a pronounced spin density on the phosphorus center (g_{xx} = 2.0094, g_{yy} = 2.0094, g_{zz} = 2.0022; $A_{xx}(^{31}P)$ = 2.5 G, $A_{yy}(^{31}P)$ = 17 G, $A_{zz}(^{31}P)$ = 261 G). According to these principal values, the spin density is mainly localized in a 3p(P) orbital (64%), with a little contribution of the 3s(P) orbital (2%), a situation already encountered for the radicals **15a** and **15b**. Therefore, similar to **15a** and **15b**, the radical **17** can be described as a phosphinyl radical linked to a phenoxide fragment in a *para* position (see the resonance structure depicted in Scheme 14).

In conclusion, suitable neutral phosphaalkenes can be used as precursor for the synthesis of phosphinyl radicals. This is mainly due to the peculiar electronic property of the starting phosphaalkenes which display a higher electron affinity than the "typical" compounds of this family (such as **14c).**

3.3.2) Oxidation of phosphaalkenes containing an electron-rich phosphorus center

It will be shown now that, by reversing the polarity of the P=C bond, the resulting inversely polarized phosphaalkenes are readily oxidized to the corresponding radical cations. Moreover, as suggested by EPR analysis and DFT calculations, these radicals can also be viewed as phosphinyl radicals.
The reductive properties of the inversely polarized phosphaalkenes **18a** and **18b** were investigated by Geoffroy et *al.*[19] These compounds are easily prepared according to scheme 15.

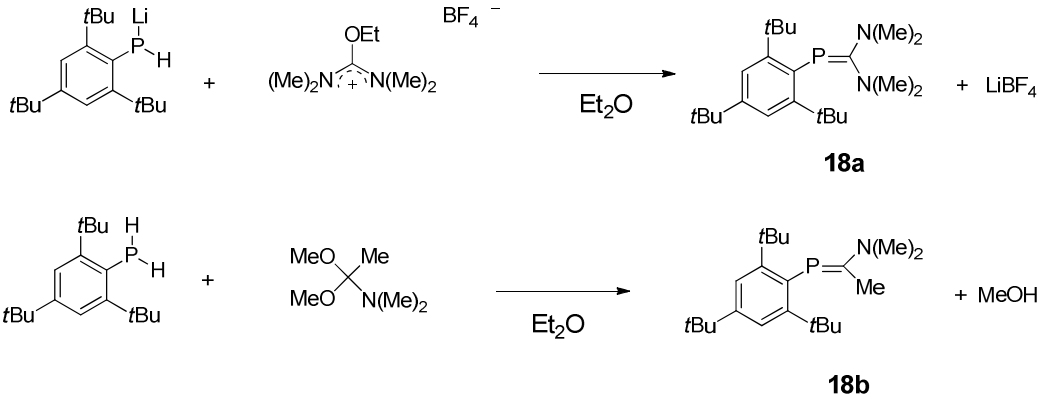

Scheme 15. Preparation of the inversely polarized phosphaalkenes **18a** and **18b**.

The electronic situation in **18a** or **18b** is opposite to the one encountered in the compounds **14a**, **14b** and **16** in which the phosphorus atoms are electron-deficient. Indeed, because of the donation of the electron lone-pairs of the nitrogens, the phosphorus centers in **18a** and **18b** are actually electron-rich as suggested by the resonance forms depicted in Scheme 16.

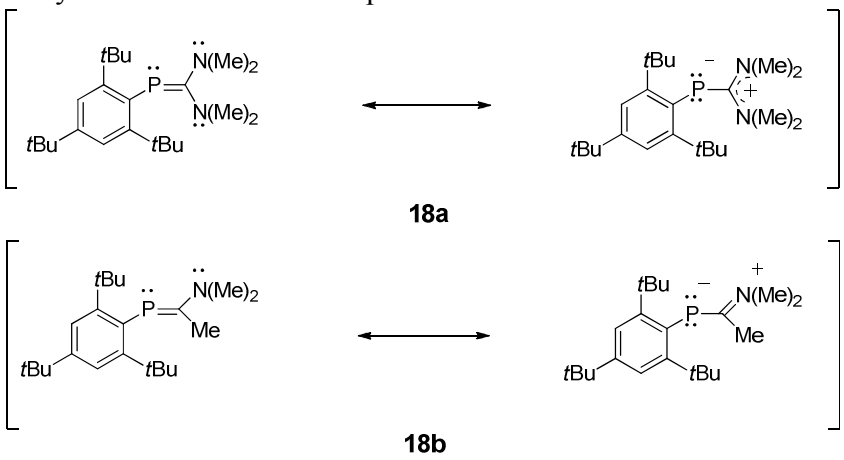

Scheme 16. Two resonance structures for compounds **18a** and **18b** outlining the electron-rich phosphorus centers.

The presence of this electron-rich phosphorus center results in interesting reducing properties for these phosphaalkenes which are indicated in the cyclic voltammograms of the THF solutions of **18a** and **18b**. Compounds **18a** and **18b** undergo a reversible one-electron oxidation at $E_{1/2}$ = +0.315 V (vs SCE) and $E_{1/2}$ = +0.553 V (vs SCE), respectively. Those potentials are significantly lower than the reported ones for typical phosphaalkenes (1.07 V-2.94 V)[20] confirming the dramatic electronic change resulting from the presence of the amino substituents. The corresponding radical cations were then chemically generated in both cases by the one-electron oxidation of the phosphaalkenes using $[Cp_2Fe]^+PF_6^-$ (Ferrocenium hexafluorophosphate) (Scheme 17). The obtained radicals were highly persistent, allowing their characterization in solution by EPR spectroscopy.

At room temperature, the EPR spectra of **19a** and **19b** are very similar and display a large isotropic hyperfine coupling with the ^{31}P nucleus (**19a**: $a_{iso}(^{31}P)$ = 105 G, **19b**: $a_{iso}(^{31}P)$ = 103 G) consistent with phosphinyl radicals.[6]

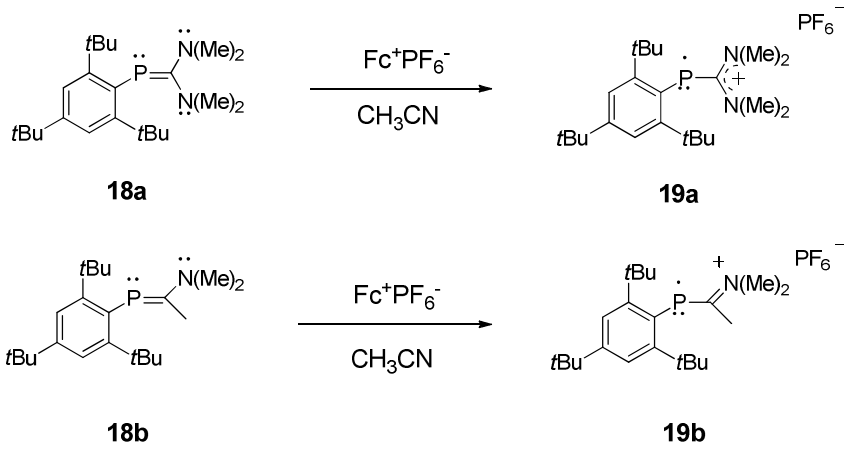

Scheme 17. Synthesis of the phosphinyl radical cations **19a** and **19b.**

The frozen solution EPR spectra reveal that in both cases, the *g* and the axially symmetric hyperfine coupling tensors are aligned (**19a**: g_{xx} = 2.0081, g_{yy} = 2.0136 and g_{zz} = 2.0032; $A_{xx}(^{31}P) \approx 0$, $A_{yy}(^{31}P)$ = 11 G and $A_{zz}(^{31}P)$ = 298 G. **19b**: g_{xx} = 2.0114, g_{yy} = 2.0109 and g_{zz} = 2.0035; $A_{xx}(^{31}P)$ = 0, $A_{yy}(^{31}P)$ = 16 G and $A_{zz}(^{31}P)$ = 290 G). These principal values show clearly that for both species the spin density is mainly localized in a 3p orbital of the phosphorus centers (around 75% in the 3p(P) orbital in both cases). Therefore, the radicals **19a** and **19b** can be described as phosphinyl radicals bearing a formamidinium or an iminium substituent respectively (Scheme 17).

3.4) Summary and objectives

Although phosphinyl radicals are extremely reactive species, their stabilization leading to persistent or even solid state stable species has been achieved. However, the only example of a solid state stable phosphinyl radical (compound **5**) displays an important delocalization of the spin density away from the phosphorus center. As a consequence its phosphinyl character is reduced. In addition, inversely polarized phosphaalkenes seem to be promising precursors for the synthesis of phosphinyl radical cations featuring an important spin density at the phosphorus center. The presence of a charge in these radicals would be an additional barrier to the dimerization. In the previous chapter, we showed that singlet carbenes were able to stabilize the paramagnetic electron-deficient $P_2^{+\cdot}$ radical cation. Therefore, we reasoned that by extending this concept, the oxidation of a suitable carbene-phosphinidene adduct (which is also an inversely polarized phosphaalkene) may result to a stable phosphinyl radical cation (Scheme 18). In addition, this phosphinyl radical cation could be also viewed as a carbene-phospheniumyl adduct.

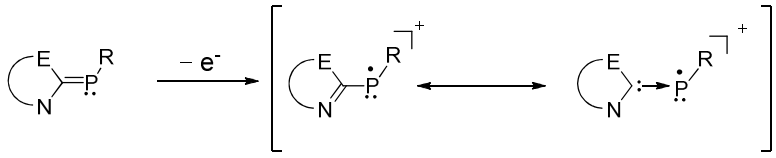

Scheme 18. One-electron oxidation of a carbene-phosphinidene adduct.

3.5) Results and discussion

3.5.1) Phosphinyl radical cations: from a transient to an isolated crystalline compound

3.5.1.1) Preliminary study

In order to verify that the generation of a phosphinyl radical from such a carbene-phosphinidene adduct was possible, we decided to study first the readily prepared phosphaalkene **22**. This simple non-hindered phosphaalkene was prepared in one step from the free carbene **20** by the reaction with pentaphenylcyclopentaphosphane **21** according to a procedure described by Arduengo *et al.* (Scheme 19).[21] Compound **22** was obtained as a yellow powder in 79% yield.

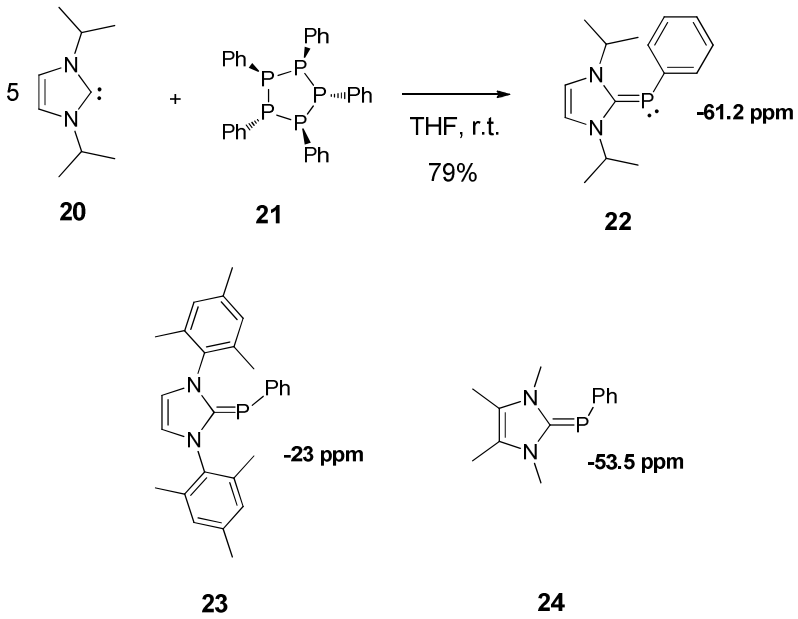

20 **21** **22** **23** **24**

Scheme 19. Synthesis of the phosphaalkene **22** and structures of the already reported similar carbene-phosphinidene adducts.[21]

Compound **22** displays in the $^{31}P\{^{1}H\}$ NMR spectrum a high field chemical shift for the phosphorus center (δ = -61.2 ppm), a feature already observed in the previously reported carbene-phosphinidene adducts **23** and **24** (Scheme 19).[21]
This high-field chemical shift is very different from the observed values for "regular" phosphaalkenes (100-400 ppm)[22] and indicates that the phosphorus center is particularly electron-rich. In the $^{13}C\{^{1}H\}$ NMR spectrum, the C2 carbon center of the imidazole ring gives rise to a doublet at 167.8 ppm due to the coupling with the phosphorus center ($^{1}J_{PC}$ = 102 Hz). Similar values were obtained for the adducts **23** (δ = 170 ppm, $^{1}J_{PC}$ = 103 Hz), **24** (δ = 169 ppm, $^{1}J_{PC}$ = 98 Hz), confirming the identity of **22**. Like compounds **23** and **24**, **22** can also be viewed as a carbene-phosphinidene adduct where the phosphorus center carries two electron lone-pairs (Scheme 20). This resonance structure suggests that the P=C double bond is not well developed due to the weak π back-bonding from the phosphorus lone-pair to the carbene center. This is also in agreement with the ^{1}H and ^{13}C NMR data which indicate that in solution, the imidazole ring is symmetrical suggesting fast rotation around the P-C bond.

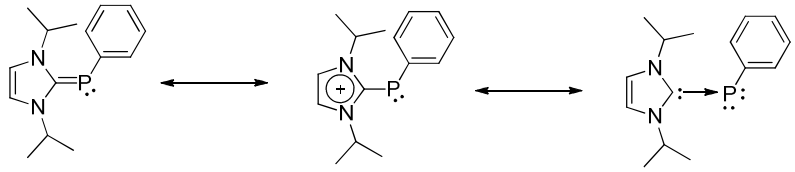

22

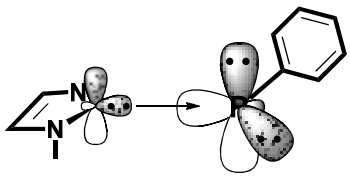

Scheme 20. Resonance structures and bonding situation for compound **22**.

The cyclic voltammetry of **22** performed in THF shows an irreversible one-electron oxidation at E_{ox} = -0.193 V (vs Fc^{+}/Fc) suggesting clearly that the corresponding radical cation is not stable under the conditions of the measure. This value is also significantly lower that the reported values for the oxidation potentials of typical phosphaalkenes (1.07 V-2.94 V)[20] consistent with a higher electron density at the phosphorus center.
However, we still decided to perform the chemical oxidation of **22** in the hope of identifying the oxidation product. Thus, after the reaction of **22** with one equivalent of ferrocenium triflate ($Fc^{+}TfO^{-}$) and subsequent work-up, the mixture of products **25a** and **25b**, not soluble in THF was isolated as a white powder in moderate yield (30%) (Scheme 21).
The $^{31}P\{^{1}H\}$ NMR spectrum of the mixture in CD_3CN consists in two singlets at δ = -49.8 ppm and δ = -57.7 ppm in a 6.3:1 ratio. The ^{1}H NMR spectrum displays

also two very similar sets of signals in the same 6.3:1 ratio, suggesting the presence of two different diastereoisomers in the mixture that we were not able to separate (major: **25a** and minor: **25b**). In addition, each set of signals indicates the presence of the carbene derived organic fragment in both products.
The imidazole ring protons give rise to a singlet at 7.92 ppm for the major product and 7.91 ppm for the minor one (in CD_3CN) which are quite downfield in comparison with the corresponding singlet for **22** (δ = 6.41 ppm, in C_6D_6). However these chemicals shifts are comparable with the corresponding one displayed by the imidazolium chloride (7.60 ppm in CD_2Cl_2) suggesting that the products contain an imidazolium fragment.

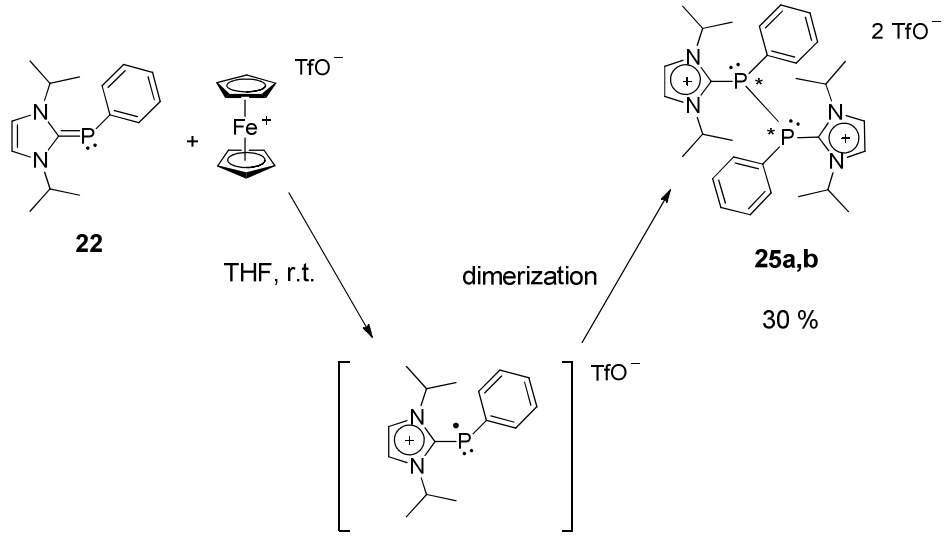

Scheme 21. One-electron oxidation of **22.**

In addition, the $^{13}C\{^1H\}$ NMR spectrum displays for the major diastereoisomer a triplet signal at 137.9 ppm due to the coupling with two phosphorus atoms ($^1J_{PC}$ = $^2J_{PC}$ = 25 Hz). This signal is attributed to the C2 imidazole carbon centers. The corresponding signal for the minor diastereoisomer was not observed, probably due to overlapping. The *ipso* carbon atoms of the phenyl rings give also rise to a triplet (major: 134.2 ppm, $^1J_{PC}$ = $^2J_{PC}$ = 12 Hz; minor: 135.6 ppm, $^1J_{PC}$ = $^2J_{PC}$ = 12 Hz). All together, these results suggest that the oxidation products are the dication **25a** and **25b** which are two diastereoisomers due to the presence of two chiral phosphorus centers. Unfortunately, we were not able to attribute the diastereoisomers (*meso* or the *rac* compounds) to the corresponding sets of signals in the NMR (major diastereoisomer and minor diastereoisomer). However, the nature of the product is clear and it results most likely from the dimerization of the generated transient radical cation (Scheme 21).
In order to prevent this dimerization, we decided to change the nature of the carbene fragment in the carbene-phosphinidene adduct. We chose the bulky cyclic (alkyl)(amino)carbene CAAC **26** (Scheme 22), hoping that the steric hindrance offered by the carbene would be efficient enough to protect the radical center. Moreover, we have seen in the second chapter that the electrophilic CAACs are

more efficient than NHCs to delocalize the spin density from the coordinated $P_2^{+\cdot}$ radical cations. This would result in a decrease of the spin density at the phosphorus center and consequently to an enhanced stabilization of the radical.

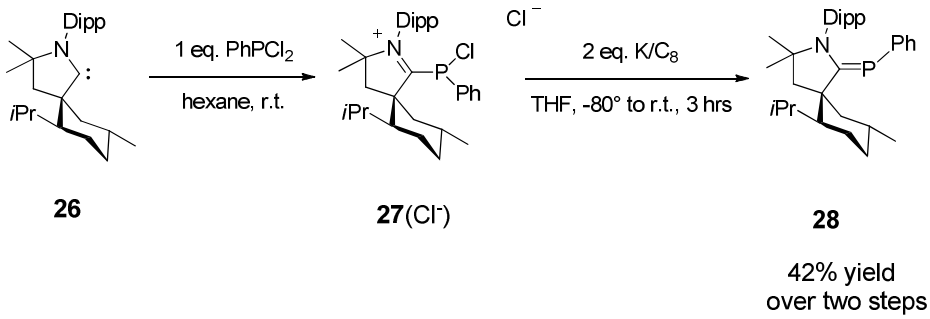

26 **27**(Cl^-) **28**

42% yield over two steps

Scheme 22. Synthesis of the carbene-phosphinidene adduct **28**.

The adduct **28** was prepared from the free carbene **26** (Scheme 22). Addition of one equivalent of dichlorophenylphosphine to a solution of the free carbene **26** in hexane resulted after one night of stirring at room temperature in the formation of the salt **27**(Cl^-) which precipitated out from the solution**.** The $^{31}P\{^1H\}$ NMR of the solid in CD_3CN displays only a singlet at δ = 162 ppm which was attributed to the chlorophosphine **27**(Cl^-). However, the ^1H and $^{13}C\{^1H\}$ NMR analysis indicated the presence of an unidentified by-product. As any attempt to isolate **27**(Cl^-) failed and resulted to decomposition, the second step was performed without any purification. The chlorophosphine **27**(Cl^-) was reduced with two equivalents of potassium graphite in THF which gave after work-up the desired product **28** as a pale yellow powder in 42% yield (over two steps). The $^{31}P\{^1H\}$ NMR spectrum of **28** in C_6D_6 displays a singlet at 56.2 ppm. In the $^{13}C\{^1H\}$ spectrum, the quaternary carbon of the pyrrolidine ring in **28** gives rise to a doublet due to the coupling with the phosphorus nucleus (δ = 191.3 ppm, $^1J_{PC}$ = 109 Hz). The *ipso* carbon of the phenyl ring gives also a doublet at 141.9 ppm ($^1J_{PC}$ = 64 Hz). The chemical shift in the ^{31}P NMR is significantly down-field in comparison with the NHC analog **22** (-61.2 ppm). This difference reflects the more important π back-bonding from the phosphorus lone-pair to the carbene center generated by the more electrophilic CAAC in comparison with the NHC.
The cyclic voltammetry of **28** in THF was performed and shows a *quasi*-reversible one-electron oxidation at $E_{1/2}$ = + 0.094 V (vs Fc^+/Fc) (Figure 3). However this oxidation occurred at a relatively high potential suggesting that the generated radical cation may be quite electrophilic. We then attempted to perform chemically the oxidation of **28** using Ag^+OTf^- (E_o = +0.41V vs Fc^+/Fc in THF)[23], however no formation of any paramagnetic product was observed. We moved therefore to the stronger commercially available triarylaminium radical cation $[N(p\text{-}C_6H_4Br)_3]^{+\cdot}SbCl_6^-$ (E_o = +0.70V vs Fc^+/Fc in CH_2Cl_2).[23] When one equivalent of the latter was added to one equivalent of **28** in THF, the solution turned immediately clear yellow and after one hour of stirring at room

temperature, the $^{31}P\{^{1}H\}$ NMR of the solution revealed that a large amount of the chlorophosphine **27** (δ = 162 ppm) was actually present in solution. While the mechanism of formation of **27** is still unclear, the chlorophosphine most likely results from the abstraction of a chlorine atom from the $SbCl_6^-$ anion present in solution (Scheme 23). This result outlines clearly the very electrophilic character of the generated radical cation.

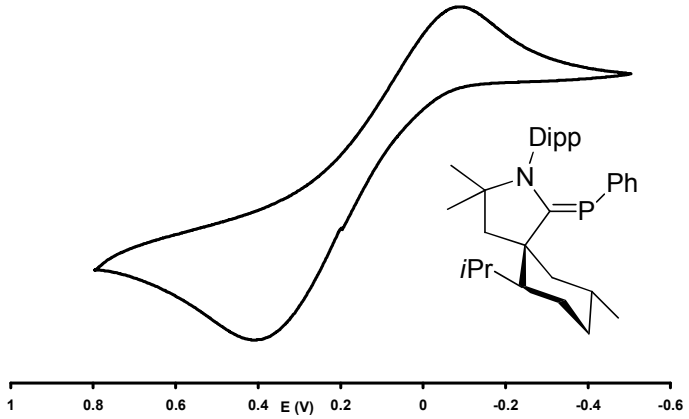

Figure 3. Cyclic voltammogram of the THF solution of **28** containing 0.1 M *n*-Bu_4PF_6 as electrolyte (potential versus Fc^+/Fc, scan rate 100 $mV.s^{-1}$).

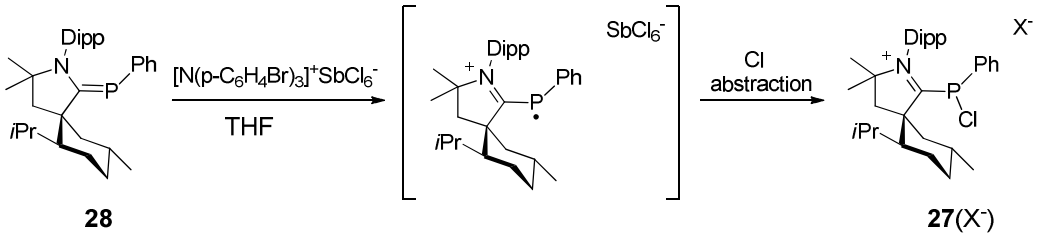

Scheme 23. Oxidation of compound **28** resulting to the formation of the chlorophosphine **27**(the counter anion of **27** is undetermined).

Whereas all the attempts to generate the radical cation by the oxidation of the phosphaalkene **28** failed, the electrochemical studies still suggest that CAACs are suitable for our purpose. The difficulty to prepare the radical cation from **28** is mainly due to the high oxidation potential of the latter, requiring inconvenient oxidative agents with usually unsuitable counter anions. Moreover, the high electrophilicity of the radical cation implies also that the latter may be really sensitive. For these reasons, we believed that by changing the phenyl subsituent at the phosphorus atom to a suitable group, we may be able to lower the oxidation potential of the resulting phosphaalkene while keeping the CAAC ligand.

3.5.1.2) Design and synthesis of CAAC-phosphinidene adducts with reduced oxidation potentials

It was previously showed that the 8-aminonaphtalene group was efficient for the hypercoordination of electron-poor phosphorus fragments and the formation of hypervalent phosphorus compounds.[24] We therefore prepared the phosphaalkene **31** (Scheme 24) hoping that the sigma donation from the nitrogen lone-pair to the phosphorus center in the corresponding radical cation would result in a lower oxidation potential.

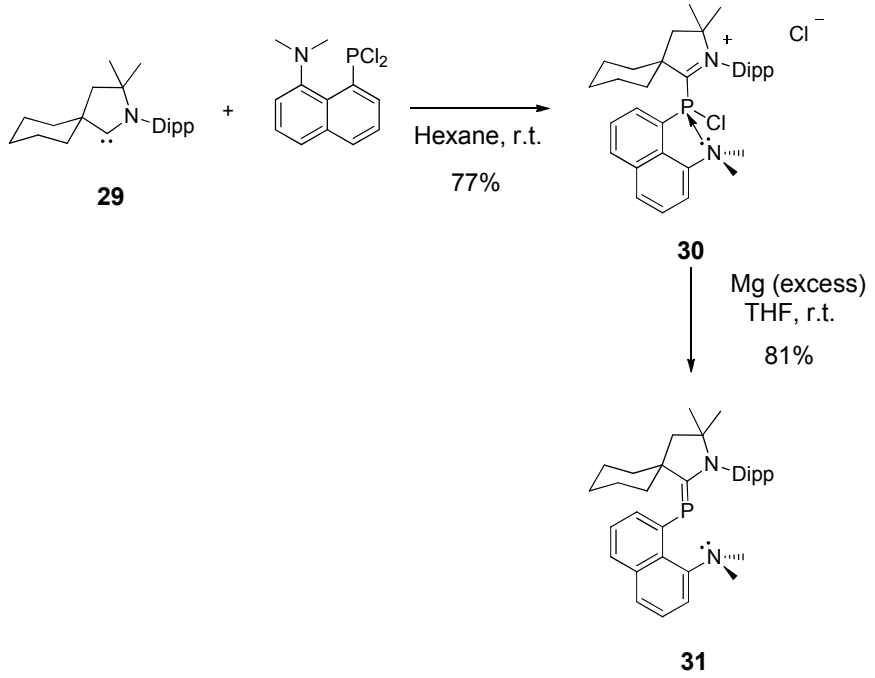

Scheme 24. Preparation of the phosphaalkene **31**

For this synthesis, we used the less sterically hindered carbene **29** which would be small enough to accommodate the naphthalene fragment. In a first step, the chlorophosphine **30** was prepared in 77% yield by the addition of **29** to 1-(dimethylamino)-8-dichlorophosphinonaphtalene. The $^{31}P\{^{1}H\}$ NMR spectrum of **30** in CD_3CN displays a broad singlet at +69.4 ppm indicative of some fluxional effects. In the ^{1}H and $^{13}C\{^{1}H\}$ NMR spectra, the signals in the aromatic region were well defined confirming the presence of the naphthalene group as well as the 2,6-diisopropylphenyl substituent in the molecule. Most of the signals in the aliphatic region were broad making their assignment difficult. However, the integration in the ^{1}H NMR spectrum is in agreement with the expected number of protons.

The chlorophosphine **30** was then reduced with an excess of magnesium powder to give the desired phosphaalkene **31** in 81% yield after work-up. The latter displays a sharp singlet at +95.2 ppm in the $^{31}P\{^{1}H\}$ NMR spectrum which is down-field in comparison with the previously described phosphaalkene **28** (+56.2

ppm). In the $^{13}C\{^1H\}$ NMR spectrum, the quaternary carbon from the pyrrolidine ring gives rise to a doublet at δ = +200 ppm ($^1J_{PC}$ = 60 Hz) comparable to the corresponding chemical shift displayed in **28** (δ = 191.3 ppm). Interestingly, the amino methyl substituents give rise to a broad singlet at 2.57 ppm in the ^1H NMR spectrum, due probably to some fluxional effects.
Unfortunately, the cyclic voltamogramm of **31** in THF showed an irreversible one-electron oxidation at E_o = - 300 mV (vs Fc^+/Fc), but the lower oxidation potential in comparison with **28** ($E_{1/2}$ = + 94 mV vs Fc^+/Fc) confirmed the expected influence of the amino group.
Despite the latter feature, we still decided to carry out the chemical oxidation of **31** in benzene using one equivalent of $Ph_3C^+B(C_6F_5)_4^-$ as the oxidant (Scheme 25) (previously reported oxidation potential for $Ph_3C^+BF_4^-$: -0.11 V versus Fc^+/Fc).[23] After work-up, a solid was obtained and the corresponding ^{31}P NMR in flurorobenzene indicated the presence of two products in a 1:1 ratio. Each compound displays a singlet in the $^{31}P\{^1H\}$ NMR spectrum (**32a**: δ= -17.9 ppm and **32b**: δ = -55.2 ppm). However in **32a** the phosphorus nucleus displays a coupling with two non-equivalent protons (**32a**: $^2J_{PH}$ = 31 Hz, $^2J_{PH}$ = 14 Hz) and in **32b**, there is a strong coupling between the phosphorus nucleus and a unique proton (**32b**: $^1J_{PH}$ = 290 Hz). In the last case, the strong coupling indicates the presence of a P-H bond which suggests that **32b** is actually the protonated phosphaalkene (Scheme 25).

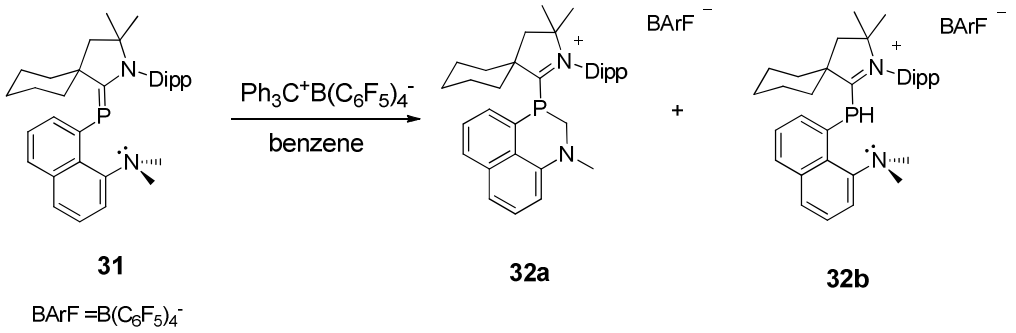

Scheme 25. Chemical one-electron oxidation of **31** affording a 1:1 mixture of the salts **32a** and **32b**.

Finally, we were able to obtain single crystals suitable for an X-ray diffraction study of the second compound **32a.** The structure of **32a** is depicted in Figure 4 and shows that the cation contains a pyramidal tricoordinated phosphorus center involved in a six member heterocycle. This phosphorus atom is involved in a 6 members ring and is connected to a methylene group which explains the coupling with the two different protons displayed in the ^{31}P NMR spectrum.
Unfortunately, all attempts to separate the products failed and no complete NMR characterisation of **32a** and **32b** was possible.
Although the mechanism for the formation of **32a** and **32b** is unclear, we can propose that first the transient phosphinyl radical cation undergoes a $H^{\cdot}$ atom shift from a methyl substituent linked to the nitrogen atom to the phosphorus center

(scheme 26). Indeed, due to the electrophilic character of the phosphinyl radical (already discussed for **28**) combined with the nucleophilic character of the resulting α-aminoalkyl radical, this transformation is favored by polar effects. These polar effects have been evocated previously in radical chemistry.[25]
After this first step, various subsequent intermolecular reactions leading to the obtained products can be proposed.

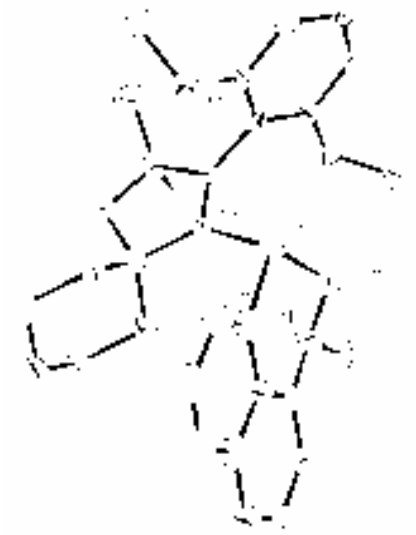

Figure 4. Solid-state structure of **32a**, 50% thermal ellipsoids are shown. Hydrogen atoms and the counter anion ($B(C_6F_5)_4^-$) are omitted for clarity. Selected bond distances [Å] and angles [°]: P(1)–C(16) 1.795(3), P(1)–C(1) 1.873(3), P(1)–C(26) 1.803(3), N(1)–C(1) 1.304(3); C(16)–P(1)–C(26) 100.07(15), C(16)–P(1)–C(1) 106.41(13), C(26)–P(1)–C(1) 98.25(13).

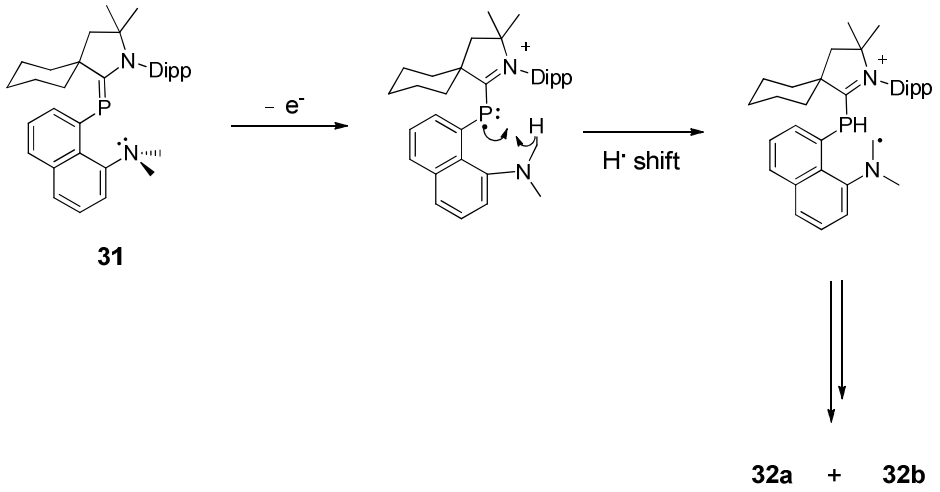

Scheme 26. Proposed mechanism for the formation of **32a** and **32b**.

The proximity of the dimethylamino substituent to the phosphorus center in **31** probably facilitates the H· transfer reaction. Therefore, in order to avoid this side-reaction, we decided to move on to the synthesis of the phosphaalkene **34** where the dimethylamino group is separated from the phosphorus center by a phenyl ring (Scheme 27). Moreover, the donation of the nitrogen lone-pair to the phosphorus center would proceed via π-conjugation through the phenyl ring, still reducing the oxidation potential in comparison with **28**.

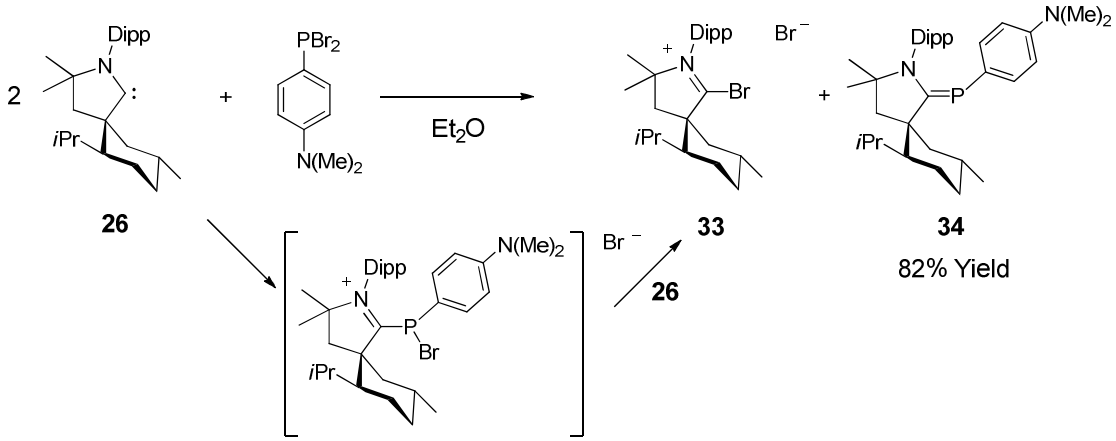

Scheme 27. Preparation of the phosphaalkene **34.**

The adduct **34** was prepared directly in one step by the reaction between two equivalents of the bulky CAAC **26** and one equivalent of dibromo(4-dimethylaminophenyl)phosphine according to Scheme 27. After three hours at room temperature, a white precipitate appeared which was removed by filtration and washed with diethyl ether. The yellowish filtrate was on the other hand evaporated to give a light yellow powder.

The $^{31}P\{^{1}H\}$ NMR spectrum of the white precipitate (**33**) in CD_3CN revealed that no phosphorus atom was present in the molecule. Moreover, the ^{1}H and the $^{13}C\{^{1}H\}$ NMR spectra indicate that **33** features a similar organic skeleton to **26**. Importantly, this species displays a downfield singlet at 187.7 ppm in the $^{13}C\{^{1}H\}$ NMR spectrum which is attributed to the quaternary carbon of the pyrrolidine ring. This spectroscopic data suggests that **33** is the bromine-CAAC adduct depicted in Scheme 27.

The $^{31}P\{^{1}H\}$ NMR spectrum of the yellow compound (**34**) in C_6D_6 displays a singlet at 58.4 ppm which is very similar to the chemical shift of the corresponding singlet displayed by the related adduct **28** (56.2 ppm). Similarly, the $^{13}C\{^{1}H\}$ NMR spectrum displays a down-field doublet at 189.6 ppm (^{1}J = 107 Hz) which is attributed to the pyrrolidine quaternary carbon linked to the phosphorus center (**28**: δ = 191.3 ppm, $^{1}J_{PC}$ = 109 Hz). All together these results indicate that **34** is the desired phosphaalkene (Scheme 27). Interestingly, here the intermediate bromophosphine resulting from the addition of the carbene to the dibromophenylphosphine is not observed. This feature indicates that this transient

compound is quickly dehalogenated by the second equivalent of carbene resulting to the salt **33** and the phosphaalkene **34** (Scheme 27).

The cyclic voltammetry of a THF solution of **34** indicated that under the conditions of the analysis, **34** undergoes a non-reversible one-electron oxidation process around $E_{ox} \approx$ -0.150 V. This potential is lower than the corresponding value for the phenyl derivative **28** ($E_{1/2}$ = + 0.094 V) reflecting the expected π donation from the amino substituent. We then performed the chemical oxidation of **34** using $Ph_3C^+B(C_6F_5)_4^-$. Immediately upon addition of toluene to an equimolar mixture of **34** and $Ph_3C^+B(C_6F_5)_4^-$, the color of the solution turned intense blue. However, after stirring the solution at room temperature during one hour, the color changed to red. The $^{31}P\{^1H\}$ NMR spectrum of the crude indicated the presence of a mixture of unidentified products, suggesting that the blue persistent radical cation **35** which is formed upon addition of the solvent is not stable and undergoes degradation in solution (Scheme 28).

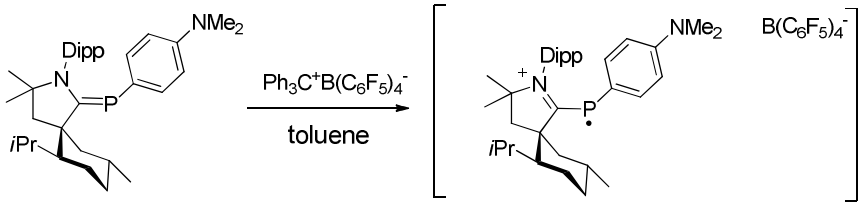

34 **35**

Scheme 28. Generation of the persistent phosphinyl radical cation **35**.

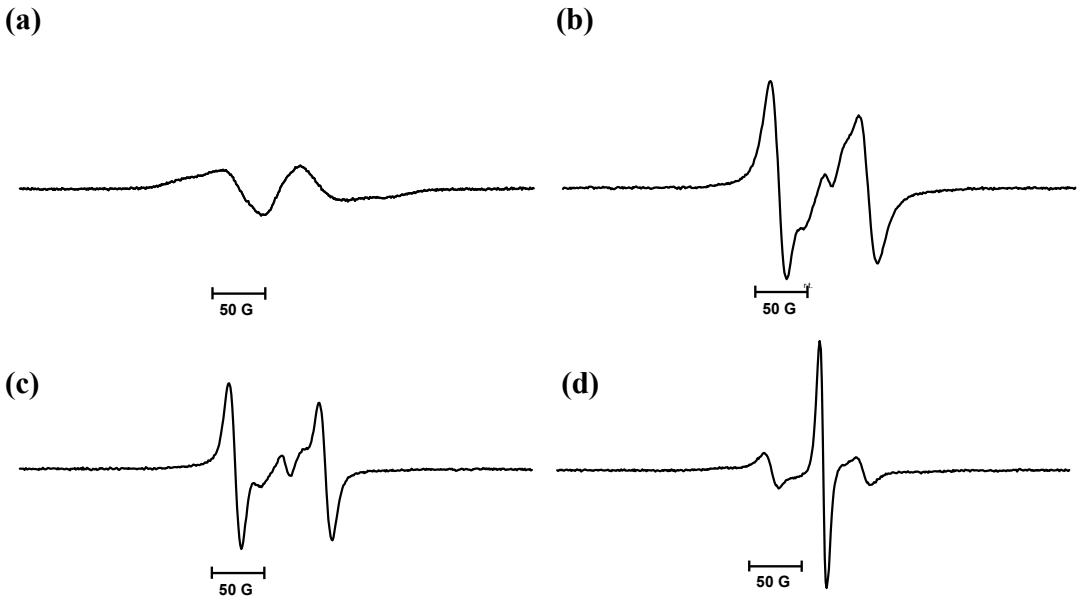

Figure 5. EPR spectra of the in-situ generated transient radical cation **35** in dichloromethane at -80°C (spectrum recorded at: **(a)**: - 80°C, **(b)**: - 50°C, **(c)**: 0°C, **(d)**: room temperature).

In order to confirm our hypothesis, we performed the EPR analysis at different temperature of the in-situ generated radical cation in CH_2Cl_2. Dichloromethane was added at -80°C to an equimolar mixture of **34** and $Ph_3C^+B(C_6F_5)_4^-$ in an EPR tube. Then, the tube was quickly inserted into the cavity of the EPR spectrometer previously cooled down at -80°C. The spectrum recorded at this temperature exhibits a broad doublet due to the hyperfine coupling with the ^{31}P nucleus, confirming the presence of the phosphinyl radical (figure 5(a)). The broadness of the spectrum is probably due to the slow tumbling of the radical in the solution. However, when the temperature of the sample was increased to -50 °C, the line width decreased allowing us to determine the EPR isotropic parameters of the radical (g = 2.005, $a_{iso}(^{31}P)$ = 89 G). The measured isotropic hyperfine coupling constant is in the expected range for phosphinyl radicals ($a(^{31}P)$ = 63-100 G) confirming the nature of **35**.

However, when the temperature of the sample is further risen, we can see that the intensity of the doublet decreases dramatically (see Figures 5(c) and 5(d)) and is almost vanished at room temperature (Figure 5(d)). This analysis indicates that the radical is only persistent at room temperature and has a half-life of a few minutes in solution. On the EPR spectrum recorded at room temperature (Figure 5(d)), the additional single line ($g \approx 2.002$) is probably attributed to the trityl radical ($^{\cdot}CPh_3$)[26] which is generated by the reduction of the trityl cation during the reaction (previously reported value for g: 2.003). Due to broadening, the hyperfine coupling with the protons is not observed for the trityl radical.

These results show that the generated radical cation **35** is only persistent at room temperature and undergoes degradation to unknown products. In order to achieve the preparation of a stable phosphinyl radical cation, we prepared the phosphaalkene **37** bearing a 2,2,6,6-tetramethylpiperidino substituent directly linked to the phosphorus center (scheme 29).[27] Such a substituent would still lower the oxidation potential relatively to the phenyl substituted phosphaalkene **28** via the π donation from the nitrogen lone-pair to the phosphorus atom. Also, it would provide enough steric hindrance around the phosphorus center and due to the lack of hydrogens in α position of the nitrogen center, no hydrogen shifts could occur.

The phosphaalkene **37** was prepared in two steps according to Scheme 29. First, the chlorophosphine **36** was isolated as a white powder in 55% yield after the reaction between the free carbene **29** and 2,2,6,6-tetramethylpiperidinedichlorophosphine in an equimolar ratio. In $CDCl_3$, the salt **36** displays a singlet in the $^{31}P\{^1H\}$ NMR spectrum at 92.3 ppm, and interestingly the ^1H and the $^{13}C\{^1H\}$ NMR data indicate the presence of diastereotopic nuclei due to the chirogenic phosphorus center in the molecule. Moreover, the quaternary carbon directly linked to the phosphorus atom gives rise to a down-field doublet at 213.3 ppm ($^1J_{PC}$ = 121 Hz).

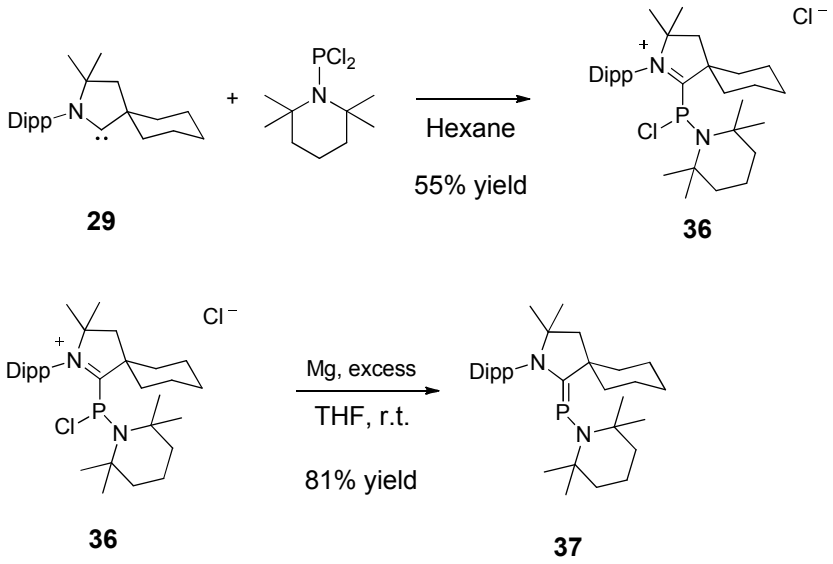

Scheme 29. Synthesis of the phosphaalkene **37**.

The reduction of **36** with an excess of magnesium proceeded smoothly at room temperature affording the desired phosphaalkene **37** in 81% yield. In the $^{31}P\{^1H\}$ NMR spectrum, the latter gives rise to a singlet at 136 ppm and the phosphaalkenic carbon resonates at 207 ppm (^1J = 95 Hz). The structure of the latter was unambiguously confirmed by an X-ray diffraction analysis performed on a single crystal of **37** (Figure 6).

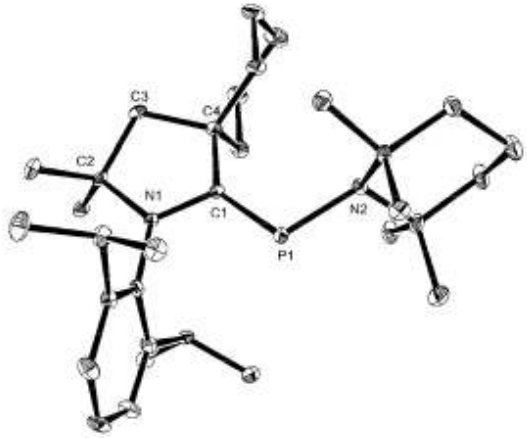

Figure 6. . Solid-state structure of the phosphaalkene **37**, 50% thermal ellipsoids are shown. Hydrogen atoms are omitted for clarity. Selected bond distances [Å] and angles [°]: P(1)-N(2) 1.7655(11), P(1)-C(1) 1.7376(14), N(1)-C(1) 1.3805(16), N(2)-P(1)-C(1), 108.90(6).

In the solid state, the cyclohexyl ring of compound **37** is flipped away from the piperidine moiety reducing steric repulsions. The phosphaalkene has a *E* configuration with a P=C bond length (1.7376 Å) in the range of the corresponding values in inversely polarized phosphaalkenes.[28] The P-N bond length (1.7655 Å) is also in agreement with a single P-N bond (typical value for a P-N single bond length: 1.77 Å)[14].

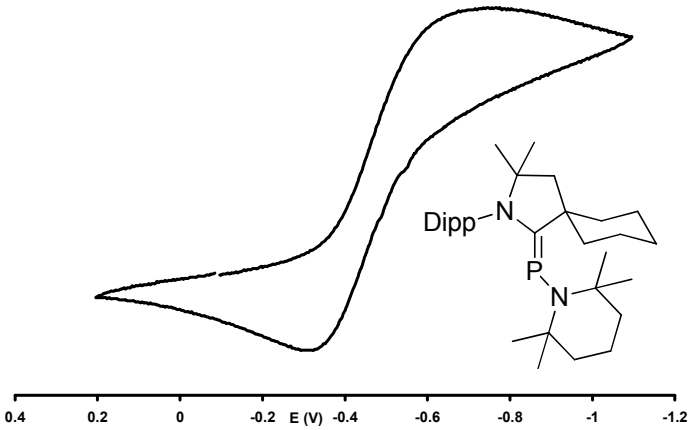

Figure 7. Cyclic voltamogramm of a fluorobenzene solution of **37** containing 0.1 M of $K^{+}B(C_6F_5)^{-}_4$ as an electrolyte.

The cyclic voltamogram of **37** in a fluorobenzene solution containing

$K^+B(C_6F_5)_4^-$ as the electrolyte (0.1 M) displays a reversible one-electron oxidation at $E_{1/2}$ = -0.412 V (vs. Fc^+/Fc) (Figure 7).
This low oxidation potential prompted us to perform the chemical one-electron oxidation of **37** using one equivalent of $Ph_3C^+B(C_6F_5)_4^-$ as the oxidant. After one hour of reaction at room temperature in benzene and subsequent work-up the radical cation **38** was isolated as a brown powder in 38% yield (Scheme 30).

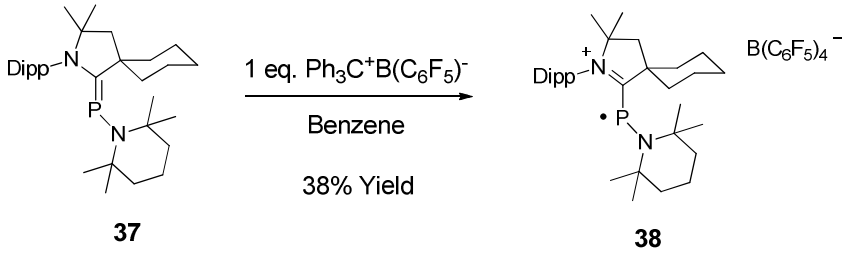

37 **38**

Scheme 30. Preparation of the phosphinyl radical cation **38**.

The $^{31}P\{^1H\}$ and $^{13}C\{^1H\}$ NMR of **38** were silent indicating the paramagnetic nature of the latter. Therefore, the EPR spectrum of a fluorobenzene solution of **38** was recorded at room temperature and at – 173 °C (Figure 8). The room temperature EPR spectrum (Figure 8, left) consists in a doublet of mutliplet (g = 2.007) due to a large hyperfine coupling constant with the phosphorus nucleus ($a(^{31}P)$ = 99 G) and a small coupling constant with one or two nitrogen nuclei ($a(^{14}N) \approx 4$ G). The hyperfine coupling constant with the ^{31}P nucleus is in the range of the ones observed for other persistent phosphinyl radicals ($a(^{31}P)$ = 63-100 G).
Moreover, according to the frozen EPR spectrum (Figure 8, right), the g and ^{31}P hyperfine coupling tensors are aligned and display axial symmetry.
After simulation, the following principal values could be obtained: $A_{xx}(^{31}P) = A_{yy}(^{31}P)$ = 23 G and $A_{zz}(^{31}P)$ = 247 G, $g_{xx} = g_{yy}$ = 2.009 and g_{zz} = 2.018. All together these EPR parameters suggest that the spin density is mainly localized in a 3p(P) orbital (57 %) with a small contribution of the 3s(P) orbital (2 %).

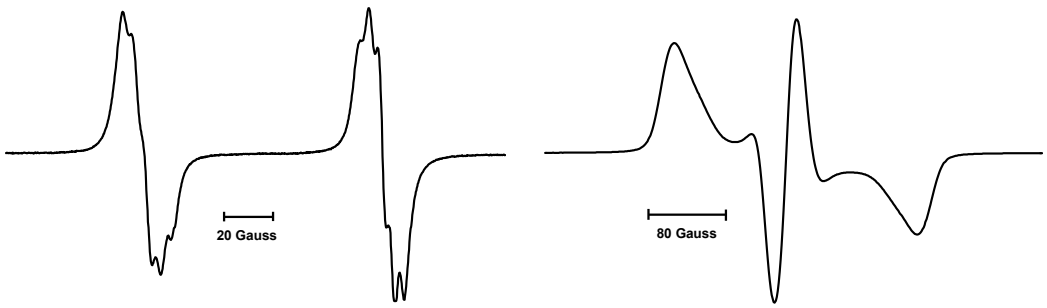

Figure 8. EPR spectra of **38** in fluorobenzene at room temperature (left) and in a frozen solution at -173 °C (right).

The structure of **38** was unambiguously determined by the use of X-ray diffraction analysis (Figure 9). In the solid state, the cation adopts a V-shaped geometry with a N(2)-P(1)-C(1) bond angle of 107.3°. Moreover, the P(1)-C(1) bond length in **38 (**1.81 Å) is longer than the corresponding one in the neutral precursor **37** (1.74 Å). This geometrical change from **37** to **38** is explained by the fact that after oxidation, there is only one electron remaining in the phosphorus 3p orbital for π back-bonding to the carbene center, reducing consequently the P=C bond order (See the bonding situation depicted in scheme 20, page 139).

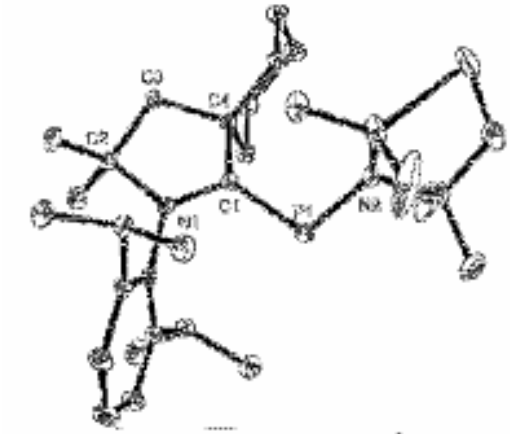

Figure 9. Solid state structure of the radical cation **38**, 50% thermal ellipsoids are shown. Hydrogen atoms and the counter anion $B(C_6F_5)_4^-$ are omitted for clarity. Selected bond distances [Å] and angles [°]: P(1)-N(2) 1.6805(14), P(1)-C(1) 1.8137(17), N(1)-C(1) 1.318(2); N(2)-P(1)-C(1) 107.26(8), N(1)-C(1)-C(4) 110.18(13).

Noteworthy, the P(1)-N(2) bond length in **38** (1.68 Å) is significantly shorter than the corresponding one in **37** (1.77 Å) indicating some π donation from the nitrogen lone-pair to the phosphorus center.
Calculations in collaboration with the group of Frenking were performed at the (U)M05-2X/def2-SVP level of theory using the NBO method. The calculations confirmed that the spin density is mainly localized on the phosphorus atom (67 %) with small contributions from the nitrogen atoms (16 % for N(2) and 10 % with N(1)). The calculated spin density at the phosphorus atom is comparable with the value deduced from the EPR analysis (59 % of spin density located on the phosphorus atom). The spin density is depicted in Figure 10.

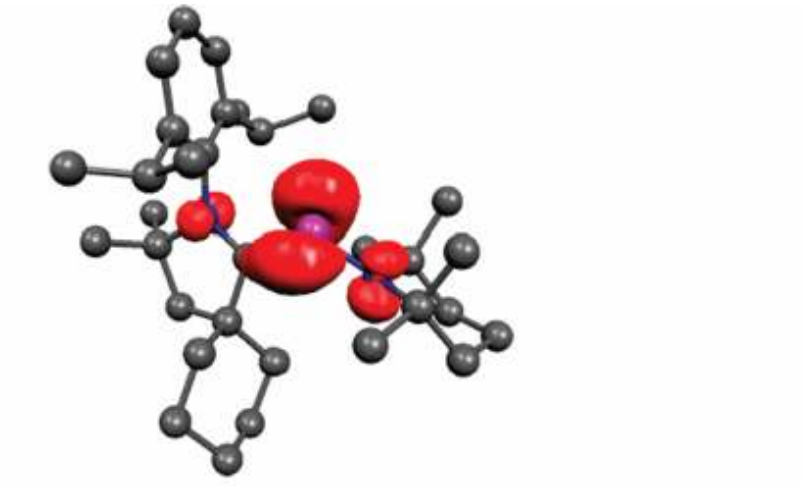

Figure 10. Spin density for the radical **38** calculated at the (U)M05-2X/def2-SVP level.

The experimental and computational analyses suggest that the radical **38** is best described as a phosphinyl radical. This was also confirmed by the reactivity of the later with *n*-Bu_3SnH. Indeed, upon addition of an excess of *n*-Bu_3SnH (5 eq.) to a solution of **38** in benzene, the color of the solution changed immediately from dark-brown to light-orange. After work-up, the phosphine **39** was obtained as pale-yellow powder in 68 % yield (Scheme 31).

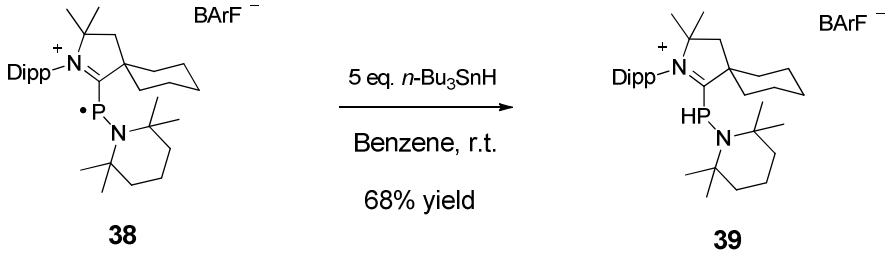

Scheme 31. H˙ abstraction reaction from *n*-Bu_3SnH by the radical **38**.

The $^{31}P\{^1H\}$ NMR spectrum of **39** in CD_2Cl_2 displays a singlet at -0.49 ppm which splits into a doublet ($^1J_{PH}$ = 283 Hz) in the ^{31}P NMR indicating the presence of a hydrogen atom linked directly to the phosphorus center. The structure of **39** was confirmed by X-ray diffraction analysis (Figure 11).

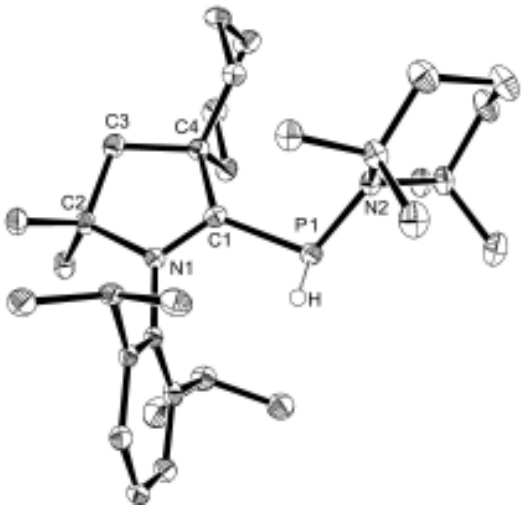

Figure 11. Solid state structure of the phosphine **39**, 50% thermal ellipsoids are shown. Hydrogen atoms (except the one linked to the phosphorus center) and the counter anion $B(C_6F_5)_4^-$ are omitted for clarity. Selected bond distances [Å] and angles [°]: P(1)-N(2) 1.678(2), P(1)-C(1) 1.842(3), N(1)-C(1) 1.310(3); N(2)-P(1)-C(1) 110.20(11), N(1)-C(1)-C(4) 110.9(2).

In conclusion, we have seen that the stable singlet carbene CAAC is able to stabilize a phosphinyl radical which can be consequently characterized in the solid state. This was also possible by the careful choice of the substituent at the phosphorus center resulting in the decrease of the oxidation potential of the phosphaalkene to a value attainable by common oxidative reactants. In comparison to the vanadium stabilized phosphorus radical **5**, the spin density in **38** is more localized at the phosphorus center (67% vs. 31%), and in consequence the phosphinyl character is more pronounced in **38** than in **5** which is confirmed by the enhanced reactivity of the former. The stability of the radical cation can be attributed to the presence of the positive charge preventing the dimerization to happen by repulsive electrostatic repulsions. Significant steric hindrance around the phosphorus center may also contribute to the stability of **38**.

3.5.2) Stable carbenes *versus* transition metals for the stabilization of a neutral phosphinyl radical

After the successful isolation of a stable phosphinyl radical cation we decided to move on to the more challenging synthesis of a neutral radical. For this purpose we used the vanadium phosphinyl radical **5** as a model.
It has been shown previously that stable singlet carbenes can mimic the reactivity of transition metal complexes. For example, they are able to activate H_2[29], CO[30], P_4[31] and sometimes they can even surpass the reactivity of transition metal complexes as exemplified by the carbene mediated activation of ammonia.[29]

We reasoned therefore that the direct replacement of the vanadium metals in **5** by carbenes may lead to a stable neutral, fully organic phosphinyl radical.
As discussed before, CAACs seemed to be more efficient than NHCs for the stabilization of the phosphinyl radical cation which is consistent with their higher electrophilicity. For this reason, we decided first to use CAACs for our new objective and the first synthetic target was the radical **42**. As outlined by the resonance forms depicted in scheme 32, we could expect a significant delocalization of the spin density into the vacant p orbitals of the carbene centers resulting therefore to some electronic stabilization.

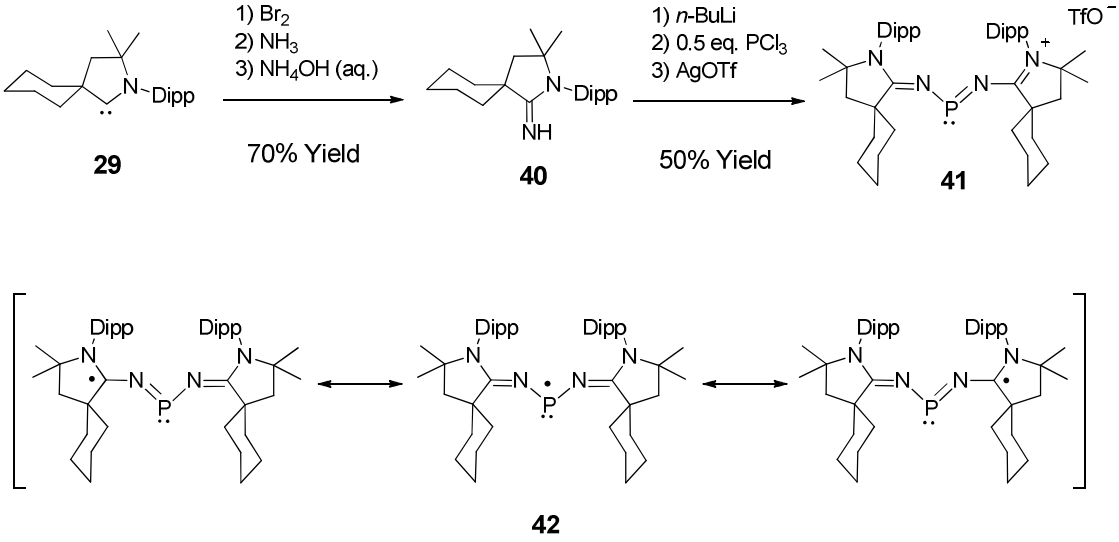

Scheme 32. Preparation of the salt **41** and resonance structure of the targeted radical **42**.

First, the amidine **40** was prepared in 70% yield in one pot from the free carbene **29** according to a modified known procedure.[32] Then **40** was deprotonated by *n*-BuLi in ether and 0.5 eq. of PCl_3 was added to the mixture. After work-up the salt **41**(Cl^-) was obtained as a white powder in 66 % yield. Compound **41**(Cl^-) displays in the $^{31}P\{^1H\}$ NMR spectrum a singlet at 182.1 ppm. This NMR chemical shift is at the lower range of the corresponding values observed for iminophosphines (100 pm – 800 ppm).[22] However, at this stage the product contained some impurities which could be removed after an anion exchange using silver triflate, affording the salt **41**(TfO^-) in 76 % yield. The $^{31}P\{^1H\}$ NMR spectrum of **41**(TfO^-) in $CDCl_3$ displays a singlet at 184.2 ppm. This chemical shift is very close from the corresponding value displayed by **41**(Cl^-). The ^1H as a well as the $^{13}C\{^1H\}$ NMR spectra of **41**(TfO^-) display only one set of signals corresponding to the carbene fragments indicating that the cation is symmetrical.
We then tried to prepare the neutral radical **42** by the one-electron reduction of **41**(TfO^-) using one equivalent of potassium graphite as a reducing agent. Unfortunately after two hours of stirring at room temperature, the $^{31}P\{^1H\}$ NMR spectrum of the solution indicated a complex mixture of unidentified products,

and all the attempts to generate the radical **42** failed suggesting that the latter is not stable. These results showed that the CAAC **29** is not suitable for the stabilization of the targeted radical, we therefore decided to change the carbene and to use the bulky NHC **43** (Scheme 33).

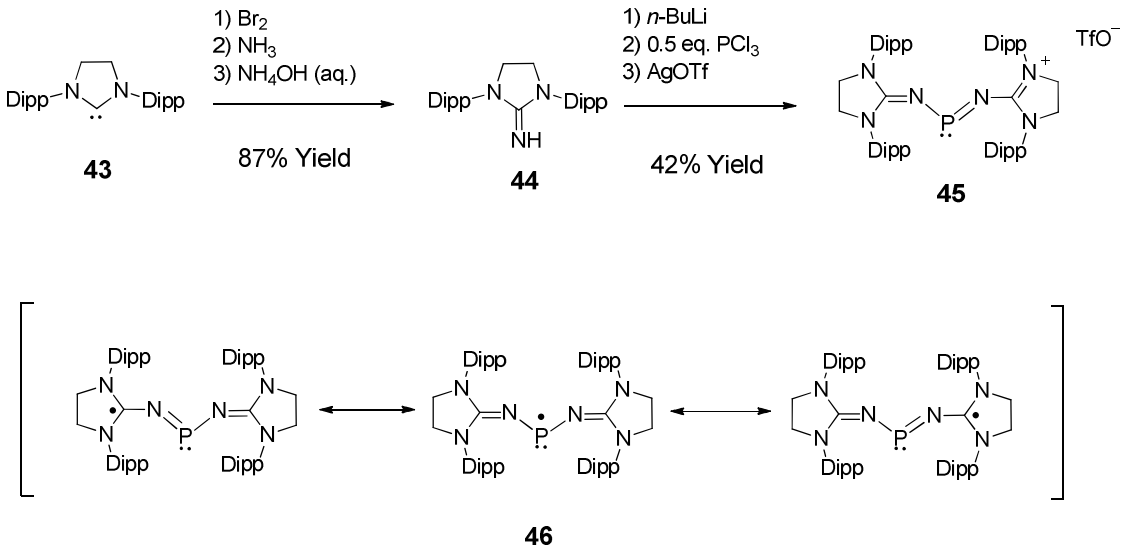

Scheme 33. Preparation of the salt **45** and structure of the corresponding radical **46**.

Following exactly the same pathway than for the CAAC derivative **41**, the radical precursor **45** was prepared from the free NHC **43** according to Scheme 33. Thus in a first step, the guanidine **44** was synthesized in 87% yield. The latter was then in-situ deprotonated using *n*-BuLi followed by the addition of 0.5 equivalent of PCl_3 affording **45**(Cl^-) as a white powder in 50 % yield. Exactly like the analogous compound **41**, the impurities present with the salt **45**(Cl^-) were eliminated after an anion exchange using silver triflate. The salt **45**(TfO^-) was then obtained as a white powder in 83 % yield. The latter gives rise in the $^{31}P\{^1H\}$ NMR spectrum to a singlet (δ = 277 ppm) and in the $^{13}C\{^1H\}$ NMR spectrum, the imidazolidine ring quaternary carbons exhibit a doublet at 158.2 ppm ($^2J_{PC}$ = 19 Hz). Paradoxically, the ^{31}P NMR signal in **45**(TfO^-) is at a lower field than the corresponding signal displayed by **41**(TfO^-). Indeed, because of the less π-accepting property of the NHC in comparison with the CAAC, the phosphorus center in **45**(TfO^-) should be more electron-rich and therefore should give rise to a higher field chemical shift.

We then performed the cyclic voltammetry of a THF solution of **45**(TfO^-) containing 0.1 M of *n*-Bu_4NPF_6 as the electrolyte (Figure 12). The cyclic voltamogramm indicates that **45**(TfO^-) undergoes a reversible one-electron reduction at $E_{1/2}$ = -1.84 V. These results prompted us to carry out the chemical reduction using one equivalent of potassium graphite as the reductant in THF. Upon addition of the solvent to an equimolar mixture of **45**(TfO^-) and K/C_8 the color of the solution turned immediately dark red. After three hours of stirring at

room temperature, the ^{31}P NMR of the solution was silent indicating the paramagnetic nature of the product. Finally, after work-up the radical **46** was obtained as a dark red powder in 85 % yield.
The EPR spectrum of **46** in a THF solution was recorded at room temperature and at -173°C and is shown below (Figure 13).

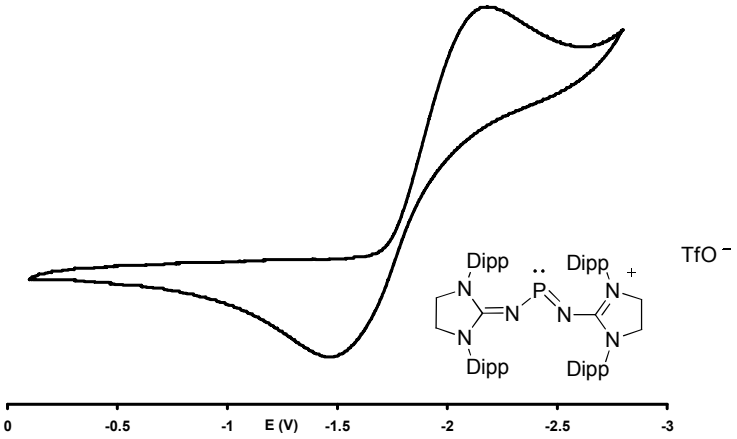

Figure 12. Cyclic voltammogram of the THF solution of **45**(TfO^-) containing 0.1 M *n*-Bu_4PF_6 as electrolyte (potential versus Fc^+/Fc, scan rate 100 $mV.s^{-1}$).

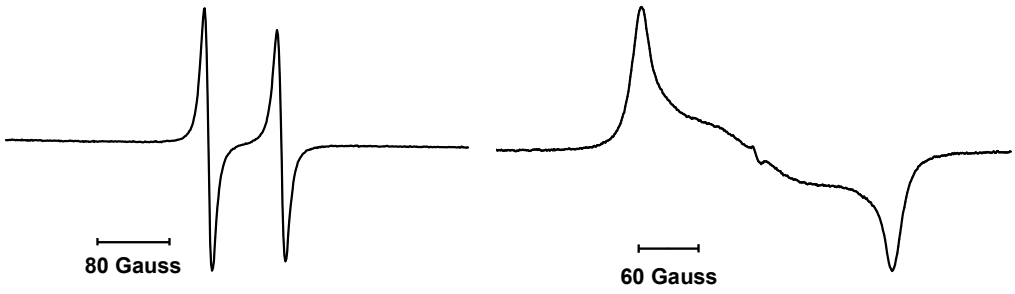

Figure 13. EPR spectra of the radical **46** in THF, recorded at room temperature (left) and at -173°C (right).

At room temperature (Figure 13, left), the spectrum displays a large splitting due to the hyperfine coupling constant with the phosphorus center (g = 2.005, $a(^{31}P)$ = 78 G). Also no coupling with a ^{14}N nucleus is observed suggesting that the spin density at the nitrogen centers is very weak. Moreover, simulation of the anisotropic frozen solution EPR spectrum (Figure 13, right) allowed us to determine the principal values for the g and the ^{31}P hyperfine coupling tensors which are aligned and display axial symetry: g_{xx} = 2.0074, g_{yy} = 2.0062 and g_{zz} = 2.0024; $A_{xx}(^{31}P) = A_{yy}(^{31}P)$ = 0 G and $A_{zz}(^{31}P)$ = 240 G. According to these

results, the spin density is mainly localized at the phosphorus center with 62% in a 3p(P) orbital and only 2% in the 3s(P) orbital. All these values are consistent with a phosphinyl radical and indicate than in **46** the spin density is significantly less delocalized from the phosphorus center than in the vanadium radical **5** (according to calculations in **5**: 31.3 % of the spin density is localized on the phosphorus center and 23 % is localized over each vanadium atom). Finally, an X-ray diffraction study performed on a single crystal of **46** confirmed the structure of the latter (Figure 14).

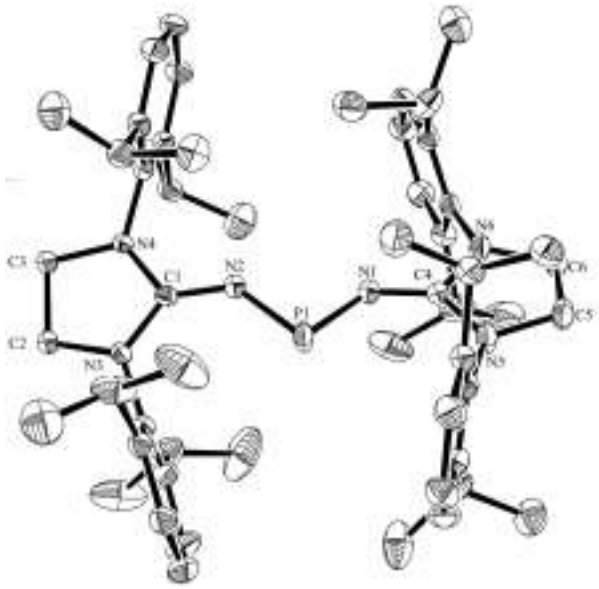

Figure 14. Solid state structure of the radical **46**, 50% thermal ellipsoids are shown. Hydrogen atoms are omitted for clarity. Selected bond distances [Å] and angles [°]: P(1)-N(2) 1.657(2), P(1)-N(1) 1.658(2), N(1)-C(4) 1.272(4), N(2)-C(1) 1.277(4); N(2)-P(1)-N(1) 96.75(13).

The asymmetric unit in the crystal structure of radical **46** contains three independent molecules. In the solid state, radical **46** adopts a V-shaped geometry with an average N(1)-P(1)-N(2) bond angle of 97.8°.
This angle is more acute than the corresponding angles in the vanadium radical **5** (110.9°) and the radical cation **38** (107.3°). The P(1)-N(1) (1.658 Å) and P(1)-N(2) (1.657 Å) bond lengths are at the lower end of the range observed for P-N single bonds and are also longer than the P-N bonds in **5** (average 1.62 Å) confirming the weaker delocalization of the radical in **46**. Importantly, **46** represents the first example of a neutral organic phosphinyl radical stable in the solid state.
In order to directly compare the electronic stabilization brought by the NHCs with the one offered by the vanadium metalloligands in **5** we undertook the synthesis of the mixed substituted phosphinyl radical **49** (Scheme 34). The distribution of the spin density in this molecule (which is directly deduced from the hyperfine

coupling with the ^{31}P and the ^{51}V nuclei) depends on the relative ability of each substituent to delocalize the radical from the phosphorus center.
In consequence, this radical **49** would provide an experimental comparison of the relative ability of each substituent to delocalize the spin density from the phosphinyl center.

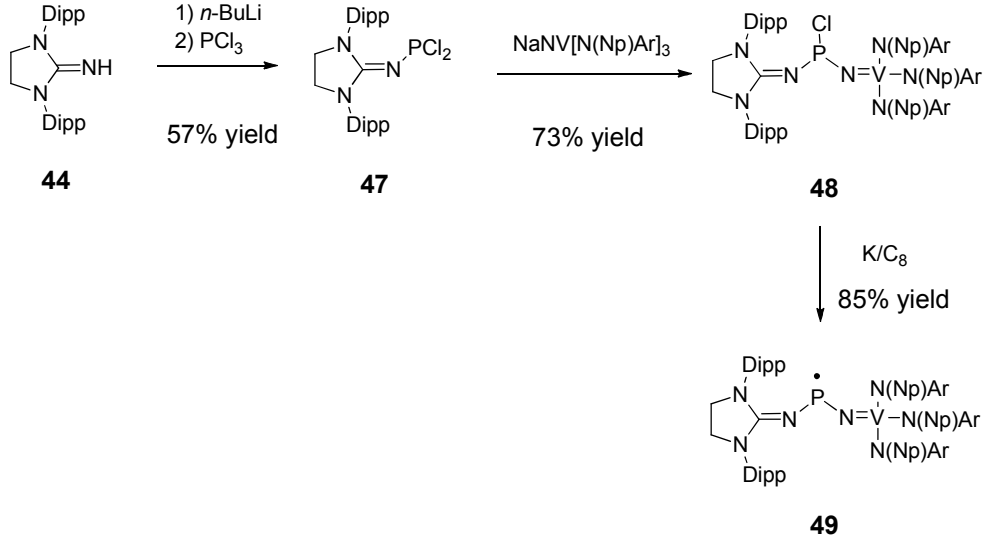

Scheme 34. Synthesis of the mixed substituted radical **49** (Np = neopentyl, Ar = 3,5-$Me_2C_6H_3$).

The radical **49** was prepared according to Scheme 34. The dichlorophosphine **47** was easily made in 57 % yield by the in-situ deprotonation of **44** followed by the addition of one equivalent of PCl_3. Compound **47** displays in the $^{31}P\{^1H\}$ NMR spectrum a singlet at 184 ppm. Substitution of a chlorine atom by the vanadium-iminato groupment was performed by the reaction between **47** and the already reported vanadium nitride anion $\{NV[N(Np)Ar]_3\}^-Na^+$.[33] The resulting product **48** displays in the $^{31}P\{^1H\}$ NMR spectrum a broad singlet at 185 ppm. The broadening is due to the ^2J coupling with the vanadium nucleus (^{51}V: I = 7/2, 99.75%). This relatively high field chemical shift shows that unlike phosphenium **45,** the chlorine atom stays coordinated to the phosphorus atom of **48**. This is also confirmed by the ^1H NMR spectrum which indicates that the pair of methylene protons in the neopentyl group are diastereotopic resulting in two doublets at 4.54 ppm and 4.44 ppm. Similarly, the isopropyl groups of the Dipp substituents give rise to two sets of signals in the ^1H and $^{13}C\{^1H\}$ spectra. This spectroscopic data indicates that the phosphorus center in **48** is chiral, consistent with the presence of the chorine atom. This structural difference between **45** and **48** suggests that the imidazolidin-2-iminato substituent is a better π-donor that the vanadium-iminato ligand.
The one-electron reduction of **48** was performed using one equivalent of K/C_8 which afforded after work-up the radical **49** as a dark red powder in 85 % yield.

The EPR spectrum of the latter in THF was recorded at room temperature and at -173°C (Figure 15).

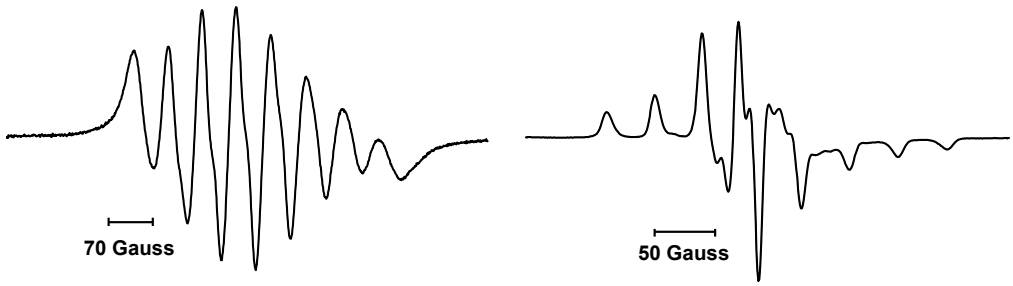

Figure 15. EPR spectra of a THF solution of **49** recorded at room temperature (left) and at -173°C (right).

The room temperature EPR spectrum displays a eight-line pattern due to the hyperfine coupling with the ^{51}V nucleus (I = 7/2, 99.75%) (g = 1.981, a(^{51}V) = 58 G) (Figure 15, left). However, the hyperfine coupling with the ^{31}P nucleus is weak, resulting only to a broadening of the lines and can not be evaluated.

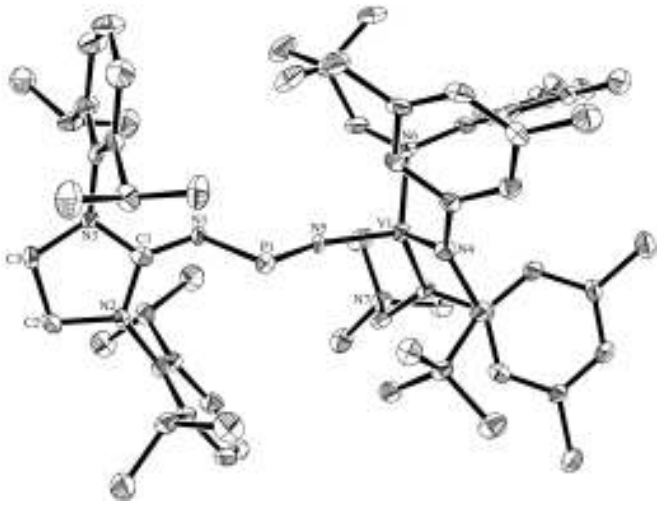

Figure 16. Solid state structure of the radical **49**, 50% thermal ellipsoids are shown. Hydrogen atoms are omitted for clarity. Selected bond distances [Å] and angles [°]: P(1)-N(5) 1.572(5), P(1)-N(1) 1.634(5), N(1)-C(1) 1.286(7), V(1)-N(5) 1.806(4), V(1)-N(6) 1.902(5), V(1)-N(7) 1.898(4); N(1)-P(1)-N(5) 109.5(3).

In order to gain more insight into the electronic structure of **49**, the frozen EPR spectrum was recorded at -173°C (figure 15, right). Simulation of the spectrum allowed us to determine the principal values of the g and hyperfine tensors which are aligned: g_{xx} = 1.9726, g_{yy} = 2.0048 and g_{zz} = 1.9583; $A_{xx}(^{51}V) = A_{yy}(^{51}V)$ = 30 G and $A_{zz}(^{51}V)$ = 121 G; $A_{xx}(^{31}P) = A_{yy}(^{31}P)$ = 7 G and $A_{zz}(^{31}P)$ = 12 G. According to these values and considering the fact that the ^{51}V hyperfine coupling tensor displays axial symmetry, the spin density is mainly localized at the

vanadium center (67 %) and lightly on the phosphorus center (1 % in the 3p orbital).
The structure of **49** was unambiguously confirmed by X-ray diffraction analysis performed on a single crystal (Figure 16). In the solid state, the radical **49** adopts a V-shaped geometry, with a N(1)-P(1)-N(5) bond angle of 109.5°. This angle is wider than the corresponding one in the organic radical **46** (96.75°) and is comparable to the angle in **5** (110.9°). The P(1)-N(5) bond length (1.572 Å) is short and lays in the range of the values observed for the iminophosphine P=N double-bond lengths (1.475-1.619 Å).[22] Also the V(1)-N(5) bond (1.806 Å) is longer than the corresponding one in **5** (1.72 Å). The EPR analysis combined with the geometrical parameters of **49** suggests that this compound can actually be described as a vanadium (IV) complex carrying an imidazolidin-2-iminatophosphinimide ligand (Scheme 35). Therefore, the vanadium center appears to be more powerful than the imidazolidin-2-iminato ligand to delocalize the spin density from the phosphorus center.

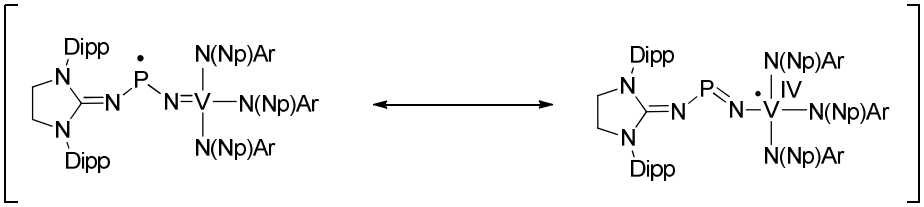

49

Scheme 35. Two resonance structures for the radical **49** showing that this compound can also be viewed as a vanadium (IV) complex (resonance form on the right) (Np = neopentyl, Ar = 3,5-$Me_2C_6H_3$).

DFT calculations on the real compounds **5**, **46** and **49** were carried out in collaboration with the group of Frenking. The calculated Mulliken atomic spin densities for the three radicals are depicted in Figure 17 (**5**: Figure 17a, **46**: Figure 17b and **49**: Figure 17c). In the neutral radical **46**, a large spin density is located on the phosphorus atom (+0.68e) with a slight delocalization on the NHC ligands (+0.1% at each quaternary carbon). Also, the spin density at the central nitrogen atoms is very low explaining why in the EPR spectrum of **46**, no hyperfine coupling was observed with the nitrogen nuclei. However, in the vanadium radical **5**, a lower spin density is found on the phosphorus center (+0.42e) due to a more important contribution of the 3d orbitals of each vanadium atoms to the SOMO (+0.43e/+0.44e).

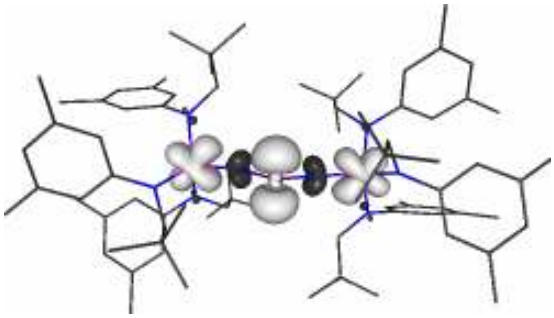

a) **5**
P: +0.42, N: -0.10/-0.11, V:+0.43/+0.44

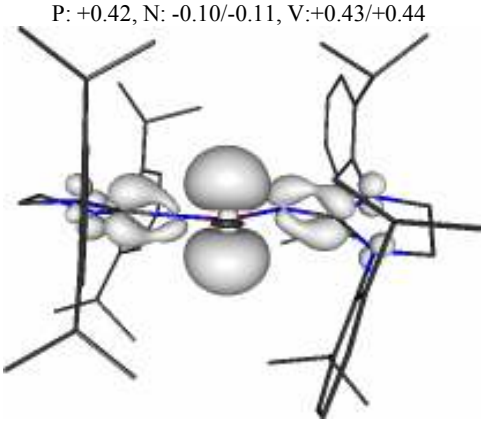

b) **46**
P: +0.68, N: -0.03/>-0.01, C: +0.09/+0.10

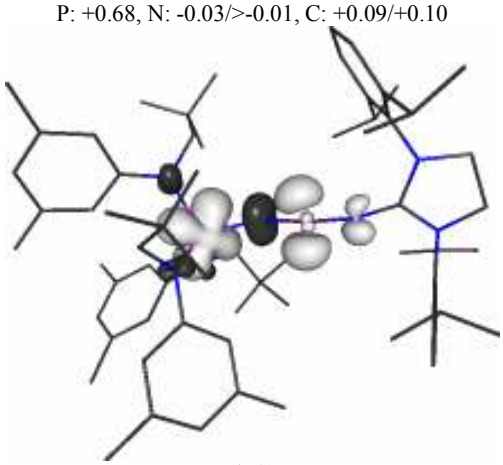

c) **49**
P: +0.24, N_V: -0.13, N_C: +0.05, V:+0.97, C:<0.01

Figure 17. Spin density (BP86/TZVPP//BP86/SVP, isosurfaces at 0.004 and -0.004 a.u) of **5**, **46** and **49**. Mulliken atomic spin densities per atom given in electrons for the atoms of the central moieties.

This comparison suggests already that the vanadium metalloligands are more powerful than the imidazolidin-2-iminato ligands to delocalize the radical from the phosphorus center. This is confirmed by the calculated spin density in the mixed compound **49**. In this radical the vanadium center possesses the highest spin density (+0.97e) which is even higher than the total spin density localized over the two vanadium centers in **5**. There is also a little contribution of the phosphorus orbitals to the SOMO (+0.24e) but weaker than in **5** or **46**. Moreover, no spin density excess is found on the NHC fragment. To conclude, the vanadium metalloligands are more effective to delocalize the spin density from the phosphorus center but NHC are efficient enough to allow the isolation of the neutral organic stable phosphinyl radical **46**. Due to the larger contribution of the phosphorus orbitals to the SOMO, the latter displays a more important phosphinyl character in comparison with **5**. Probably, the steric hindrance provided by the NHC moieties in the radical **46** accounts for its stability even in the solid state.

3.6) Conclusion

Various strategies have been attempted prior to our work for the stabilization of phosphinyl radicals. However, so far the use of transition metals was the only successful way allowing for the complete characterisation of a phosphinyl radical. This is mainly due to the fact that on the contrary of main group elements, transition metals are susceptible to undergo one-electron redox chemistry. However during the last past years it has been shown that singlet carbenes are able to mimic transition metals, and we have now shown that they are also useful tools for the stabilization of phosphinyl radicals.

Two different types of radicals have been prepared: a radical cation where the phosphinyl center is directly linked to the carbene, and a neutral radical where nitrogen atoms bridge the phosphinyl center to the carbenes. The last one represents the first example of a neutral, organic phosphinyl radical which is stable in solution and in the solid state. Importantly, in these last two examples, the phosphinyl nature of the radicals are still conserved which is not the case for the vanadium stabilized radical where important delocalization occur.

By employing the same strategy we could hope that some other main group elements based radicals could be prepared.

References

[1] a) J. K. Kochi and Editor, *Free Radicals*, Vol. 2, **1973**, p. 906 pp; b) S. Marque and P. Tordo, *Top. Curr. Chem.* **2005**, 250, 43-76.
[2] S. Ito, M. Kikuchi, M. Yoshifuji, A. J. Arduengo, III, T. A. Konovalova and L. D. Kispert, *Angew. Chem., Int. Ed.* **2006**, 45, 4341-4345.
[3] M. Scheer, C. Kuntz, M. Stubenhofer, M. Linseis, R. F. Winter and M. Sierka, *Angew. Chem., Int. Ed.* **2009**, 48, 2600-2604.
[4] P. Agarwal, N. A. Piro, K. Meyer, P. Mueller and C. C. Cummins, *Angew. Chem., Int. Ed.* **2007**, 46, 3111-3114.
[5] U. Schmidt, K. Kabitzke, K. Markau and A. Mueller, *Chem. Ber.* **1966**, 99, 1497-1501.
[6] P. P. Power, *Chem. Rev.* (Washington, DC, U. S.) **2003**, 103, 789-809.
[7] L. J. Berliner and Editor, *Molecular Biology: Spin Labeling. Theory and Applications*, **1976**, p. 592 pp.
[8] a) S. Loss, A. Magistrato, L. Cataldo, S. Hoffmann, M. Geoffroy, U. Rothlisberger and H. Grutzmacher, *Angew. Chem., Int. Ed.* **2001**, 40, 723-726; b) L. Cataldo, C. Dutan, S. K. Misra, S. Loss, H. Gruetzmacher and M. Geoffroy, *Chem.--Eur. J.* **2005**, 11, 3463-3468.
[9] a) M. J. S. Gynane, A. Hudson, M. F. Lappert, P. P. Power and H. Goldwhite, J. *Chem. Soc., Chem. Commun.* **1976**, 623-624; b) M. J. S. Gynane, A. Hudson, M. F. Lappert, P. P. Power and H. Goldwhite, *J. Chem. Soc., Dalton Trans.* **1980**, 2428-2433.
[10] a) S. L. Hinchley, C. A. Morrison, D. W. H. Rankin, C. L. B. Macdonald, R. J. Wiacek, A. Voigt, A. H. Cowley, M. F. Lappert, G. Gundersen, J. A. C. Clyburne and P. P. Power, *J. Am. Chem. Soc.* **2001**, 123, 9045-9053; b) S. L. Hinchley, C. A. Morrison, D. W. H. Rankin, C. L. B. Macdonald, R. J. Wiacek, A. H. Cowley, M. F. Lappert, G. Gundersen, J. A. C. Clyburne and P. P. Power, *Chem. Commun. (Cambridge)* **2000**, 2045-2046.
[11] J.-P. Bezombes, K. B. Borisenko, P. B. Hitchcock, M. F. Lappert, J. E. Nycz, D. W. H. Rankin and H. E. Robertson, *Dalton Trans.* **2004**, 1980-1988.
[12] J.-P. Bezombes, P. B. Hitchcock, M. F. Lappert and J. E. Nycz, *Dalton Trans.* **2004**, 499-501.
[13] a) C. E. Holloway, F. E. Mabbs and W. R. Smail, *J. Chem. Soc. A* **1968**, 2980-2984; b) D. C. Bradley, R. H. Moss and K. D. Sales, *J. Chem. Soc. D* **1969**, 1255-1256.
[14] D. W. J. Cruickshank, *Acta Crystallogr.* **1964**, 17, 671-672.
[15] A. Al Badri, M. Chentit, M. Geoffroy and A. Jouaiti, *J. Chem. Soc., Faraday Trans.* **1997**, 93, 3631-3635.
[16] G. Maerkl and K. M. Raab, *Tetrahedron Lett.* **1989**, 30, 1077-1080.
[17] H. Kawanami, K. Toyota and M. Yoshifuji, *Chem. Lett.* **1996**, 533-534.
[18] S. Sasaki, F. Murakami and M. Yoshifuji, *Angew. Chem., Int. Ed.* **1999**, 38, 340-343.
[19] P. Rosa, C. Gouverd, G. Bernardinelli, T. Berclaz and M. Geoffroy, *J. Phys. Chem. A* **2003**, 107, 4883-4892.
[20] W. W. Schoeller, J. Niemann, R. Thiele and W. Haug, *Chem. Ber.* **1991**, 124, 417-421.
[21] a) A. J. Arduengo, III, J. C. Calabrese, A. H. Cowley, H. V. R. Dias, J. R. Goerlich, W. J. Marshall and B. Riegel, *Inorg. Chem.* **1997**, 36, 2151-2158; b) A. J. Arduengo, III, H. V. R. Dias and J. C. Calabrese, *Chem. Lett.* **1997**, 143-144.

[22] M. Regitz, O. J. Scherer and Editors, *Multiple Bonds and Low Coordination in Phosphorus Chemistry*, **1990**, p. 478 pp.
[23] N. G. Connelly and W. E. Geiger, *Chem. Rev. (Washington, D. C.)* **1996**, 96, 877-910.
[24] a) C. Chuit, R. J. P. Corriu, P. Monforte, C. Reye, J.-P. Declercq and A. Dubourg, *J. Organomet. Chem.* **1996**, 511, 171-175; b) C. Chuit, R. J. P. Corriu, P. Monforte, C. Reye, J. P. Declercq and A. Dubourg, *Angew. Chem.* **1993**, 105, 1529-1531 (See also *Angew Chem , Int Ed Engl* , 1193, 1532(1510), 1430-1532); c) F. H. Carre, C. Chuit, R. J. P. Corriu, W. E. Douglas, D. M. H. Guy and C. Reye, *Eur. J. Inorg. Chem.* **2000**, 647-653.
[25] a) C. T. Walling, *Free Radicals in Solution*, 1957, p. 631 pp; b) B. P. Roberts, *Chem. Soc. Rev.* **1999**, 28, 25-35.
[26] J. Sinclair and D. Kivelson, *J. Am. Chem. Soc.* **1968**, 90, 5074-5080.
[27] O. Back, M. A. Celik, G. Frenking, M. Melaimi, B. Donnadieu and G. Bertrand, *J. Am. Chem. Soc*. **2010**, 132, 10262-10263.
[28] L. Weber, *Eur. J. Inorg. Chem.* **2000**, 2425-2441.
[29] G. D. Frey, V. Lavallo, B. Donnadieu, W. W. Schoeller and G. Bertrand, *Science (Washington, DC, U. S.)* **2007**, 316, 439-441.
[30] V. Lavallo, Y. Canac, B. Donnadieu, W. W. Schoeller and G. Bertrand, *Angew. Chem., Int. Ed.* **2006**, 45, 3488-3491.
[31] a) J. D. Masuda, W. W. Schoeller, B. Donnadieu and G. Bertrand, *Angew. Chem., Int. Ed.* **2007**, 46, 7052-7055; b) J. D. Masuda, W. W. Schoeller, B. Donnadieu and G. Bertrand, *J. Am. Chem. Soc.* **2007**, 129, 14180-14181; c) O. Back, G. Kuchenbeiser, B. Donnadieu and G. Bertrand, *Angew. Chem., Int. Ed.* **2009**, 48, 5530-5533.
[32] R. Kinjo, B. Donnadieu and G. Bertrand, *Angew. Chem., Int. Ed.* **2010**, 49, 5930-5933.
[33] J. K. Brask, V. Dura-Vila, P. L. Diaconescu and C. C. Cummins, *Chem. Commun. (Cambridge, U. K.)* **2002**, 902-903.

Experimental part

Synthesis of 22:

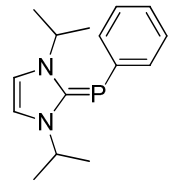

In the glovebox, pentaphenylcyclopentaphosphine **21** (0.318 g, 0.59 mmol) was added at room temperature to a stirring solution of the free carbene **20** (0.448 g, 2.95 mmol) in 8 mL of THF. Immediately upon addition the color of the solution turned red. The solution was then stirred at room temperature overnight. All the volatiles were removed under vacuum and the resulting yellow solid was washed 2 times with 10 mL of hexane and then dried under vacuum to afford **22** as a fine yellow powder. Yield 79% (0.610 g, 2.34 mmol).

^{31}P{^{1}H} (C_6D_6, 162 MHz): δ -61.2.

^{1}H NMR (C_6D_6, 400 MHz): δ 0.94 (d, J = 7.2 Hz, 12 H), 5.07 (dsept, J = 7.2 Hz, J = 4 Hz, 2 H), 6.41 (s, 2 H), 6.86 (t, J = 7.2 Hz, 1 H), 7.03 (t, J = 7.2 Hz 2 H), 7.54 (t, J = 7.2 Hz, 2 H).

^{13}C{^{1}H} NMR (C_6D_6, 100 MHz): δ 22.3, 50.4 (d, J_{PC} = 9 Hz), 116.3, 122.2, 128.3, 132.0 (d, J_{PC} = 20 Hz), 151.1 (d, J_{PC} = 50 Hz), 167.8 (d, J_{PC} = 102 Hz, $C_{carbene}$).

Synthesis of 25a and 25b:

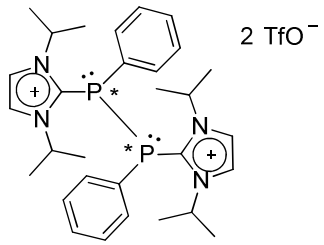

15 mL of THF was added at room temperature to a mixture of adduct **22** (0.600 g, 2.31 mmol) and ferrocenium triflate ($Fc^{+}TfO^{-}$) (0.773 g, 2.31 mmol). The mixture was then stirred at room temperature during 2 hours. During the course of the reaction a precipitate appeared and was filtered via cannula. The product was then extracted with 30 mL of acetonitrile and the solvent was removed under vacuum. The residue was then washed 4 times with 10 mL of THF in order to remove the remaining ferrocenium triflate. The resulting solid was dried under vacuum affording a mixture of the diastereoisomers **25a** and **25b** as a white powder. Yield 30 % (0.280 g, 0.34 mmol).

Diastereoisomer **25a** (major):

$^{31}P\{^{1}H\}$ (CD_3CN, 162 MHz): δ -49.8.

^{1}H (CD_3CN, 400 MHz): δ 1.28 (d, J = 6.8 Hz, 12 H), 1.44 (d, J = 6.0 Hz, 12 H), 5.18-5.34 (m, 4 H), 7.26-7.34 (m, 4 H), 7.46-7.52 (m, 4 H), 7.54-7.62 (m, 2 H), 7.92 (s, 4 H).

$^{13}C\{^{1}H\}$ (CD_3CN, 125.75 MHz): δ 22.6, 24.1, 55.2 (t, J_{PC} = 9 Hz), 122.4 (q, J_{CF} = 316 Hz, CF_3), 125.8, 131.6, 133.1, 134.2 (t, J_{PC} = 12 Hz), 137.9 (1, J_{PC} = 25 Hz, $C_{carbene}$).

Diastereoisomer **25b** (minor):

$^{31}P\{^{1}H\}$ (CD_3CN, 162 MHz): δ -57.7.

^{1}H (CD_3CN, 400 MHz): δ 0.78 (d, J = 6.0 Hz, 12 H), 1.60 (d, J = 6.0 Hz, 12 H), 5.04-5.16 (m, 4 H), 7.91 (s, 4 H), because of overlapping aromatic protons could not be observed.

$^{13}C\{^{1}H\}$ (CD_3CN, 125.75 MHz): δ 22.9, 23.4, 54.2, 122.4 (q, J_{CF} = 316 Hz, CF_3), 125.9, 131.0, 132.9, 135.6 (t, J_{PC} = 12 Hz), the quaternary carbons of the imidazolium rings were not observed.

Synthesis of 28:

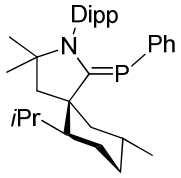

Dichlorophenylphosphine (0.492 g, 2.75 mmol) was added at room temperature to a solution of the free carbene **26** (1.050 g, 2.75 mmol) in 15 mL of hexane. Immediately upon addition the solution turned blue and a precipitate appeared. The mixture was then stirred at room temperature overnight, during this time the solution turned colorless. The precipitate was filtered via cannula and then washed 2 times with 20 mL of hexane. The resulting solid was dried under vacuum.
Potassium graphite (0.744 g, 5.50 mmol) was added to the solid followed by the addition at -80 °C of 20 mL of THF. The mixture was then stirred at room temperature during 3 hours and the graphite was then removed by filtration via cannula. After evaporation of the solvent, compound **28** was obtained as a pale yellow powder. Yield 42% (0.565 g, 1.15 mmol).

$^{31}P\{^{1}H\}$ (C_6D_6, 121 MHz): δ 56.2.

^{1}H (C_6D_6, 500 MHz): δ 0.99 (d, J = 6.8 Hz, 3 H), 1.00 (d, J = 6.8 Hz, 3 H), 1.00 (s, 3 H), 1.06 (d, J = 6.8 Hz, 3 H), 1.13 (d, J = 6.8 Hz, 3 H), 1.14 (d, J = 6.8 Hz, 3 H), 1.16 (d, J =

6.8 Hz, 3 H), 1.24 (s, 3 H), 1.2-1.4 (m, 2 H), 1.51 (d, J = 6.8 Hz, 3 H),1.56-1.70 (m, 2 H), 1.59 (d, J = 12.9 Hz, 1 H), 1.99 (d, J = 13.1 Hz, 1 H), 2.31 (sept, J = 6.8 Hz, 1 H), 2.47 (d, J = 12.9 Hz, 1 H), 2.50 (d, J = 13.1 Hz, 1 H), 2.86 (qt, J = 13.4 Hz, J = 4.2 Hz, 1 H), 3.10-3.35 (m, 1 H), 3.26 (sept, J = 6.8 Hz, 1 H), 6.7-7.0 (m, 8 H), 1 H belonging to the cyclohexyl ring couldn't be observed because of overlapping.

^{13}C{^{1}H} (C_6D_6, 125.75 MHz): δ 21.5 (d, J_{PC} = 10 Hz), 22.9, 23.7, 24.9, 25.0 (d, J_{PC} = 21 Hz), 25.4, 25.8, 26.2, 27.4, 27.6, 29.2, 30.1, 30.3, 30.8, 36.3, 51.6, 54.7, 56.1 (d, J_{PC} = 10 Hz), 58.6 (d, J_{PC} = 27 Hz), 68.9, 125.8, 126.1 (d, J_{PC} = 6 Hz), 127.7 (d, J_{PC} = 6 Hz), 129.36, 134.6, 134.8, 138.2, 138.6, 141.9 (d, J_{PC} = 64 Hz), 149.9 (d, J_{PC} = 12 Hz), 191.3 (d, J_{PC} = 109 Hz, $C_{carbene}$).

Synthesis of 27(X$^-$):

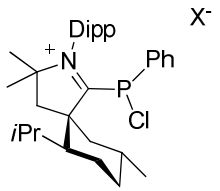

THF (6 mL) was added at room temperature to a mixture of **28** (0.350 g, 0.72 mmol) and $[N(C_6H_4Br\text{-}4)_3]^+SbCl_6^-$ (0.584 g, 0.72 mmol). Immediately upon addition the solution turned clear yellow. The mixture was then stirred at room temperature during 1 hour.

^{31}P{^{1}H} (THF, 121 MHz): δ 162 ppm.

Synthesis of 30:

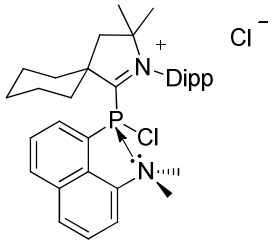

A solution of the free carbene **29** (0.777 g, 2.39 mmol) in 6 mL of hexane was added at room temperature to a stirring solution of 1-(dimethylamino)-8-dichlorophosphinonaphtalene (0.647 g, 2.39 mmol) in 6 mL of hexane. The mixture was then stirred at room temperature overnight. The precipitate was filtered via cannula and washed 3 times with 20 mL of ether. The resulting solid was dried under vacuum to afford the salt **30** as a fine yellow powder. Yield: 77% (1.120 g, 1.88 mmol).
^{31}P{^{1}H} (CD_3CN, 162 MHz): δ 69.4 (br s).

^{1}H (CD_3CN, 400 MHz): δ 0.95-1.80 (m, 10 H), 1.25 (d, J = 6.4 Hz, 3 H), 1.38 (d, J = 6.4 Hz, 6 H), 1.59 (s, 3 H), 1.71 (s, 3 H), 1.90-2.10 (m, 2 H), 2.15-2.35 (m, 3 H), 2.65-3.00 (m, 5 H), 2.72 (s, 3 H), 7.28 (d, J = 7.4 Hz, 1 H), 7.40-7.55 (m, 2 H), 7.63 (d, J = 5.0 Hz, 2 H), 7.70-7.80 (m, 2 H), 7.88 (td, J = 4.6 Hz, J = 1.6 Hz, 1 H), 8.19 (d, J = 8.0 Hz, 1 H).

^{13}C{^{1}H} (CD_3CN, 100 MHz): δ 22.1 (d, J_{PC} = 3 Hz), 22.8, 23.0, 25.0, 25.31, 25.34, 25.87, 25.89, 29.7, 29.9, 30.3, 35.3, 35.5, 44.5, 48.1, 48.3, 63.2, 85.4 (d, J_{PC} = 8 Hz), 122.5, 127.2, 127.3 (d, J_{PC} = 5 Hz), 127.6, 128.0, 128.5, 129.5, 129.7, 131.8 (d, J_{PC} = 5 Hz), 132.6, 135.1, 136.1, 145.6, 147.3 (d, J_{PC} = 7 Hz), 149.9 (d, J_{PC} = 5 Hz), the quaternary carbon of the pyrrolidinium ring was not observed.

Synthesis of 31:

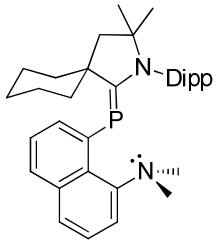

15 mL of THF was added at room temperature to a mixture of salt **30** (1.100 g, 1.84 mmol) and magnesium (325 mesh, 99.5%, purchased from Aldrich, 0.090 g, 3.69 mmol). The mixture was then stirred at room temperature during 4 hours. All the volatiles were removed under vacuum and the product was extracted 2 times with 15 mL of hexane. After evaporation of the filtrate the phosphoalkene **31** was obtained as a fine yellow powder. Yield 81% (0.785 g, 1.49 mmol).

^{31}P{^{1}H} (C_6D_6, 162 MHz): δ 95.2.

^{1}H (C_6D_6, 400 MHz): δ 0.80-1.32 (m, 8 H), 1.07 (s, 6 H), 1.36 (d, J = 6.8 Hz, 6 H), 1.41 (d, J = 10.8 Hz, 2 H), 1.73 (s, 2 H), 1.76 (d, J = 6.8 Hz, 6 H), 2.57 (br s, 6 H), 3.32 (sept, J = 6.8 Hz, 2 H), 7.04 (d, J = 8.8 Hz, 1 H), 7.20-7.34 (m, 5 H), 7.49 (d, J = 7.6 Hz, 1 H), 7.66 (d, J = 6.8 Hz,1 H), 7.88 (t, J = 6.4 Hz, 1 H).

^{13}C{^{1}H} NMR (C_6D_6, 100 MHz): δ 23.8, 24.9, 26.0, 28.2 (br s), 29.4, 30.0 (br s), 38.8 (d, J_{PC} = 5.4 Hz), 50.5, 54.7, 54.8, 66.3, 116.5, 124.6, 124.8, 125.6, 125.9, 128.9, 129.4, 134.6, 136.1, 136.4, 137.9, 138.5, 138.6, 153.0, 200.5 (d, J_{PC} = 60 Hz, $C_{carbene}$).

Synthesis of 32a and 32b:

Benzene (8 mL) was added at room temperature to a mixture of **31** (0.206 g, 0.39 mmol) and $Ph_3C^+B(C_6F_5)_4^-$ (0.300 g, 0.33 mmol). Immediately upon addition, the solution turned dark brown. The mixture was then stirred at room temperature during 1h30 and the solvent was removed under vacuum to give a red solid. The resulting solid was washed three times with a benzene/hexane mixture (3 mL/15 mL) and was dried under vacuum. Single crystals of **32a** were obtained by layering hexane on top of a fluorobenzene solution of **32a**.

Compound 32a:

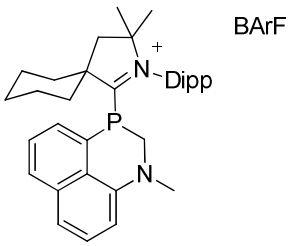

$^{31}P\{^1H\}$ (C_6H_5F, 121 MHz): δ -17.9.

^{31}P (C_6H_5F, 121 MHz): δ -17.9 (d, $^2J_{PH}$ = 31 Hz, $^2J_{PH}$ = 14 Hz).

Compound 32b:

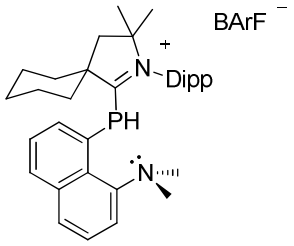

$^{31}P\{^1H\}$ (C_6H_5F, 121 MHz): δ -55.2.

^{31}P (C_6H_5F, 121 MHz): δ -55.2 (d, $^1J_{PH}$ = 290 Hz).

Synthesis of 34:

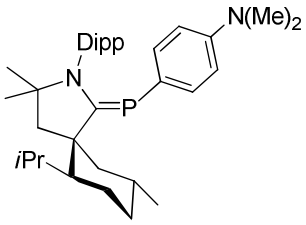

Ether (15 mL) was added at room temperature to a mixture of carbene **26** (0.735 g, 1.98 mmol) and dibromo(4-methoxyphenyl)phosphine (0.305 g, 0.99 mmol). The mixture was then stirred at room temperature during 3 hours. Over the course of the reaction a white precipitate appeared. The precipitate was filtered via cannula and washed with 10 mL of ether. After evaporation of the filtrate the phosphoalkene **34** was obtained as a light yellow powder. Yield 82% (0.430 g, 0.81 mmol).

$^{31}P\{^{1}H\}$ (C_6D_6, 202.5 MHz): δ 58.4.

^{1}H (C_6D_6, 500 MHz): δ 1.01 (d, *J* = 6.5 Hz, 3 H), 1.03 (s, 3 H), 1.12 (d, *J* = 7.0 Hz, 3 H), 1.14 (d, *J* = 6.5 Hz, 3 H), 1.15 (d, *J* = 7.0 Hz, 3 H), 1.19 (d, *J* = 7.0 Hz, 3 H), 1.21 (d, *J* = 7.0 Hz, 3 H), 1.27 (s, 3 H), 1.34 (dd, *J* = 6.5 Hz, *J* = 2.5 Hz, 1 H), 1.56 (d, *J* = 6.5 Hz , 3H), 1.64 (dd, *J* = 12.5 Hz, *J* = 1.5 Hz, 2 H), 1.72 (dd, *J* = 13.5 Hz, *J* = 6.5 Hz, 1 H), 2.01 (d, *J* = 12.5 Hz, 1 H), 2.35 (sept, *J* = 6.5 Hz, 1 H), 2.45 (s, 6 H), 2.50 (d, *J* = 12.5 Hz, 2 H), 2.55 (d, *J* = 13.0 Hz, 1 H), 2.95 (dt, *J* = 13 Hz, *J* = 4.5 Hz, 1 H), 3.22-3.34 (m, 1 H), 3.38 (sept, *J* = 7.0 Hz, 1 H), 3.39 (sept, *J* = 7.0 Hz, 1 H), 6.25 (d, *J* = 8.5 Hz, 2 H), 6.62 (d, *J* = 8.5 Hz, 1 H), 6.63 (d, *J* = 8.5 Hz, 1 H), 7.00-7.08 (m, 2 H), 7.23 (t, *J* = 8.5 Hz, 1 H).

$^{13}C\{^{1}H\}$ (C_6D_3, 125.75 MHz): δ 21.5 (d, J_{PC} = 10 Hz), 23.8, 25.0, 25.2, 25.3 (d, J_{PC} = 6 Hz), 26.0 (d, J_{PC} = 8 Hz), 27.4, 27.5, 27.7, 29.3 (d, J_{PC} = 8 Hz,), 30.2, 30.4, 30.9, 36.5, 40.5, 51.6, 54.8, 56.2 (d, J_{PC} = 10 Hz), 58.3, 58.5, 68.5, 112.6, 112.7, 125.6, 125.9, 129.1, 135.5, 135.7, 138.9, 149.4, 150.1, 189.6 (d, J_{PC} = 107 Hz, $C_{carbene}$).

Synthesis of 35:

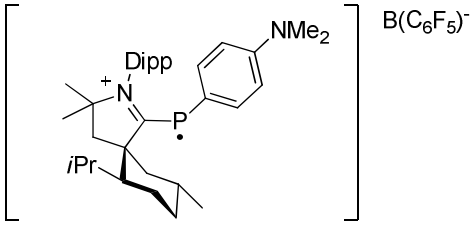

Dichloromethane (1mL) was added at -80 °C to a mixture of phosphoalkene **34** (0.020 g, 0.04 mmol) and $Ph_3C^+B(C_6F_5)_4^-$ (0.035 g, 0.04 mmol) in an E.P.R. tube. Immediately upon addition the solution turned blue. The E.P.R. tube was then inserted into the cavity

of an E.P.R. spectrometer cooled down at -80 ° C for the analysis. The E.P.R. spectra were then successively recorded at -80°C, -50°C, 0 °C and finally room temperature.

Synthesis of 36:

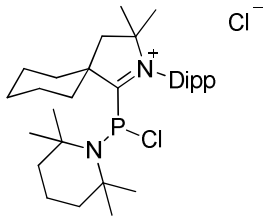

2,2,6,6-tetramethylpiperidinedichlorophosphine (0.311 g, 1.29 mmol) was added at room temperature to a solution of CAAC **29** (0.419 g, 1.29 mmol) in 10 mL of hexane. The mixture was stirred at room temperature overnight. During the course of the reaction a white precipitate appeared. The suspension was filtered via cannula and the resulting white solid was washed 2 times with 15 mL of ether. After drying under vacuum the salt **36** was obtained as a white powder. Yield 55% (0.405 g, 0.715 mmol).

Mp: 177 ^{o}C.

^{31}P{^{1}H} ($CDCl_3$, 121 MHz): δ 92.3.

^{1}H ($CDCl_3$, 300 MHz): δ 1.15-1.90 (m, 12 H), 1.25 (d, *J* = 6.7 Hz, 3 H), 1.28 (d, *J* = 6.4 Hz, 3 H), 1.29 (d, *J* = 6.7 Hz, 3 H), 1.30 (d, *J* = 6.4 Hz, 3 H), 1.38 (s, 6 H), 1.42 (s, 3 H), 1.45 (s, 3 H), 1.67 (s, 6 H), 2.03 (d, *J* = 12.7 Hz, 1 H), 2.12 (d, *J* = 12.7 Hz, 1 H), 2.26 (t, *J* = 12.8 Hz, 1 H), 2.35-2.55 (m, 1 H), 2.44 (sept, *J* = 6.7 Hz, 1 H), 2.48 (d, *J* = 13.8 Hz, 1 H), 2.63 (sept, *J* = 6.4 Hz, 1 H), 2.72 (d, *J* = 13.8 Hz, 1 H), 7.19 (dd, *J* = 8 Hz, *J* = 1.4 Hz, 1 H), 7.22 (dd, *J* = 8 Hz, *J* = 1.4 Hz, 1 H), 7.43 (dd, *J* = 7.8 Hz, *J* = 7.8 Hz, 1 H).

^{13}C{^{1}H} ($CDCl_3$, 75 MHz): δ 16.8, 22.5, 22.6, 24.6, 25.2, 25.4, 25.8 (d, J_{PC} = 7 Hz), 27.5, 28.9, 29.5, 29.9, 30.3 (d, J_{PC} = 7 Hz), 31.7, 32.3, 36.1, 36.5, 36.8, 39.4, 39.8 (d, J_{PC} = 6 Hz), 40.9 (d, J_{PC} = 26 Hz), 44.4, 61.5 (d, J_{PC} = 10 Hz), 62.8 (d, J_{PC} = 33 Hz), 63.6 (d, J_{PC} = 7 Hz), 85.6 (d, J_{PC} = 6 Hz), 126.1, 126.2, 131.4, 131.5, 145.0, 145.3, 213.3 (d, J_{PC} = 121 Hz, $C_{carbene}$).

Synthesis of 37:

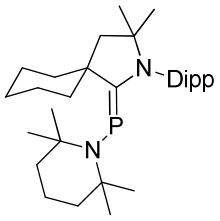

60 mL of THF was added at room temperature to a mixture of magnesium (325 mesh, 99.5%, purchased from Aldrich, 0.192 g, 7.91 mmol) and salt **36** (2.24 g, 3.96 mmol). The mixture was then stirred at room temperature overnight. During the course of the reaction the color of the solution turned yellow and the white precipitate disappeared. The solvent was then removed under vacuum and the product was extracted with 60 mL of hexane. Evaporation of the filtrate provided the phosphoalkene **37** as a yellow solid. Single crystals suitable for X-ray diffraction analysis were obtained slow evaporation of a ether solution of **37** Yield 81 % (1.60 g, 3.22 mmol).

Mp: 188 ^{o}C.

^{31}P{^{1}H} (C_6D_6, 121 MHz): δ 135.4.

^{1}H (C_6D_6, 500 MHz): δ 1.05 (s, 6 H), 1.28-1.75 (m, 12 H), 1.29 (s, 6 H), 1.31 (d, J = 7 Hz, 6 H), 1.62 (s, 6 H), 1.66 (d, J = 7 Hz, 6 H), 1.86-1.91 (m, 2 H), 1.90 (s, 2H), 3.04 (t, J = 13 Hz, 2 H), 3.15 (sept, J = 7 Hz, 2 H), 7.15-7.25 (m, 3 H).

^{13}C{^{1}H} (C_6D_6, 125.75 MHz): δ 18.6, 23.9, 24.7, 25.0 (d, J_{PC} = 12.4 Hz), 26.7, 27.9 (d, J_{PC} = 8 Hz), 29.1, 30.4, 38.1 (d, J_{PC} = 4 Hz), 38.2 (d, J_{PC} = 6 Hz), 43.2, 49.1, 55.4 (d, J_{PC} = 12 Hz), 56.9 (d, J_{PC} = 6 Hz), 66.8, 125.5, 129.0, 134.2, 149.0 (d, J_{PC} = 4 Hz), 207.3 (d, J_{PC} = 95 Hz, $C_{carbene}$).

Synthesis of 38:

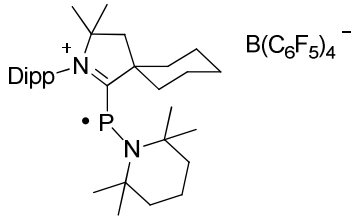

8 mL of benzene was added at room temperature to a mixture of $Ph_3C^+B(C_6F_5)_4^-$ (0.390 g, 0.42 mmol) and phosphoalkene **37** (0.210g, 0.42 mmol). Immediately upon addition,

the color turned dark brown and the mixture biphasic. The mixture was then stirred at room temperature during 1 hour. The solvent was then removed via vaccum and the resulting brown residue was washed three times with a mixture benzene/ hexane (1.5 mL/ 20 mL) and was dried under vacuum to afford the radical **38** as a fine brown powder. Single crystals suitable for X-ray diffraction analysis were obtained by layering hexane on top of a fluorobenzene solution of **38** at 5 ^{o}C. Yield 38 % (0.190 g, 0.16 mmol).

Mp: 94 ^{o}C.

Synthesis of 39:

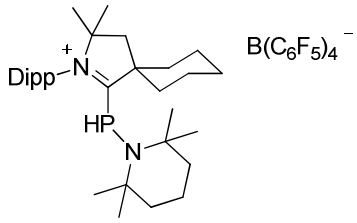

$HSn(nBu)_3$ (0.594 g, 2.04 mmol) was added at room temperature to a biphasic mixture of radical **38** (0.480 g, 0.41 mmol) in 5 mL of benzene while stirring. Upon addition the color turned clear orange. The mixture was stirred at room temperature overnight and the upper phase was then removed. The resulting orange oil was washed two times with 6 mL of benzene and one time with 6 mL of hexane. The oil was dried under vacuum to afford **39** as a fine pale orange powder. Single crystals suitable for X-ray diffraction analysis were obtained by layering hexane on top of a fluorobenzene solution of **39** at 5 ^{o}C. Yield 68 % (0.325 g, 0.28 mmol).

Mp: 171-173 ^{o}C.

^{31}P{^{1}H} (CD_2Cl_2, 162 MHz): δ –0.49.

^{31}P (CD_2Cl_2, 162 MHz): δ.–0.49 (d, J_{PH} = 283 Hz).

^{1}H ($CDCl_3$, 500 MHz): δ 0.8-1.8 (m, 18 H), 1.14 (s, 6 H), 1.35 (d, J = 6.5 Hz, 6 H), 1.38 (d, J = 6.5 Hz, 6 H) , 1.43 (s, 6 H), 1.80-1.96 (m, 2 H), 1.92 (d, J = 11.5 Hz, 2 H), 2.57 (br s, 4 H), 5.57 (d, J_{PH} = 283 Hz, 1 H), 7.42 (d, J = 8 Hz, 2 H), 7.55 (t, J = 8 Hz, 1 H).

^{13}C{^{1}H} ($CDCl_3$, 125.75 MHz): δ 13.6, 16.6, 22.0, 24.5, 24.8, 27.3, 27.8, 29.4, 36.6, 40.8, 45.1, 58.9, 61.5, 82.1 , 115.5 (d, J_{PC} = 21 Hz), 124.2 (br s), 127.6, 130.2 (d, J_{PC} = 8 Hz), 132.5, 136.4 (d, J_{CF} = 241 Hz), 138.4 (d, J_{CF} = 243 Hz), 144.9 (br s), 148.4 (d, J_{CF} = 239 Hz), 218.8 (d, J_{PC} = 68 Hz, $C_{carbene}$).

Synthesis of 40:

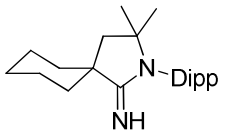

Elemental bromine (0.688 g, 4.30 mmol) was added at - 78°C to a solution of CAAC **29** (1.400 g, 4.30 mmol) in 20 mL of hexane. Immediately upon addition a yellow precipitate appeared. The mixture was then stirred at room temperature overnight and the precipitate was filtered via cannula. The resulting solid was washed with 25 mL of ether and dried under vacuum. 25 mL of THF was then added to the yellow solid, and ammonia gas was bubbled through the suspension at room temperature while stirring during 30 minutes. The mixture was then quenched with 20 mL of an aqueous solution of NH_4OH (14.87 M) and stirred at room temperature during 30 minutes. 50 mL of ether was then added to the mixture and the organic phases was washed with brine and dried over $MgSO_4$. After filtration, the volatiles were removed under vacuum to afford **40** as a yellow powder. Yield 70% (1.030 g, 3.03 mmol).

^{1}H (C_6D_6, 400 MHz): δ 0.96 (s, 6 H), 1.12 (d, *J* = 6.8 Hz, 6 H), 1.15 (d, *J* = 6.8 Hz, 6 H), 1.18-1.26 (m, 3 H), 1.5-1.7 (m, 5 H), 1.75 (s, 2 H), 2.06 (br s, 2 H), 3.05 (sept, *J* = 6.8 Hz, 2 H), 7.05-7.18 (m, 3 H), N*H* was not observed.

^{13}C{^{1}H} (C_6D_6, 100 MHz): δ 23.5, 23.6, 26.4, 26.9, 29.4, 30.2, 38.1, 45.9, 48.2, 62.5, 125.1, 129.4, 131.9, 150.9, 174.2.

Synthesis of 41(Cl^-):

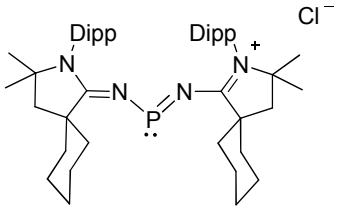

^{n}BuLi (2.5 M in hexane, 1.27 mL, 3.18 mmol) was added at -78°C to a solution of **40** (1.030 g, 3.03 mmol) in 25 mL of ether. The mixture was warmed up at room temperature and then stirred during 2 hours. The mixture was then cooled down at - 78°C and PCl_3 (0.208 g, 1.51 mmol) was added. The mixture was then stirred at room temperature overnight. The precipitate was filtered via cannula and 25 mL of chloroform was added to the solid. After removal of LiCl by filtration all the volatiles were removed under vacuum. The residue was then washed with 25 mL of ether and dried under vacuum to afford **41**(Cl^-) as a white powder. Yield 66 % (0.740 g, 0.99 mmol).

^{31}P{^{1}H} ($CDCl_3$, 162 MHz): δ 182.1.

^{1}H ($CDCl_3$, 400 MHz): δ 1.00 (d, *J* = 6.4 Hz, 12 H), 1.04-1.72 (m, 20 H), 1.22 (d, *J* = 6.4 Hz, 12 H), 1.28 (s, 12 H), 2.22 (s, 4 H), 2.63 (sept, *J* = 6.4 Hz, 4 H), 7.20 (d, *J* = 7.6 Hz, 4 H), 7.38 (t, *J* = 7.6 Hz, 2 H).

^{13}C ($CDCl_3$, 100 MHz): δ 21.8, 23.5, 24.9, 26.8 (d, J_{PC} = 4 Hz), 29.2, 29.7, 35.1, 45.7, 49.1, 68.7, 125.1, 128.9, 130.3, 147.1, 171.4 ($C_{carbene}$).

Synthesis of 41(TfO^-):

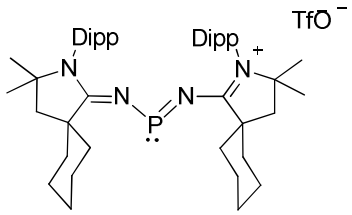

15 mL of chloroform was added at room temperature to a mixture of **41**(Cl^-) (0.740 g, 0.99 mmol) and AgOTf (0.255 g, 0.99 mmol). The mixture was then stirred at room temperature in the dark during 1 hour. Over the course of the reaction a precipitate appeared which was removed via filtration. The filtrate was evaporated under vacuum and the resulting solid was washed 2 times with 15 mL of ether and then dried under vacuum affording **41**(TfO^-) as a white powder. Yield 76 % (0.650 g, 0.76 mmol).

^{31}P{^{1}H} ($CDCl_3$, 121 MHz): δ 184.2.

^{1}H ($CDCl_3$, 300 MHz): δ 0.9-1.8 (m, 20 H), 1.07 (d, *J* = 6.7 Hz, 12 H), 1.27 (d, *J* = 6.7 Hz, 12 H), 1.33 (s, 12 H), 2.28 (s, 4 H), 2.66 (sept, *J* = 6.7 Hz, 4 H), 7.26 (d, *J* = 7.8 Hz, 4 H), 7.43 (t, *J* = 7.8 Hz, 2 H).

^{13}C{^{1}H} ($CDCl_3$, 75 MHz): δ 21.7, 23.6, 24.9, 26.8 (d, J_{PC} = 4 Hz), 29.2, 29.6, 35.1, 45.4, 49.1, 69.2, 125.2, 128.8, 130.4, 147.0, 171.5 ($C_{carbene}$), CF_3 was not observed.

^{19}F ($CDCl_3$, MHz): -77.1.

Synthesis of 44:

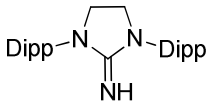

Elemental bromine (1.257 g, 7.87 mmol) was added at -78°C to a slurry of NHC **42** (3.070 g, 7.87 mmol) in 60 mL of hexane. The mixture was stirred at room temperature overnight. The precipitate was filtered via cannula and washed with 40 mL of ether. 40 mL of THF is then added to the resulting yellow solid and ammonia gas was bubbled through the suspension at room temperature during 30 minutes. The mixture was then quenched with 20 mL of an aqueous solution of NH_4OH (14.87 M), stirred at room temperature during 30 minutes and 100 mL of ether was then added to the mixture. The organic phase was washed with brine and dried over $MgSO_4$. After filtration, the volatiles were removed under vacuum to afford **44** as a white powder. Yield 87% (2.770 g, 6.83 mmol).

Mp: 190 ^{o}C.

^{1}H (C_6D_6, 400 MHz): δ 1.21 (d, *J* = 6.8 Hz, 12 H), 1.29 (d, *J* = 6.8 Hz, 12 H), 3.19 (sept, *J* = 6.8 Hz, 4 H), 3.25 (s, 4 H), 7.07 (d, *J* = 8 Hz, 4 H), 7.17 (t, *J* = 8 Hz, 2 H), N*H* was not observed.

^{13}C{^{1}H} (C_6D_6, 100 MHz): δ 24.5, 25.2, 29.4, 48.8, 124.8, 129.3, 135.8, 149.6, 160.1.

Synthesis of 45(Cl^-):

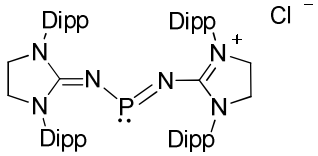

^{n}BuLi (2.5 M in hexane, 2.45 mL, 6.13 mmol) was added at -78°C to a solution of **44** (2.365 g, 5.84 mmol) in 40 mL of ether. The mixture was warmed up at room temperature and then stirred during 3 hours. Then the solution was cooled down at -78°C and PCl_3 (0.404 g, 2.92 mmol) was added. The mixture was then stirred at room temperature overnight. The white precipitate was filtered via cannula and 20 mL of CH_2Cl_2 was added. After filtration of LiCl, all the volatiles were removed under vaccum and the yellowish residue was washed with 25 mL of ether. The residue was dried under vacuum to afford **45**(Cl^-) as a white powder. At this stage the product contains some impurities which cannot be separated. Yield 50 % (1.29 g, 1.48 mmol).

^{31}P{^{1}H} (CD_3CN, 162 MHz): δ 276.3.

^{1}H (CD_3CN, 400 MHz): δ 0.78 (d, J = 7.2 Hz, 24 H), 1.43 (d, J = 7.2 Hz, 24 H), 2.79 (sept, J = 7.2 Hz, 8 H), 3.92 (s, 8 H), 7.09 (d, J = 7.6 Hz, 8 H), 7.37 (t, J = 7.6 Hz, 4 H).

^{13}C{^{1}H} (CD_3CN, 100 MHz): δ 25.0 (d, J_{PC} = 3 Hz), 25.5, 30.0, 50.4, 126.1, 131.9, 132.3, 148.9, 159.6 (d, J_{PC} = 17 Hz, $C_{carbene}$).

Synthesis of 45(TfO^-):

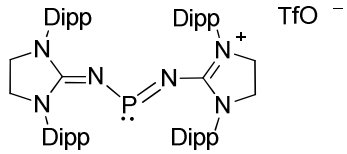

20 mL of CH_2Cl_2 was added at room temperature to a mixture of **45**(Cl^-) (1.270 g, 1.45 mmol) and AgOTf (0.373 g, 1.45 mmol). The mixture was then stirred at room temperature in the dark during two hours. During the course of the reaction a precipitate appeared which was removed by filtration. Evaporation of the volatiles under vacuum gave a yellow residue which was washed two times with 20 mL of ether. The solid was dried under vacuum to afford **45**(TfO^-) as a white powder. Yield 83% (1.19 g, 1.20 mmol).

Mp: 374°C (decomposition).

^{31}P{^{1}H} ($CDCl_3$, 162 MHz): δ 277.0.

^{1}H ($CDCl_3$, 400 MHz): δ 0.72 (d, J = 6.8 Hz, 24 H), 1.15 (d, J = 6.8 Hz, 24 H), 2.67 (sept, J = 6.8 Hz, 8 H), 3.93 (s, 8 H), 6.99 (d, J = 8.0 Hz, 8 H), 7.30 (t, J = 8.0 Hz, 4 H).

^{13}C{^{1}H} (CD_3CN, 100 MHz): δ 24.0, 24.6, 29.0, 49.3, 121.1 (q, J_{CF} = 319 Hz, CF_3), 124.6, 130.5, 130.7, 147.3, 158.2 (d, J_{PC} = 19 Hz, $C_{carbene}$).

Synthesis of 46:

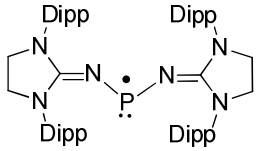

15 mL of THF was added at room temperature to a mixture of salt **45**(TfO^-) (1.080 g, 1.09 mmol) and KC_8 (0.155 g, 1.15 mmol). The mixture was then allowed to stir at room temperature during three hours. The solvent was removed under vacuum and the product extracted with 20 mL of benzene. After evaporation of the solvent the radical **46** was obtained as a fine red microcrystalline powder. Yield 72% (0.660 g, 0.79 mmol).

Mp: 208°C-211°C.

Synthesis of 47:

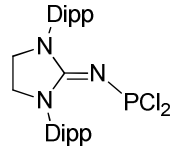

^{n}BuLi (2.5 M in hexane, 1.20 mL, 3.01 mmol) was added at -78°C to a solution of **44** (1.160 g, 2.86 mmol) in 25 mL of THF. The mixture was then stirred at room temperature during 3 hours. The solution was cooled down at -78°C and PCl_3 (0.413 g, 3.01 mmol) was then added. The mixture was stirred at room temperature overnight and all the volatiles were removed under vacuum. Benzene was then added to the residue and LiCl was filtered off via cannula. After evaporation of the solvent the yellow residue was washed two times with 20 mL of pentane. The remaining solid was dried under vacuum to afford **47** as a white powder. Yield 57% (0.820 g, 1.62 mmol).

Mp: 271 ^{o}C.

^{31}P{^{1}H} (C_6D_6, 162 MHz): δ 183.7.

^{1}H (C_6D_6, 400 MHz): δ 1.18 (d, J = 6.8 Hz, 12 H), 1.47 (d, J = 6.8 Hz, 12 H), 3.14 (sept, J = 6.8 Hz, 4 H), 3.33 (s, 4 H), 7.07 (d, J = 8.0 Hz, 4 H), 7.19 (t, J = 8.0 Hz, 2 H).

^{13}C{^{1}H} (C_6D_6, 100 MHz): δ 24.6, 25.5, 29.6, 49.0, 125.1, 130.6, 133.6, 148.5, 155.9 (d, J_{PC} = 17 Hz, $C_{carbene}$).

Synthesis of 48:

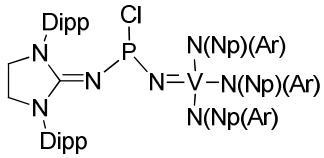

30 mL of THF was added at - 78°C to a mixture of **47** (0.820 g, 1.62 mmol) and the vanadium nitride anion **6** (1.067 g, 1.62 mmol). The mixture was then stirred at room temperature during six hours. All the volatiles were removed under vacuum and 30 mL of benzene was then added to the dark red residue. After removal of NaCl by filtration, the solvent was removed under vacuum. The dark red residue was then washed with 10 mL of acetonitrile and dried under vacuum to afford **48** as dark red powder. Yield 73 % (1.340 g, 1.19 mmol).

Mp: 128°C-131°C.

$^{31}P\{^{1}H\}$ (C_6D_6, 162 MHz): δ 185.5 (bs).

^{1}H (C_6D_6, 400 MHz): δ 0.90 (s, 27 H), 1.24 (d, *J* = 6.8 Hz, 6 H), 1.26 (d, *J* = 6.8 Hz, 6H), 1.65 (d, *J* = 6.8 Hz, 6H), 1.69 (d, *J* = 6.8 Hz, 6H), 2.10 (s, 18H), 3.37 (sept, *J* = 6.8 Hz, 2 H), 3.37-3.45 (m, 2 H), 3.46-3.52 (m, 2H), 3.54 (sept, *J* = 6.8 Hz, 2 H), 4.44 (d, *J* = 13.2 Hz, 3 H), 4.54 (d, *J* = 13.2 Hz, 3 H), 6.37 (s, 6 H), 6.53 (s, 3 H), 7.18 (d, *J* = 7.6 Hz, 4 H), 7.26 (t, *J* = 7.6 Hz, 2 H).

$^{13}C\{^{1}H\}$ (C_6D_6, 100 MHz): δ 21.9, 25.1, 25.4, 25.9, 26.1, 29.4, 29.6, 29.9, 36.4, 50.1, 77.7, 122.7, 124.9, 125.3, 125.8, 129.9, 135.9, 137.5, 148.3, 148.5, 157.9 (d, J_{PC} = 23 Hz, $C_{carbene}$), 158.3.

Synthesis of 49:

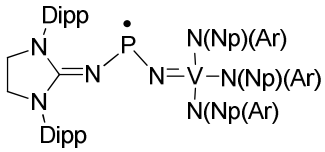

15 mL of THF was added at room temperature to a mixture of **48** (1.230 g, 1.11 mmol) and KC_8 (0.160 g, 1.17 mmol). The mixture was then stirred at room temperature during three hours and the solvent was removed under vacuum. 25 mL of benzene was then added to the dark red residue and KCl and graphite were removed via filtration. All the volatiles were removed under vacuum to afford the radical **49** as a dark red powder. Yield 85 % (1.010 g, 0.94 mmol).

Mp: 98°C-102°C.